Superelevation Criteria for Sharp Horizontal Curves on Steep Grades

DETAILS

182 pages | 8.5 x 11 | PAPERBACK
ISBN 978-0-309-30790-1 | DOI 10.17226/22312

AUTHORS

þÿTorbic, Darren J.; O Laughlin, Mitchell K.; Harwood, Douglas W.; Bauer, Karin M.; Bokenkroger, Courtney D.; Lucas, Lindsay M.; Ronchetto, John R.; Brennan, Sean; Donnell, Eric; Brown, Alexander; and Tejas Varunjikar

NATIONAL COOPERATIVE HIGHWAY RESEARCH PROGRAM

NCHRP REPORT 774

Superelevation Criteria for Sharp Horizontal Curves on Steep Grades

Darren J. Torbic
Mitchell K. O'Laughlin
Douglas W. Harwood
Karin M. Bauer
Courtney D. Bokenkroger
Lindsay M. Lucas
John R. Ronchetto
MRIGLOBAL
Kansas City, MO

Sean Brennan
Eric Donnell
Alexander Brown
Tejas Varunjikar
THOMAS D. LARSON PENNSYLVANIA TRANSPORTATION INSTITUTE
AT THE PENNSYLVANIA STATE UNIVERSITY
University Park, PA

Subscriber Categories
Design • Operations and Traffic Management • Safety and Human Factors

Research sponsored by the American Association of State Highway and Transportation Officials
in cooperation with the Federal Highway Administration

TRANSPORTATION RESEARCH BOARD

WASHINGTON, D.C.
2014
www.TRB.org

NATIONAL COOPERATIVE HIGHWAY RESEARCH PROGRAM

Systematic, well-designed research provides the most effective approach to the solution of many problems facing highway administrators and engineers. Often, highway problems are of local interest and can best be studied by highway departments individually or in cooperation with their state universities and others. However, the accelerating growth of highway transportation develops increasingly complex problems of wide interest to highway authorities. These problems are best studied through a coordinated program of cooperative research.

In recognition of these needs, the highway administrators of the American Association of State Highway and Transportation Officials initiated in 1962 an objective national highway research program employing modern scientific techniques. This program is supported on a continuing basis by funds from participating member states of the Association and it receives the full cooperation and support of the Federal Highway Administration, United States Department of Transportation.

The Transportation Research Board of the National Academies was requested by the Association to administer the research program because of the Board's recognized objectivity and understanding of modern research practices. The Board is uniquely suited for this purpose as it maintains an extensive committee structure from which authorities on any highway transportation subject may be drawn; it possesses avenues of communications and cooperation with federal, state and local governmental agencies, universities, and industry; its relationship to the National Research Council is an insurance of objectivity; it maintains a full-time research correlation staff of specialists in highway transportation matters to bring the findings of research directly to those who are in a position to use them.

The program is developed on the basis of research needs identified by chief administrators of the highway and transportation departments and by committees of AASHTO. Each year, specific areas of research needs to be included in the program are proposed to the National Research Council and the Board by the American Association of State Highway and Transportation Officials. Research projects to fulfill these needs are defined by the Board, and qualified research agencies are selected from those that have submitted proposals. Administration and surveillance of research contracts are the responsibilities of the National Research Council and the Transportation Research Board.

The needs for highway research are many, and the National Cooperative Highway Research Program can make significant contributions to the solution of highway transportation problems of mutual concern to many responsible groups. The program, however, is intended to complement rather than to substitute for or duplicate other highway research programs.

NCHRP REPORT 774

Project 15-39
ISSN 0077-5614
ISBN 978-0-309-30790-1
Library of Congress Control Number 2014946500

COPYRIGHT INFORMATION

NOTICE

The project that is the subject of this report was a part of the National Cooperative Highway Research Program, conducted by the Transportation Research Board with the approval of the Governing Board of the National Research Council.

The members of the technical panel selected to monitor this project and to review this report were chosen for their special competencies and with regard for appropriate balance. The report was reviewed by the technical panel and accepted for publication according to procedures established and overseen by the Transportation Research Board and approved by the Governing Board of the National Research Council.

The opinions and conclusions expressed or implied in this report are those of the researchers who performed the research and are not necessarily those of the Transportation Research Board, the National Research Council, or the program sponsors.

The Transportation Research Board of the National Academies, the National Research Council, and the sponsors of the National Cooperative Highway Research Program do not endorse products or manufacturers. Trade or manufacturers' names appear herein solely because they are considered essential to the object of the report.

Published reports of the

NATIONAL COOPERATIVE HIGHWAY RESEARCH PROGRAM

are available from:

Transportation Research Board
Business Office
500 Fifth Street, NW
Washington, DC 20001

and can be ordered through the Internet at:

http://www.national-academies.org/trb/bookstore

Printed in the United States of America

THE NATIONAL ACADEMIES

Advisers to the Nation on Science, Engineering, and Medicine

The **National Academy of Sciences** is a private, nonprofit, self-perpetuating society of distinguished scholars engaged in scientific and engineering research, dedicated to the furtherance of science and technology and to their use for the general welfare. Upon the authority of the charter granted to it by the Congress in 1863, the Academy has a mandate that requires it to advise the federal government on scientific and technical matters. Dr. Ralph J. Cicerone is president of the National Academy of Sciences.

The **National Academy of Engineering** was established in 1964, under the charter of the National Academy of Sciences, as a parallel organization of outstanding engineers. It is autonomous in its administration and in the selection of its members, sharing with the National Academy of Sciences the responsibility for advising the federal government. The National Academy of Engineering also sponsors engineering programs aimed at meeting national needs, encourages education and research, and recognizes the superior achievements of engineers. Dr. C. D. Mote, Jr., is president of the National Academy of Engineering.

The **Institute of Medicine** was established in 1970 by the National Academy of Sciences to secure the services of eminent members of appropriate professions in the examination of policy matters pertaining to the health of the public. The Institute acts under the responsibility given to the National Academy of Sciences by its congressional charter to be an adviser to the federal government and, upon its own initiative, to identify issues of medical care, research, and education. Dr. Victor J. Dzau is president of the Institute of Medicine.

The **National Research Council** was organized by the National Academy of Sciences in 1916 to associate the broad community of science and technology with the Academy's purposes of furthering knowledge and advising the federal government. Functioning in accordance with general policies determined by the Academy, the Council has become the principal operating agency of both the National Academy of Sciences and the National Academy of Engineering in providing services to the government, the public, and the scientific and engineering communities. The Council is administered jointly by both Academies and the Institute of Medicine. Dr. Ralph J. Cicerone and Dr. C. D. Mote, Jr., are chair and vice chair, respectively, of the National Research Council.

The **Transportation Research Board** is one of six major divisions of the National Research Council. The mission of the Transportation Research Board is to provide leadership in transportation innovation and progress through research and information exchange, conducted within a setting that is objective, interdisciplinary, and multimodal. The Board's varied activities annually engage about 7,000 engineers, scientists, and other transportation researchers and practitioners from the public and private sectors and academia, all of whom contribute their expertise in the public interest. The program is supported by state transportation departments, federal agencies including the component administrations of the U.S. Department of Transportation, and other organizations and individuals interested in the development of transportation. **www.TRB.org**

www.national-academies.org

COOPERATIVE RESEARCH PROGRAMS

CRP STAFF FOR NCHRP REPORT 774

Christopher W. Jenks, *Director, Cooperative Research Programs*
Christopher Hedges, *Manager, National Cooperative Highway Research Program*
David A. Reynaud, *Senior Program Officer*
Megan A. Chamberlain, *Senior Program Assistant*
Eileen P. Delaney, *Director of Publications*
Natalie Barnes, *Senior Editor*

NCHRP PROJECT 15-39 PANEL
Field of Design—Area of General Design

Norman H. Roush, *West Virginia DOT* (retired)*, Racine, OH* (Chair)
Kenneth T. Briggs, *KCI Technologies Inc., Sparks, MD*
Antonette C. Clark, *California DOT, Sacramento, CA*
James R. Kladianos, *Wyoming DOT, Laramie, WY*
John Roccanova, *California DOT, Stockton, CA*
Larry F. Sutherland, *Parsons Brinckerhoff, Columbus, OH*
Jeffrey Shaw, *FHWA Liaison*
Stephen F. Maher, *TRB Liaison*

AUTHOR ACKNOWLEDGMENTS

This report was prepared by Dr. Darren J. Torbic, Mr. Douglas W. Harwood, Ms. Karin M. Bauer, Ms. Lindsay M. Lucas, and Mr. John R. Ronchetto of MRIGlobal; Dr. Sean Brennan, Dr. Eric Donnell, and Mr. Alexander Brown of the Thomas D. Larson Pennsylvania Transportation Institute at the Pennsylvania State University; Mr. Mitchell K. O'Laughlin of Kiewit (formerly of MRIGlobal); Ms. Courtney D. Bokenkroger of Elanco (formerly of MRIGlobal); and Mr. Tejas Varunjikar of Nexteer Automotive (formerly of the Thomas D. Larson Pennsylvania Transportation Institute at the Pennsylvania State University). The authors wish to thank the state departments of transportation of California, Maryland, Pennsylvania, Washington, and West Virginia for their assistance in this research.

FOREWORD

By David A. Reynaud
Staff Officer
Transportation Research Board

This report provides superelevation criteria for horizontal curves on steep grades. A series of field studies and vehicle dynamics simulations were undertaken to investigate combinations of horizontal curve and vertical grade design. The report should be of interest to state and local highway design practitioners.

Sharp, horizontal curves on steep downgrades represent a potential safety concern for vehicles, especially heavy vehicles. Examples where this combination may occur are interchange ramp movements, curves on mountainous roads, or high-speed downgrade curves on controlled-access roadways. At these locations, the complicating factors of grade, pavement cross slope, and pavement friction fully tax the driver's ability to provide correct vehicle positioning without compromising control of the vehicle. Superelevation criteria, horizontal curvature, and other associated geometric criteria needed to be developed for situations where steep grades are located on sharp horizontal curves.

The objective of NCHRP Project 15-39 was to develop superelevation criteria for horizontal curves on steep grades. Other criteria associated with design of horizontal curves (e.g., tangent-to-curve transitions, spiral transitions, lateral shift of vehicles traversing the curve, need for pavement widening, and determination of curve radii) were also considered.

The research was performed by MRIGlobal and the Pennsylvania State University. Design criteria were developed based on a series of field studies and vehicle dynamic simulations. Field studies were conducted to collect vehicle speed and lane-changing maneuver data from locations across the United States, as well as representative samples of tire–pavement friction data for various pavement surface conditions. Vehicle dynamic simulations used AASHTO design criteria in combination with field-measured data. Three classes of passenger vehicles and three classes of trucks were considered for safety analysis. The report provides design guidance based on the analyses for sharp horizontal curves on steep grades.

CONTENTS

Note: Many of the photographs, figures, and tables in this report have been converted from color to grayscale for printing. The electronic version of the report (posted on the Web at www.trb.org) retains the color versions.

SUMMARY

Superelevation Criteria for Sharp Horizontal Curves on Steep Grades

Geometric design policy for horizontal curves is established by the American Association of State Highway and Transportation Officials (AASHTO) and published in *A Policy on Geometric Design of Highways and Streets* (referred to as the *Green Book*). Design criteria for horizontal curves are based on a mathematical model that represents the vehicle as a point mass. As a vehicle traverses a horizontal curve, it undergoes a centripetal acceleration that is balanced by a combination of superelevation and friction at the tire–pavement interface. Horizontal curves designed in accordance with AASHTO policy have been shown to provide a substantial margin of safety with respect to vehicle skidding and rollover for both passenger cars and trucks under normal conditions. However, the policy indicates that vehicles traveling on steep downgrades or upgrades may require some adjustment in superelevation rates, to maintain an adequate margin of safety, for grades steeper than 5%. The superelevation adjustment is made by assuming a slightly higher design speed for horizontal curves on steep downgrades and, because vehicles slow down on an upgrade, adding superelevation in the curve. The recommendation to adjust the design speed and superelevation on steep grades has not been fully investigated.

The purpose of this research was to develop superelevation criteria for sharp horizontal curves on steep grades. A series of field studies and vehicle dynamics simulations were undertaken to investigate the combination of horizontal curve and vertical grade design criteria. The field studies included collecting vehicle speed and lane-change maneuver data from 20 locations across the United States. Additionally, tire–pavement friction data were collected at eight locations, representative of pavement surface conditions on multilane, divided highways. Crash data were acquired for the data collection locations and statistical models of the predicted number of crashes were estimated as a function of traffic volume and margins of safety for skidding and rollover. The vehicle dynamics simulations used the AASHTO design criteria, in combination with the field-measured data, to investigate the margins of safety against skidding and rollover for several vehicle types on sharp horizontal curves with steep grades. The point-mass model was the simplest model considered, while more complex models such as the bicycle and multibody models were also considered which simulate vehicles accounting for multiple axles and multiple tires, respectively.

The following vehicle types were considered in this research:

- **Passenger Vehicles:**
  - E-class sedan (i.e., mid-class sedan)
  - E-class sport utility vehicle (i.e., mid-size SUV)
  - Full-size SUV

- **Trucks:**
  - Single-unit truck
  - Tractor semi-trailer truck
  - Tractor semi-trailer/full-trailer truck (double)

The vehicle maneuver scenarios studied in this research for vehicles on curves include the following:

- Vehicle maintains constant speed equal to the design speed of the curve (no deceleration, i.e., 0 ft/s^2)
- Vehicle brakes at a deceleration rate that drivers typically use when entering a curve (–3 ft/s^2)
- Vehicle brakes on the curve at a deceleration rate equivalent to that assumed for stopping sight distance design criteria (–11.2 ft/s^2)
- Vehicle brakes on the curve at a deceleration rate greater than that assumed for stopping sight distance design criteria, equivalent to the deceleration used in an emergency braking maneuver (–15 ft/s^2)

Each of these vehicle maneuver scenarios was considered for a vehicle maintaining its lane position and also for a vehicle changing lanes while traversing the curve and decelerating, as described above.

The vehicle maneuver scenarios were assessed, and it was concluded that the following scenarios occur so rarely that they do not represent a reasonable basis for design:

- Deceleration at rates greater than –11.2 ft/s^2 while traversing a curve (i.e., an emergency stop with deceleration greater than that assumed for stopping sight distance design criteria)
- Deceleration at rates of –11.2 ft/s^2 or greater (i.e., a controlled stop with deceleration greater than or equal to that assumed for stopping sight distance design criteria) while traversing a curve and simultaneously changing lanes on the curve

Thus, modifications to current AASHTO *Green Book* horizontal curve–superelevation design policy should be based on the assumption that a vehicle should be able to maintain its desired trajectory within the same lane while undergoing deceleration equivalent to that considered for stopping sight distance design criteria (–11.2 ft/s^2).

For this research, a sharp horizontal curve is defined as a minimum-radius curve as determined from the maximum rate of superelevation and maximum side friction factor for each design speed, in accordance with the design criteria in the AASHTO *Green Book.* The results obtained here should assure that, if a vehicle can brake on a minimum-radius curve without loss of control, then that same vehicle will be able to brake on larger-than-minimum-radius curves without loss of control.

The following conclusions were drawn from the research effort:

- The AASHTO *Green Book* maximum side friction factors (f_{max}) used in horizontal curve design are below friction supply curves for lateral (cornering) and longitudinal (braking) directions, for both passenger vehicles and trucks, as measured in the field for design speeds greater than 20 mph. Thus, current horizontal curve design policy appears to provide reasonable lateral friction margins against skidding in most situations. However, the more complex vehicle dynamics models (i.e., the transient bicycle and multibody models) indicate that the point-mass model generally overestimates the margins of safety against skidding and rollover across all vehicle types.

- There is no concern of a passenger vehicle rolling over while traveling at the design speed on a sharp horizontal curve with a steep downgrade, when designed according to current AASHTO *Green Book* policy.
- Based upon a review of the literature, the lowest rollover thresholds for tanker trucks (i.e., liquid-cargo tank trucks) are in the range of 0.28 to 0.30. Because carriers are discouraged from hauling half-filled tanks, because completely filled and empty tanks produce rigid-load behaviors that are generally more predictable and the rollover thresholds are closer to 0.56 than 0.30, and because crash data show that few crashes involve vehicles with rollover thresholds less than 0.35, horizontal curve design and superelevation criteria should not be based upon tanker trucks with rollover thresholds of 0.28 to 0.30. Rather horizontal curve design and superelevation criteria should be based upon more typical loading and truck configurations. For vehicles considered in the simulation modeling in this study, the minimum rollover threshold was 0.56.
- On downgrades, the lowest margins of safety against skidding and rollover generally occur at design speeds of 40 mph and lower for all vehicle types. This appears to be the result of higher side friction factors used in design for horizontal curves with lower design speeds.
- Steep vertical downgrade–sharp horizontal curve combinations that necessitate braking to maintain a constant speed (and maintain lane position) from the approach tangent through a horizontal curve for a passenger car sedan have large margins of safety against skidding (>0.33) for design speeds ranging from 25 to 85 mph (see Figure 87). Similarly, positive margins of safety against skidding (≥0.23) for passenger cars that decelerate at a rate of −3 ft/s^2 (similar to rates measured in the field for the present study and reported by Bonneson [2000b]) or at a rate of −11.2 ft/s^2 (stopping sight distance deceleration) exist for all design speed–downgrade combinations considered in the present study. Deceleration rates of −15 ft/s^2 (emergency braking) produce negative margins of safety for many design speeds for vertical downgrade–sharp horizontal curve combinations when the passenger car sedan enters the horizontal curve. However, the latter scenario does not seem likely to occur with sufficient frequency to constitute a reasonable basis for design.
- Steep vertical downgrade–sharp horizontal curve combinations that necessitate braking to maintain a constant speed (and maintain lane position) from the approach tangent through a horizontal curve for a mid-size SUV have large margins of safety against skidding (>0.34) for design speeds ranging from 25 to 85 mph (see Figure 88). Similarly, margins of safety against skidding for a mid-size SUV that decelerates at a rate of −3 ft/s^2 exceed 0.3 for all design speeds for vertical downgrade–sharp horizontal curve combinations considered in the present study. When mid-size SUVs must decelerate at a rate of −11.2 ft/s^2 (stopping sight distance braking), positive margins of safety (>0.15) were produced for all design speeds for vertical downgrade–sharp horizontal curve combinations considered in the present study. Deceleration rates of −15 ft/s^2 (emergency braking) produce negative margins of safety for most designs considered in the present study. However, the latter scenario does not seem likely to occur with sufficient frequency to constitute a reasonable basis for design.
- The margins of safety against skidding for a full-size SUV were similar to those reported for the mid-size SUV (see Figures 88 and 89).
- Steep vertical downgrade–sharp horizontal curve combinations that necessitate braking for a single-unit truck to maintain a constant speed (and maintain lane position) from the approach tangent through a horizontal curve have large margins of safety against skidding (>0.25) for design speeds ranging from 25 to 85 mph (see Figure 90). Similarly, margins of safety against skidding for the single-unit truck that decelerates at a rate of −3 ft/s^2 exceed 0.10 for all design speeds for vertical downgrade–sharp horizontal curve combinations considered in the present study. Based upon the steady-state

and transient bicycle models for a vehicle, when single-unit trucks must decelerate at a rate of −11.2 ft/s^2 (stopping sight distance braking) or a rate equivalent to emergency braking (−15 ft/s^2), significant negative margins of safety against skidding result across all design speed–downgrade combinations considered in the present study. However, based on multibody model analyses for deceleration rates of −11.2 ft/s^2 and −15 ft/s^2 by a single-unit truck on a curve, the single-unit truck is able to maintain control on the curve when equipped with an anti-lock brake system (ABS).

- Steep vertical downgrade–sharp horizontal curve combinations that necessitate braking for a tractor semi-trailer to maintain a constant speed (and maintain lane position) from the approach tangent through a horizontal curve have large margins of safety against skidding (>0.28) for design speeds ranging from 25 to 85 mph (see Figure 91). Similarly, margins of safety against skidding for a tractor semi-trailer that decelerates at a rate of −3 ft/s^2 exceed 0.26 for all design speeds for vertical downgrade–sharp horizontal curve combinations considered in the present study, and when a tractor semi-trailer must decelerate at a rate of −11.2 ft/s^2, the margins of safety exceed 0.11. For emergency braking (−15 ft/s^2), a tractor semi-trailer will experience negative lateral friction margins at low design speeds (e.g., 35 mph or less). The margins of safety against skidding were slightly higher for the tractor semi-trailer/full-trailer truck when compared to the tractor semi-trailer. The emergency braking scenario does not seem likely to occur frequently enough to constitute a reasonable basis for design.
- When maintaining a vehicle operating speed at or near the design speed on a horizontal curve, grade and maximum superelevation rate (e_{max}) appear to have little effect on the margins of safety against skidding and rollover for all vehicle types.
- Eck and French (2002) suggest that high superelevation rates (e.g., between 8% and 16%) make horizontal curves on steep downgrades more forgiving. The vehicle dynamics simulations in the present study suggest that maximum rates of superelevation should not exceed 12% on downgrades because the superelevation transition occurring on the approach tangent can begin to reduce the margins of safety against skidding prior to curve entry. On curves designed with e_{max} greater than 12%, the margin of safety against skidding by a vehicle may be smaller in the superelevation transition area than on the curve proper. Thus, the results of this research do not support the recommendation by Eck and French that e_{max} values up to 16% should be considered in some cases. On upgrades of 4% and greater, e_{max} should be limited to 9% for minimum-radius curves with design speeds of 55 mph and higher, to avoid the possibility of wheel-lift events. Alternatively, e_{max} values up to 12% could be used for minimum-radius curves if it can be verified that the available sight distance is such that deceleration at −11.2 ft/s^2 is unlikely to be required.
- When vehicles change lanes in a horizontal curve, the margins of safety against skidding decrease considerably for all vehicle types considered in the present study. When lane changing occurs during a stopping sight distance or emergency braking maneuver, all vehicles exhibit negative margins of safety against skidding, as shown in Figures 132 through 143. For those situations (i.e., combinations of horizontal curvature, grade, and vehicle maneuvers) in which the transient bicycle model predicted skidding (i.e., negative lateral friction margins), the multibody model showed that if a vehicle has ABS, and the driver properly responds to minor lateral skidding, then the vehicle can maintain its intended path. In cases where the driver does not correct the steering input in response to a lateral shift, and the vehicle is not equipped with ABS, the transient bicycle model showed the lateral skidding of passenger sedan vehicles with negative margins of safety is small (i.e., less than 1.5 ft in lateral direction) across all combinations of vertical downgrade, design speed, deceleration rate, and lane-change maneuvers. A mid-size SUV, full-size SUV, and single-unit truck without ABS all exhibit large lateral shifts when the margin

of safety against skidding is negative in certain conditions, most notably situations when more aggressive braking is needed such as deceleration rates similar to those used to develop stopping sight distance or emergency braking design criteria (−11.2 or −15 ft/s^2). The case of a tractor semi-trailer without ABS need not be considered because all tractor semi-trailers are mandated to have ABS. [Note: Federal Motor Vehicle Safety Standard No. 121 mandates ABS on all new airbraked vehicles with gross vehicle weight ratings of 10,000 lb or greater. ABS is required on tractors manufactured on or after March 1, 1997, and airbraked semi-trailers and single-unit trucks manufactured on or after March 1, 1998 (Allen, 2010).]

- Based on current AASHTO *Green Book* horizontal curve–superelevation design policy, a vehicle that performs an emergency braking maneuver (−15 ft/s^2 deceleration) on a steep downgrade–horizontal curve combination will likely skid off the roadway in many cases if the vehicle is not equipped with ABS.
- The method used in the current AASHTO *Green Book* policy to distribute superelevation and side friction on tangent–curve transitions is adequate and produces positive margins of safety against skidding and rollover for all vehicle types on horizontal curves designed using maximum superelevation and minimum curve radii. However, the superelevation attained at the point of curve entry should be checked and compared to a lateral friction margin condition to ensure that the lateral friction margin on the curve entry is not less than the margin within the curve.
- AASHTO policy uses superelevation to balance the effects of sharper curvature. This balance may be imperfect when axle-to-axle differences are considered. The balancing effect is slightly more conservative with higher superelevation rates, often resulting in lower lateral friction margins occurring for lower superelevations (e.g., 0% superelevation). However, differences in lateral friction margins between different superelevations are very small.
- The crash analysis performed in the present study showed that the predicted number of single-vehicle run-off-road and single-vehicle rollover crashes decreases as the margins of safety against skidding and rollover increase for both passenger vehicles and trucks.

The recommended design guidance developed based on the research conducted in the present study is as follows:

- Figures 30 and 32 of this report show passenger vehicle and truck tire measurements of skidding wet-tire friction in the lateral (cornering) and longitudinal (braking) directions. It is recommended that the lateral friction curves (two standard deviations below mean) be integrated into AASHTO *Green Book* Figures 3-4 and 3-5, which show the maximum side friction factors used in horizontal curve design for high-speed and low-speed streets and highways (respectively). Incorporating these curves into Figures 3-4 and 3-5 of the *Green Book* would be informative to designers. The modified figures would, for the first time, illustrate friction measurements that take into consideration the effects of cornering. For a conservative design policy, horizontal curve–superelevation design policy recommendations should be based upon the 2nd percentile (i.e., mean friction minus two standard deviations) of the friction supply provided at the tire–pavement interface.
- For a simple horizontal curve, the maximum rate of superelevation should not exceed 12% on a downgrade. If considering a maximum superelevation rate greater than 12%, a spiral curve transition is recommended to increase the margins of safety against skidding between the approach tangent and horizontal curve. On upgrades of 4% or more, the maximum superelevation rate should be limited to 9% for minimum-radius curves with design speeds of 55 mph and higher, to avoid the possibility of wheel-lift events. Alternatively, if it can be verified that the available sight distance is such that deceleration

at −11.2 ft/s^2 is unlikely to be required on upgrades of 4% or more (i.e., the available sight distance is greater than minimum stopping sight distance design values), e_{max} values up to 12% may be used for minimum-radius curves.

- For sharp horizontal curves (or near minimum-radius curves) on downgrades of 4% or more, the "Stay in Lane" sign (R4-9) should be installed in advance of the curve on multilane highways. Consideration may also be given to using solid white lane line markings to supplement the R4-9 sign.
- Sharp horizontal curves (or near minimum-radius curves) on downgrades of 4% or more should not be designed for low design speeds (i.e., 30 mph or less). In the event that such situations cannot be avoided, warning signs to reduce speeds well in advance of the start of the horizontal curve should be used.
- The following condition should be used to check that the superelevation achieved at the point of curvature (PC) of a simple horizontal curve (i.e., with no spiral transition curves) is less than the threshold value computed based on the given design speed–curve radius combination:

$$\frac{e}{100} < \frac{1}{1 + p_{tangent}} \times \frac{V^2}{gR}$$

where:

e = superelevation at PC of horizontal curve,
$p_{tangent}$ = proportion of the maximum superelevation that is attained at the PC of horizontal curve,
V = design speed (ft/s),
g = gravitational constant (32.2 ft/s^2), and
R = radius of horizontal curve (ft).

If the condition presented above is met, the superelevation transition may be placed as indicated in *Green Book* Table 3-18. If the condition presented above is not met, designers should reduce the proportion of the maximum superelevation attained at the PC of the horizontal curve, or introduce a spiral transition curve between the approach tangent and simple horizontal curve. Based on an analysis completed for the present study, the condition above is satisfied for maximum-superelevation–minimum-radius curves for all design speeds. However, the condition above may be violated when using greater than minimum horizontal curve radii. In such cases, it is important to check the superelevation condition above, and if the condition is not met, it is recommended that a lower proportion of the superelevation runoff (e.g., 70%) be introduced prior to horizontal curve entry.

SECTION 1

Introduction

1.1 Background

Geometric design policy for horizontal curves is set by the American Association of State Highway and Transportation Officials (AASHTO) in *A Policy on Geometric Design of Highways and Streets*, commonly known as the *Green Book*, and by the design manuals of individual highway agencies. These criteria are based on the physics of the interaction between vehicles and the roadway, as well as consideration of vehicle stability and driver behavior.

As a vehicle traverses a horizontal curve, it undergoes centripetal acceleration equal to the square of the vehicle speed divided by the radius of the vehicle's curved path. This acceleration is balanced by a combination of superelevation and friction between the pavement and tires on the vehicle. Horizontal curves designed in accordance with *Green Book* criteria, even minimum-radius curves, have been shown to provide a substantial margin of safety with respect to both vehicle skidding and rollover under normal circumstances for both passenger vehicles and trucks (Harwood et al., 1989; Harwood and Mason, 1994; Harwood et al., 2003).

Geometric design criteria for horizontal curves are based on a simple mathematical model that represents the vehicle as a point mass. Research (MacAdam et al., 1985) has shown that the vertical loads on tires, in particular on trucks, and the side friction that can be supplied between the tires and pavement surface when traversing a horizontal curve vary dynamically and can be represented by a more sophisticated model than the point-mass model. Braking and tractive forces associated with vehicle maneuvering on grades also lead to variations between tires in vertical load and side friction supply. These variations in tire loads and vertical forces may lead to skidding or rollover at lateral accelerations less than those suggested by the point-mass model. Finally, the simple point-mass model assumes that the vehicle is on a planar surface. However, the combination of a superelevated curve and a steep grade creates a road surface that is clearly not planar.

The variation in the side friction factor values and tire loads suggested by the point-mass model in the AASHTO *Green Book* is expected to increase for horizontal curves on steep grades, but this phenomenon has not been thoroughly investigated. *NCHRP Report 439* (Bonneson, 2000b) included a preliminary investigation of this issue, based on a two-wheel "bicycle" model to represent a vehicle in a more complex form than the point-mass model. The *Green Book* has implemented the results from *NCHRP Report 439* for horizontal curves on grades with the following policy statement:

> On long or fairly steep grades, drivers tend to travel faster in the downgrade than in the upgrade direction. Additionally, research has shown that the side friction demand is greater on both downgrades (due to braking forces) and steep upgrades (due to the tractive forces). Some adjustment in superelevation rates should be considered for grades steeper than 5%. This adjustment is particularly important on facilities with high truck volumes and on low-speed facilities with intermediate curves using high levels of side friction demand.
>
> In the case of a divided highway with each roadway independently superelevated, or on a one-way ramp, such an adjustment can be readily made. In the simplest practical form, values from Tables 3-8 to 3-12, presented in Section 3.3.5, can be used directly by assuming a slightly higher design speed for the downgrade. Since vehicles tend to slow on steep upgrades, the superelevation adjustment can be made by not reducing the design speed for the upgrade. The appropriate variation in speed depends on the particular conditions, especially the rate and length of grade and the magnitude of the curve radius compared to other curves on the approach highway section.
>
> On two-lane and multilane undivided roadways, the adjustment for grade can be made by assuming a slightly higher design speed for the downgrade and applying it to the whole traveled way (both upgrade and downgrade sides). The added superelevation for the upgrade can help counter the loss of available side friction due to tractive forces. On long upgrades, the additional superelevation may cause negative side friction for slow-moving vehicles (such as large trucks). This effect is mitigated by the slow speed of the vehicle, allowing time to counter steer, and the increased experience and training for truck drivers. (AASHTO, 2011)

The approach suggested in the *Green Book* of adjusting the design speed to determine the appropriate superelevation for curves located on steep grades is a suitable approach given the current state of research knowledge. Additional knowledge is needed, however, to make such guidance more quantitative for specific combinations of curvature and grade.

1.2 Research Objective and Scope

The objective of this research was to develop superelevation criteria for sharp horizontal curves on steep grades. The basic elements of horizontal curve design, in addition to superelevation, include the radius of curvature, curve length, side friction factor, and superelevation transition. These basic elements of horizontal curve design, in addition to superelevation, were considered in this research.

This research was based on quantitative analyses. Data for the quantitative analyses were based on theoretical considerations and simulation, supported by actual field data collected at horizontal curves on steep grades.

This research investigated operational and vehicle dynamics data for horizontal curves on grades of 4% and greater. The research documented in *NCHRP Report 439* and incorporated in the 2011 *Green Book* indicates that an adjustment in superelevation rates should be considered for grades steeper than 5%. Rather than assuming the current superelevation criteria are sufficient for grades of 5% and below, this research investigated the impact on superelevation of grades as low as 4%. By considering grades of 4% and greater, this research more clearly and explicitly defined the boundary at which superelevation rates on grades should be adjusted.

The results of this research are applicable for urban and rural high-speed facilities including freeways, multilane divided and undivided highways, and two-lane roads; turning roadways (particularly ramps); and low-speed facilities. Both passenger vehicles and trucks were considered in developing the superelevation criteria. This research focused on superelevation criteria for sharp horizontal curves on steep downgrades; however, because undivided facilities must also be considered, upgrades were studied as well.

This research does not address issues related to pavement/shoulder cross-slope breaks on horizontal curves.

1.3 Overview of Research Methodology

In Phase I of the research, the research team summarized the literature related to superelevation criteria for sharp curves on steep grades. Topics covered in the review included horizontal curve design, the effects of heavy truck characteristics on horizontal curve design, the relationship between safety and horizontal curve design, driver comfort studies on horizontal curves, friction studies on horizontal curves, an overview of vehicle dynamics simulation modeling, and a summary of current horizontal curve design practice used across a range of state transportation agencies in the United States. The research team also identified critical parameters to be considered during field data collection and vehicle dynamics simulation modeling.

In Phase II the research team conducted speed studies, an instrumented vehicle study, and friction testing at sites in the eastern and western parts of the United States. Data collection sites were identified through a review of geometric design data and crash data when available. Vehicle dynamics simulation models were used to model vehicle dynamics at the actual field data collection sites and a range of hypothetical horizontal and vertical geometries. The field data were used to validate the vehicle dynamics simulation models. The simulation models used in this research ranged in complexity from the point-mass model (least complex) to the bicycle model to multibody models (most complex). The vehicle dynamics simulation models were used to identify combinations of horizontal curves and grades where skidding and/or vehicle rollover may be of concern for either passenger vehicles and/or trucks. A crash analysis was also conducted to investigate the relationship between lateral friction and rollover margins and crashes. Based upon the results of the simulation models and the crash analysis, recommended design criteria for superelevation on sharp curves on steep grades were developed.

1.4 Key Terms

The following list provides key terms used throughout this report and their definitions:

Centripetal Acceleration (a_r): an object that moves in a circular path (i.e., horizontal curve) with a constant speed follows a path that is tangent to the curve. Because the velocity vector undergoes a change in direction, the object (i.e., vehicle) undergoes an acceleration perpendicular to the path and toward the center of the horizontal curve. The centripetal acceleration is equal to the square of the vehicle speed divided by the radius of the circular path.

Lateral Acceleration: a term used by highway engineers that is equivalent to centripetal acceleration for the purposes of horizontal curve design.

Radius of Curve (R): describes a horizontal curve with a constant radius.

Minimum Radius of Curve (R_{min}): minimum radius of horizontal curve, which is a function of the maximum rate of superelevation and the maximum demand side friction used in horizontal curve design.

Side Friction Supply ($f_{tire\text{-}pavement}$): friction available between the pavement surface and vehicle tires to prevent skidding

on a horizontal curve, also referred to as the coefficient of friction. The maximum side friction supply is utilized when a vehicle is at the point of impending skid.

Side Friction Factor (f): the unbalanced portion of lateral acceleration or the portion of lateral acceleration that is not balanced by superelevation. The side friction factor represents demand side friction and is also referred to as net lateral acceleration in the point-mass model.

Rollover Threshold ($f_{rollover}$): the maximum lateral acceleration that a vehicle can experience without overturning.

Maximum Side Friction (f_{max}): the maximum side friction demand set forth in the AASHTO *Green Book* for use in horizontal curve design. The maximum side friction is based on driver comfort levels (i.e., tolerance for lateral acceleration) and is also referred to as the limiting side friction factor.

Sharp Horizontal Curve: a minimum-radius curve as determined from the maximum rate of superelevation and maximum side friction factor for each design speed, in accordance with the design criteria in the AASHTO *Green Book*.

Lateral Friction Margin: the difference between the available tire–pavement friction and the friction demand of the vehicle as it tracks the curve [i.e., side friction supply ($f_{tire\text{-}pavement}$) – side friction factor (f)]. This friction margin represents the additional lateral acceleration that a vehicle could undergo without skidding. A positive margin indicates a vehicle can undergo additional lateral acceleration without skidding, while a negative margin indicates the vehicle tires will skid given the level of friction supplied between the tire and pavement for the condition in question.

Rollover Margin: defined in two ways in the present study. One rollover margin is based on lateral acceleration, which represents the difference between the current lateral acceleration and the maximum lateral acceleration that a vehicle can experience without overturning. Rollover margin is also defined by the proximity of the load-transfer ratio to an absolute value of unity, e.g., how close an axle is to experiencing wheel lift. In both cases, a value of zero indicates the onset of wheel lift.

Steep Grade: in the present study, a vertical grade of at least 4%.

Point-Mass Model: a vehicle cornering model, where the vehicle is assumed to be a single object whose overall size does not influence its behavior.

Maximum Rate of Superelevation (e_{max}): the maximum banking or cross slope of the roadway cross section within a horizontal curve; this value ranges from 4% to 12%, depending on climatic conditions, area type, terrain, and the frequency of very slow-moving vehicles in the traffic stream.

Trucks: a range of vehicle types that include single-unit, tractor semi-trailer, and tractor semi-trailer/full-trailer trucks.

Design Speed (V_{DS}): selected speed used to determine the various geometric design features of the roadway.

Operating Speed: the speed at which drivers are observed operating their vehicles during free-flow conditions. The most common measure of operating speed is the 85th percentile of the free-flow speed distribution.

Bicycle Model: a vehicle dynamics model that treats each axle of a vehicle as a single tire located at the midline of the axle.

Multibody Model: a vehicle dynamics model that treats each tire of a vehicle as a separate kinematic body.

Transient Vehicle Behavior: when a driver changes the steering input on a vehicle (e.g., during transition from an approach tangent to a horizontal curve), the vehicle will enter the curve with motions that are initially unsteady (i.e., the spin of the vehicle, the yaw rate, will not at first match that of the curve) but settle out to a constant turning path on the curve. The behavior of the vehicle in this time period is called its "transient response."

Steady-State Vehicle Behavior: at the conclusion of the period of transient response resulting from a steering input change, the yaw rate of the vehicle will become constant, which is referred to as "steady-state response."

1.5 Outline of Report

This report documents the entire research effort. The remainder of this report is organized as follows. Section 2 summarizes the literature related to superelevation criteria for sharp curves on steep grades and presents current design policy. Section 3 describes the field studies conducted as part of this research and presents the results. Section 4 presents the analytical and simulation modeling work performed to investigate superelevation criteria for sharp horizontal curves on steep grades. Section 5 summarizes a crash analysis that investigated the relationship between crashes and lateral friction margins and rollover margins. Section 6 presents the final conclusions and recommendations of the research, including recommended design guidance and the need for future research. The remainder of the report consists of a list of references and three appendixes. Appendix A provides the nomenclature of the various symbols used throughout this report along with their definitions. Appendix B shows the vehicle input parameters used in the simulation modeling, and Appendix C presents changes proposed for consideration in future editions of the *Green Book* and *Manual on Uniform Traffic Control Devices* (MUTCD), based on the findings and conclusions of this research.

SECTION 2

Literature Review

This section summarizes the literature related to superelevation criteria for sharp curves on steep grades and also summarizes current practice on this issue. The topics are organized as follows:

- Horizontal curve design
- Heavy trucks
- Driver comfort
- Friction studies
- Vehicle dynamics models
- Current practice

2.1 Horizontal Curve Design

Current AASHTO policy on horizontal curve design is based upon a point-mass model. From the basic laws of Newtonian physics, consider a point mass traveling in a curved roadway with a constant radius (R) and a constant velocity (V), as shown in Figure 1. The point mass undergoes a centripetal acceleration which acts toward the center of curvature. The centripetal acceleration is given as:

$$a_r = \frac{V^2}{R} \tag{1}$$

Assume that the point mass is a vehicle. The acceleration is balanced by the side friction developed between the vehicle's tires and the pavement surface, the component of vehicle's weight acting parallel to the road due to superelevation, or a combination of both, as shown in Figure 2. Let the banking angle of roadway be α (radians). The superelevation (e) is typically defined by the rise (change in elevation) in feet per 100 ft across the road (i.e., in the transverse direction). Hence, $e/100 = \tan\alpha$. There are three forces acting on the point mass as shown in Figure 2:

1. Normal reaction from the road (N)
2. The tire–pavement friction cornering force acting at the road toward the center of the rotation (F_c)
3. Vehicle weight ($W = mg$; where m is the mass and g is the gravitational acceleration).

Performing a force balance in the y-axis direction (referring to the axis system shown in Figure 2), one obtains:

$$m \cdot a_r = \sum F_y$$

$$\Rightarrow m\frac{V^2}{R} = N_y + W_y + F_{cy} \tag{2}$$

And in the z-axis direction:

$$0 = \sum F_z = N_z + W_z + F_{cz} \tag{3}$$

The force components are given as:

$$\begin{aligned} N_z &= -N\cos\alpha, & N_y &= N\sin\alpha \\ F_{cz} &= F_c\sin\alpha, & F_{cy} &= F_c\cos\alpha \\ W_z &= mg, & W_y &= 0 \end{aligned} \tag{4}$$

Expressions for the friction factor and superelevation are:

$$f = F_c/N \quad e/100 = \tan\alpha \tag{5}$$

Equation 3 can be solved for mass by substituting values from Equation 4 to obtain $m = 1/g \cdot (-F_c sin(\alpha) + Ncos(\alpha))$. Substituting this into Equation 2, and then simplifying the result by substituting expressions from Equation 5, one obtains:

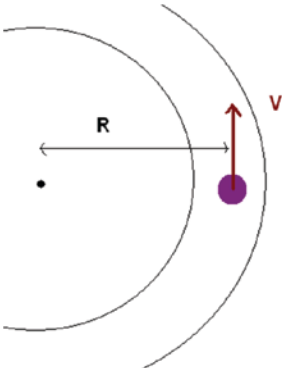

Figure 1. Point-mass model: vehicle traveling on a horizontal curve.

$$\frac{V^2}{gR} = \frac{f + \tan\alpha}{(1 - f \cdot \tan\alpha)} = \frac{f + e/100}{1 - f \cdot e/100} \tag{6}$$

Rearranging terms, one gets the basic curve formula:

$$\frac{V^2}{gR} = \left(\frac{f + 0.01e}{1 - 0.01fe}\right) \tag{7}$$

The product $f \cdot e/100$ in the denominator is usually small and is generally ignored. The simplified formula can be used to solve for the curve radius allowable as a function of the maximum friction factor, the design speed, and the superelevation.

$$R = \left(\frac{V^2}{g \cdot (f + 0.01 \cdot e)}\right) \tag{8}$$

The limiting factor for road design is the side friction factor *f*. Also, the superelevation rate for a curve will not exceed a maximum value selected by the designer. Hence, for a given design speed of a roadway, practical lower limits on the radius of curvature, R_{min}, are given by:

$$R_{min} = \frac{V_{DS}^2}{g \cdot (f_{max} + 0.01 \cdot e_{max})} \tag{9}$$

Here, f_{max} is the maximum demand side friction factor used in horizontal curve design, and e_{max} is the maximum superelevation rate for a given design speed, V_{DS}. AASHTO uses Equation 9 for determining the minimum radius of curvature. This usage is generally justified since it provides a more conservative design than Equation 8.

The basic side friction formula can be obtained by rearranging terms in Equation 8 as follows:

$$f = \frac{V_{DS}^2}{g \cdot R} - 0.01 \cdot e \tag{10}$$

In AASHTO policy, *f* is called the "side friction factor" which represents the portion of lateral acceleration that is not balanced by superelevation. The term *f* represents a friction "demand" which must be resisted by the available "supply" of friction generated at the tire–pavement interface. In addition, the unbalanced lateral acceleration creates an overturning moment on the vehicle that must be resisted by the vehicle's roll stability, which depends on vehicle design, loading, and suspension characteristics. The term "side friction factor," as used in the *Green Book*, represents friction demand, not friction supply.

AASHTO design policy for horizontal curves is based on the assumption that the value of *f* can be determined as a function of vehicle speed, curve radius, and superelevation. An inherent assumption is that vehicles follow the curved path exactly.

The tire–pavement interface can supply friction ($f_{tire\text{-}pavement}$) to resist the tendency of the vehicle to skid due to lateral acceleration as the vehicle traverses a curved path. The pavement friction generated at the tire–pavement interface is proportional to the normal load transmitted to the tire through the vehicle suspension which depends on tire and pavement properties. From the viewpoint of a point-mass model, the vehicle will skid if $f > f_{tire\text{-}pavement}$, where $f_{tire\text{-}pavement}$ represents the maximum amount of friction that can be generated at the tire–pavement interface to counteract lateral acceleration and prevent skidding.

Similarly, from the viewpoint of a point-mass model, the vehicle will overturn if $f > f_{rollover}$, where $f_{rollover}$ represents the maximum lateral acceleration that a vehicle can experience without overturning. $f_{rollover}$ is referred to as the

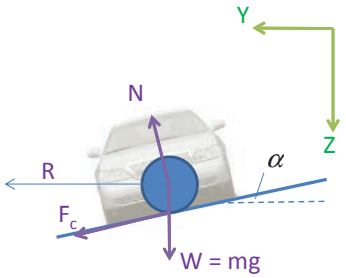

Figure 2. Lateral forces acting on point mass during cornering.

"rollover threshold" of the vehicle. Rollover thresholds are a characteristic of vehicle design and loading that can be estimated from static tests, but are best determined from dynamic tests.

The *Green Book* design criteria for horizontal curves are not based on any formal assumptions about the magnitudes of $f_{\text{tire-pavement}}$ and f_{rollover}. Rather, horizontal curve design is based on limiting the value of f to be less than or equal to a specified value, $f_{\max}$, which has been selected based on driver comfort levels (i.e., driver tolerance for lateral acceleration). A further assumption, stated but not explicitly demonstrated in AASHTO policy, is that the values of $f_{\max}$ used in design have been selected such that $f_{\max} < f_{\text{tire-pavement}}$ and $f_{\max} < f_{\text{rollover}}$. The first criterion, $f_{\max} < f_{\text{tire-pavement}}$, is addressed in *Green Book* Figure 3-5, which shows that the values of $f_{\max}$ used in design are less than the values of $f_{\text{tire-pavement}}$. The second criterion, $f_{\max} < f_{\text{rollover}}$, is asserted but not demonstrated in the *Green Book*. Research by others, including Harwood et al. (1989) and Harwood et al. (2003), has shown that the assumptions of $f_{\max} < f_{\text{tire-pavement}}$ and $f_{\max} < f_{\text{rollover}}$ do appear to be generally applicable to both passenger vehicles and trucks for horizontal curves designed in accordance with AASHTO policy.

The point-mass model works reasonably well for the conceptual design of horizontal curves; however, there are several limitations to this simple approach to horizontal curve design (Easa and Abd El Halim, 2006). First, the model does not account for differences in vehicle dynamics between passenger vehicles and trucks, and the model ignores tire force differences between the front/rear or left/right tires of a vehicle (i.e., the forces acting on all tires are assumed to be the same). Second, the point-mass model ignores the combined characteristics of the highway alignment such that the horizontal alignment is designed in isolation without accounting for the overlapping vertical alignment. Third, the point-mass model assumes that vehicles traverse curves following a path of constant radius equal to the radius of the curve; however, it has been shown that at some points on a horizontal curve, some vehicles will over steer the curve, following a path less than the radius of the curve (Glennon and Weaver, 1972). Fourth, the point-mass model assumes vehicles traverse the curve at a constant speed and does not account for situations when vehicles may have to decelerate (i.e., apply the brakes) while traversing through the curve.

Several research efforts have evaluated the adequacy of the current point-mass model approach to horizontal curve design. In the mid-1990s, Harwood and Mason (1994) evaluated the adequacy of the AASHTO geometric design policy to safely accommodate both passenger vehicles and trucks on horizontal curves. Harwood and Mason concluded there does not appear to be a need to modify existing high-speed criteria for determining the radius and superelevation of horizontal curves designed in accordance with current AASHTO policy. Existing design policies provide adequate margins of safety against skidding and rollover for both passenger vehicles and trucks as long as the design speed of the curve is selected realistically. Special care should be taken for curves with design speeds of 30 mph or less to assure that the selected design speed will not be exceeded, particularly by trucks. Design of superelevation transitions according to the ⅔-⅓ rule provides an acceptable design, while spiral transitions would provide marginally lower lateral accelerations. For minimum-radius horizontal curves designed in accordance with AASHTO low-speed criteria, AASHTO policy generally provides adequate margins of safety against skidding and rollover for passenger vehicles traveling at the design speed, but for design speeds of 10 to 20 mph, minimum-radius curves may not provide adequate margins of safety for trucks with poor tires on a poor, wet pavement or for trucks with low rollover thresholds. Revision of the AASHTO low-speed horizontal design criteria should be considered, especially for locations with substantial truck volumes.

In other research, Bonneson (1999) estimated statistical models of curve speed and side friction demand to develop limiting values of side friction demand for use in horizontal curve design. The relationship between maximum side friction demand and horizontal curve approach speed derived for passenger vehicles is shown in Figure 3. The model illustrates that side friction demand decreases as the curve approach speed increases, while the side friction demand increases as the speed reduction between the curve approach speed and the speed at the mid-point of a horizontal curve ($V_a - V_c$) increases. The side friction demand related to no speed reduction between the approach tangent and mid-point of a horizontal curve ($V_a - V_c = 0$ mph) was proposed as the desirable upper limit on maximum design side friction factors. However, a maximum desirable speed reduction of

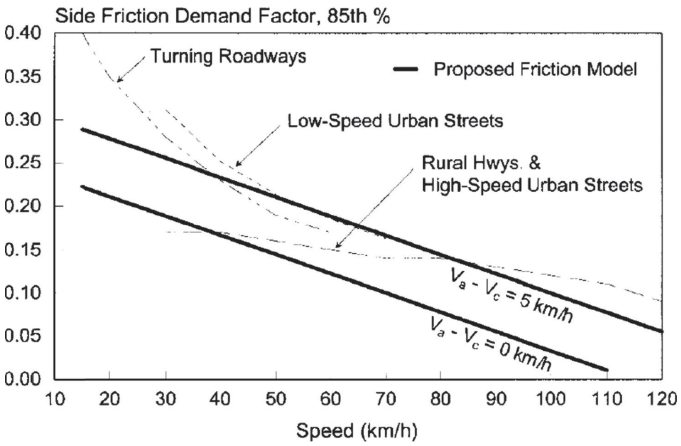

Figure 3. Relationship between side friction demand and speed (Bonneson, 1999).

3 mph (5 km/h) was proposed to balance traffic flow and construction cost, thus allowable maximum side friction demands corresponding to the $V_a - V_c = 3$ mph (5 km/h) trend line were recommended.

To assess the margin of safety for the proposed side friction demand factors, Bonneson (2000b) compared side friction supply for both slide and roll failure to the proposed side friction demand factors. A graphical representation of this assessment is shown in Figure 4 where the side friction demand for speed reductions of 0 to 1.86 mph (0 and 3 km/h) is plotted for both passenger vehicle and truck margins of safety against slide and roll failure. The results show that grades, particularly steep upgrades, reduce the margin of safety, particularly for trucks. Another trend observed was that roll failure is only observed in trucks on low-speed curves. Finally, Figure 4 shows that slide failure will occur prior to roll failure for passenger vehicles at any speed, and at higher speeds for trucks. Bonneson (2000a) also proposed limiting superelevation rates of 8.2%, 9.8%, 10.8%, 11.4%, and 11.8% proposed for design speeds of 18.6, 24.8, 31.0, 37.3, and 43.5 mph, respectively, and determined the optimal proportion of the superelevation runoff located prior to the point of curvature (PC) to be 80% at 18.6 mph and 70% at 74.6 mph for two-lane highways. A 10% increase in the proportion was proposed for each additional travel lane to be rotated on the transition curve. Later, Bonneson (2001) proposed a superelevation distribution method for horizontal curves based on established minimum and maximum superelevation rate boundary conditions.

Awadallah (2005) more recently proposed a method to determine design side friction factors based on side friction supply factors for skid and roll, and, about the same time, Tan (2005) replicated experiments conducted in the 1930s and 1940s to determine comfortable net lateral acceleration on horizontal curves. Tan concluded that AASHTO design side

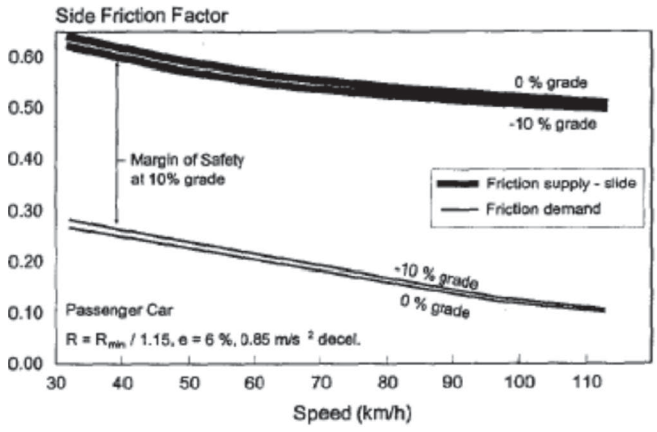

a. Speed reduction of 3 km/h.

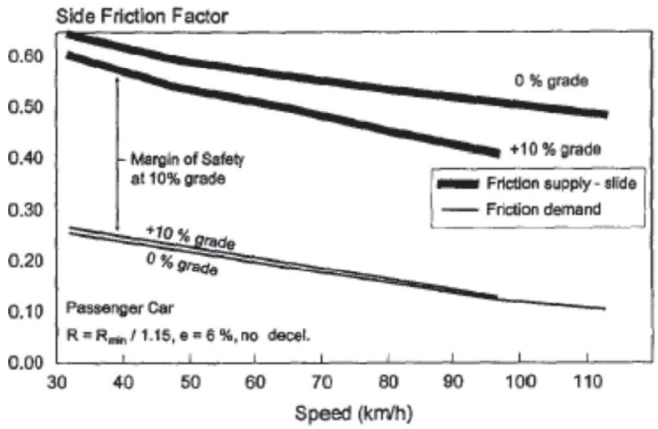

b. No speed reduction.

Effect of speed reduction on passenger car margin of safety against slide failure.

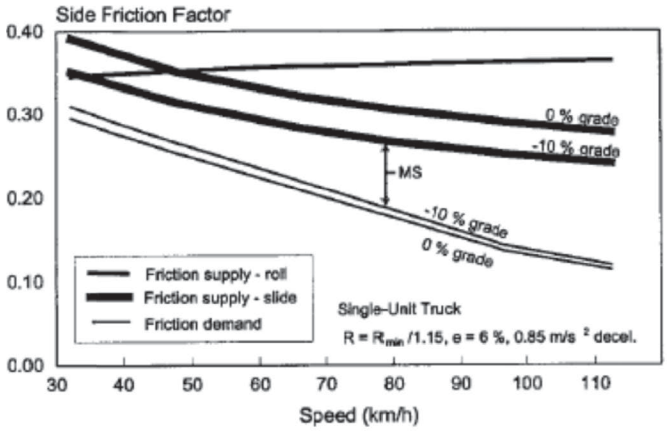

a. Speed reduction of 3 km/h.

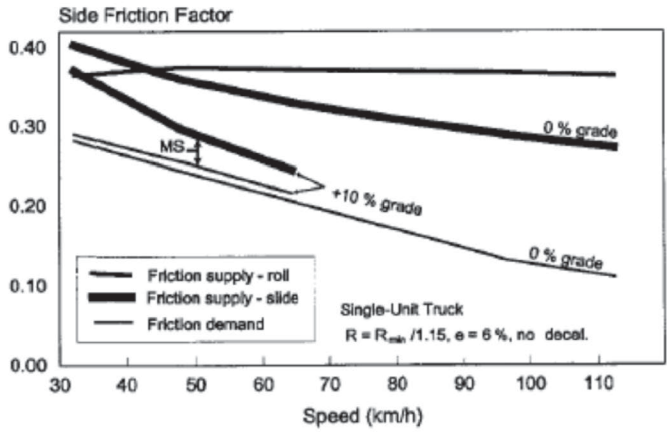

b. No speed reduction.

Effect of speed reduction on truck margin of safety against slide or roll failure.

Figure 4. Margin of safety between side friction supply and demand (Bonneson, 2000b).

friction values are conservative for contemporary passenger vehicles traveling at the design speed and recommended that the coefficient of friction at impending skid be revisited in the AASHTO *Green Book* to reflect current pavement design practices and performance.

2.2 Heavy Trucks

Eck and French (2002) investigated problems faced by trucks on sharp curves on steep grades to determine appropriate superelevation rates for trucks under these conditions. The primary findings and conclusions from this research included the following:

- On downgrades, a portion of the available friction (side friction supply) is consumed in maintaining a steady speed. This leaves less than the maximum friction available for side friction demand. This is not a significant problem under normal steady-speed conditions, but the available side friction is severely reduced when braking. The downgrade also adds to the lateral acceleration. Two theoretical models support the use of additional superelevation on sharp curves on steep downgrades.
- High superelevation rates (e.g., between 0.08 and 0.16) make horizontal curves on steep downgrades more forgiving. These high superelevation rates do not necessarily permit higher speeds but can better accommodate drivers making errors in safe speed selection for the curve and grade combination.
- Reducing the superelevation of existing curves is not good highway geometric design practice, unless there is another safety issue that requires this reduction. Where the superelevation rate has been reduced, significant increases in passenger vehicle crashes have been observed and are partially attributable to violation of driver expectancy.

2.3 Driver Comfort

A key consideration in AASHTO's policy in selecting maximum side friction factors (f_{max}) for use in design is the level of centripetal or lateral acceleration sufficient to cause drivers to experience a feeling of discomfort and to react instinctively to avoid higher speeds. The general policy follows the assumption that at low speeds drivers are more tolerant to discomfort and hence higher values of side friction are sought, while at higher speeds a greater margin of safety should be sought; hence, the use of lower side friction factors at high speeds. This approach for selecting maximum side friction factors for design is based upon research from the 1930s and 1940s (Barnett et al., 1937; Moyer and Berry, 1940; Meyer, 1949; Stonex and Noble, 1940). More recent studies by Bonneson (2000b) and Tan (2005) reaffirmed the appropriateness of the side friction factors currently recommended in AASHTO policy for horizontal curve design.

2.4 Friction Studies

The basic side friction formula (Equation 10) gives an estimate of the side friction for a vehicle maneuver on a horizontal curve. One of the earliest studies on measuring the coefficient of friction at the point of impending skid on a roadway was done by Moyer (1934). Table 1 lists different coefficient of friction values recorded by Moyer, and Figure 5 shows variation in friction levels (for different skid conditions) with respect to speed. In Figure 5, the side skid coefficients of friction reported are higher than straight skid coefficients of friction, which is usually not the case in modern measurements of tire behavior. The differences might be explained by Wong (2008) where he notes that modern passenger vehicles now use synthetic rubber which has significantly different properties from natural rubber, which is still sometimes used in truck tires. The difference is that natural rubber has much better wear properties,

Table 1. Coefficient of friction vs. speed (Moyer, 1934).

Type of surface	Type of skid	Remarks	Coefficient of friction					
			Speed (mph)					
			5	10	15	20	25	30
Portland cement concrete, 19 × 4.75 tires, no chains	Side	Dry surface	1.01	1.01	0.97	0.95	0.92	0.89
	Straight	Dry surface	0.94	0.90	0.86	0.83	0.80	0.77
	Side	Wet surface	0.78	0.75	0.72	0.69	0.66	0.64
	Straight	Wet surface	0.67	0.63	0.59	0.55	0.51	0.46
Ice on pavement, no chains	Side	Smooth tread	0.20	0.19	0.19	0.20	–	–
	Side	New tread	0.19	0.19	0.22	0.19	–	–
Ice on pavement, 16 × 7.00 tires, no chains	Straight	New tread	0.18	0.15	0.17	0.21	–	–
	Impending	New tread	0.17	0.19	0.19	0.19	–	–
	Side	New tread	0.19	0.19	0.19	0.18	–	–

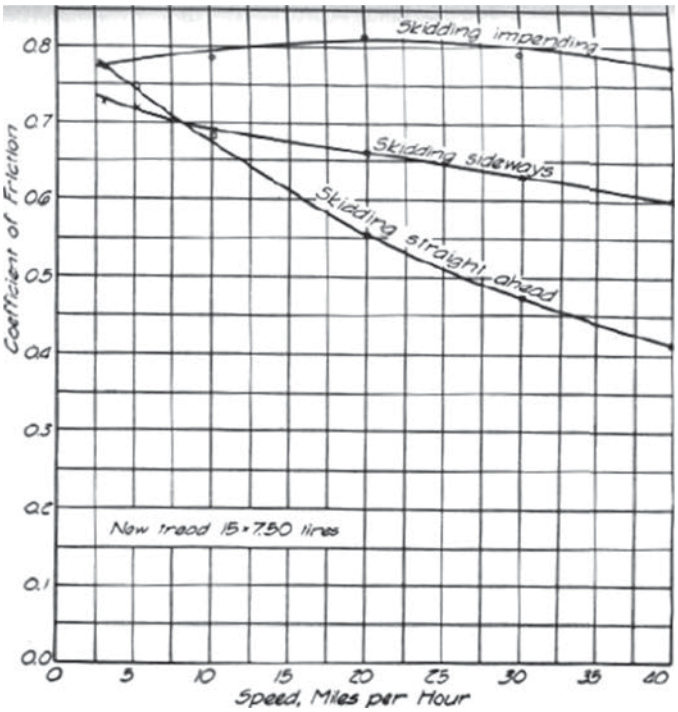

Figure 5. Relation between static, side skid, and straight skid coefficients of friction on wet portland cement concrete (Moyer, 1934).

ideal for trucks; but the coefficient of friction is much less for natural rubber tires, with the result that trucks have a stopping distance of 1.65 to 2.65 times farther than a passenger vehicle, assuming both are using high-grip tires of good condition.

More recent work examining stopping distance includes that of Olson et al. (1984). Olson et al. proposed Equation 11 to calculate the skid number for a given velocity (V):

$$SN_V = SN_{40}e^{P(V-40)} \tag{11}$$

where:

SN_V = Skid Number (= 100 × coefficient of friction) at given speed
V = Speed in mph
P = Normalized skid gradient (<0)

Table 2 summarizes the formulae given by Olson et al. for sliding friction and maximum rolling friction for passenger vehicle tires and truck tires. The friction coefficients for truck tires are less than those for passenger vehicles. Olson et al.'s study also indicates a decrease in friction with the increasing speed.

Table 3 lists the values of maximum and side friction coefficients of friction for different tires on dry as well as wet roads as determined by Fancher et al. (1986).

Because of tire deformation characteristics, a wheel will exhibit different curves and different maximum friction values depending on whether the force is in the lateral direction or longitudinal direction, the condition of the tires, whether an anti-lock braking system (ABS) is employed, and the loading of the tires. The use of braking forces will reduce the available lateral friction, and the use of lateral force will reduce the available braking forces. This interrelationship between lateral and longitudinal forces is called the friction ellipse.

The sliding friction limit for a tire, regardless of direction, is determined by the coefficient of sliding friction times the load. The friction can be used for lateral force, brake force, or a combination of the two, in either the positive or negative directions (Gillespie, 1992). However, the vector total of the two forces cannot exceed the friction limit. This leads to the friction ellipse (or circle) concept. As shown in Figure 6, utilization of friction in one direction decreases the friction reserve in the other direction. The friction ellipse equation represents the operating range of tire forces and is given by Equation 12 (Wong, 2008):

$$\left(\frac{F_y}{F_{y,\max}}\right)^2 + \left(\frac{F_x}{F_{x,\max}}\right)^2 = n^2 \le 1 \tag{12}$$

Here F_x is the tire's longitudinal (braking) force, F_y is the tire's lateral (cornering) force, and $F_{x,\max}$ and $F_{y,\max}$ are the maximum possible forces available in braking and cornering, respectively. The term n represents the total utilized friction and has a value of 1 when the tires are at the friction limit. Values below 1 represent situations within the friction ellipse, whereas values above 1 are beyond the tire's force capabilities. Thus, as long as the value of n is less than 1, the operating point (i.e., tire forces in x and y direction) lies inside the friction ellipse (i.e., the tire–pavement can generate required friction force). Equation 12 can be related

Table 2. Formulae for forward friction coefficients (Olson et al., 1984).

	Passenger vehicle tire	Truck tire
Sliding friction (μ_s)	1.2 SN_V	0.84 SN_V
Maximum rolling friction (μ_p)	0.2 + 1.12 μ_s	μ_s

Table 3. Coefficients of road adhesion for truck tires on dry and wet concrete pavement at 40 mph (Fancher et al., 1986).

Tire type	Tire construction	Dry		Wet	
		μ_p	μ_s	μ_p	μ_s
Goodyear Super Hi Miler (Rib)	Bias-ply	0.850	0.596	0.673	0.458
General GTX (Rib)	Bias-ply	0.826	0.517	0.745	0.530
Firestone Transteel 1 (Rib)	Radial-ply	0.809	0.536	0.655	0.477
Firestone Transport 1 (Rib)	Bias-ply	0.804	0.557	0.825	0.579
Goodyear Unisteel R-1 (Rib)	Radial-ply	0.802	0.506	0.700	0.445
Firestone Transteel Traction (Lug)	Radial-ply	0.800	0.545	0.600	0.476
Goodyear Unisteel L-1 (Lug)	Radial-ply	0.768	0.555	0.566	0.427
Michelin XZA (Rib)	Radial-ply	0.768	0.524	0.573	0.443
Firestone Transport 200 (Lug)	Bias-ply	0.748	0.538	0.625	0.476
Uniroyal Fleet Master Super Lug	Bias-ply	0.739	0.553	0.513	0.376
Goodyear Custom Cross Rib	Bias-ply	0.716	0.546	0.600	0.455
Michelin XZZ (Rib)	Radial-ply	0.715	0.508	0.614	0.459
Average		0.756	0.540	0.641	0.467

to pavement friction values in the lateral and longitudinal directions through a simple transformation since the friction factor is defined as force divided by vertical load. Specifically, the longitudinal and lateral friction demands are derived from the demanded tire forces as follows:

$$\text{Longitudinal Friction Factor} \quad f_x = \frac{F_x}{N} \tag{13}$$

$$\text{Lateral (i.e., Side) Friction Factor} \quad f_y = \frac{F_y}{N} \tag{14}$$

Where F_x and F_y are braking and cornering forces on the tire, and N is the normal load the tire carries. Depending on the level of model complexity, this "tire" could be construed to represent either an individual tire or the sum of force effects on multiple tires. With these substitutions, the friction ellipse equation can be written in terms of the friction factors as:

$$\left(\frac{f_y}{f_{y,\max}}\right)^2 + \left(\frac{f_x}{f_{x,\max}}\right)^2 = n^2 \le 1 \tag{15}$$

Unless the tire is at an extreme angle to the road, the normal force, F_z, in the tire's coordinate system can be assumed to be the normal force, N, acting on the tire from the road as shown in Figure 2.

The term n in Equations 12 and 15 can be referred to as the utilized amount of tire–pavement friction or the measure of friction supplied (often referred to as friction reserve by vehicle dynamicists). Again, one can usually infer that enough friction supply is available as long as $n < 1$. When $n > 1$, friction supply is exceeded.

For the dry pavements, there is little to no significant change in the tire–road pavement friction with increasing speed, perhaps 10% to 20% at most, but there is a noticeable decrease in friction on wet surfaces with increasing speeds. The friction is found to be decreasing with increasing speeds as shown in Figure 7 (Wong, 2008). This variation also depends on the type of road, condition of tire treads, etc. The shapes of these curves roughly match the driver comfort friction demand curves empirically determined for use in the design of horizontal curves. It thus seems likely that driver "comfort" may simply be a driver's perception of inferred friction supply on wet roads.

To summarize, the maximum lateral force acting on a tire or the maximum side friction factor depends on a range of main factors, including:

- The normal force on the tire;
- Longitudinal tire force;
- Road surface condition (dry, wet, snow, ice, etc.);
- Vertical load acting on the tire;
- Speed (mainly for wet surfaces);
- Tire condition (new, worn out); and
- Tire composition.

2.5 Vehicle Dynamics Models

Although the point-mass model serves as the basis for horizontal curve design, over the past few decades some researchers have proposed two-axle models (i.e., the bicycle model) for horizontal curve design (Figure 8). The models in these studies represent modifications to the classical bicycle model used in vehicle stability analysis. This model is derived and discussed in detail in subsequent sections. The modifications include factors such as inclusion of grade, braking/acceleration, consideration of the friction ellipse, etc. The advantage of the bicycle

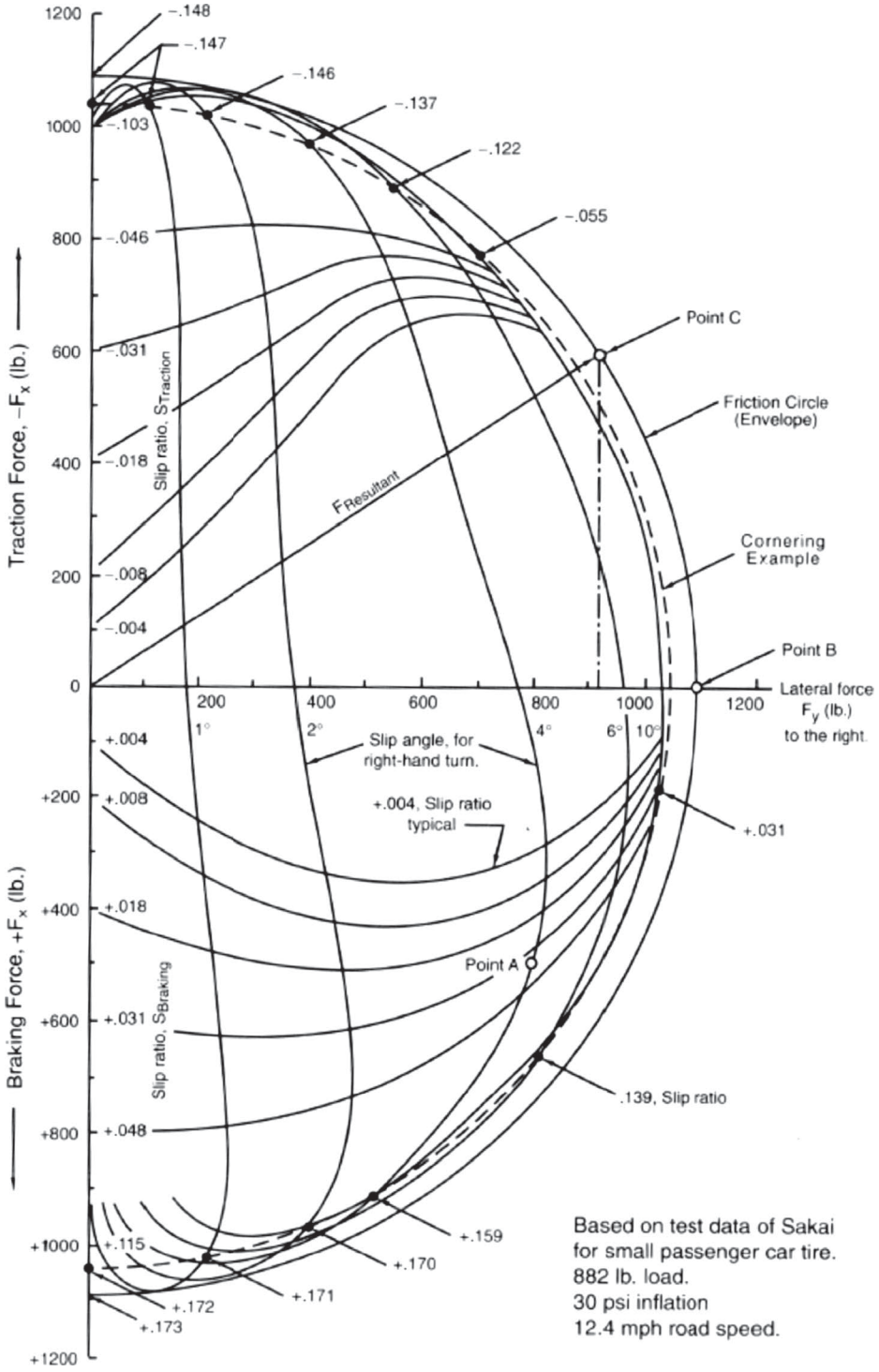

Figure 6. Friction ellipse diagram (right turn) (Milliken and Milliken, 1995).

model versus the point-mass model is that it examines not only force balance, but also moment balance. The moment balance in particular prevents the vehicle from "spinning out" on a roadway. Further, it is useful to examine whether individual axles will exhibit skidding prior to the entire vehicle exhibiting skidding.

Using the bicycle model, Psarianos et al. (1998) studied the influence of vehicle parameters on horizontal curve design. Psarianos et al. indicate that the friction reserve might be exceeded for a passenger vehicle traveling 12 mph higher than the design speed of 50 mph on a minimum-radius curve (obtained from basic point-mass model) for downgrades

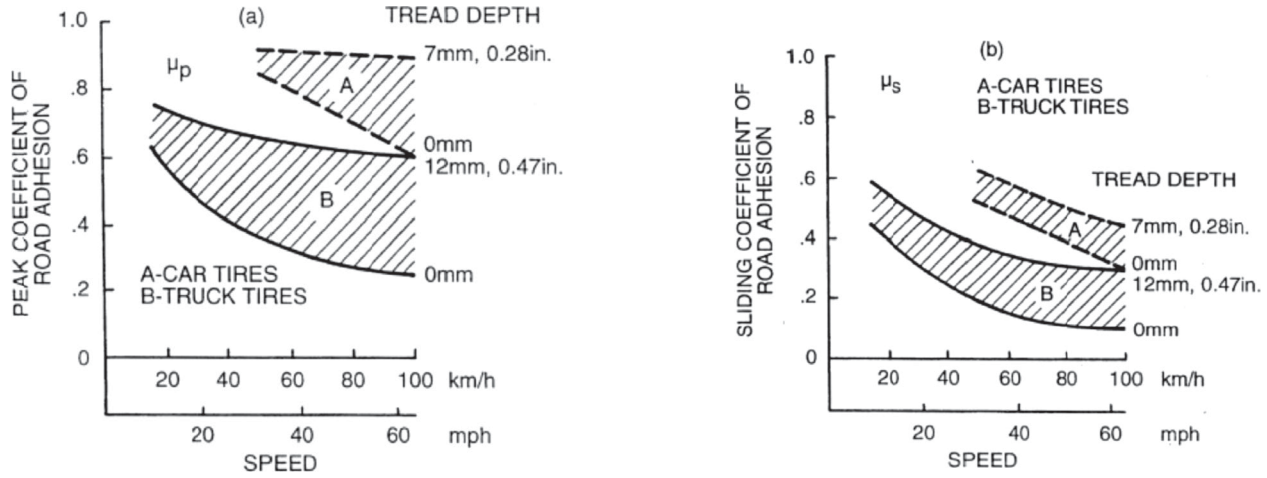

Figure 7. Effect of speed on coefficient of road adhesion (Wong, 2008).

steeper than 5%. They pointed out that these maneuvers will be more critical for trucks since they have lower maximum side friction factors.

Kontaratos et al. (1994) also developed an analytical two-axle vehicle model to determine the minimum horizontal curve radius as a function of vertical grade. In their bicycle-like model, Kontaratos et al. added the effects of the grade and superelevation, front-wheel versus rear-wheel drive, air resistance, etc. Their results suggest that the margins of safety against skidding are lower on steeper grades.

Bonneson (2000b) developed a two-axle vehicle model in his analysis of horizontal curve design. In the analysis Bonneson considered mild braking representative of the speed reduction upon entry to the curve. He developed slide (skid) failure and roll failure models separately to check if vehicle maneuvers are safe for given conditions. A decrease in the margin of safety (for the side friction factor) for trucks and passenger vehicles was reported on grades.

None of the studies mentioned above consider a multi-axle vehicle model and thus omit all tractor semi-trailers. Further, few of these studies considered a tire model inclusive of the friction ellipse and representative combined braking/turning situations. They also did not address load transfer, transient instabilities, and many steady-state instabilities as well. Also, except Bonneson (2000b), who used the Highway-Vehicle-Object Simulation Model (HVOSM) for a part of his study, there was no use of a multibody simulation model to comprehensively analyze vehicle stability while traversing a horizontal curve.

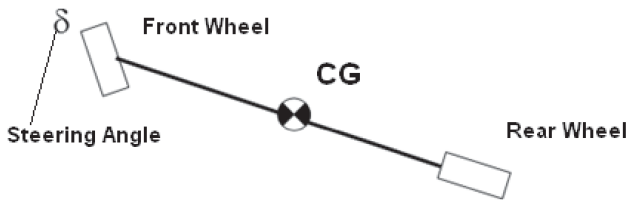

Figure 8. Plan view of bicycle model.

In the vehicle dynamics literature, many papers and textbooks (e.g., Dugoff, 1968; Ito, 1990; Milliken and Milliken, 1995; Wong, 2008; Gillespie, 1992) relevant to vehicle stability on a horizontal curve have been published, although none of these are clearly used at present in AASHTO policy. Of particular interest, if a driver applies a steady steering input (e.g., during transition from a tangent to a horizontal curve) and maintains it, the vehicle will enter a curve of constant radius after a transition period. The behavior of the vehicle in this transition time period is called its "transient response characteristics." Bundorf (1968) pointed out that such a behavior is quite important and the handling qualities of an automobile depend greatly upon its transient response. The bicycle model can predict curve onset transient behavior and other transient effects, for example, maneuvers such as a lane change where the radius of the curve is changing.

2.6 Current Practice

The design policies/manuals of 40 state highway agencies were reviewed to understand their current practice concerning superelevation design criteria, specifically seeking to determine if state policies differed from AASHTO guidance on superelevation criteria for sharp horizontal curves on grades. Of the 40 state design policies/manuals reviewed, most referred to the *Green Book* for detailed design procedures concerning superelevation. Only two state design policies/manuals provided statements concerning superelevation design criteria on grades. The other state design policies/manuals are silent on this issue.

The design manual for the Indiana Department of Transportation (INDOT) recommends the use of a higher speed in superelevation calculations than the design speed for the following conditions:

- **Transition area.** Where a highway is transitioning from a predominantly rural environment to an urban environment, travel speeds in the transition area within the urban environment may be higher than the urban design speed.
- **Downgrade.** Where a horizontal curve is located at the bottom of a downgrade, travel speeds on the curve may be higher than the overall project design speed. As suggested adjustments, the design speed used for the horizontal curve may be 5 mph (grade of 3% to 5%) or 10 mph (grade > 5%) higher than the project design speed. This adjustment may be more appropriate for a divided facility than for a two-lane, two-way highway.
- **Long tangent.** Where a horizontal curve is located at the end of a long tangent section, a design speed of up to 10 mph higher than the project design speed may be appropriate.

The design manual for the Ohio Department of Transportation (ODOT) provides the following guidance for designing superelevation on steep grades:

> On long and fairly steep grades, drivers tend to travel somewhat slower in the upgrade direction and somewhat faster in the downgrade direction than on level roadways. In the case of divided highways, where each pavement can be superelevated independently, or on one-way roadways, such as ramps, this tendency should be recognized to see whether some adjustment in the superelevation rate would be desirable and/or feasible. On grades of 4% or greater with a length of 1000 ft (300 m) or more and a superelevation rate of 0.06 or more, the designer may adjust the superelevation rate by assuming a design speed which is 5 mph (10 km/h) less in the upgrade direction and 5 mph (10 km/h) higher in the downgrade direction, providing that the assumed design speed is not less than the legal speed. On two-lane, two-way roadways and on other multilane, undivided roadways, such adjustments are less feasible, and should be disregarded.

In summary, the guidance provided in the design policies/manuals for INDOT and ODOT is very much consistent with AASHTO's policy on superelevation criteria for curves on steep grades, but both provide more detail than AASHTO's policy. Where AASHTO policy suggests assuming a higher design speed for the downgrade, the Indiana and Ohio policies/manuals provide specific guidance on how much to increase the design speed. Also, Ohio's manual indicates a specific length of grade for consideration.

SECTION 3

Field Studies

Three types of field studies were conducted as part of this research. Results of the field studies were used as inputs into the vehicle dynamics simulation models and/or served to validate the model outputs. Section 4 describes in more detail how the results from the field studies were used in the vehicle dynamics simulation modeling portion of the research.

The field studies conducted during this research consisted of:

- Speed and vehicle maneuver studies,
- Instrumented vehicle studies, and
- Friction testing.

The field studies were conducted in mountainous regions in the eastern and western parts of the United States. This section of the report provides a brief description of the site selection process to identify sites for inclusion in one or more of the field studies, presents the general characteristics of the sites, describes the field studies, and presents the primary results.

3.1 Site Selection

The goal of the site selection process was to identify sharp horizontal curves on grades of 4% or more, on a range of roadway types (freeways, other divided highways, and undivided highways) including high- and low-speed facilities in both rural and urban areas. For site selection purposes, a sharp horizontal curve was defined as a horizontal curve that, under current AASHTO policy, would require superelevation of at least 6% when designed with criteria applicable to a maximum superelevation rate of 8% (i.e., sites with above-minimum-radius curves were included in the field studies). Sharp horizontal curves were also identified for inclusion in the field studies based on the presence of curve warning signs and/or advisory speed signs. It was also desirable to collect data in different geographical locations throughout the United States. Initially, the research team identified the states of Pennsylvania, Maryland, and West Virginia in the eastern United States and California, Colorado, Utah, and Washington in the western United States, as potential locations for the field studies.

Several steps were taken to identify candidate data collection sites:

- Where available, roadway inventory data were obtained to find areas with sharp curves on steep grades in the selected states whose geometrics fit the selection criteria.
- Crash data were obtained where available to conduct a system-wide review to find sites with concentrations of lane departure and rollover crashes involving trucks and/or passenger vehicles.
- An online survey was distributed to state trucking associations in the respective states requesting that their safety offices and/or drivers identify locations which they were familiar with that have sharp horizontal curves on steep grades.
- The transportation agencies from the respective states were also contacted for suggestions of candidate data collection sites.

Through these various means, close to 100 candidate data collection sites were identified. The research team then conducted site selection trips in the states of California, Maryland, Pennsylvania, Washington, and West Virginia to gather detailed geometric data in the field and to select the final sites for inclusion in the field studies.

Twenty sites were selected for inclusion in one or more of the field studies. Table 4 presents location information, grade, and horizontal curve data for each of the sites. The grade and curve data were obtained from a combination of roadway inventory files, plan and profiles sheets, and field measurements. Seventeen of the sites were located on downgrade sections, while three of the sites were on upgrades. Most of the sites were on freeways, but several sites were on two-lane or multilane highways, and one site was a freeway-to-freeway ramp. The grade represents the maximum grade

Table 4. Data collection sites and site characteristic information.

Site	State	Route (direction)	County	MP	Nearest city	Roadway type	Grade (%)	Length of grade (mi)	Curve radius (ft)	Curve length (mi)	e_{max} (%)	Spiral	Curve direction
CA1	CA	I-5 (NB)	Kern	1.6-2.1	Lebec	Freeway	–3.1	>1.0	2,000	0.47	2	Absent	Left
CA2	CA	SR 17 (NB)	Santa Clara	2.0-3.0	Los Gatos	Multilane	–6.2	0.25	537	0.21	12	Absent	Right
CA3	CA	SR 17 (SB)	Santa Cruz	10.3-9.7	Scotts Valley	Multilane	–6.3	0.25	575	0.13	8.8	Absent	Left
MD1	MD	I-68 (WB)	Garrett	5.5-7.0	Friendsville	Freeway	–4.1	0.78	1,909	0.31	6	Absent	Left
MD2[2]	MD	I-68 (WB)	Washington	74.5-75.0	Hancock East	Freeway	6.0	>1.0	1,909	0.42	5.5	Absent	Right
MD3	MD	I-68 (WB)	Washington	72.5-73.5	Hancock West	Freeway	–5.7	0.21	1,900	0.32	4.5	Absent	Right
PA1	PA	I-79 (NB)	Washington	Interchange I-70/I-79	Washington	Ramp	–5.0	1.0	Comp[1]	0.19	6.25	Absent	Right
PA2	PA	I-80 (EB)	Jefferson	79.5-80.5	Brookville	Freeway	–4.0	0.67	1,637	0.27	8.3	Present	Left
WA1	WA	I-90 (WB)	Grant	137.5-138	Vantage	Freeway	–4.9	>1.0	955	0.23	9.3	Present	Right
WA2	WA	I-82 (WB)	Kittitas	15.14-15.94	Ellensburg	Freeway	–5.0	>1.0	1,600	0.24	10	Absent	Left
WA3	WA	I-82 (WB)	Kittitas	4.00-4.63	Ellensburg	Freeway	–5.0	>1.0	2,400	0.19	7	Absent	Right
WA4	WA	I-82 (EB)	Kittitas	21.75-22.5	Ellensburg	Freeway	–3.8	0.6	1,600	0.33	5.8	Absent	Right
WA5[2]	WA	US 97 (NB)	Kittitas	162.7-163	Ellensburg	Two-lane	6.0	0.86	1,637	0.19	2	Absent	Left
WA6	WA	I-90 (EB)	Kittitas	131.48-31.69	Ellensburg	Freeway	–2.9	>1.0	2,800	0.33	7	Absent	Right
WA7[2]	WA	US 2 (EB)	King	60.0-60.7	Skykomish	Multilane	5.9	>1.0	577	0.25	10	Present	Left
WV1	WV	I-77 (SB)	Mercer	20.6-21.4	Camp Creek	Freeway	–4.9	>1.0	1,206	0.50	8	Present	Left
WV2	WV	I-68 (WB)	Monongalia	9.9-10.6	Cheat Lake	Freeway	–5.7	>1.0	1,909	0.49	7.8	Present	Left
WV3	WV	I-79 (SB)	Kanawha	2.05-2.5	Mink Shoals	Freeway	–3.7	0.75	1,146	0.05	8	Present	Left
WV4	WV	I-77 (NB)	Kanawha	76.5-78.0	Cabin Creek	Freeway	–5.2	>1.0	1,041	0.26	8	Present	Right
WV5	WV	I-64 (EB)	Kanawha	49.7-50.5	Institute	Freeway	–5.0	0.58	1,637	0.33	7.2	Present	Left

[1] Compound curve with four radii: 430 ft, 230 ft, 150 ft, and 310 ft.
[2] Upgrade sites.

either approaching the curve or in the curve. Similarly, the superelevation represents the maximum superelevation on the curve. In a few cases, the selection criteria were relaxed to include sites in the field studies.

Three types of field studies were conducted as part of this research. Table 5 provides a matrix indicating if data from the respective site were used for the given field study. Table 5 also shows if crash data from the site were included in the crash analysis. Section 5 of this report provides details on the crash analysis.

3.2 Speed and Vehicle Maneuver Studies

The primary purpose of the speed portion of the studies was to determine, at each data collection site, the distribution of vehicle speeds on the approach tangent and on the curve for both passenger vehicles and trucks. These speed distributions were used in the vehicle dynamics simulation modeling.

The primary purpose of the vehicle maneuver portion of the studies was to determine the duration of lane-change maneuvers at sharp horizontal curves on steep grades and the proportion of vehicles that change lanes. The data on duration of lane-change maneuvers were used in the vehicle dynamics simulation modeling, and the proportion of vehicles that change lanes indicates the extent or the frequency of such maneuvers.

3.2.1 Data Collection Methodology

Speed data were collected using laser guns. Laser guns collect speeds and distances of subject vehicles in a continuous fashion. By comparing distances to benchmark locations/distances, speeds were determined at specific locations along the study site such as upstream of the curve, the beginning of the curve (i.e., PC), and the mid-point of the curve.

In general, speed data were collected beginning at least 500 ft upstream of the curve and at least through the mid-point of the curve. Depending on the geometry and available sight distance, one or two laser guns were used to collect speed data for vehicles over the length of the study area. The laser guns were operated by a researcher inside of a vehicle parked on the side of the roadway in a location chosen based on several criteria:

- Location was safe;
- Data collectors and equipment were situated as inconspicuously as possible such that they had no (or minimal) impact on driver behavior or desired operating speeds; and

Table 5. Data collection sites, field studies, and crash analysis matrix.

Site	Speed data	Vehicle maneuver data	Instrumented vehicle data	Friction testing data	Crash data
CA1	X	X			X
CA2	X	X			X
CA3	X	X			X
MD1	X	X	X	X	X
MD2	X	X	X	X	X
MD3	X	X	X	X	X
PA1	X		X		X
PA2	X	X			X
WA1	X	X			
WA2	X	X			X
WA3	X	X			X
WA4	X	X			X
WA5	X	X			X
WA6	X	X			X
WA7	X				X
WV1	X	X		X	X
WV2	X		X	X	X
WV3	X	X		X	X
WV4	X	X		X	X
WV5	X	X		X	X

- Subject vehicles tracked from the rear as they drove away from the laser gun.

Figure 9 illustrates the general field setup for the speed studies.

At each site speed data were collected over the course of a single day. Speed data were collected for both passenger vehicles and trucks under free-flow conditions. During post-processing of the data, vehicles were grouped into vehicle classes as follows:

- **Passenger vehicles:**
  - Sedan
  - Sport utility vehicle (SUV)
  - Pickup
  - Van

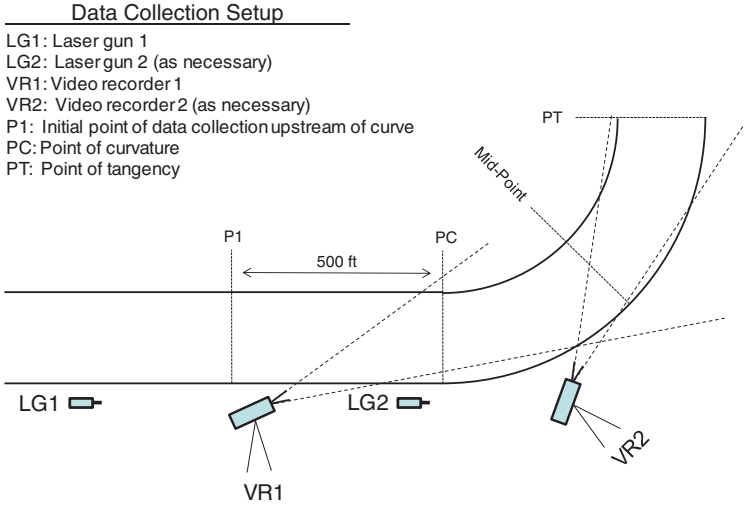

Figure 9. General data collection setup for speed and vehicle maneuver studies.

- **Trucks:**
  - Single-unit truck
  - Tractor semi-trailer truck
  - Tractor semi-trailer/full-trailer truck (double)

While collecting speed data, one or two video cameras were also positioned on the roadside to record vehicle maneuvers at the sites. The field of view for each camera was as follows:

- Camera 1—approach and upstream end of the horizontal curve
- Camera 2—mid-point and downstream end of the horizontal curve

The videos from the cameras were reviewed in the office to document the number of vehicles and types (e.g., passenger vehicles and trucks) at the site, the number of vehicles changing lanes, and the duration and direction of the lane-change maneuvers. Figure 10 shows a tractor semi-trailer maneuver from the left to the right lane at one of the data collection sites. At a few sites, the perspective of the camera did not provide a sufficient view to document lane-change information.

3.2.2 Analysis Results of Speed Data

Figure 11 shows the locations on the approach tangent and horizontal curve at which speed data were collected. The zero point of each measurement distribution represents the beginning of the curve (i.e., PC). In most cases, a maximum of 3% to 6% of the observations were obtained at a specific location along the study site. At a few sites (e.g., CA1, CA2, and WV5), the geometrics and roadside characteristics prohibited collecting speed data over the desired coverage area.

Table 6 provides summary statistics of the speed data for passenger vehicles located 500 ft upstream of the curve, at the beginning of the curve (i.e., PC), and 500 ft downstream of the PC at each data collection site. The Table also provides the posted speed limit at each site and the advisory speed (if posted). The third column provides the average vehicle count (i.e., number of observations) at the three respective locations included in the table. At some sites, passenger vehicle speeds decreased going from 500 ft upstream of the curve to the beginning of the curve, while at other sites speeds increased. At most sites passenger vehicle speeds decreased going from the beginning of the curve to 500 ft downstream of the curve.

Table 7 provides the corresponding summary statistics for trucks. At most sites truck speeds decreased going from 500 ft upstream of the curve to the beginning of the curve. Similarly, at most sites truck speeds decreased going from the beginning of the curve to 500 ft downstream of the beginning of the curve.

Table 8 provides detailed speed information collected at Maryland site MD1 for both passenger vehicles and trucks at 100 ft intervals. These speed data were entered into the simulation models (i.e., CarSim and TruckSim) to determine friction supply curves (and the corresponding lateral friction and rollover margins) for passenger vehicles and trucks at each of the data collection sites based upon actual operating speeds measured at the sites.

3.2.3 Analysis Results of Lane-Change Maneuver Data

The primary measures of interest from the lane-change analysis consisted of the frequency and duration of the maneuvers. Table 9 provides summary statistics on the frequency and percentage of lane-change maneuvers observed at each site by vehicle type and grade direction (i.e., downgrade and upgrade). The Table provides data on total vehicles by vehicle type and whether the lane change consisted of a maneuver from the right lane to the left lane (identified as *left* in the table) or from the left lane to the right lane (i.e., *right* in the table). As long as the lane-change maneuver occurred within the field of view of the video camera, the lane-change maneuver was documented. Thus, in some cases the lane change may have occurred on the approach tangent, on the approach tangent and into the curve, or entirely within the curve. At

Figure 10. Video of tractor semi-trailer maneuvering from left lane to right lane.

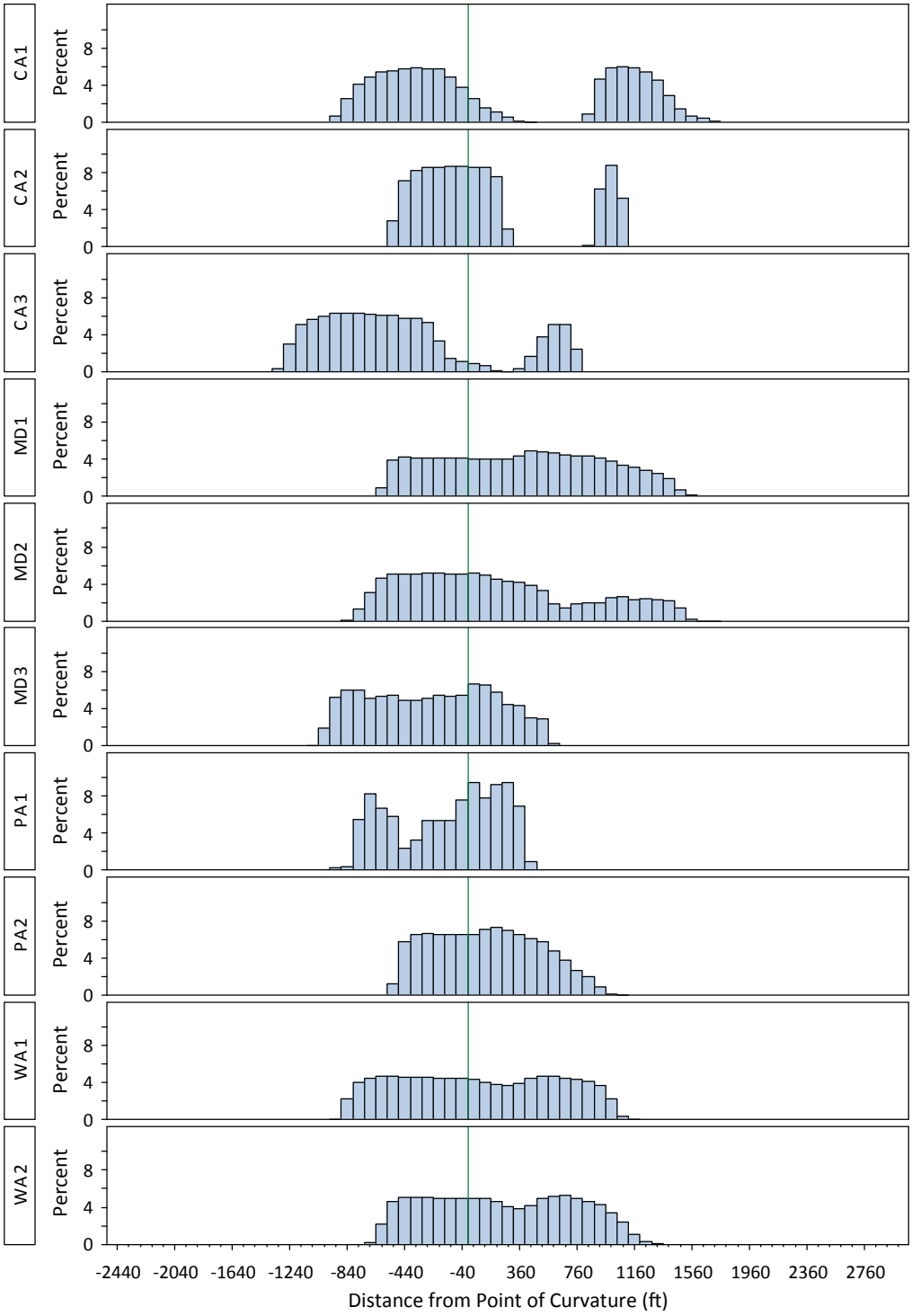

Figure 11. Speed measurement coverage at data collection sites.

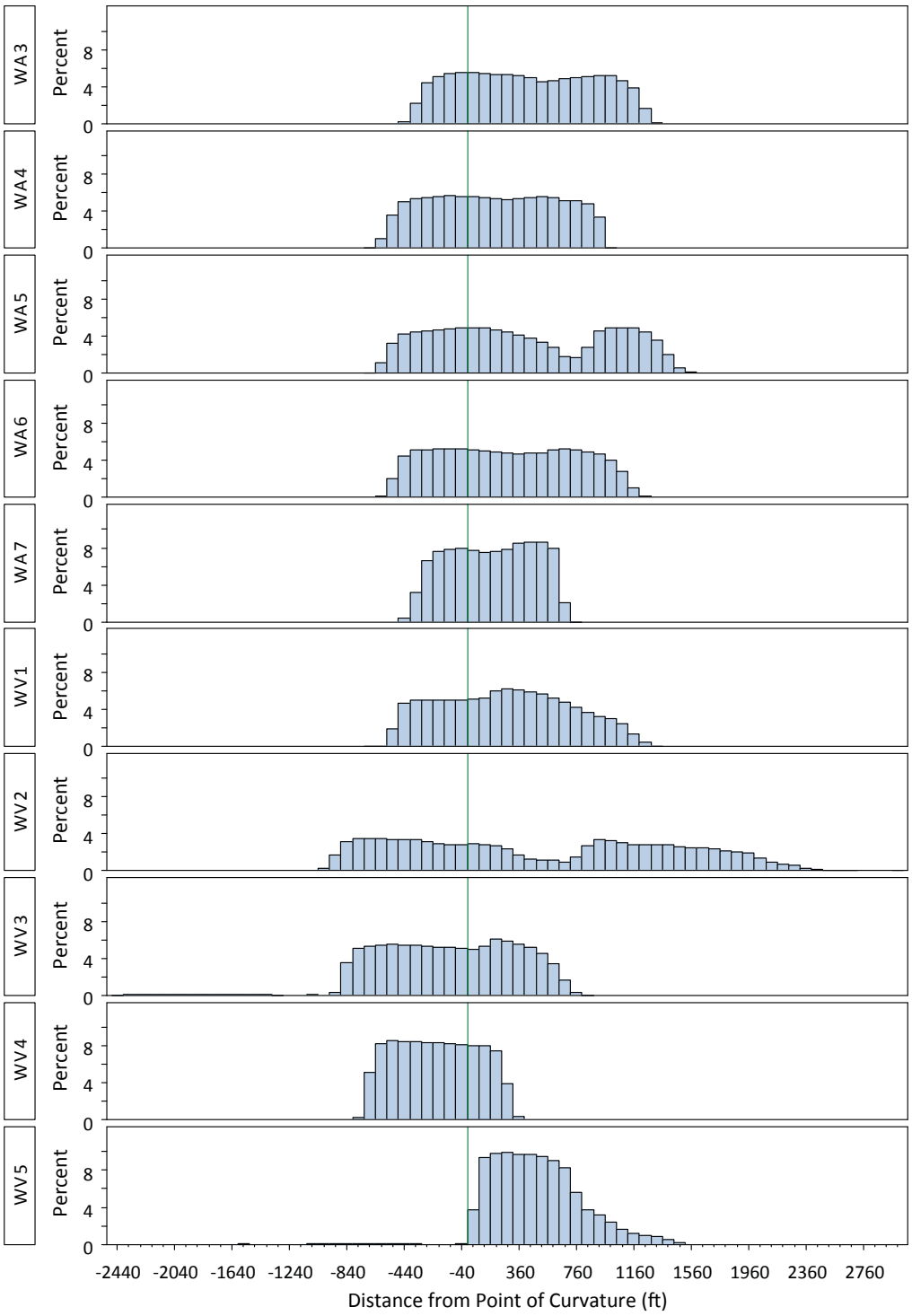

Figure 11. **(Continued).**

Table 6. Summary of speed data near curves (passenger vehicles).

Site	Posted speed limit/ advisory speed (mph)	Avg veh count	500 ft upstream of curve				Beginning of curve (i.e., PC)				500 ft downstream of PC			
			Mean speed (mph)	85th %tile speed (mph)	Std dev (mph)	Percent exceed posted speed limit >5 mph	Mean speed (mph)	85th %tile speed (mph)	Std dev (mph)	Percent exceed posted speed limit >5 mph	Mean speed (mph)	85th %tile speed (mph)	Std dev (mph)	Percent exceed posted speed limit >5 mph
CA1	65	27	66.0	73.4	7.0	30	NA	NA	NA	NA	NA	NA	NA	NA
CA2	40/45	53	51.3	55.9	5.0	90	53.0	57.1	4.8	93	NA	NA	NA	NA
CA3	50/40	55	53.9	58.0	4.1	33	NA	NA	NA	NA	49.1	52.0	3.4	0
MD1	65	70	65.4	71.0	5.2	17	65.5	70.8	4.7	20	65.0	69.5	4.7	14
MD2	65	65	63.9	70.0	7.5	3	63.2	69.9	7.8	12	61.2	68.6	9.9	9
MD3	65	76	68.4	73.5	4.9	32	68.0	73.1	5.2	26	67.1	72.5	5.0	20
PA1	40/25	61	NA	NA	NA	NA	36.6	40.4	4.0	2	NA	NA	NA	NA
PA2	65	66	63.5	67.0	4.5	9	66.8	72.0	4.6	20	67.0	72.5	4.5	19
WA1	70/50	79	64.4	70.8	5.1	0	62.4	68.8	5.3	0	57.3	62.9	6.0	0
WA2	70	42	69.4	72.6	4.0	2	69.2	74.0	4.4	2	68.6	72.4	4.6	2
WA3	70	73	NA	NA	NA	NA	70.2	74.6	4.4	11	69.5	74.4	4.5	8
WA4	70	66	67.8	71.5	3.8	2	67.8	71.9	4.0	0	66.3	70.6	4.3	0
WA5	60	55	57.9	62.5	4.3	24	58.4	64.0	5.8	33	56.8	64.2	6.5	24
WA6	70	54	68.2	73.0	3.6	0	68.9	72.9	3.6	3	68.5	72.6	3.8	5
WA7	60/40	114	NA	NA	NA	NA	51.0	56.0	5.8	82	48.2	52.8	4.7	72
WV1	70/50	53	64.3	70.4	5.2	0	66.9	72.0	5.6	6	67.1	71.2	5.2	6
WV2	70/50	45	67.8	74.1	6.8	13	68.4	73.5	5.9	13	68.9	76.4	4.8	15
WV3	70/50	86	67.7	73.2	5.4	7	67.2	73.0	5.0	7	65.3	71.3	5.2	1
WV4	60/50	94	64.2	69.7	5.6	35	62.6	68.0	5.3	26	NA	NA	NA	NA
WV5	60	69	NA	NA	NA	NA	NA	NA	NA	NA	68.5	73.5	4.4	72

Table 7. Summary of speed data near curves (trucks).

Site	Posted speed limit/ advisory speed (mph)	Avg veh count	500 ft upstream of curve				Beginning of curve (i.e., PC)				500 ft downstream of PC			
			Mean speed (mph)	85th %tile speed (mph)	Std dev (mph)	Percent exceed posted speed limit >5 mph	Mean speed (mph)	85th %tile speed (mph)	Std dev (mph)	Percent exceed posted speed limit >5 mph	Mean speed (mph)	85th %tile speed (mph)	Std dev (mph)	Percent exceed posted speed limit >5 mph
CA1	55[1]	47	53.3	56.9	3.8	3	51.9	55.5	3.3	0	NA	NA	NA	NA
CA2	35[1]/45	32	42.5	48.1	5.1	56	41.8	48.1	5.3	51	NA	NA	NA	NA
CA3	50/40	23	39.8	48.0	6.6	4	NA	NA	NA	NA	38.0	45.0	5.1	0
MD1	65	48	63.2	66.3	3.7	0	63.0	66.4	3.1	0	61.7	65.8	3.7	0
MD2	65	65	43.0	60.0	13.4	1	41.5	59.0	13.4	1	39.1	54.6	13.2	0
MD3	65	63	64.5	69.1	5.5	7	64.1	68.0	5.4	11	64.3	69.9	5.7	14
PA1	40/25	46	33.7	38.6	5.5	2	26.2	30.4	3.8	0	NA	NA	NA	NA
PA2	65	54	64.5	67.2	3.7	4	65.0	68.9	4.6	9	65.3	69.1	4.3	11
WA1	60[1]/50	54	56.8	60.4	5.1	0	54.5	58.7	3.7	0	50.0	54.1	4.0	0
WA2	60[1]	44	60.8	65.1	5.0	14	60.3	65.1	4.4	7	60.1	64.7	4.4	7
WA3	60[1]	38	NA	NA	NA	NA	58.7	65.0	6.1	17	58.3	63.8	6.0	11
WA4	60[1]	34	58.8	62.9	4.4	0	58.5	62.0	4.0	6	57.8	62.0	4.2	3
WA5	60	52	45.9	56.0	11.4	2	44.4	56.0	11.9	3	41.1	54.0	12.0	0
WA6	60[1]	40	61.2	66.2	3.5	19	61.8	65.4	3.0	16	61.1	63.6	2.5	4
WA7	60/40	15	NA	NA	NA	NA	36.7	48.2	11.2	47	36.1	47.2	10.6	36
WV1	70/50	48	61.5	67.3	5.3	0	62.5	67.0	5.0	0	62.0	66.3	5.0	0
WV2	50[1]/50	37	55.8	62.7	7.4	40	54.6	58.6	6.8	38	55.5	66.0	8.0	37
WV3	70/50	49	63.9	69.1	4.7	0	63.4	69.0	4.8	0	62.5	66.5	4.9	0
WV4	60/50	71	58.6	63.3	4.1	7	57.3	61.9	3.8	0	NA	NA	NA	NA
WV5	60	49	NA	NA	NA	NA	NA	NA	NA	NA	65.8	69.9	3.9	53

[1] Dual speed limits for passenger vehicles and trucks.

Table 8. Speed distribution data for passenger vehicles and trucks at Maryland site MD1.

Dist (ft)	Passenger vehicles								Trucks							
	# of Obs	Avg speed (mph)	Std dev (mph)	Speed percentiles (mph)					# of Obs	Avg speed (mph)	Std dev (mph)	Speed percentiles (mph)				
				Min	25th	Median	85th	Max				Min	25th	Median	85th	Max
–500	69	65.4	5.2	51.4	61.6	65.1	71.0	76.0	49	63.2	3.7	51.0	60.6	63.9	66.3	69.0
–400	70	65.7	4.9	53.2	61.9	65.5	71.1	75.5	48	63.2	3.6	51.0	61.2	64.0	66.4	69.1
–300	72	65.9	4.7	54.7	62.0	65.5	72.0	75.4	48	63.2	3.5	51.0	60.9	64.0	66.4	69.1
–200	73	65.7	4.8	55.2	62.1	65.1	72.0	75.5	47	63.3	3.1	55.6	60.9	64.1	66.4	69.1
–100	72	65.7	4.8	54.7	62.1	64.9	72.0	75.6	47	63.2	3.1	56.2	60.9	63.9	66.5	69.2
0	71	65.5	4.7	54.0	62.2	65.0	70.8	75.5	47	63.0	3.1	56.4	60.8	63.8	66.4	69.2
100	71	65.4	4.7	53.3	62.0	65.0	70.8	75.3	46	62.8	3.2	55.8	60.7	63.1	66.7	69.2
200	72	65.4	4.8	52.8	62.0	65.2	70.9	75.1	46	62.5	3.3	55.3	59.9	62.9	66.4	69.2
300	71	65.4	4.7	52.6	61.7	65.5	70.7	75.0	45	62.3	3.4	54.8	59.9	62.7	66.1	69.2
400	72	65.3	4.7	52.9	61.9	65.4	70.4	74.8	47	61.9	3.7	52.7	59.4	62.4	66.0	69.0
500	71	65.0	4.7	53.5	61.5	65.2	69.5	74.7	48	61.7	3.7	52.9	59.5	62.2	65.8	68.9
600	69	64.9	4.7	54.2	61.5	65.2	69.9	74.6	49	61.5	3.7	53.0	59.4	61.8	65.7	68.8
700	68	64.9	4.8	54.5	61.7	65.2	70.0	75.2	48	61.2	3.7	53.0	59.0	61.6	65.8	68.5
800	66	64.9	4.8	54.0	61.7	65.1	70.5	75.0	47	60.9	3.7	53.0	58.5	61.1	65.6	68.1
900	65	64.9	4.7	53.8	61.9	64.8	70.0	75.2	46	60.6	3.7	52.9	58.3	60.7	65.4	67.7
1,000	61	64.8	4.5	53.8	61.8	64.8	69.7	73.3	46	60.5	3.7	52.8	58.0	60.7	65.2	67.4
1,100	55	64.5	4.4	53.8	61.4	64.9	68.5	74.6	42	60.7	3.9	52.4	57.9	60.9	65.0	67.0
1,200	49	64.3	4.6	53.7	61.3	64.4	69.6	75.2	39	60.4	4.1	52.1	57.7	61.0	64.9	66.7
1,300	35	65.3	4.6	53.9	61.5	65.2	70.6	76.0	38	60.3	4.2	51.7	57.6	61.0	64.9	66.4
1,400	19	64.4	4.1	54.0	61.2	65.1	69.6	72.7	31	59.6	4.2	51.1	56.7	60.1	64.5	65.9

NOTE: Posted speed limit at site is 65 mph.

Table 9. Summary of lane-change maneuvers by vehicle type and grade direction.

Site	Passenger vehicles				Trucks				All vehicles combined			
	Total vehicles	Lane-change count (%)			Total vehicles	Lane-change count (%)			Total vehicles	Lane-change count (%)		
		Left	Right	Total		Left	Right	Total		Left	Right	Total
Downgrade												
CA1	2,432	25 (0.01)	20 (0.01)	45 (0.02)	1,271	5 (0.00)	19 (0.01)	24 (0.02)	3,703	30 (0.01)	39 (0.01)	69 (0.02)
CA2	2,344	57 (0.02)	39 (0.02)	96 (0.04)	141	3 (0.02)	4 (0.03)	7 (0.05)	2,485	60 (0.02)	43 (0.02)	103 (0.04)
CA3	2,804	30 (0.01)	37 (0.01)	67 (0.02)	148	1 (0.01)	0 (0.00)	1 (0.01)	2,952	31 (0.01)	37 (0.01)	68 (0.02)
MD1	321	27 (0.08)	36 (0.11)	63 (0.20)	88	12 (0.14)	4 (0.05)	16 (0.18)	409	39 (0.10)	40 (0.10)	79 (0.19)
MD3	924	37 (0.04)	12 (0.01)	49 (0.05)	208	4 (0.02)	3 (0.01)	7 (0.03)	1,132	41 (0.04)	15 (0.01)	56 (0.05)
PA2	944	20 (0.02)	38 (0.04)	58 (0.06)	439	10 (0.02)	39 (0.09)	49 (0.11)	1,383	30 (0.02)	77 (0.06)	107 (0.08)
WA1	669	12 (0.02)	10 (0.01)	22 (0.03)	262	1 (0.00)	8 (0.03)	9 (0.03)	931	13 (0.01)	18 (0.02)	31 (0.03)
WA2	426	25 (0.06)	20 (0.05)	45 (0.11)	138	6 (0.04)	1 (0.01)	7 (0.05)	564	31 (0.05)	21 (0.04)	52 (0.09)
WA3	610	8 (0.01)	34 (0.06)	42 (0.07)	121	4 (0.03)	4 (0.03)	8 (0.07)	731	12 (0.02)	38 (0.05)	50 (0.07)
WA4	488	19 (0.04)	43 (0.09)	62 (0.13)	119	4 (0.03)	5 (0.04)	9 (0.08)	607	23 (0.04)	48 (0.08)	71 (0.12)
WA6	475	5 (0.01)	13 (0.03)	18 (0.04)	168	0 (0.00)	7 (0.04)	7 (0.04)	643	5 (0.01)	20 (0.03)	25 (0.04)
WV1	953	8 (0.01)	103 (0.11)	111 (0.12)	278	2 (0.01)	122 (0.44)	124 (0.45)	1,231	10 (0.01)	225 (0.18)	235 (0.19)
WV3	957	53 (0.06)	38 (0.04)	91 (0.10)	102	10 (0.10)	11 (0.11)	21 (0.21)	1,059	63 (0.06)	49 (0.05)	112 (0.11)
WV4	625	9 (0.01)	17 (0.03)	26 (0.04)	380	7 (0.02)	5 (0.01)	12 (0.03)	1,005	16 (0.02)	22 (0.02)	38 (0.04)
WV5	1,687	6 (0.00)	13 (0.01)	19 (0.01)	328	6 (0.02)	7 (0.02)	13 (0.04)	2,015	12 (0.01)	20 (0.01)	32 (0.02)
Upgrade												
MD2	1,204	27 (0.02)	36 (0.03)	63 (0.05)	257	13 (0.05)	3 (0.01)	16 (0.06)	1,461	40 (0.03)	39 (0.03)	79 (0.05)
WA5	188	4 (0.02)	3 (0.02)	7 (0.04)	86	1 (0.01)	3 (0.03)	4 (0.05)	274	5 (0.02)	6 (0.02)	11 (0.04)

most sites, less than 10% of the vehicles changed lanes near or on the curve. At two of the sites (MD1 and WV1), nearly 20% of the vehicles changed lanes. This was most likely due to entrance/exit ramps located in the vicinity of these curves.

Table 10 presents summary statistics of lane-change duration data for passenger vehicles on both downgrades and upgrades. Lane-change duration was defined to be the amount of time from when the right tires of a vehicle crossed the lane lines to when the left tires crossed the lane lines for a right maneuver and when the left tires of a vehicle crossed the lane lines to when the right tires crossed the lane lines for a left maneuver. Thus, the actual lane-change duration from when the driver initiated the maneuver when positioned near the center of one travel lane until the time the driver completed the maneuver to the center of the other travel lane was longer than what is reported here, but for consistency and an objective measure for determining the start and end times of the maneuvers, the definition above was used. From Table 10 it is assessed that on downgrades, passenger vehicles had similar mean durations for maneuvers to the left (2.85 s) and to the right (2.94 s). On upgrades, passenger vehicles took slightly longer to maneuver to the right (3.25 s) compared to the left (2.95 s).

Table 11 presents summary statistics of lane-change duration data for trucks on both downgrades and upgrades. On downgrades, trucks had similar mean durations for maneuvers to the left (4.00 s) and to the right (4.09 s). On upgrades, trucks took longer to maneuver to the right (5.81 s) than to the left (4.47 s).

Tables 12 and 13 provide lane-change summary statistics for passenger vehicles and trucks by curve direction to assess whether lane-change duration is affected by whether the maneuver is made with the curve (i.e., left maneuver on a curve to the left or a right maneuver on a curve to the right) or against the curve (i.e., left maneuver on a curve to the right or a right maneuver on a curve to the left).

A split-plot model was used to estimate the statistical differences between mean lane-change durations for:

- Two grade directions (i.e., upgrade and downgrade);
- Two curve directions (i.e., left and right);
- Two vehicle types (i.e., passenger vehicles and trucks); and
- Two lane-change directions (i.e., left and right).

The 17 field sites were included in the model as random effects, assuming that the sites were chosen from a larger population of potential sites. This allows for estimation of the main effects on lane-change duration accounting for the added variability associated with using data from multiple sites.

Table 10. Lane-change duration statistics for passenger vehicles by grade direction.

Site	Left maneuver (s)					Right maneuver (s)				
	Veh count	Mean	Std dev	Min	Max	Veh count	Mean	Std dev	Min	Max
Downgrade										
CA1	25	2.84	0.80	1.00	4.00	20	3.35	1.27	2.00	8.00
CA2	57	2.63	0.98	1.00	7.00	39	2.28	0.76	1.00	4.00
CA3	30	3.13	0.43	2.00	4.00	37	3.35	0.59	2.00	4.00
MD1	27	3.03	0.55	2.15	4.53	36	3.24	0.72	1.94	5.28
MD3	37	2.57	0.60	1.65	4.16	12	2.55	0.59	1.56	3.53
PA2	20	2.70	0.68	1.69	4.84	38	2.44	0.58	1.53	3.87
WA1	12	2.67	0.65	2.00	4.00	10	3.00	1.33	1.00	5.00
WA2	25	2.92	0.81	2.00	5.00	20	3.10	1.25	2.00	7.00
WA3	8	2.88	0.83	2.00	4.00	34	3.00	0.85	2.00	5.00
WA4	19	3.21	0.71	2.00	5.00	43	2.72	0.85	1.00	5.00
WA6	5	3.00	1.22	2.00	5.00	13	3.69	1.44	2.00	6.00
WV1	8	3.12	0.65	2.25	3.97	103	2.92	0.60	1.69	4.57
WV3	53	2.95	0.80	1.72	5.38	38	3.12	0.75	1.62	4.66
WV4	9	2.88	0.52	2.34	3.81	17	3.37	0.60	2.69	4.65
WV5	6	2.26	0.29	1.91	2.63	13	2.47	0.48	1.90	3.31
Downgrade average	341	2.85	0.76	1.00	7.00	473	2.94	0.86	1.00	8.00
Upgrade										
MD2	27	3.02	0.53	2.15	4.53	36	3.24	0.72	1.94	5.28
WA5	4	2.50	1.29	1.00	4.00	3	3.33	1.53	2.00	5.00
Upgrade average	31	2.95	0.67	1.00	4.53	39	3.25	0.78	1.94	5.28

Table 11. Lane-change duration statistics for trucks by grade direction.

Site	Left maneuver (s)					Right maneuver (s)				
	Veh count	Mean	Std dev	Min	Max	Veh count	Mean	Std dev	Min	Max
Downgrade										
CA1	5	5.60	0.89	4.00	6.00	19	6.37	1.46	3.00	8.00
CA2	3	4.00	1.00	3.00	5.00	4	3.00	0.82	2.00	4.00
CA3	1	3.00		3.00	3.00	0				
MD1	12	4.31	0.45	3.75	5.16	4	5.21	1.25	3.35	5.97
MD3	4	3.65	0.45	2.99	4.03	3	3.10	0.46	2.79	3.63
PA2	10	3.13	0.62	2.50	4.78	39	3.35	0.66	2.22	5.18
WA1	1	6.00		6.00	6.00	8	6.63	1.06	5.00	8.00
WA2	6	5.33	1.63	3.00	7.00	1	7.00		7.00	7.00
WA3	4	4.75	1.50	4.00	7.00	4	5.50	1.29	4.00	7.00
WA4	4	4.50	1.00	4.00	6.00	5	4.60	0.89	3.00	5.00
WA6	0					6	7.17	1.60	5.00	9.00
WV1	2	3.94	1.73	2.72	5.16	122	3.72	0.80	2.28	5.50
WV3	10	3.28	0.74	2.13	4.15	11	3.50	1.00	2.03	4.90
WV4	7	3.84	0.77	2.88	4.83	5	3.57	1.01	2.24	4.72
WV5	6	2.82	0.62	2.16	3.84	7	3.18	0.57	2.31	4.18
Downgrade average	75	4.00	1.18	2.13	7.00	238	4.09	1.41	2.00	9.00
Upgrade										
MD2	13	4.43	0.63	3.75	5.97	3	4.96	1.40	3.35	5.84
WA5	1	5.00		5.00	5.00	3	6.67	2.08	5.00	9.00
Upgrade average	14	4.47	0.63	3.75	5.97	6	5.81	1.84	3.35	9.00

Table 12. Lane-change duration statistics for passenger vehicles by curve direction.

Site	Left maneuver (s)					Right maneuver (s)				
	Veh count	Mean	Std dev	Min	Max	Veh count	Mean	Std dev	Min	Max
Curve left										
CA1	25	2.84	0.80	1.00	4.00	20	3.35	1.27	2.00	8.00
CA3	30	3.13	0.43	2.00	4.00	37	3.35	0.59	2.00	4.00
MD1	27	3.03	0.55	2.15	4.53	36	3.24	0.72	1.94	5.28
PA2	20	2.70	0.68	1.69	4.84	38	2.44	0.58	1.53	3.87
WA2	25	2.92	0.81	2.00	5.00	20	3.10	1.25	2.00	7.00
WA5	4	2.50	1.29	1.00	4.00	3	3.33	1.53	2.00	5.00
WV1	8	3.12	0.65	2.25	3.97	103	2.92	0.60	1.69	4.57
WV3	53	2.95	0.80	1.72	5.38	38	3.12	0.75	1.62	4.66
WV5	6	2.26	0.29	1.91	2.63	13	2.47	0.48	1.90	3.31
Left curve average	198	2.92	0.72	1.00	5.38	308	3.00	0.80	1.53	8.00
Curve right										
CA2	57	2.63	0.98	1.00	7.00	39	2.28	0.76	1.00	4.00
MD2	27	3.02	0.53	2.15	4.53	36	3.24	0.72	1.94	5.28
MD3	37	2.57	0.60	1.65	4.16	12	2.55	0.59	1.56	3.53
WA1	12	2.67	0.65	2.00	4.00	10	3.00	1.33	1.00	5.00
WA3	8	2.88	0.83	2.00	4.00	34	3.00	0.85	2.00	5.00
WA4	19	3.21	0.71	2.00	5.00	43	2.72	0.85	1.00	5.00
WA6	5	3.00	1.22	2.00	5.00	13	3.69	1.44	2.00	6.00
WV4	9	2.88	0.52	2.34	3.81	17	3.37	0.60	2.69	4.65
Right curve average	174	2.78	0.79	1.00	7.00	204	2.90	0.94	1.00	6.00

Table 13. Lane-change duration statistics for trucks by curve direction.

Site	Left maneuver (s)					Right maneuver (s)				
	Veh count	Mean	Std dev	Min	Max	Veh count	Mean	Std dev	Min	Max
Curve left										
CA1	5	5.60	0.89	4.00	6.00	19	6.37	1.46	3.00	8.00
CA3	1	3.00		3.00	3.00	0				
MD1	12	4.31	0.45	3.75	5.16	4	5.21	1.25	3.35	5.97
PA2	10	3.13	0.62	2.50	4.78	39	3.35	0.66	2.22	5.18
WA2	6	5.33	1.63	3.00	7.00	1	7.00		7.00	7.00
WA5	1	5.00		5.00	5.00	3	6.67	2.08	5.00	9.00
WV1	2	3.94	1.73	2.72	5.16	122	3.72	0.80	2.28	5.50
WV3	10	3.28	0.74	2.13	4.15	11	3.50	1.00	2.03	4.90
WV5	6	2.82	0.62	2.16	3.84	7	3.18	0.57	2.31	4.18
Left curve average	53	3.94	1.24	2.13	7.00	206	3.95	1.27	2.03	9.00
Curve right										
CA2	3	4.00	1.00	3.00	5.00	4	3.00	0.82	2.00	4.00
MD2	13	4.43	0.63	3.75	5.97	3	4.96	1.40	3.35	5.84
MD3	4	3.65	0.45	2.99	4.03	3	3.10	0.46	2.79	3.63
WA1	1	6.00		6.00	6.00	8	6.63	1.06	5.00	8.00
WA3	4	4.75	1.50	4.00	7.00	4	5.50	1.29	4.00	7.00
WA4	4	4.50	1.00	4.00	6.00	5	4.60	0.89	3.00	5.00
WA6	0					6	7.17	1.60	5.00	9.00
WV4	7	3.84	0.77	2.88	4.83	5	3.57	1.01	2.24	4.72
Right curve average	36	4.28	0.90	2.88	7.00	38	5.13	1.85	2.00	9.00

The degrees of freedom were calculated using the Welch–Satterthwaite equation, and variance components were used for the variance-structure of the split-plot model. Main effect results are shown in Table 14, and statistically significant interaction effects are shown in Table 15.

There is no evidence of a statistically significant difference in vehicle lane-change duration means at upgrade sites compared to downgrade sites (p-value = 0.2385) or at sites with a curve to the left compared to a curve to the right (p-value = 0.7898). There is a statistically significant difference in lane-change duration means between passenger vehicles and trucks (p-value < 0.0001) where passenger vehicles execute the lane-change maneuver about 1.4 s quicker than trucks. There is also a statistically significant difference in mean lane-change duration for vehicles maneuvering into the left lane compared to vehicles maneuvering into the right lane (p-value = 0.0066), but for practical purposes, this difference in lane-change duration (i.e., 0.27 s) is minimal or insignificant.

Interactions between main effects were also important relationships to examine, because one main effect can vary greatly

Table 14. Analysis results of lane-change durations (main effects).

Main effect	Group	Vehicle count	Mean (s)	Std dev (s)	Difference in means (s)	p-value[a]
Grade	Upgrade	90	4.14	1.07	0.67	0.2385
	Downgrade	1,127	3.47	1.08		
Curve	Left	765	3.45	1.04	–0.32	0.7898
	Right	452	3.77	1.20		
Vehicle type	Passenger vehicles	884	2.90	0.82	–1.43	<0.0001
	Trucks	333	4.33	1.34		
Lane-change maneuver	Left	461	3.48	0.82	–0.27	0.0066
	Right	756	3.75	1.28		

[a] p-values below 0.05 indicate statistical significance at the 95% confidence level.

Table 15. Analysis results of lane-change durations (interaction effects).

Interaction effect	Group	Vehicle count	Mean (s)	Std dev (s)	Difference in means (s)	p-value[a]
Grade direction and vehicle type	Upgrade, passenger vehicles	70	3.13	0.63	0.23	0.0039
	Downgrade, passenger vehicles	814	2.90	0.81		
	Upgrade, trucks	20	5.14	1.38	1.09	
	Downgrade, trucks	313	4.05	1.30		
Curve direction and lane-change direction	Left curve, left maneuver	251	3.43	1.01	–0.10	0.0551
	Right curve, left maneuver	210	3.53	0.85		
	Left curve, right maneuver	514	4.98	1.06	0.96	
	Right curve, right maneuver	242	4.02	1.47		

[a] p-values below 0.05 indicate statistical significance at the 95% confidence level.

at different levels of another main effect. All interaction effects were tested in this model, but only two were found to be statistically significant. For the interaction between vehicle type and grade type, lane-change durations for trucks are much higher if they occur on an upgrade compared to a downgrade (difference in means = 1.09 s) compared to lane-change durations for passenger vehicles along an upgrade compared to a downgrade (difference in means = 0.23 s). For the interaction between curve direction and lane-change direction, there is also some evidence that curve direction has less of an effect on a vehicle making a left maneuver (difference in means between left curve sites and right curve sites = 0.10 s) than on a vehicle making a right maneuver (difference in means between left curve and right curve sites = 0.96 s; p-value = 0.0551).

3.3 Instrumented Vehicle Studies

At five data collection sites (see Table 5 for specific sites), the research team collected a range of data using an instrumented vehicle. The purposes were to:

1. Measure the road geometry (i.e., grade, curvature, and cross slope) of each site to confirm whether the vehicle-based road measurements were in agreement with information from roadway inventory files, plan and profile sheets, and field measurements;
2. Obtain in-vehicle dynamics measurements for comparison with simulation outputs to check the fidelity of the vehicle simulation software; and
3. Measure the continuous speed profiles of vehicles traversing the entire lengths of the data collection site (i.e., along the entire grade and curve) since laser gun measurements were collected primarily on the tangent approaching the curve and through the curve, and not along the entire length of the downgrade or upgrade.

3.3.1 Data Collection Methodology

Roadway geometry, cross-slope, and vehicle dynamic data were collected at five sites from in-vehicle sensors while the test vehicle followed free-flow vehicles through the sites. At each site data were collected while following behind five separate passenger vehicles and two tractor semi-trailers.

The instrumented vehicle was a 2010 Dodge Durango. This vehicle was chosen because of its capacity to hold the data collection equipment and because the vehicle's inertial and kinematic parameters align well with those of a standard full-size SUV as defined within CarSim. The vehicle was instrumented with a defense-grade global positioning system (GPS) coupled to a ring-laser-gyro inertial measurement unit (IMU) that gives accurate absolute measures of position and orientation. GPS/IMU data were collected at 100 Hz. In addition, a roof-mounted light detection and ranging (LIDAR) sensor was mounted to a gantry behind and above the vehicle. This road-scanning system was installed to look down perpendicular to the road to give 180° cross-section measurements of the road surface at 0.5° intervals, out to a distance of 260 ft from the sensor, for a total of 361 points per sweep. Each LIDAR sweep obtained 361 data points at 37.5 Hz while capturing the intensity of the LIDAR return. A camera was mounted to the dashboard of the vehicle and manually aligned so that the vanishing point of straight-line driving corresponds roughly to the center of the image. And finally, a steering angle sensor was installed to capture the driver's steering inputs directly. All sensor inputs were collected using Player/Stage software, and each measurement was time-stamped with the computer's local clock. At the beginning of each day of testing, the vehicle was calibrated. A diagram of the data collection system is shown in Figure 12, and an example screenshot from the forward-facing camera on the dashboard is shown in Figure 13.

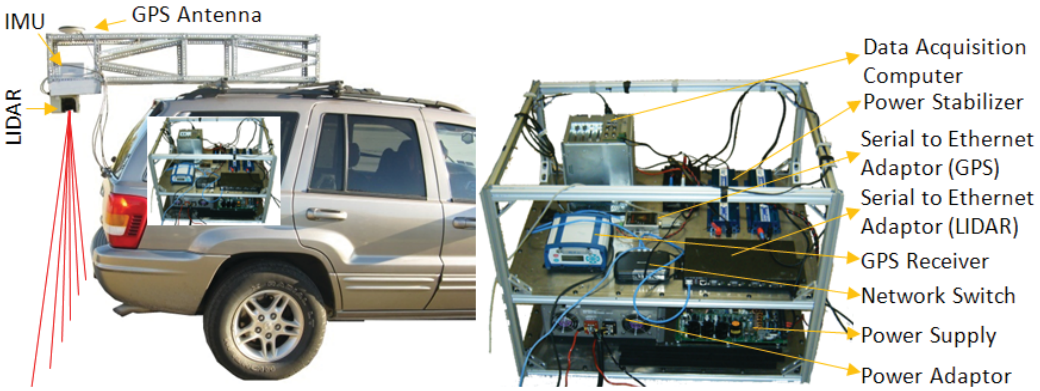

Figure 12. Instrumented vehicle data collection system.

The instrumented vehicle was driven behind vehicles in the traffic stream chosen randomly but selected such that the vehicles were not following other vehicles that would influence their speed. The instrumented vehicle was maintained at a constant following distance—approximately 300 ft behind the lead vehicle as shown in Figure 13. Selected vehicles were followed beginning at the top/bottom of the grade and followed down/up the entire grade and through the curve. The data collection system provided a range of data, including the following:

- **Vehicle data**
  - Velocities on each of the three axes
  - Acceleration/deceleration on each of the three axes
  - Steering angle
  - Roll, pitch, and yaw angles and rates about each axis
  - Position of the vehicle in latitude, longitude, and elevation

Figure 13. Screenshot from instrumented vehicle during data collection.

- **Roadway data**
  - Vertical alignment
  - Horizontal alignment
  - Normal cross slope
  - Transition from normal cross slope to full superelevation
  - Full superelevation in curve

3.3.2 Analysis of Results

Roadway geometry data were obtained from the LIDAR measurements. Standard coordinate transformations were used to convert from LIDAR coordinates, to vehicle coordinates, and finally to globally referenced coordinates (see Vemulapalli and Brennan [2009] for details). The resulting point-cloud data were filtered to develop a smoothed road profile that provided grade, horizontal alignment, and cross-slope information for each site (Varunjikar, 2011). An example illustration of the resulting road profile after processing is shown in Figure 14.

One of the first confirmations conducted on the measured data was to verify that the measured grades matched

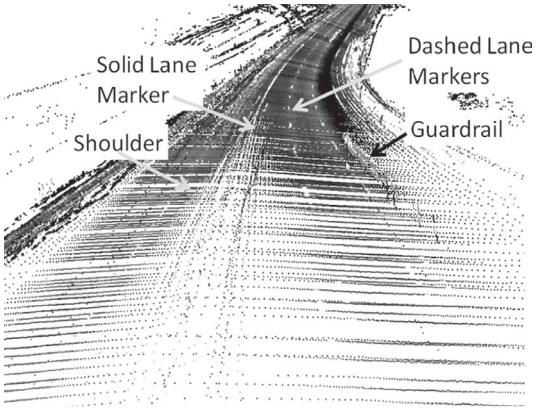

Figure 14. Three-dimensional point cloud obtained by instrumented vehicle data (site MD1).

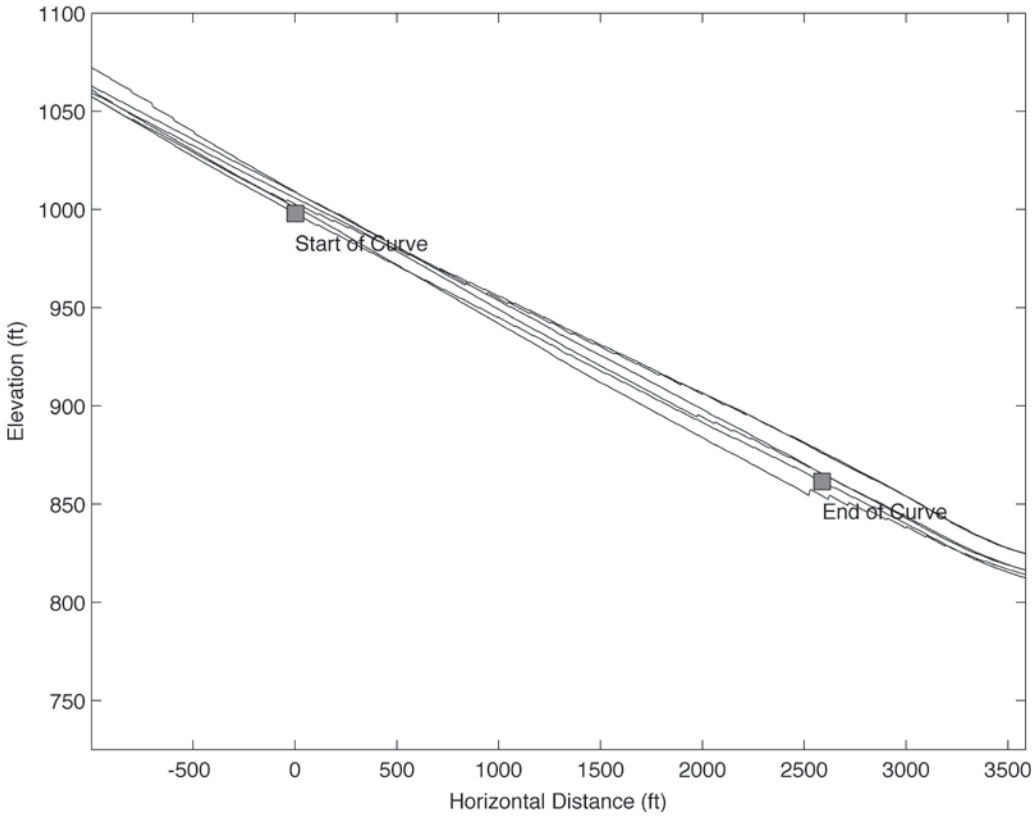

Figure 15. Measured elevations and horizontal distance for all traversals (site WV2).

the grades as reported on profile sheets for the sites. As an example, the measured grades were inferred from the height (z) versus horizontal alignment measurements as shown in Figure 15 for the WV2 site. In Figure 15 (and all subsequent figures), the zero point on the horizontal alignment depicts the beginning of the curve (i.e., PC). Positive values for the horizontal alignment represent the relative position along the length of the curve, and negative values represent the relative position on the approach tangent to the curve. In Figure 15 the inferred grade is −5.6% which is consistent with the grade obtained from the profile sheets for this same site. A similar level of consistency between measured grades and grades obtained from profile sheets was found across all five sites in the instrumented vehicle study (Table 16).

The second level of consistency checks focused on horizontal alignment. The measured horizontal alignment of the WV2 site is shown Figure 16. The Figure illustrates a curve to the left. Through visual inspection, comparisons were made of the collected horizontal geometry, as shown in Figure 16, and CAD drawings created by the research team of the road plans. Additionally, the collected horizontal vehicle trajectory was compared to Google Earth satellite images to further confirm geometric consistency. These comparisons indicated

Table 16. Comparison of grades from instrumented vehicle data and profile sheets.

Site	Percent grade	
	Measured using instrumented vehicle	Obtained from profile sheets
MD1[a]	−4.07 ± 0.27	−4.1
MD2	+6.17 ± 0.33	6.0
MD3	−5.61 ± 0.25	−5.7
PA1[a]	−5.19 ± 0.16	−5.0
WV2	−5.62 ± 0.22	−5.7

[a] Slope for approach is different than the curve. The values shown here are for the approach geometry, not the curve itself.

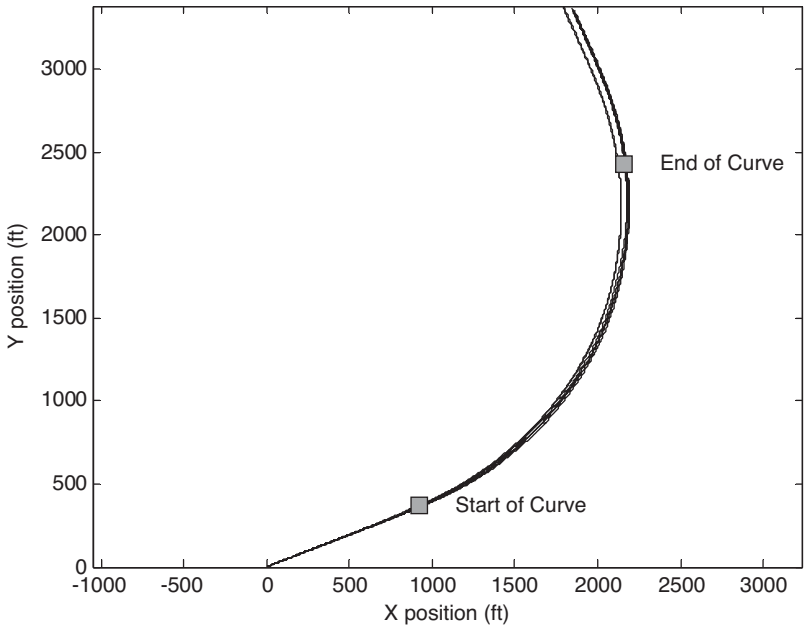

Figure 16. Horizontal alignment from instrumented vehicle for all traversals (site WV2).

a high level of agreement between the instrumented vehicle data and the actual roadway plans.

After it was confirmed that the in-vehicle geometric measurements agreed well with horizontal and vertical alignment information obtained from roadway plans and profiles, the horizontal and vertical alignment data were imported into CarSim to simulate the vehicle's dynamics to compare simulation results to instrumented vehicle measurements. An example of this comparison is shown in Figure 17 for the WV2 site. Note, the horizontal and vertical alignment data and cross-section data (i.e., cross-slope and superelevation data) used to represent the site geometry in CarSim were based upon

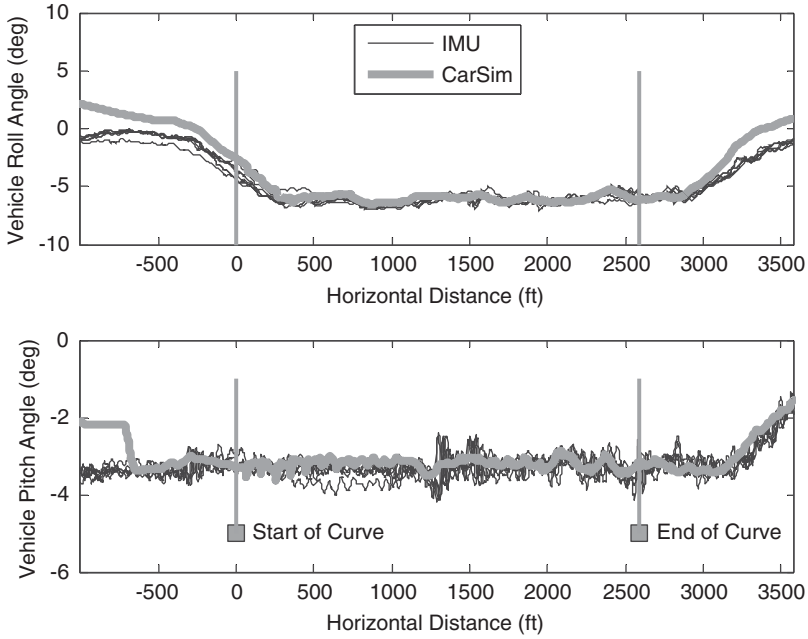

Figure 17. Comparison of CarSim simulation results and instrumented vehicle measurements for all traversals (site WV2).

information obtained from plans and profiles (and/or a combination of roadway inventory files and field measurements). In Figure 17, from a visual perspective, the simulation outputs closely agree with the measured data, including many of the transient effects such as oscillations in the entry and exit of the curve.

Confirmation that the simulation outputs closely agreed with the data from the instrumented vehicle was important in several respects. First, it confirmed the fidelity and/or accuracy of the CarSim model for use in subsequent phases of this research. Second, it provided a reasonable level of confirmation that horizontal and vertical alignment and cross-slope/superelevation data obtained from combinations of plans and profiles, roadway inventory files, and field measurements could be used to accurately model the geometrics of the 20 data collection sites within CarSim, without the need to use the instrumented vehicle to collect this information.

3.3.3 Continuous Speed Profiles

One of the purposes of the instrumented vehicle study was to measure the continuous speed profiles of vehicles traversing each field site for the entire length of the site (i.e., from the top of the grade through the curve or from the bottom of the grade through the curve), since roadside laser gun measurements of speed are limited in their coverage to shorter segments of the sites. Figure 18 shows all the speed traces from the instrumented vehicle traversals versus the mean speeds measured using laser guns for the WV2 site. This particular site had full coverage of the curve from the roadside laser gun locations. The Figure illustrates some of the phenomenon of a typical passenger vehicle. For example, the instrumented vehicle study showed that most vehicles that were followed maintained relatively constant speed through the curve, punctuated by areas of short changes. This behavior was readily observed in most of the traversals. For some vehicles, however, there are very large speed changes within the curve. For example, Figure 18 shows a situation where one followed vehicle changed speed from approximately 80 mph before the curve, to 50 mph within the curve, and then back to 80 mph after the curve.

Figure 19 shows the corresponding acceleration/deceleration of the subject vehicles while traversing the data collection site, as measured from the instrumented vehicle. Shown in this figure are the individual data traces for each vehicle traversal, the mean acceleration at each point in the curve, and the upper and lower bounds created from two standard deviations from the mean at each location. Prior work by Bonneson (2000b) suggested that vehicles slow down slightly on the entrance to a curve, with very minor deceleration rates of −3 ft/s^2. This deceleration on the entrance to a curve was not conclusively or consistently seen in the speed data collected from the instrumented vehicle; indeed, several of the followed vehicles actually accelerated rather than decelerated upon entrance to the curve. However, the upper and lower bounds on the accelerations throughout the curve are approximately bounded by 3 ft/s^2 deviations from zero acceleration (e.g., constant speed).

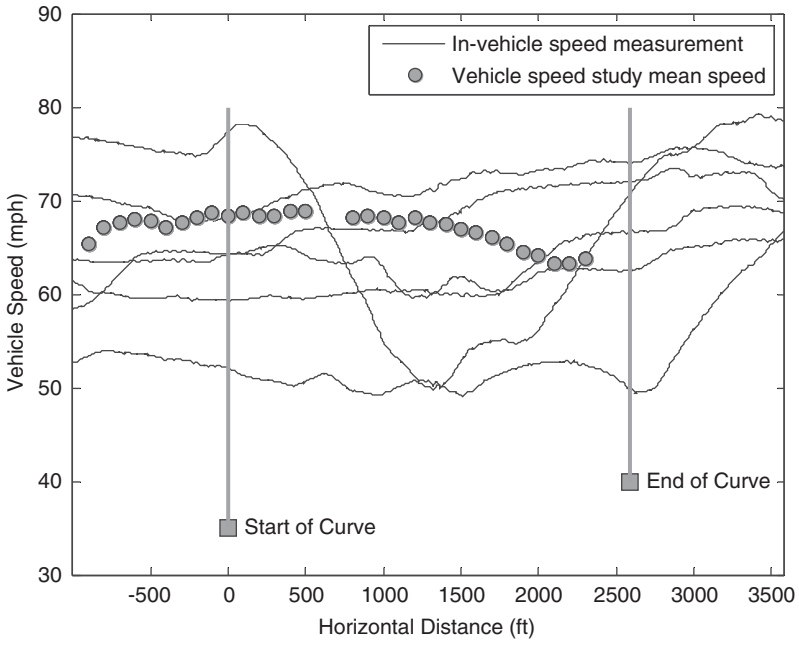

Figure 18. Comparison of speed profiles from instrumented vehicle and mean speeds from laser guns (site WV2).

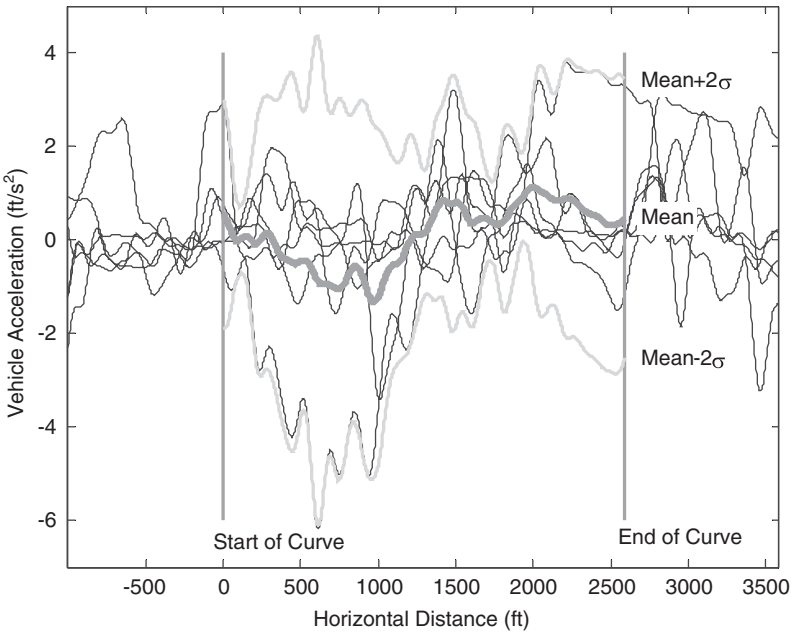

Figure 19. Longitudinal acceleration profiles from instrumented vehicle (site WV2).

Several general findings regarding the speed data collected from the instrumented vehicle are as follows:

- Overall, the mean speed profiles measured by the instrumented vehicle agreed with the speed data collected from the laser guns.
- The variability in the vehicle acceleration within a curve was approximately between 3 and −3 ft/s^2; this magnitude is consistent with the curve-entry deceleration reported by Bonneson (2000b). Hereafter, this deceleration level is denoted as "curve-entry deceleration," even though the field data indicate that the deceleration may occur throughout the curve.

3.3.4 Summary of Instrumented Vehicle Study

Consistent with the main goals of the instrumented vehicle study, several observations can be inferred from the analysis results presented above. First, the horizontal and vertical alignment and cross-slope/superelevation data obtained from combinations of plans and profiles, roadway inventory files, and field measurements agreed with the corresponding data measured from the instrumented vehicle. Because plans and profiles, roadway inventory files, and field measurements were available for all 20 data collection sites, and the instrumented vehicle results were available at only 5 sites, horizontal and vertical alignment and cross-slope/superelevation data obtained from combinations of plans and profiles, roadway inventory files, and field measurements were used for all site-specific simulations.

Second, the outputs from the vehicle dynamics simulations agreed closely with the instrumented vehicle data. This agreement gives confidence in the fidelity of the simulation results.

Third, the speed profiles of the instrumented vehicle study were found to be in agreement with the speed data collected from the laser guns. In addition, the magnitude of the decelerations observed from the instrumented vehicle speed data is consistent with the findings of *NCHRP Report 439* (Bonneson, 2000b). Thus, for the simulations (see Section 4), some scenarios were performed assuming minor decelerations of −3 ft/s^2 as curve-entry deceleration levels.

3.4 Friction Testing

3.4.1 Purpose

The purpose of the friction testing was to establish friction values for tires on both passenger vehicles and trucks suitable for modeling a vehicle's expected behavior on steep grades and through sharp horizontal curves where both lateral and longitudinal forces must be generated. The friction data were used in conjunction with the simulation analyses (see Section 4) to determine the difference between the AASHTO design friction curves and the friction supply and demand on representative grades and horizontal curves. This

section of the report (1) explains the data collection methodology used to collect friction data in the field, (2) presents general processing procedures to translate the raw field data into friction values for use in the simulation modeling, and (3) summarizes the results focusing on how the friction data were utilized in the simulation modeling.

3.4.2 Data Collection Methodology

A dynamic friction (DF) tester was used to evaluate the skid resistance of the pavements at the field study sites. Testing was performed in accordance with American Society for Testing and Materials (ASTM) E1911-09a, *Standard Test Method for Measuring Pavement Surface Frictional Properties Using the Dynamic Friction Tester.* The DF tester measures the necessary torque to turn three small rubber pads in a circular path on the measured surface at different speeds. The apparatus consists of a horizontal spinning disk fitted with three spring-loaded rubber sliders that contact the paved surface as the disk rotational speed decreases due to the friction supplied between the sliders and the paved surface. A water supply unit delivers water to the paved surface being tested. The torque generated by the slider forces measured during the spin down is used to calculate the friction supply as a function of speed. Typical test speeds range from 55 to 3 mph. The DF tester is shown in Figure 20.

The device was manually placed on the pavement surface at each testing site location. A laptop computer was used to control the test and record the data. When a test was initiated, the disk was accelerated to the standard spinning speed of 55 mph. The spinning disk was then dropped to the ground, at which time automated data acquisition began. The test was complete when the disk stopped.

A circular track (CT) meter was used with the DF tester to measure road surface texture characteristics. The CT meter measures surface texture on the same circular track as the DF tester. The CT meter calculates the mean profile depth (MPD) of the road surface and the International Friction Index (IFI).

Raw data from the DF tester and CT meter were filtered to calculate the friction supply at the tire–pavement interface. The data were used to prepare friction supply curves for wet and dry pavements similar to those presented in the AASHTO *Green Book* as shown in Figure 21 (e.g., see the "New tires–wet concrete pavement" curve).

The following protocol was used during field testing:

1. Each test section was divided into two segments:
   - The first segment consisted of 450 ft of the approach tangent upstream of the horizontal curve.
   - The second segment was the entire length of the horizontal curve.
2. The first segment was subdivided into three equal lengths (i.e., 150 ft sectors). Friction measurements were collected at the beginning and end points of these sectors using the DF tester and CT meter devices. This yielded four total friction supply measurement locations on the approach tangent to the horizontal curve. The intent of measuring friction at multiple locations on the approach tangent was to understand variability in pavement friction for areas

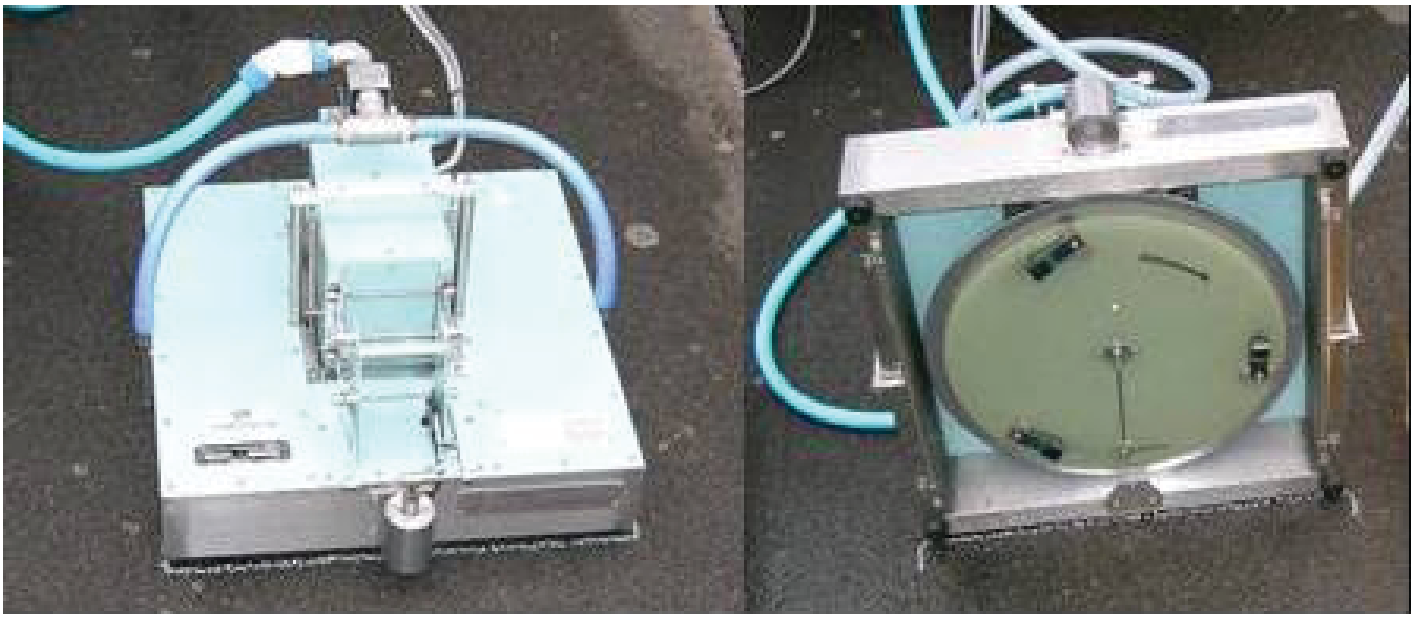

Figure 20. DF tester.

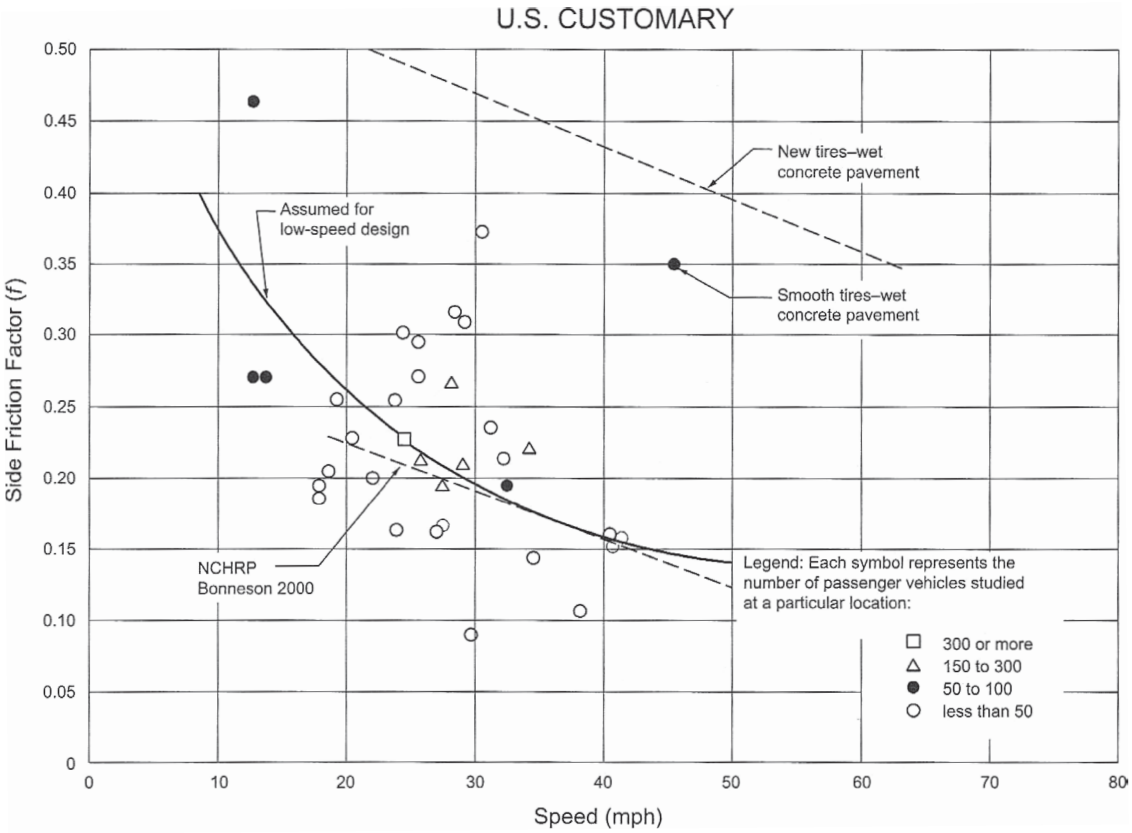

Figure 21. AASHTO side friction factors for low-speed design and friction supply curves (AASHTO, 2011).

of normal travel and slight deceleration. All friction measurements on the approach tangent were taken in the left wheel path.

3. The second segment (i.e., horizontal curve) was similarly divided into three equal length sectors yielding four physical measurement locations. The intent of measuring friction supply at four locations within the horizontal curve was to provide information about the variability in friction supply within limits of the curve.
4. Each measurement location within a sector was defined as a 6 ft long straight line. The beginning, middle, and end points of the 6 ft line were separately measured using the DF tester and CT meter devices, producing three individual measurement points for each location.
5. Within each horizontal curve segment, the measurement location was determined as follows:
   – On curves to the right, measurements were recorded in the left wheel path as this location will experience more polishing and therefore will supply less friction than the right wheel path.
   – On curves to the left, friction supply was measured in the right wheel path.

A diagram of the testing points/locations on the approach tangent and horizontal curve is shown in Figure 22.

Friction data were collected at eight field sites (see Table 5 for specific sites). The travel lanes at each of the sites consisted of asphalt pavement that appeared to be in good condition. The resulting DF tester and CT meter values are presented in Table 17.

3.4.3 Summary of Friction Testing

Friction measurements were recorded at 21 locations approaching and within a curve at each of eight field sites. These field measurements were then processed to obtain tire force curves for representative passenger vehicle and truck tires on the roads where friction measurements were taken. Section 4.2 describes the general procedures for taking the field measurements and generating tire force curves.

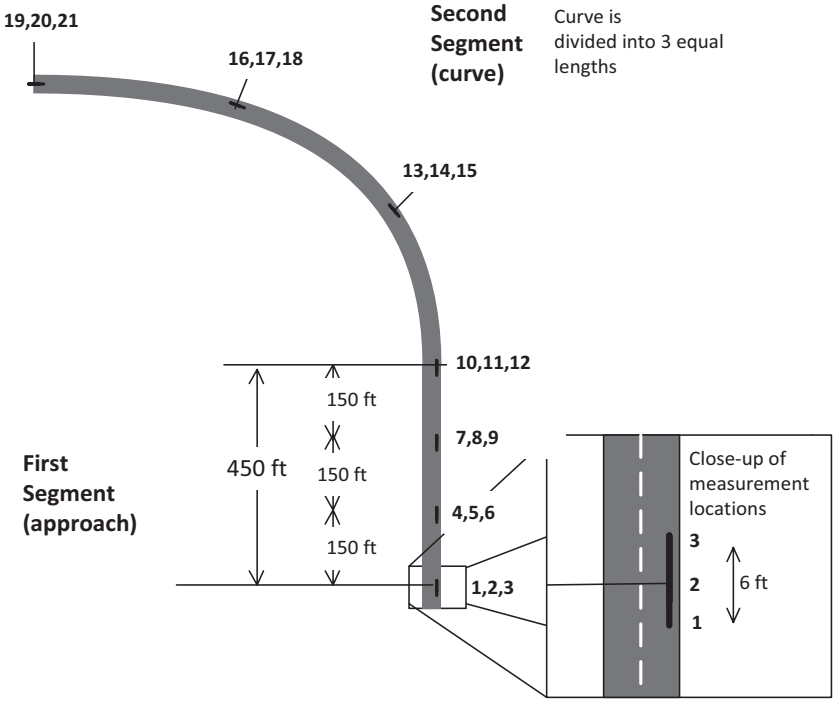

Figure 22. Friction measurement locations at a site.

Table 17. DF tester and CT meter values for field sites.

	Dynamic friction tester—DFT20 (coefficient of friction)																				
Site	1	2	3	4	5	6	7	8	9	10	11	12	13	14	15	16	17	18	19	20	21
MD1	0.70	0.69	0.70	0.67	0.67	0.65	0.67	0.66	0.66	0.64	0.64	0.65	0.67	0.65	0.66	0.65	0.66	0.67	0.63	0.63	0.64
MD2	0.40	0.44	0.43	0.46	0.44	0.43	0.44	0.42	0.43	0.42	0.44	0.44	0.44	0.46	0.44	0.46	0.43	0.42	0.49	0.47	0.52
MD3	0.53	0.52	0.51	0.56	0.56	0.52	0.38	0.50	0.50	0.50	0.50	0.50	0.44	0.45	0.45	0.48	0.49	0.48	0.45	0.44	0.43
WV1	0.38	0.41	0.45	0.48	0.46	0.48	0.48	0.48	0.48	0.50	0.51	0.47	0.47	0.48	0.47	0.50	0.50	0.51	0.51	0.51	0.53
WV2	0.52	0.58	0.59	0.59	0.59	0.59	0.57	0.58	0.57	0.57	0.57	0.56	0.52	0.52	0.52	0.52	0.52	0.51	0.47	0.44	0.46
WV3	0.51	0.59	0.60	0.60	0.61	0.60	0.61	0.63	0.59	0.57	0.59	0.60	0.47	0.50	0.48	0.44	0.47	0.45	0.57	0.53	0.54
WV4	0.51	0.54	0.57	0.56	0.57	0.58	0.60	0.56	0.60	0.62	0.58	0.59	0.58	0.58	0.53	0.57	0.56	0.57	0.55	0.56	0.35
WV5	0.50	0.52	0.54	0.58	0.56	0.57	0.55	0.55	0.54	0.54	0.53	0.54	0.47	0.48	0.48	0.38	0.46	0.48	0.53	0.54	0.58

	Circular track meter—Mean profile depth (in.)																				
Site	1	2	3	4	5	6	7	8	9	10	11	12	13	14	15	16	17	18	19	20	21
MD1	0.02	0.02	0.02	0.02	0.02	0.02	0.02	0.02	0.02	0.02	0.02	0.02	0.02	0.02	0.02	0.02	0.02	0.02	0.02	0.02	0.02
MD2	0.03	0.03	0.03	0.02	0.02	0.02	0.03	0.03	0.03	0.02	0.02	0.02	0.02	0.03	0.03	0.03	0.02	0.02	0.02	0.02	0.02
MD3	0.03	0.03	0.03	0.03	0.03	0.03	0.03	0.03	0.03	0.03	0.02	0.03	0.03	0.04	0.03	0.05	0.04	0.04	0.03	0.03	0.03
WV1	0.02	0.03	0.03	0.03	0.03	0.03	0.03	0.03	0.03	0.03	0.03	0.03	0.03	0.02	0.02	0.03	0.03	0.03	0.03	0.03	0.03
WV2	0.03	0.03	0.02	0.03	0.03	0.03	0.03	0.03	0.03	0.03	0.03	0.03	0.03	0.03	0.03	0.06	0.04	0.03	0.03	0.03	0.03
WV3	0.05	0.05	0.05	0.05	0.04	0.05	0.05	0.05	0.05	0.05	0.05	0.05	0.06	0.08	0.09	0.07	0.07	0.06	0.06	0.06	0.05
WV4	0.03	0.02	0.03	0.03	0.02	0.03	0.03	0.03	0.03	0.03	0.03	0.03	0.02	0.02	0.03	0.02	0.02	0.03	0.02	0.03	0.02
WV5	0.03	0.04	0.03	0.03	0.04	0.04	0.03	0.03	0.03	0.03	0.03	0.03	0.04	0.04	0.04	0.04	0.05	0.05	0.04	0.05	0.05

SECTION 4

Analytical and Simulation Modeling

This section presents the analytical and simulation modeling work performed to investigate superelevation criteria for sharp horizontal curves on steep grades. Section 4.1 presents the step-by-step analysis approach which integrates both field and simulation data and is based upon an increasingly detailed analysis using progressively more sophisticated simulation models. Sections 4.2 through 4.12 present the individual steps of the analysis, first describing the goal and methodology for the step, followed by background information and individual results, concluding with a summary of the key results for the respective step/analysis. The analysis considers a range of horizontal curve and vertical grade combinations and six vehicle types (i.e., three types of passenger vehicles and three types of trucks). The analysis considers situations in which vehicles maintain a constant speed through the curve and situations with progressively more aggressive deceleration. The analysis also considers situations where the vehicle's desired trajectory is to maintain the same lane from the approach tangent through the curve and situations with a lane-change maneuver. The primary performance measures of interest from the analyses are lateral friction and rollover margins that indicate whether a vehicle can successfully follow its desired trajectory through a geometric condition (i.e., horizontal curve and vertical grade combination) without experiencing a skidding or rollover event. The severity of skidding and rollover events is also described in some situations by considering the duration of the event and the lateral deviation from the desired vehicle trajectory. Most of the analyses/steps focus purely on the dynamic capabilities of the vehicle to traverse the given geometric condition. It is only in the most sophisticated and complex analyses (i.e., multibody models) that the inputs and capabilities of a driver are considered. Section 4.13 summarizes the main, overarching findings from the analytical and simulation modeling.

For the analytical and simulation modeling, a sharp horizontal curve was defined as a minimum-radius curve as determined from the maximum rate of superelevation and maximum side friction factor for given design speeds.

4.1 Analysis Approach

The analysis was designed to use a combination of field data (see Section 3) and simulation results to evaluate geometric design criteria specific to sharp horizontal curves on steep grades. The general framework for the analysis is shown in Figure 23.

The overall goal of the evaluation framework was to develop recommended modifications to existing AASHTO design policy to improve conditions that may generate concerns at sharp horizontal curves on steep grades. The notion of "substantial error" in the evaluation framework was one where differences were observed in field data versus simulations, and between simulations of different fidelity. Where field data were available to compare with simulation results, the field data were used to verify that simulations were providing reasonable results.

In several of the key steps, the primary focus was to determine whether friction demand, f, exceeds supply friction, $f_{\text{tire-pavement}}$. These design conditions should be avoided because they increase the risk of a vehicle skidding and being unable to maintain the desired trajectory on the horizontal alignment. For each analysis, the $f_{\text{tire-pavement}}$ values are represented by a friction ellipse that encompasses the maximum friction supply in the longitudinal or x-direction (braking) and lateral or y-direction (side) as shown in Figure 24. Both limits change as a function of speed, tire type, and pavement condition.

To determine whether a vehicle can traverse a horizontal curve without skidding or overturning, a minimum requirement is that the "operating point" representing the friction demand remains within this friction ellipse. Departure of the operating point from within the friction ellipse represents cases where friction demand exceeds friction supply, resulting in skidding of the tire. The operating point changes depending on the curve radius, the superelevation, steering maneuvers, and braking forces used in the horizontal curve. Much of the simulation work focuses on calculating the operating point of a vehicle within the friction ellipse under different maneuvers and assumptions.

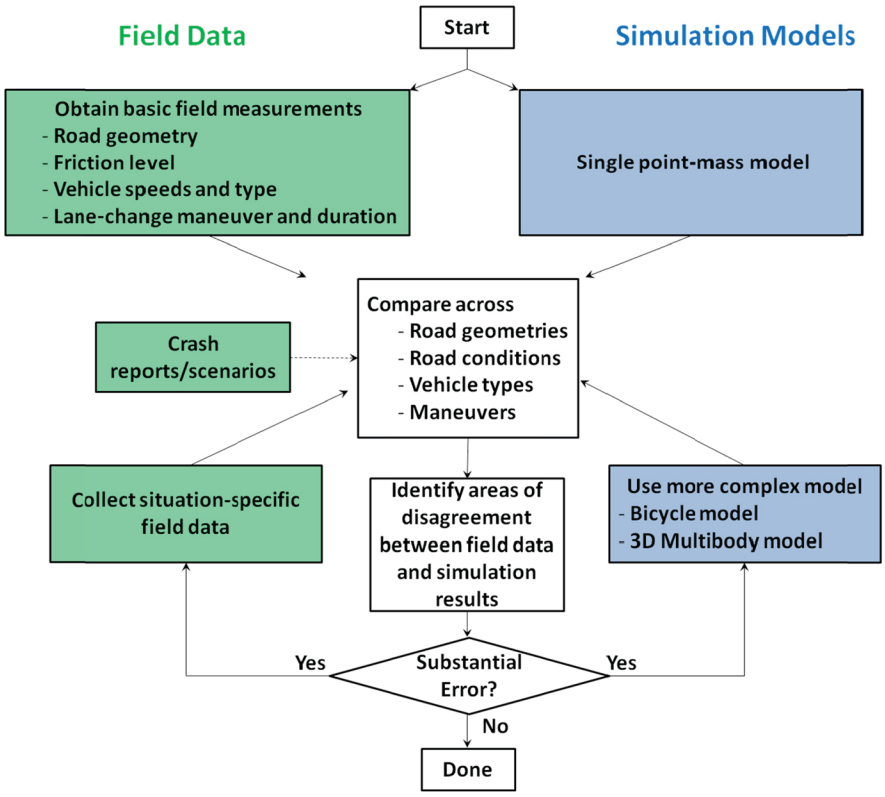

Figure 23. Framework for evaluating analytical and simulation models.

To ascertain whether the operating point (f_x, f_y) lies inside the friction supply ellipse for a given combination of cornering and braking demand, the constraint of Equation 15 must be met. While this equation serves as a good check of whether friction supply limits have been exceeded by the vehicle's demand, it is less useful as a definition of lateral friction margins because it weights braking and cornering margins equally. In practice, however, braking forces should be given priority because, when a vehicle begins to skid, the tire forces are in the opposite direction of the skid, and therefore the cornering forces are greatly diminished. Thus, having excess cornering margins but zero braking margins is not very meaningful since the cornering margins will mean little if the vehicle is unable to steer.

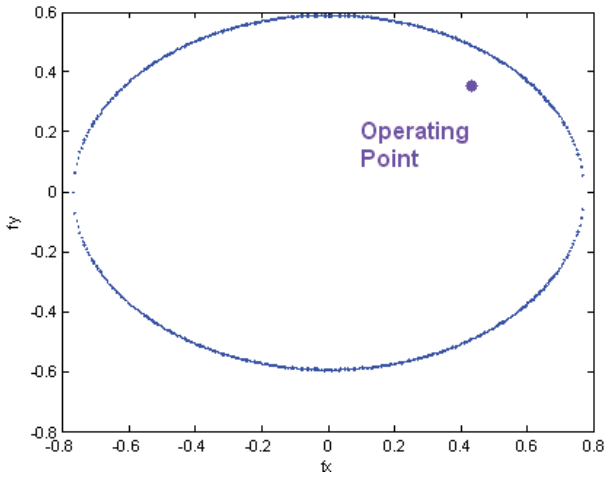

Figure 24. Friction ellipse (tire–pavement model).

The goal, therefore, is to define lateral friction margin for the purposes of this study. This definition must be mathematically tractable, must give priority to braking margins first, and should remain consistent with the definition of margin of safety against skidding used in highway design. The definition should also reflect the friction ellipse concept.

To develop a definition of lateral friction margin, consider the simple definition in Equation 16:

$$f_{margin} = f_{y,supply} - f_y \tag{16}$$

In other words, the lateral friction margin is defined as lateral friction supply minus the lateral friction (i.e., cornering friction). Because braking friction demand decreases available lateral supply friction below the nominal value of $f_{y,max}$, as demonstrated by Equation 15, the following modification is made to $f_{y,max}$ to obtain $f_{y,supply}$ by rearranging the friction ellipse equation:

$$f_{y,supply} = f_{y,max}\sqrt{1-\left(\frac{f_x}{f_{x,max}}\right)^2} \tag{17}$$

Combining Equations 16 and 17 obtains a usable definition of the lateral friction margin:

$$f_{margin} = f_{y,max}\sqrt{1-\left(\frac{f_x}{f_{x,max}}\right)^2} - f_y \quad (18)$$

This definition of the lateral friction margin therefore depends on the tire's demanded side force, f_y, the demanded braking, f_x, and maximum dimensions of the friction ellipse in the braking and lateral directions, $f_{x,max}$ and $f_{y,max}$. This lateral friction margin, where braking forces are assumed to be required first before lateral forces are available, is consistent with tire behavior near skidding. At the onset of a skid, the tire's force will be applied only opposite the direction of the skid, with little side forces available. This is generally in the braking direction, and thus there are little to no side forces available if braking is maximized. The definition of lateral friction margin above appropriately reflects this.

With this definition of lateral friction margin, values greater than zero imply that the maneuver will not cause skidding, whereas values less than zero may cause skidding. This definition is used in simulations regardless of the complexity or structure of the simulation. For example, when using the modified point-mass model, the "tire" considered is actually a lumped representation of the sum of forces on *all tires* possessed by the real vehicle. When considering the per-axle (bicycle) model, each "tire" considered represents two tires lumped together, or even eight tires in the case of the rear tractor and trailer axles. For the per-tire simulations using high-order multibody simulation software, the "tire" considered is consistent with a single "tire" on the physical vehicle. This is important because changing normal loads during a simulation due to weight transfer affect the ultimate supply friction available on true tires due to tire load sensitivity, and also change the friction demand on each modeled tire as the model structure complexity increases to approach reality.

When evaluating lateral friction margins and rollover margins, the following general qualitative categorization was assumed:

- Lateral friction margin ≥ 0.2: Large margin of safety
- 0.1 ≤ lateral friction margin < 0.2: Medium margin of safety
- 0 ≤ lateral friction margin < 0.1: Low margin of safety
- Lateral friction margin < 0: Unacceptable margin of safety

For modern roadway designs in nominal conditions, the lateral friction margins are expected to be quite high. The side friction demand in horizontal curve design is usually quite low relative to the side friction that can be supplied by the tire–pavement interface. AASHTO policy for horizontal curve design suggests some maximum friction demand levels, f_{max}, for use in the design of roadways. These values are particularly conservative because they are based on driver comfort thresholds rather than skidding or rollover thresholds. Because this study is examining potential modifications to this policy, a research approach was developed to identify situations where the friction demand curves used by AASHTO can be violated due to sharp horizontal curves on steep grades and to investigate these situations further. From this analysis, specific changes in superelevation policy can be recommended to correct for areas of concern.

The approach to the analytical and simulation modeling comprises 11 steps as follows:

Step 1: Define basic tire–pavement interaction model(s) and estimate lateral friction margins against skidding in AASHTO's current horizontal curve policy
Step 2: Define road geometries and variable ranges for use in subsequent steps
Step 3: Develop side friction demand curves and calculate lateral friction margins against skidding considering grade using the modified point-mass model
Step 4: Define vehicles and maneuvers to use in non-point-mass models
Step 5: Predict wheel lift using quasi-static models
Step 6: Predict skidding of individual axles during steady-state behavior on a curve
Step 7: Predict skidding of individual axles during braking and lane-change maneuvers on a curve
Step 8: Predict skidding of individual axles during transient steering maneuvers and severe braking
Step 9: Predict skidding of individual wheels
Step 10: Predict wheel lift of individual wheels during transient maneuvers
Step 11: Analysis of upgrades

The goals, details, and primary results of each step are presented in the corresponding sections.

At the start of the research it was generally assumed that vehicle operations on steep downgrades were the more critical situations to investigate compared to steep upgrades. Therefore, much of the analytical and simulation analysis focused on investigating horizontal curves in combination with steep downgrades, but to be thorough, some analyses were performed to investigate vehicle operations on sharp horizontal curves on steep upgrades. Steps 1 through 10 (Sections 4.2 through 4.11) focus on downgrades, while Step 11 (Section 4.12) addresses upgrades.

Six classes of vehicles were considered in the analytical and simulation modeling, as appropriate, including three classes of passenger vehicles and three classes of trucks. In presenting results of the first few steps, most of the discussion focuses on

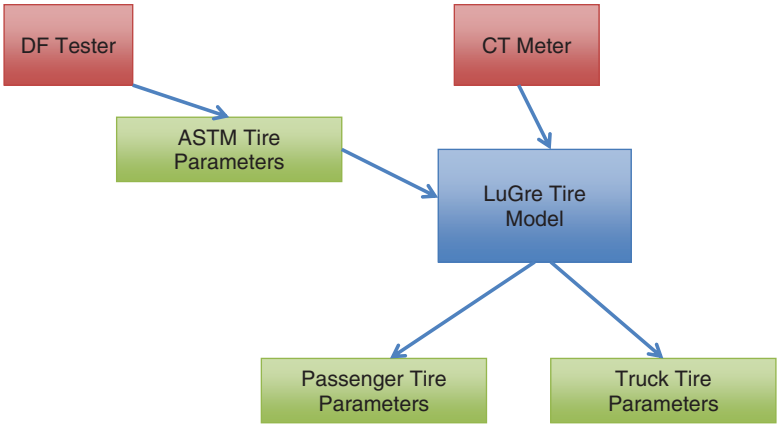

Figure 25. Sequence to convert field measurements to representative tire parameters.

the simulation results for passenger vehicles with a brief discussion on the simulation results for trucks. It is not until the last few steps (i.e., beginning with Step 7) that more detailed results for the different truck classes are presented, as the differences between trucks and passenger vehicles become more pronounced with these increasingly complex simulation models.

4.2 Step 1: Define Basic Tire–Pavement Interaction Model(s) and Estimate Lateral Friction Margins against Skidding in AASHTO's Current Horizontal Curve Policy

The objective of Step 1 was to develop and refine tire–pavement interaction model(s) that estimate(s) friction supply on typical roads, $f_{\text{tire-pavement}}$, for use in subsequent simulations. The model(s) predict tire forces as a function of tire type, vehicle speed, friction supply measurements, and pavement wetness. Friction supply curves from model estimates were then compared to AASHTO's side friction design curves to estimate lateral friction margins against skidding presently assumed in current AASHTO horizontal curve policy.

4.2.1 Analysis Approach

Data from the friction testing (see Section 3.4) were combined using the general procedure in Figure 25 to obtain tire force curves for representative passenger vehicle and truck tires on the roads where friction measurements were taken. First, the DF tester measurements (see top portion of Table 17) were fit to a tire force curve for the ASTM tire. This generates the reference skid number measurements of a road. The measured skid numbers are shown in Table 18 for the longitudinal direction (i.e., *x*-direction) corresponding to tests at 40 mph.

Additionally, the CT meter data (see bottom portion of Table 17) and DF tester data can be transformed into lateral forces to generate representative skid numbers for the lateral direction (i.e., *y*-direction). The corresponding values for passenger vehicle tires are shown in Table 19. These lateral skid numbers are not typically reported in the literature. They are reported here for the passenger tire as these values are more appropriate for horizontal curve design than longitudinal skid numbers as they represent the measured values of limiting side force available to a tire before sideways skidding. Comparing Tables 18 and 19, the lateral skid numbers are generally 9 to 25 lower than the longitudinal skid numbers.

Table 18. Skid numbers in longitudinal direction at skidding (40 mph).

	Measurement location																						
Site	1	2	3	4	5	6	7	8	9	10	11	12	13	14	15	16	17	18	19	20	21	Avg	Min
MD1	77	77	77	74	72	72	78	75	76	73	73	76	74	75	73	77	78	76	71	71	77	74.9	71
MD2	59	61	63	62	60	58	62	62	61	58	60	59	59	67	64	63	59	57	64	62	67	61.3	57
MD3	71	69	70	74	74	70	56	68	68	70	65	68	65	67	65	71	70	70	63	63	62	67.6	56
WV1	74	81	85	87	87	87	89	90	87	87	90	88	78	76	75	78	80	80	90	86	88	84.0	74
WV2	71	75	73	78	78	78	73	74	76	76	76	75	70	70	71	76	74	70	67	63	64	72.8	63
WV3	74	83	83	84	84	83	85	87	82	81	83	84	70	72	68	65	69	67	81	77	78	78.1	65
WV4	69	68	73	73	72	76	76	74	76	81	77	74	73	72	69	70	67	73	71	72	53	71.9	53
WV5	71	73	75	77	77	78	75	74	72	72	71	73	68	70	70	58	69	71	75	77	82	72.8	58

Table 19. Skid numbers in lateral direction at skidding (40 mph).

	Measurement location																						
Site	1	2	3	4	5	6	7	8	9	10	11	12	13	14	15	16	17	18	19	20	21	Avg	Min
MD1	61	62	61	58	57	56	63	59	62	59	58	62	58	62	58	62	64	61	56	56	63	59.9	56
MD2	51	52	55	53	51	49	53	54	53	50	49	48	48	58	56	54	50	48	52	52	56	52.0	48
MD3	61	59	60	63	63	60	48	58	59	61	54	58	56	59	57	63	62	62	53	55	54	58.3	48
WV1	47	50	53	55	56	56	58	57	58	59	61	57	55	49	52	59	58	58	62	58	60	56.1	47
WV2	61	63	60	67	68	68	62	62	65	65	66	65	61	60	61	67	65	61	59	55	55	62.7	55
WV3	66	74	75	76	75	75	76	79	75	73	75	76	62	61	56	56	60	58	73	69	70	69.5	56
WV4	59	57	62	62	61	65	64	63	64	69	67	62	61	60	59	58	54	62	59	61	44	60.6	44
WV5	61	64	65	67	69	69	65	64	61	62	60	63	60	61	61	52	61	63	67	69	74	63.7	52

Additional information about the road surface is needed to capture the full tire force curves in combined longitudinal and lateral skidding, across a range of skidding values from normal driving to full skids. In particular, the skid numbers only provide the skidding values and therefore do not give a good indication of tire forces transitioning from maximum friction to skidding friction conditions. To describe partial skidding phenomenon, the LuGre tire model was used.

The LuGre tire model predicts tire forces by estimating the local deflection, z, of each portion of the tire using a model similar to a spring/damper system sliding along a surface with a relative velocity, v_r. As an analogy, the tire's deformation is treated like "bristles" on a brush sliding along a contact area moving below; thus, sometimes the LuGre model is referred to as a Bristle tire model. Under these assumptions, the braking force of the tire element, F_{xi}, can be calculated using the following:

$$F_x/F_n = \underbrace{\sigma_0 z}_{\substack{\text{Stiffness}\\ \text{Effect}}} + \underbrace{\sigma_1 \frac{dz}{dt}}_{\substack{\text{Damping}\\ \text{Effect}}} + \underbrace{\sigma_2 v_r}_{\substack{\text{Viscous}\\ \text{Effect}}}$$

$$F_{xi}/F_{zi} = \underbrace{\sigma_0 z}_{\substack{\text{Stiffness}\\ \text{Effect}}} + \underbrace{\sigma_1 \frac{dz}{dt}}_{\substack{\text{Damping}\\ \text{Effect}}} + \underbrace{\sigma_2 v_r}_{\substack{\text{Viscous}\\ \text{Effect}}} \quad (19)$$

where F_{zi} is the normal force on the tire contact patch and σ_0, σ_1, σ_2 are model constants that depend solely on the properties of the tire, and thus are different for passenger vehicle and truck tires.

Once the tire properties are determined, the tire models can predict tire friction for pure braking, pure cornering (until skid), and combinations of braking and cornering. The resulting curves form an ellipse that represents the available tire forces. Figure 26 shows an example friction ellipse for the WV2 site at the second measurement location (see Figure 22).

To investigate whether friction changes within a curve in characteristic patterns—for example whether the friction may be lower on the entrance to the curve—the tire models were used to predict the maximum supply tire friction for pure braking and pure cornering across all speeds in the study, at all locations and all sites. The results showed no clear trends to suggest that friction values are different at the beginning, middle, or end of the curve. These results indicated that, for each site, the mean friction and statistical variation in the friction values can be used to model vehicle behavior, rather than detailed location-by-location modeling of friction values.

4.2.2 Analysis Results

To determine the range of friction values to consider as representative of a road surface, the statistical distribution of friction values measured from each site and each measurement location were examined. Figure 27 shows the distributions of the maximum braking and cornering friction values across all sites at 40 mph for passenger vehicle tires. Figure 28 shows the same data for 85 mph. These friction values follow roughly a normal distribution, with a mean friction supply between 0.65 and 0.88 for wet-road conditions. These numbers are in agreement with published data for wet roads, at 40 mph test speeds, for well-maintained pavement surfaces and passenger vehicle tires which suggest wet-road friction values of 0.6 or higher.

The distribution of the friction data can also be used to determine the minimum values of supply friction to consider when evaluating lateral friction margins against skidding. In this case a Gaussian (normal) probability distribution function was used to fit the data. Taking a conservative approach, the worst-case (i.e., minimum) friction values selected for use in evaluating lateral friction margins against skidding were the 2nd percentile of the distributions, determined by the mean friction minus two standard deviations in the friction data. This suggests minimum supply friction values roughly between 0.5 and 0.7 (as seen in Figures 27 and 28) for evaluating lateral friction margins against skidding.

Figures 27 and 28 illustrate the probability distribution functions of the friction data for two speed levels (40 and 85 mph). To cover the full range of speeds considered in this evaluation, friction supply curves for wet-weather conditions were generated for full braking and full cornering for speeds between 25 to 85 mph for both passenger vehicle and truck

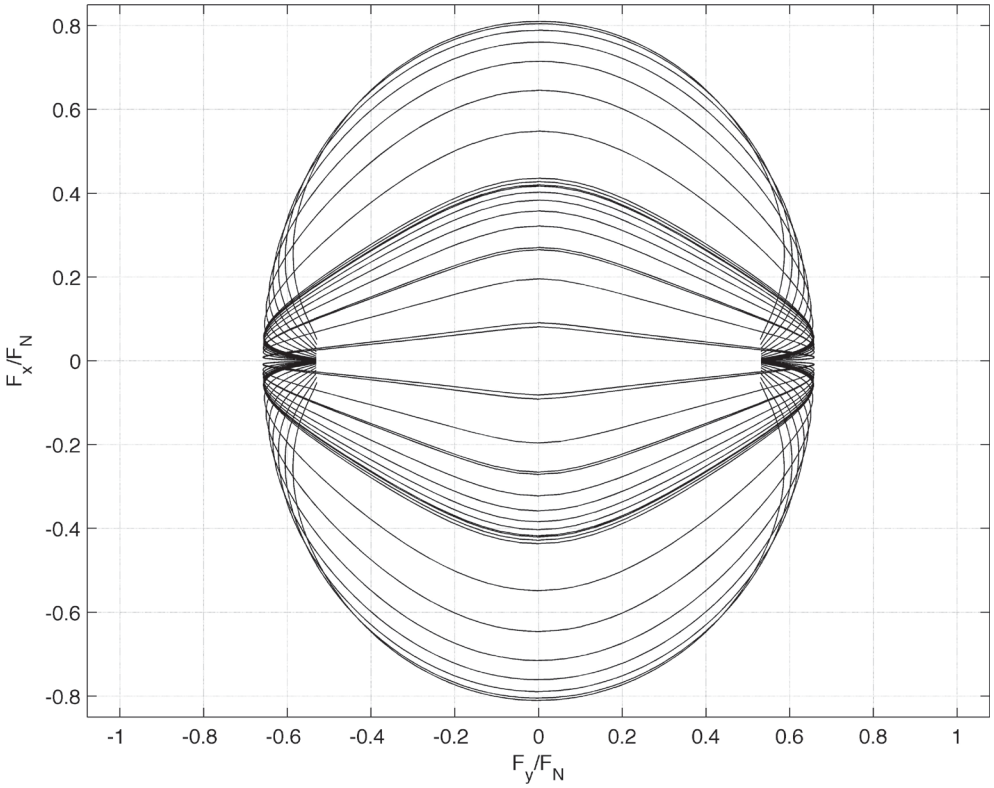

Figure 26. Friction ellipse for friction data collection location 2 (site WV2).

tires. Figure 29 illustrates the friction supply curves for the maximum friction measurements, providing both average values and two standard deviations below the average values, for both the full braking and full cornering conditions. Figure 30 presents similar information based on the skidding friction values rather than the maximum friction values. Equivalent curves for truck tires are shown in Figures 31 and 32. For comparison, Figures 29 through 32 also show the AASHTO maximum side friction factors used in horizontal curve design.

A goal of this analysis was to define reasonable estimates of the friction supply, $f_{\text{tire-pavement}}$, as a function of speed, and to represent the values in a manner easily interpreted in terms of lateral friction margins against skidding. The vehicle dynamics literature contains a wide array of tire–pavement models, and the choice of the LuGre model is a tradeoff between its comparatively high accuracy and modest computational demands. Because normal driving does not involve significant skidding, this tire model captures the vast majority of phenomenon of importance in this study. Further, the difference between the AASHTO maximum side friction factors used in horizontal curve design and the field-measured friction curves gives an estimate of the difference between the current geometric design policy based on the point-mass model and the friction levels demanded by more complex models. In Figures 29 through 32, the braking-only and cornering-only curves show a significant lateral friction margin against skidding between these and the AASHTO maximum side friction factors used in horizontal curve design, and thus the main areas of design concern are likely to arise primarily from interaction of braking and cornering forces.

In later sections where lateral friction margins are reported, the margins generally represent the difference between friction supply and friction demand. To avoid skidding or departure from a desired trajectory, the lateral friction margin should be positive.

To simplify the simulation process, the demanded friction levels are obtained from vehicle dynamic simulations that are run hereafter under "dry-road" assumptions. These dry-road simulations will demand much more tire force than can be achieved in wet-road or icy-road conditions. In contrast, the supply friction will be obtained from the passenger vehicle and truck curves in Figures 29 to 32, which are based on *wet-road* conditions. This difference in dry-road assumptions for calculating demand versus wet-road conditions for estimating friction supply is not only easier to simulate, but also it produces more conservative results. This conservatism accommodates friction transitions that commonly occur on roads but are hard to consider analytically. For example, a vehicle that is maneuvering on a dry road may encounter a wet patch of road within that maneuver (e.g., an area of the road that is drying more slowly than the surrounding road segments). In such a case, the tires could be demanding forces on entrance to the maneuver that are from a dry road, but friction availability along other portions of the road may be limited by wet-road conditions.

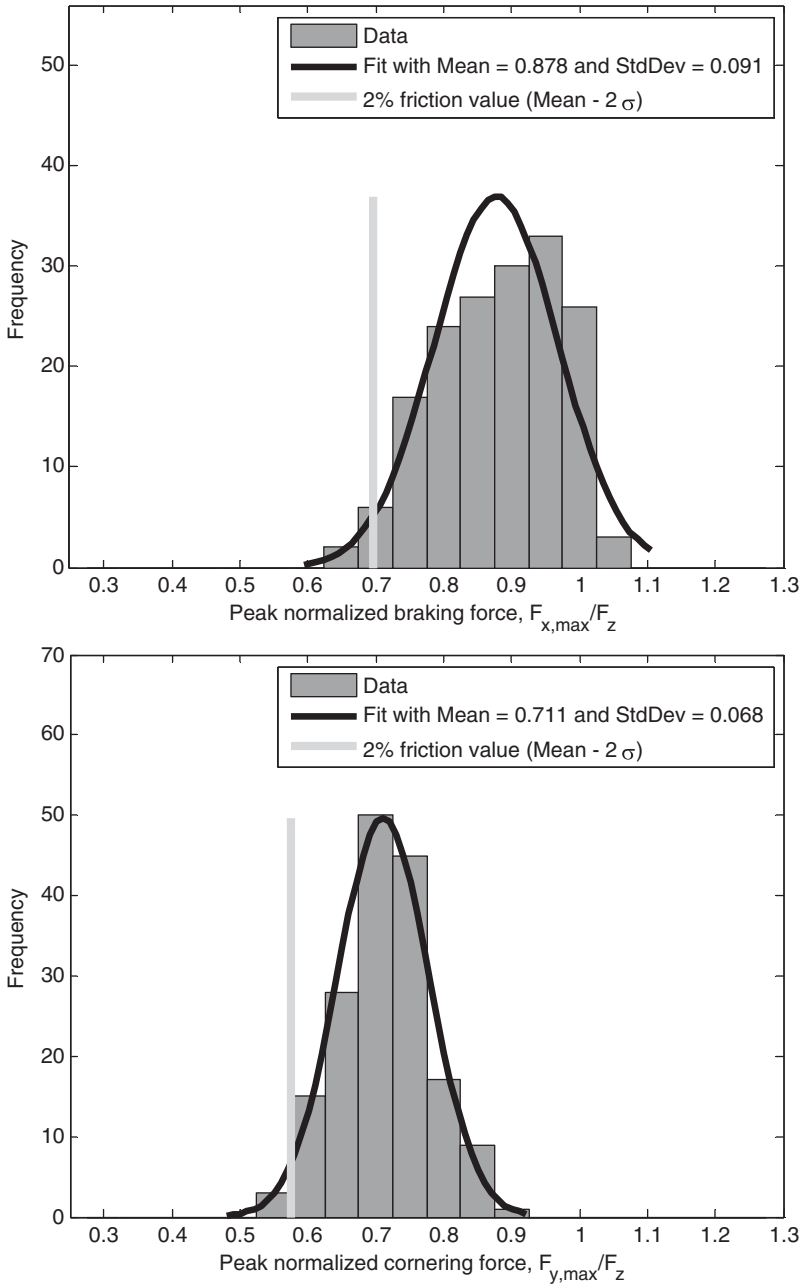

Figure 27. Distribution of maximum friction for longitudinal (braking) and lateral (cornering) directions across all sites for passenger vehicle tires (40 mph).

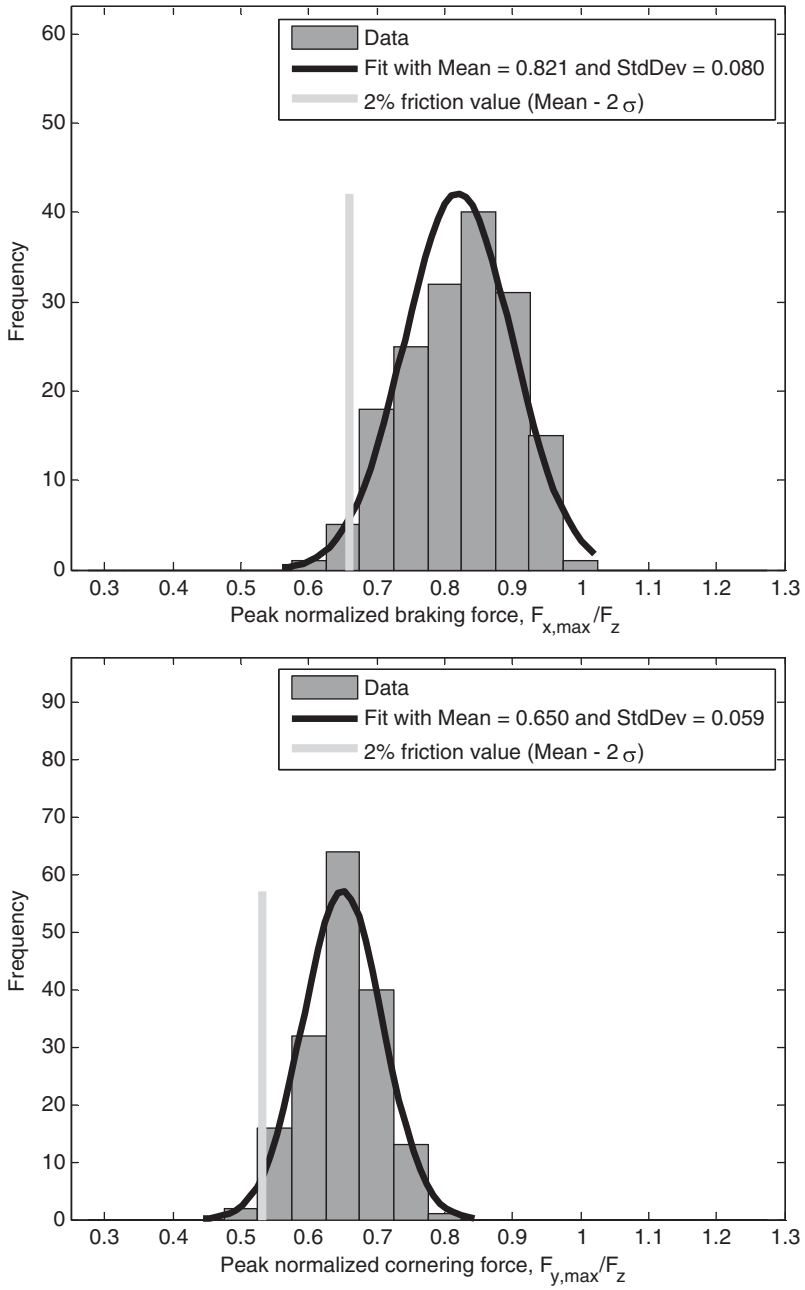

Figure 28. Distribution of maximum friction for longitudinal (braking) and lateral (cornering) directions across all sites for passenger vehicle tires (85 mph).

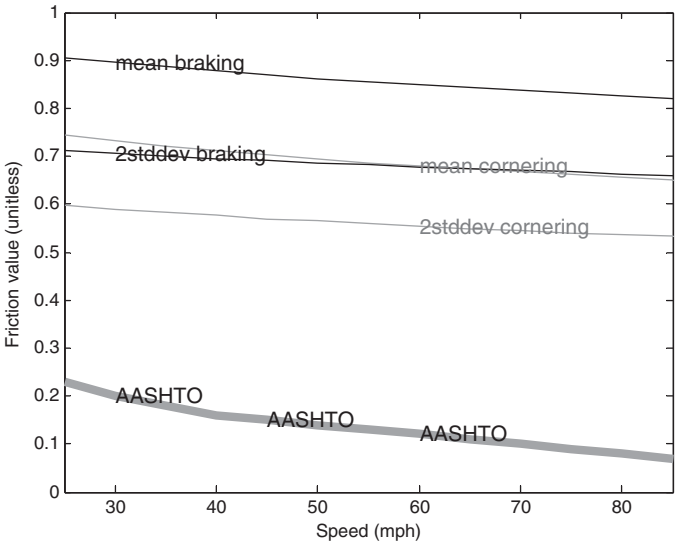

Figure 29. Passenger vehicle tire measurements of maximum wet-tire friction in longitudinal (braking) and lateral (cornering) directions (mean and two standard deviations below mean of the maximum friction supply).

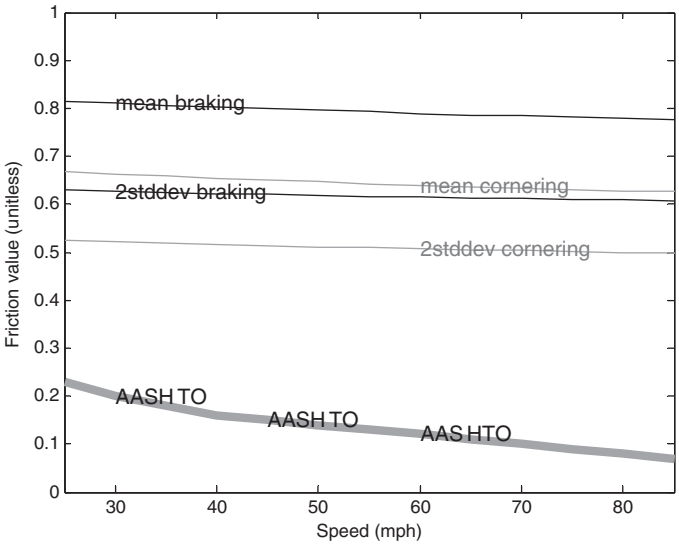

Figure 31. Truck tire measurements of maximum wet-tire friction in longitudinal (braking) and lateral (cornering) directions (mean and two standard deviations below mean of the maximum friction supply).

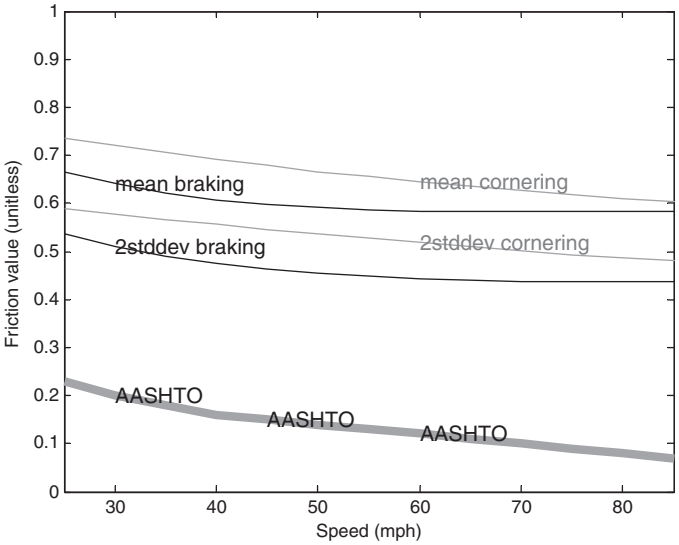

Figure 30. Passenger vehicle tire measurements of skidding wet-tire friction in longitudinal (braking) and lateral (cornering) directions (mean and two standard deviations below mean of the skidding friction supply).

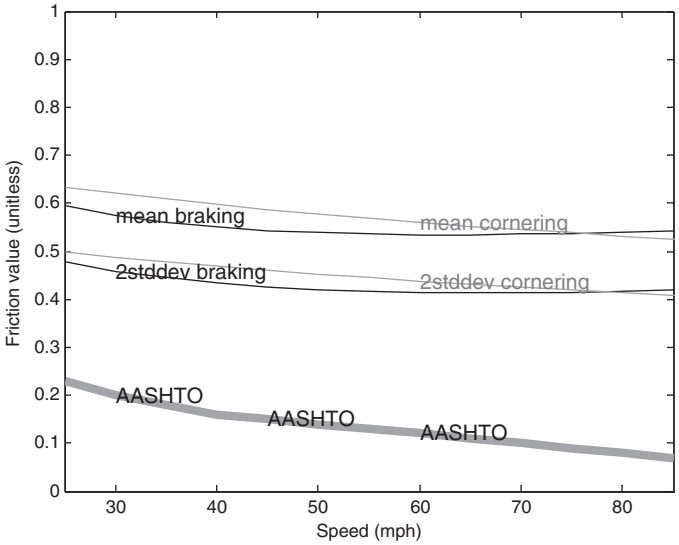

Figure 32. Truck tire measurements of skidding wet-tire friction in longitudinal (braking) and lateral (cornering) directions (mean and two standard deviations below mean of the skidding friction supply).

4.2.3 Summary of Key Results from Step 1

The results shown in Figures 29 to 32 allow comparisons between road friction measurements and the maximum side friction, f_{max}, used in the current AASHTO design policy for horizontal curves. The friction supply curves for both the lateral (cornering) and longitudinal (braking) directions for both passenger vehicles and trucks are higher than the maximum friction demand curves given by AASHTO policy. Thus, current horizontal curve design policy appears to provide reasonable lateral friction margins against skidding. The lowest friction supply curves in Figures 29 to 32 correspond to trucks in skidding conditions on roads whose friction is estimated to be two standard deviations below the mean; but even in these cases, the friction supply curve is at least 0.25 to 0.3 above the AASHTO maximum side friction. These figures already suggest a finding that is supported in later sections of the report: if there is going to be an area of concern based upon AASHTO's current design policy, it will likely arise primarily from the interaction of braking and cornering forces.

It is also worth noting that in most cases, the differences between the friction supply curves and demand side friction curves increase with speed, and the friction supply curves are generally the same shape as the maximum side friction curves assumed by AASHTO for horizontal curve design.

Finally, there is no indication that friction values vary in a consistent manner based upon location within a curve (e.g., upstream of the curve, at the PC, and within the curve).

4.3 Step 2: Define Road Geometries and Variable Ranges for Use in Subsequent Steps

The objective of Step 2 was to define the range of superelevations, horizontal curve radii, side friction levels, and grades to be considered in the analytical and simulation modeling analyses. Table 3-7 (Minimum Radius Using Limiting Values of *e* and *f*) in the 2011 *Green Book* provides a range of design values for consideration in this research. For example, design speeds range from 10 to 80 mph in 5 mph increments. Maximum superelevation ranges from 4% to 12%, in increments of 2%; and the maximum side friction factor ranges from 0.08 to 0.38. Current AASHTO policy also indicates some adjustment in superelevation rates should be considered for grades steeper than 5%. At minimum, it was important to investigate the full range of design values to sufficiently address the scope of this research and investigate design values that deviate from the norm to address potential concerns and/or modifications to the existing policy.

4.3.1 Analysis Approach

Table 20 illustrates the range of design values considered in the analytical and simulation modeling procedures. Basically, minimum-radius curves on grades of 0% and 4% to 9% in 1% increments were designed for design speeds of 25 to 85 mph, in 5 mph increments; for superelevation rates of 0% and 4% to 16%, in 1% intervals; and for side friction factors from 0.08 to 0.23 (as defined in Table 3-7 in the *Green Book*). For 85 mph, a side friction factor of 0.07 was assumed. Similarly, horizontal curves designed with curve radii of 0.8 R_{min} were analyzed. In addition to analyses of the hypothetical geometrics, the horizontal and vertical alignments and cross slopes of the 20 field sites (see Table 5) were fully defined for analysis purposes.

For analysis of the hypothetical geometries, speeds/decelerations of the vehicles also had to be defined. Four speeds/deceleration levels were selected for analyses:

- No deceleration (0 ft/s^2; i.e., constant speed)
- Curve-entry deceleration equivalent to –3 ft/s^2 based upon typical deceleration rates when entering a horizontal curve (see Section 3.3.3)
- Deceleration rates used in calculating stopping sight distance (i.e., –11.2 ft/s^2)
- Deceleration rates assumed for emergency braking maneuvers (i.e., –15 ft/s^2; analyzed for select cases)

For analyses of the 20 field sites, speed distributions of vehicles collected in the field were used (see Section 3.2).

For the variations in the minimum design radius, reducing the design radius from R_{min} to 80% of R_{min} can either be analyzed as a geometric change, a speed change, or a friction change. This is best understood by considering the point-mass model on which the AASHTO policy is based and considering

Table 20. Range of design values for analytical and simulation modeling.

Variable input parameter	Range
R	R_{min}, $0.8R_{min}$
V	25 to 85 mph (5-mph interval)
e	0%, 4% to 16% (1% interval)
G	0%, 4% to 9% (1% interval) (downgrades and upgrades)
a_x	Four levels of deceleration (0, –3, –11, and –15 ft/s^2)

a horizontal curve with no superelevation. From Equation 7, the relationship between radius, speed, and friction will be approximately:

$$\frac{V^2}{gR} = f + 0.01e \tag{20}$$

From this equation, if the speed is kept the same while the radius is reduced by 80%, then the acceleration would be balanced if the demanded friction and superelevation are both increased by a factor of 1/0.8, or 1.25. Similarly, on the left-hand side of the equation, the effect of decreasing the radius by 0.8 and keeping the speed fixed is equivalent to increasing the speed by 11.8% (the square-root of 1/0.8) and keeping the radius fixed. For horizontal curves without superelevation, the right-hand side of the equation is simply the demanded friction. In this case, a decrease in radius by 0.8 requires an increase in demand friction by 1.25. This, in turn, corresponds to forcing a systematic downward shift of the friction margins for the R_{min} case to the $0.8R_{min}$. Thus interpretation of the reduced-radius case can be used to additionally understand outcomes for situations of overspeed, low superelevation, or reduced friction margins.

Although not explicitly indicated in Table 20, the analyses primarily focus on sharp horizontal curves on steep downgrades; however, consideration is also given to sharp horizontal curves on steep upgrades in Section 4.12.

4.3.2 Summary of Key Results from Step 2

The primary purpose of this step was to define the full range of design values for consideration in the analytical and simulation modeling. The range of design values selected for detailed investigation include the following:

- Speed: 25 to 85 mph (and actual speeds measured at the study sites)
- Superelevation: 0%, 4% to 16%
- Grades: 0, 4% to 9%
- Curve radius: minimum curve radii (R_{min}) based upon current AASHTO policy (and curves with radii of $0.8R_{min}$)
- Deceleration: 0, −3, −11.2, and −15 ft/s^2

4.4 Step 3: Develop Side Friction Demand Curves and Calculate Lateral Friction Margins against Skidding Considering Grade Using the Modified Point-Mass Model

The objective of Step 3 was to develop side friction demand curves for hypothetical geometries covering the full range of design values defined in Step 2 using the modified point-mass model and calculate lateral friction margins against skidding considering the friction supply curves ($f_{tire\text{-}pavement}$) developed in Step 1. Using the modified point-mass model, the calculated side friction factors account for grade and vehicle deceleration on the curve. The adjusted side friction factors were compared to the friction supply curves from Step 1 to estimate the lateral friction margins against skidding.

4.4.1 Analysis Approach

The point-mass model (see Section 2.1), which serves as the basis for horizontal curve design, was modified to account for the effects of grade and deceleration. For a given curve radius, superelevation, grade, and design speed, physics is used to calculate the tire force utilization for steady driving. This is done via a force balance on the point mass, while using a simple friction ellipse representation of the tire to define skidding events. To develop side friction demand curves, a modified point-mass model was derived for a vehicle traversing a downgrade with superelevation. The assumption of small angle representation (i.e., $\cos\theta = 1$ and $\sin\theta = \theta$) is made to maintain simplicity within equations. The free body diagrams for the point-mass model are shown in Figure 2 for the lateral direction, and in Figure 33 for the longitudinal direction.

In Figures 33 and 2, F_b and F_c represent the braking and cornering forces acting on the vehicle point mass while γ and α represent the grade and superelevation angles, respectively. The deceleration, a_x, is directed along the vehicle's longitudinal axis. After applying a force balance using Newton's second law for a body rotating with angular velocity around a curve with constant radius, R, the three governing equations for vehicle motion in the X-, Y-, and Z-directions can be obtained as follows (Varunjikar, 2011).

Braking Equation: $$F_b = ma_x - mg\frac{G}{100} \tag{21}$$

Cornering Equation: $$F_c = m\frac{V^2}{R} - mg\frac{e}{100} \tag{22}$$

Weight Balance Equation: $$N = mg \tag{23}$$

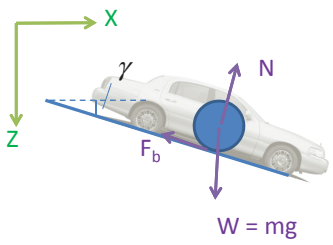

Figure 33. Longitudinal forces acting on a vehicle point-mass model.

These equations can be simplified by substituting Equation 23 into Equations 21 and 22, and then simplifying the result using the friction factors from Equations 13 and 14 to obtain:

$$f_x = \frac{a_x}{g} - \frac{G}{100} \tag{24}$$

$$f_y = \frac{V^2}{g \cdot R} - \frac{e}{100} \tag{25}$$

Here, the terms f_x and f_y represent the friction demand in the braking (longitudinal) and cornering (lateral) directions. These depend on a_x, which is the braking-induced deceleration; g, the gravitational constant; G, the road grade (which is negative for downgrades); V, the vehicle forward speed; R, the curve radius; and e, the road superelevation (positive values lean the vehicle to the inside of the curve).

Comparing Equations 24 and 25 to Equation 10 used by AASHTO, Equation 25 is equivalent, while Equation 24 adds an additional equation for the longitudinal friction factor. This point-mass section is restrained to constant curves, i.e., curves with a minimum constant-radius design, so the radius, R_{min}, is given by Equation 9. If Equation 9 is substituted into Equation 25, $f_y = f_{max}$, Equation 25 implies that the side friction demand is independent of the superelevation, grade, or braking demand. However, both grade and braking deceleration influence longitudinal friction demand f_x through Equation 24, which in turn reduces the overall lateral friction margin through Equation 18. Thus, in the absence of braking forces, this point-mass vehicle will have the same lateral friction margins for each superelevation and grade. With the addition of braking forces, however, the conditions change slightly as the total friction demand of a point-mass model for a vehicle is represented by f_x and f_y together.

4.4.2 Analysis Results

Plots of friction supply and lateral friction margins are shown in Figures 34 and 35 for passenger vehicles for a range of grades and design speeds, assuming a superelevation of 8% and constant speed. In Figure 34, the effective lateral supply friction values (Equation 17) are plotted versus the AASHTO design friction values. For the point-mass model, the lateral friction demand is equal to the AASHTO design friction for minimum-radius curves. In Figure 34, the deceleration of the vehicle is zero, meaning that braking is applied at a level sufficient to prevent the vehicle from accelerating down the grade. Both the mean lateral friction supply and the lower-bound lateral friction supply (mean minus two standard deviations, e.g., the 2-sigma values) are shown to illustrate the statistical range in friction supply.

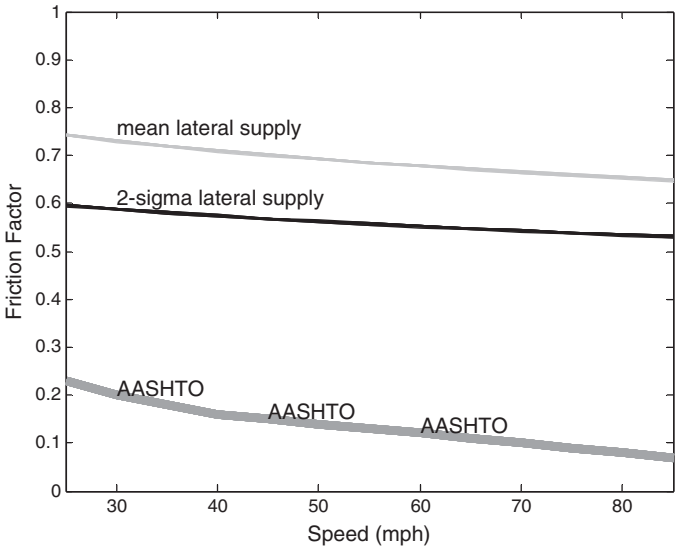

Figure 34. Lateral friction factors from modified point-mass model for passenger vehicle (G = 0% to −9%, e = 8%) (a_x = 0 ft/s²).

In Figure 35 the lateral friction margins are plotted for the same situations. The friction margin is simply the difference between the lateral friction demand and the effective lateral friction supply. For this case (e.g., the modified point-mass model), the lateral friction margins increase slightly with speed. Throughout nearly all the results that follow, the mean lateral friction margin is roughly 0.12 higher than the 2-sigma lateral friction margin, and so only the 2-sigma lateral margin is shown in the plots hereafter.

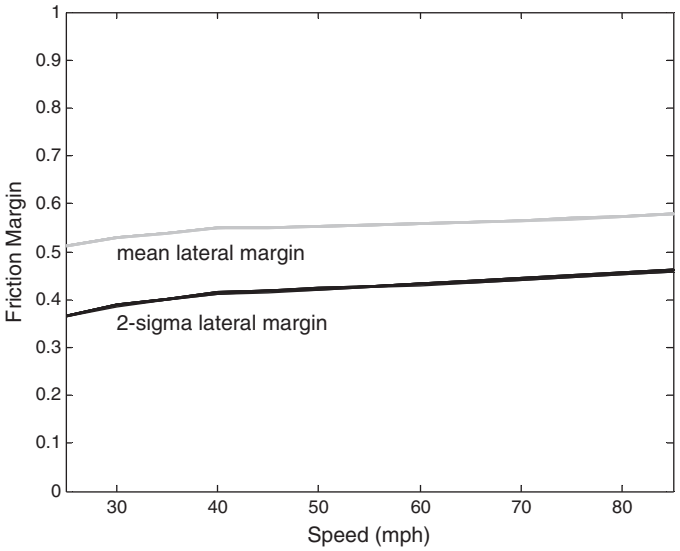

Figure 35. Lateral friction margins from modified point-mass model for passenger vehicle (G = 0% to −9%, e = 8%) (a_x = 0 ft/s²).

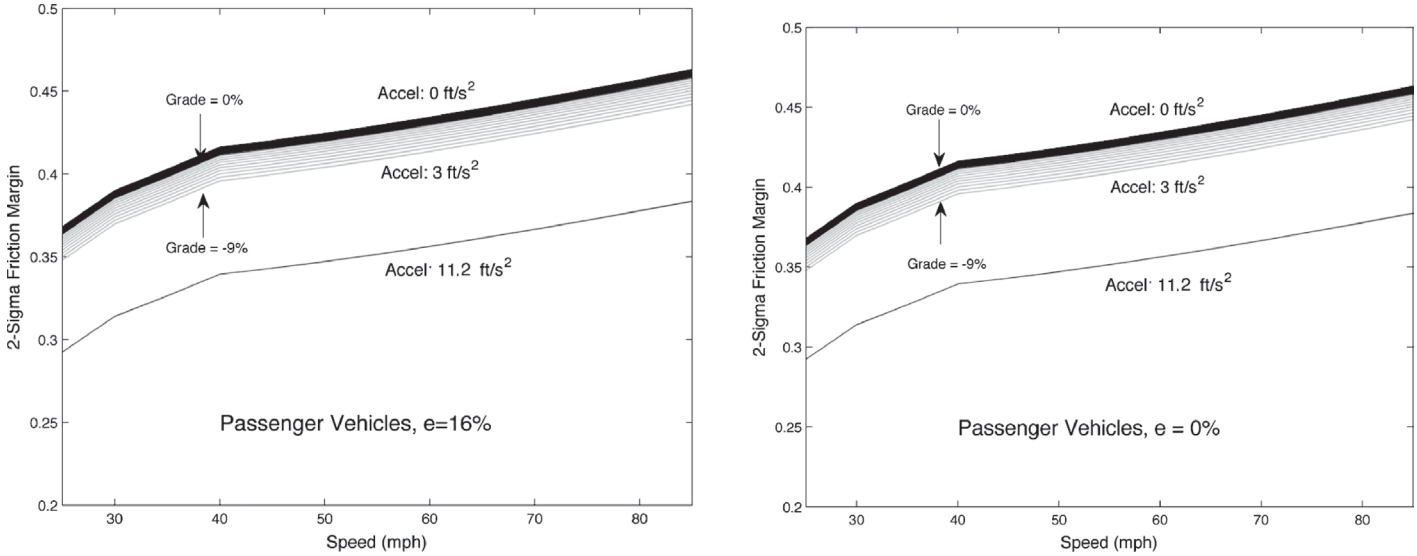

Figure 36. Lateral friction margins from modified point-mass model for passenger vehicles (G = 0% to −9%, e = 0 and 16%) (a_x = 0, −3, and −11.2 ft/s²).

For different braking values, the lateral friction margins change because the braking forces utilize some of the reserve lateral friction available. Three decelerations levels (0, −3, and −11.2 ft/s²) are shown in Figure 36 for passenger vehicles and in Figure 37 for trucks. The grades range from 0% to −9% (downgrade) and, to illustrate the effects of superelevation, lateral friction margins are shown for superelevations of 0% and 16%. These figures illustrate that, for the modified point-mass model, lateral friction margins decrease with increased braking and the addition (or lack) of superelevation has no effect on the lateral friction margins. This result may seem counterintuitive, but the primary influence of superelevation for the modified point-mass model is to change the minimum radius. Thus, the effect of superelevation is negated by the respective flattening or tightening of the curve radius.

4.4.3 Summary of Key Results from Step 3

Key findings from Step 3 are as follows:

1. Lateral friction margins decrease substantially with increased braking, and also decrease slightly with increasingly steeper downgrades.
2. Current AASHTO policy provides increasing lateral friction margins for increasing speeds for both passenger vehicles and trucks. Results presented in later sections show

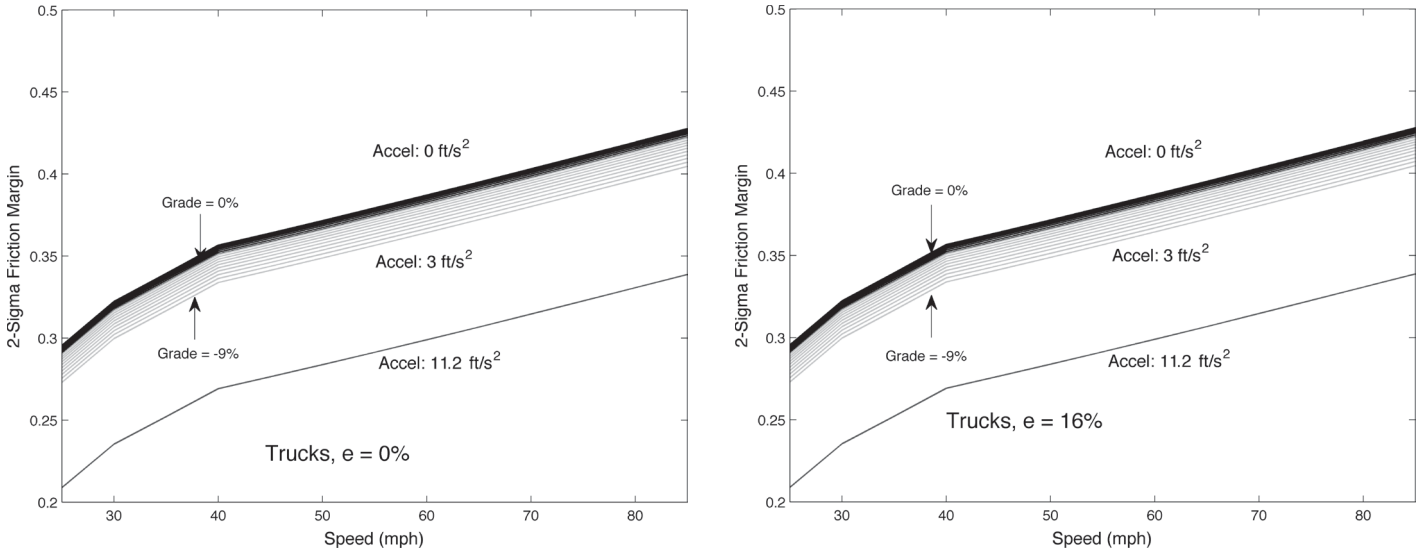

Figure 37. Lateral friction margins from modified point-mass model for trucks (G = 0% to −9%, e = 0 and 16%) (a_x = 0, −3, and −11.2 ft/s²).

that this might not apply to more realistic (i.e., complex) vehicle models.

3. In general, trucks have a lateral friction margin about 0.06 less than passenger vehicles, simply due to differences in the tire friction curves.
4. The –3 ft/s^2 deceleration case on a level road (0% grade) corresponds roughly to the zero deceleration case for a grade of –9%; these two curves overlap. In other words, if a driver was trying to maintain a constant speed while approaching an unfamiliar downgrade section and was expecting a downgrade of no more than 9%, the expected behavior would be to hit the brakes immediately prior to the downgrade. The amount of lateral friction margin utilized under this situation is consistent with –3 ft/s^2 deceleration on a level road. The Bonneson (2000b) study, as well as the measured variation in driver decelerations throughout downgrades that this work measured via the instrumented vehicle, suggests that drivers are comfortable with these friction margins. Roadway designs that necessitate deceleration requirements outside the usual variations seen in both this study and by Bonneson (2000b)—e.g., grades outside of 9% magnitudes—may require additional levels of caution and driver warning.
5. For the –11.2 ft/s^2 deceleration case, the friction utilizations are all the same, regardless of grade. This is because the stopping sight distance deceleration is assumed in the AASHTO *Green Book* to vary with grade. This variation nullifies grade's influence on friction margins. The deceleration value used in simulation was modified as per AASHTO stopping sight distance deceleration policy; specifically, the deceleration used in the actual simulation, a'_x, is given by:

$$a'_x = a_x - g\frac{G}{100} \tag{26}$$

Where G is defined as a positive number representing *downgrade*, and g is the gravitational constant. This stopping sight distance deceleration formula used by AASHTO is based on a simplistic vehicle dynamics model, which ignores potentially important effects like weight transfer, tire load sensitivity due to said weight transfer, and the static weight and friction demand differences between individual axles and tires on a vehicle.

4.5 Step 4: Define Vehicles and Maneuvers to Use in Non-Point-Mass Models

The objective of Step 4 was to define the family of vehicles and range of maneuvers (e.g., lane changes, deceleration levels) to be considered in subsequent analyses by models other than the modified point-mass model.

4.5.1 Analysis Approach

Six classes of vehicles were selected for consideration in subsequent analyses:

- **Passenger vehicles**
  - E-class sedan (i.e., mid-class sedan)
  - E-class SUV (i.e., mid-size SUV)
  - Full-size SUV
- **Trucks**
  - Single-unit truck
  - Tractor semi-trailer truck
  - Tractor semi-trailer/full-trailer truck (double)

These vehicle classes were selected because they represent a high proportion of vehicles in the current vehicle fleet, because of their operating characteristics, and in particular because of their propensity for involvement in rollover crashes. In addition, these vehicle classes are commonly incorporated in vehicle dynamic simulation packages. Tractor semi-trailer trucks with an attached tanker trailer were not specifically considered in the simulation analyses because existing vehicle dynamics models do not have the capability to simulate the dynamic effects of liquid sloshing in a tank trailer.

To "define" a vehicle, each of the models requires a number of vehicle input parameters. A set of vehicle parameters representative of general vehicle classes were defined through a combination of literature review and default values found in the vehicle dynamics software. The range of input parameters needed for simulation analyses included the following:

1. Inertia properties: mass, z-axis mass moment of inertia about the center of gravity (CG) of the total vehicle, mass of payloads for trucks
2. Dimensions: wheelbase, CG height, distances from CG of sprung/unsprung mass to front/rear axle along x-axis, track width, and location of payloads and hitch points on trucks
3. Suspension: The natural frequency and damping ratio of the vehicle in pitch (Note: results for the bicycle models in Section 4.8 showed that suspension did not have an appreciable effect on friction margins.)

Appendix B includes the vehicle input parameters selected for use in the simulation modeling.

As indicated in Step 2, four deceleration levels were considered to resemble various driving conditions for steady-state and transient behavior for use in non-point-mass models. These maneuvers each provide the braking force required to simulate constant speed (0 ft/s^2), natural speed reduction upon curve entry (–3 ft/s^2), stopping sight distance deceleration (–11.2 ft/s^2), and emergency braking situations (–15 ft/s^2). By increasing the amount of brake force, it will decrease the force

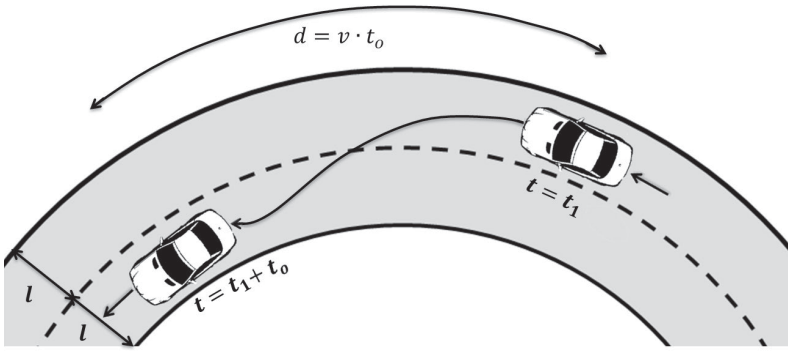

Figure 38. Lane-change maneuver.

available in the lateral direction and thus decrease the cornering abilities of the vehicle. Speed distributions of vehicles collected in the field were also used to confirm that simulations were using a range of speeds similar to those measured from vehicles at the actual field sites.

To initiate a braking scenario, the simulated vehicle is initialized so that it operates in a steady-state cruising situation. For most analyses that follow, the vehicle enters the horizontal curve from a tangent section. The initial constant speed is the design speed for the curve. The vehicle brakes and a step steering input is applied at various points in the curve. Since the deceleration, a_x, is assumed to be constant, the braking inputs are found using a brake-proportioning model that rapidly changes the braking forces to match deceleration. Because suspension dynamics are ignored in the bicycle models that follow, the weight shift due to deceleration is assumed to be rapid compared to the vehicle's motion through the curve. In the multibody models, the suspension dynamics are included and considered.

To determine the worst portion of the curve to initiate a brake maneuver, a set of simulations was performed using a transient bicycle model for an E-class SUV cruising at design speed of 60 mph on the tangent section and then entering the curve around $t = 2$ s with a constant deceleration rate of -3 ft/s^2. The steady braking was initiated at different portions of the curve for each simulation:

- **Case 1:** brakes applied after the vehicle enters steady state on the curve
- **Case 2:** brakes applied after the vehicle enters the curve but before it reaches steady state
- **Case 3:** brakes applied at the same time as steering input initiated entering the curve

The results for each case were very similar, but the maximum lateral friction demand was obtained when the vehicle brakes after reaching steady state (Case 1). These results were confirmed as well in Step 7 (see Section 4.8). In the sections that follow, when braking maneuvers are applied, they are applied well after the onset of the curve unless otherwise noted.

A common lane-change maneuver was also considered for analysis in later sections. Initially traveling at steady state on a curve at the design speed, the vehicle moves from a low-speed lane to a high-speed lane at a constant speed as shown in Figure 38. It was assumed that the curve was to the left, and therefore, the lane change was toward the inside of the curve. A lane width, l, of 12 ft is assumed for analysis purposes. The steering input used for the lane-change simulations is one sine wave with a time period of t_s. This sine wave steering input is applied in addition to the nominal steering input, δ_{curve}, required for traveling on a curve as shown in Figure 39. Data on lane-change maneuvers were also collected as part of the speed and vehicle maneuvers studies (see Section 3.2); and in particular, the duration of lane-change maneuvers measured in the field were considered in Steps 7 through 10 of the simulation modeling.

4.5.2 Summary of Key Results from Step 4

In this step the primary vehicle input parameters were selected for use in the simulation modeling. Appendix B provides more detail on the vehicle input parameters. Also it

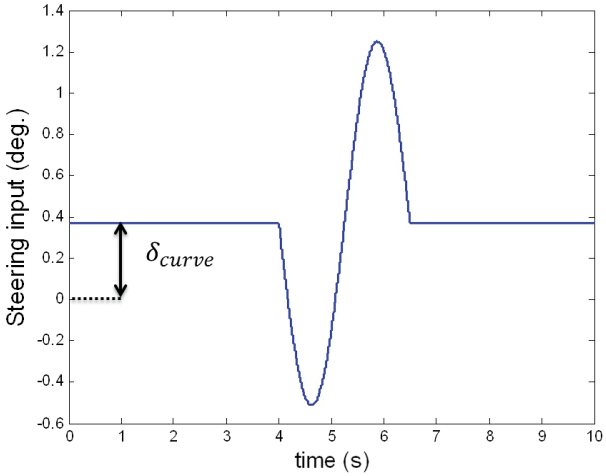

Figure 39. Steering input for lane-change maneuver.

was determined that the maximum lateral friction demand is required when the vehicle brakes after reaching steady state (Case 1). Therefore, in subsequent analyses investigating braking maneuvers, the brakes are applied well after the onset of the curve unless otherwise noted.

4.6 Step 5: Predict Wheel Lift Using Quasi-static Models

The objective of Step 5 was to find the static rollover thresholds for the six vehicle classes included in this study to check if vehicle maneuvers at design speeds on downgrades with curves could induce wheel-lift events for a given road geometry considering horizontal curvature, grade, and superelevation. Because roadway design is focused on providing low levels of side friction demand for vehicles relative to the maximum side friction supply at the tire–pavement interface, it is possible that a vehicle could experience wheel lift prior to a skid event occurring. This step is aimed at predicting wheel lift for a vehicle traveling on a curve using quasi-static models.

4.6.1 Analysis Approach

In this step, a rollover model to predict wheel lift was developed to account for the effect of superelevation. The prediction of wheel lift involves expressing the rollover threshold of the vehicle using laws of mechanics. For roads without superelevation or grade, the rollover threshold for a rigid-vehicle model using quasi-static analysis is

$$f_{rollover} = \frac{T}{2h} \tag{27}$$

where T is the track width and h is the CG height (Gillespie, 1992). This is a well-known and classic result, but it does not include superelevation effects or suspension effects.

To include superelevation and suspension within the classical analysis, this step involved the following tasks:

1. Derive the quasi-static rollover model for a rigid and/or suspended vehicle accounting for superelevation.
2. Find rollover threshold for each representative vehicle and compare it with the lateral accelerations obtained from the modified point-mass analysis in previous steps.
3. Identify those roadway conditions, for further investigation, where the lateral accelerations generated are higher than the rollover threshold.

The static rollover/wheel-lift predictions do not directly depend on the tire–pavement friction. However, this method will indicate whether a wheel-lift event or a skidding event will occur first as vehicle speed increases. For example, if the wheel-lift threshold for lateral acceleration is higher than the friction limit, then skidding will take place before wheel lift. Further, if the wheel-lift threshold is significantly higher than the actual lateral acceleration necessary to negotiate the curve, then again wheel lift is unlikely during normal maneuvers on a curve.

The quasi-static rollover model for use on superelevated roads is based on a static force balance on a simplified representation of a vehicle, which includes only a rudimentary representation of suspension effects. The approach is nearly identical to the point-mass, rigid-vehicle model analysis that produces Equation 27, except superelevation is considered and the roll axis of the vehicle is added. The setup of the model is shown in Figure 40 which illustrates the rear view of a suspended vehicle traversing a curve to the right. Figure 40 shows the forces acting on the suspended vehicle. Due to lateral load transfer, the normal load on the outside wheel, F_{zo}, increases. This can be associated with the sprung mass rolling with a lateral shift in the CG toward the outside of the curve. The sprung-mass CG rotates about a point called the roll center, whose position depends on the suspension geometry. For the analysis, it is assumed that the roll-center position:

- Does not change,
- Is aligned with the center of the vehicle, and
- Is a fixed height above the road surface.

The parameters in the static rollover model shown in Figure 40 are defined as follows:

h = Height of sprung-mass CG
h_r = Height of roll center
T = Track width
ϕ = Roll angle
F_{zi} = Normal load on inner tires
F_{zo} = Normal load on outer tires
F_{yi} = Lateral force on inner tires
F_{yo} = Lateral force on outer tires

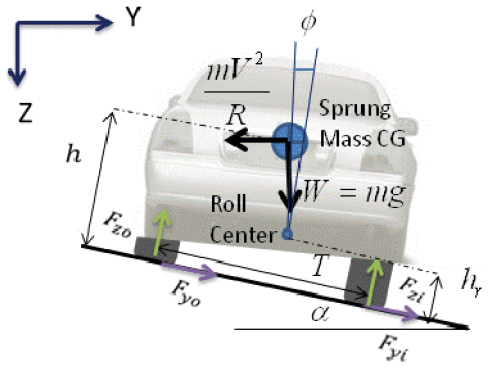

Figure 40. Static rollover model modified to include superelevation.

This model associates the rollover event with the onset of wheel lift, characterized by the normal load on the inside wheels going to zero ($F_{zi} = 0$). It can be assumed that $F_{zi} \approx 0$ just before wheel lift occurs. Balancing the moments about the outer tire contact point,

$$\sum M = -h \cdot \left(m\frac{V^2}{R} - mg \cdot \sin(\alpha) \right) + \left(\frac{T}{2} - (h - h_r) \cdot \phi \right) \cdot mg \cdot \cos(\alpha) = 0 \quad (28)$$

Substituting $a_y = V^2/R$ into Equation 28, and using the small angle approximation yields:

$$-h \cdot \left(\frac{a_y}{g} - \alpha \right) + \left(\frac{T}{2} - (h - h_r) \cdot \phi \right) = 0 \quad (29)$$

and therefore:

$$\frac{a_y}{g} + \frac{(h - h_r)}{h} \cdot \phi = \frac{T}{2h} + \frac{e}{100} \quad (30)$$

For steady-state analysis, the roll angle of the vehicle body can be written as a roll gain, in rad/g, multiplied by the lateral acceleration in g's (e.g., $\phi = R_\phi \cdot \frac{a_y}{g}$). Substituting this expression, Equation 30 can be rewritten in the final form used in this study:

$$\frac{a_y}{g} + \frac{(h - h_r)}{h} \cdot R_\phi \cdot \frac{a_y}{g} = \frac{T}{2h} + \frac{e}{100}, \text{ or}$$

$$\frac{a_y}{g} = \frac{\frac{T}{2h} + \frac{e}{100}}{1 + \left(1 - \frac{h_r}{h}\right) \cdot R_\phi} \quad (31)$$

Equation 32 gives the rollover margin based on lateral acceleration, which represents the difference between the maximum lateral acceleration allowable before wheel lift and the curve-induced lateral acceleration, a_y.

$$RM_{ay} = \underbrace{\frac{\frac{T}{2h} + \frac{e}{100}}{1 + \left(1 - \frac{h_r}{h}\right) \cdot R_\phi}}_{\text{maximum steady acceleration prior to wheel lift}} - \underbrace{\frac{a_y}{g}}_{\text{normalized acceleration within curve}} \quad (32)$$

This rollover margin is for a rigid vehicle considering a simple suspension model and the superelevation of the roadway.

From Equation 32, a few observations can be made immediately. First, since Equation 32 only depends on lateral forces, the grade of the road has no effect on wheel lift, nor does speed influence the rollover threshold. For vehicles with suspension, the worst-case conditions are those vehicles with a high roll gain (R_ϕ) and low roll axis compared to CG height (e.g., h_r/h is close to zero or even negative). This agrees with intuition, as these assumptions represent top-heavy vehicles with "soft" suspensions.

Further, if one assumes a rigid vehicle without suspension (e.g., $R_\phi = 0$), then Equation 32 becomes:

$$RM_{ay} = \left(\frac{T}{2h} + \frac{e}{100} \right) - \frac{a_y}{g} \quad (33)$$

For this rigid-vehicle model, increasing superelevation directly shifts the rollover threshold upward. This agrees with intuition, as well as the current AASHTO design policy which allows tighter curve radii in the presence of higher superelevation. For a vehicle without any suspension roll and on a road without any superelevation, the rollover threshold portion of Equation 33 reduces to $T/2h$, which agrees exactly with Equation 27.

To develop approximate estimates of how a suspension-vehicle model will differ from a rigid-vehicle model, an approximate value of $R_\phi = 0.17$ rad/g was assumed given the fact that most vehicles exhibit approximately 1° of roll per 0.1 g of lateral acceleration (10°/g corresponds to 0.17 rad/g). The ratio of h_r/h is generally between 0.25 and 0.75 for most vehicles, but a worst-case value would be to set this ratio to zero. Similarly, the worst-case road is one without superelevation. Therefore, the worst-case rollover margin would be approximately:

$$RM_{ay} \approx \frac{\frac{T}{2h} + \frac{e}{100}}{1 + R_\phi} - \frac{a_y}{g} \approx \frac{1}{1.17}\left(\frac{T}{2h}\right) - \frac{a_y}{g} \approx 0.85\left(\frac{T}{2h}\right) - \frac{a_y}{g} \quad (34)$$

4.6.2 Analysis Results

Sample rollover thresholds ($T/2h$ values) for the vehicles used in this study are given in Table 21 considering a superelevation of 4%. For trucks, these margins are given for their trailers, as the trailer margins are far lower than the tractor; however, the trailer can be loaded in an infinite number of configurations, resulting in a wide range of margins that could potentially be achieved. The maximum side friction (f_{max}) recommended by AASHTO policy, for the speeds considered in this study, ranges from 0.07 for a design speed of 85 mph to 0.23 for a design speed of 25 mph. Comparing the rollover thresholds to AASHTO's maximum side friction values for

Table 21. Rollover thresholds (*T*/2*h*) for vehicles used in this research.

Vehicle class	Rollover threshold in *g*'s	Adjusted rollover threshold (~0.85 *T*/2*h*)[a]
E-class sedan	1.36	1.16
E-class SUV	1.10	0.94
Full-size SUV	1.22	1.04
Single-unit truck	0.87	0.74
Tractor semi-trailer truck	0.56 (trailer)	0.48
Tractor semi-trailer/full-trailer truck	0.56 (trailer)	0.48

[a] Rollover threshold (*T*/2*h*) = ~ 0.85 × rollover threshold in *g*'s.

design speeds of 25 mph or greater, it can be deduced that wheel lift will not occur for passenger vehicles or trucks driving at the design speed on a curve designed according to current AASHTO policy. Note, though, that at design speeds below the scope of this research (i.e., design speeds of 10 and 15 mph), the maximum side frictions according to current AASHTO policy are 0.32 and 0.38, respectively. The rollover margin at these low design speeds is still positive, but the margin is decreasing with speed because the maximum side friction (f_{max}) recommended by AASHTO policy increases with speed.

Note also that Harwood et al. (2003) reported conservative (worst-case) rollover thresholds for trucks to be approximately 0.35. Assuming 85% of this value gives approximately 0.30 for the estimated rollover threshold, when accounting for superelevation and suspension. Thus, at lower design speeds rollover becomes more of a concern.

For tractor semi-trailers, the truck configuration and type of cargo influences the vehicle's roll stability. The effects of liquids in cargo tank trucks are of particular concern. While detailed simulations of fluid–vehicle interaction is beyond the scope of this research, previous work provides good approximations of rollover thresholds suitable to estimate situations that may lead to the onset of a rollover. Notable work includes that of Gillespie and Verma (1978) who found that lateral acceleration at wheel lift was 0.36 for liquid-cargo tank trucks (due to their higher CG and different suspension) versus 0.54 for the typical tractor semi-trailer—a value similar to the 0.56 value found in modern simulations and studies (Table 21). Their work also noted that liquid-cargo tank trucks were much more susceptible to rollover due to rearward amplification effects. A comprehensive study of slosh dynamic effects was conducted by Ervin et al. (1985) to assist in federal rule making for liquid-cargo transport. They found that, of 30 reported crashes from California data, 22 crashes occurred during transport of underfilled cargo containers; definitive cause/effect relationships between liquid-cargo motion and vehicle rollover, however, could not be established. Subsequent analyses revealed that some rollover cases would have occurred even for rigid-cargo motion. Ervin et al. note that peak liquid force amplitudes were 2 to 3 times larger for liquid cargo than for the same mass of rigid cargo. These amplification factors closely agree with the amplification factor of 2 numerically computed by Modaressi-Tehrani et al. (2007).

To quantify the effect of liquid-cargo influence, Evrin et al. examined the difference in lateral accelerations resulting in overturn. These results indicate that liquid-cargo tank trucks may have rollover thresholds that are half of comparable rigid-cargo rollover thresholds. However, the minimum lateral rollover thresholds for liquid-cargo tank trucks are nearly always the same as that of an empty tanker. All lateral rollover thresholds were 0.25 to 0.30, which are similar to the rollover thresholds assumed by Harwood et al. (2003) for truck rollover stability when accounting for superelevation and suspension effects.

Ervin et al. (1985) also note that the worst-case lateral slosh frequencies are between 0.5 and 0.8 Hz, with lower frequencies corresponding to less-full cases. The effect of sight distance on a vehicle's excitation at various frequencies is also considered, with results showing that roads with more limited sight distance will tend to cause more excitation at frequencies of liquid-cargo resonance (between 0.2 and 0.4 Hz) versus typical steering input excitations for roads with unrestricted sight distance, which tend to contain frequencies around 0.15 Hz. For these oscillation frequencies, Ervin et al. note that lateral accelerations of 0.25 or less will generally not cause overturn based on a harmonic analysis. Again, these results are in agreement with the experimental results presented earlier and assumptions by Harwood et al. Further, both results suggest that the 50% full-loading condition is likely the "worst-case" loading situation for harmonic fluid motion. For braking, recent work by Biglarbegian and Zu (2006) showed that liquid-cargo tank trucks require approximately 30% more distance than rigidly loaded trucks due to weight-transfer effects of the fluid.

Thus, the most conservative interpretation of the literature on liquid-cargo tank trucks is to assume a lateral rollover threshold value of 0.30 or half a rigid vehicle's nominal value, whichever is less. The lowest rollover threshold for trucks in

Table 21 is 0.56, and half this value is 0.28, which for practical purposes is the same as a rollover threshold value of 0.30. This suggests that the lateral accelerations in curves, and hence the maximum side friction values used for design, should be limited to values less than 0.30. In general practice, a rollover threshold of 0.28 to 0.30 is particularly conservative since the default loading of most trucks is expected to have nominal $T/2h$ values of approximately 0.56 as noted in Table 21. Further, liquid-cargo tank trucks in modern practice are generally discouraged from carrying half-filled tanks, and thus the completely filled or empty tanks produce rigid-load behaviors that are generally more predictable and more in agreement with the 0.56 value than 0.30. The difference between the 0.56 rollover threshold value expected in practice, versus the 0.30 rollover threshold value based on the summary of previous research, suggests that there is conservatism added to the low-order model analysis that likely includes extreme cases (i.e., partially filled liquid-cargo tanks) as well as expected errors inherent in such a simple rollover vehicle model. It should also be noted that in the *Comprehensive Truck Size and Weight Study* (FHWA, 1995), an appendix states that crash data show so few fatalities with rollover thresholds less than 0.35 that rates cannot be calculated, suggesting that few vehicles on the road have rollover thresholds less than 0.35.

4.6.3 Summary of Key Results from Step 5

The following findings were obtained from the analysis in Step 5 focusing on roll margins for *steady-state driving*, e.g., driving without abrupt steering inputs that might excite transient lateral accelerations:

1. For passenger vehicles, the rollover thresholds are far higher than the available friction on the road. There seems to be no concern of a passenger vehicle rolling over while traveling at the design speed on a curve designed according to current AASHTO policy. This is simply because the tires will skid before the rollover threshold is reached.
2. For trucks, the rollover thresholds are much lower. For design speeds greater than 30 mph, trucks are not expected to exhibit wheel lift under current AASHTO design policy. At design speeds of 25 or 30 mph, AASHTO policy allows maximum side friction values that are nearer to the rollover thresholds for trucks, but not sufficient to cause rollover. For design speeds below the scope of this research (e.g., 10 and 15 mph), the rollover margins are still positive but are decreasing with speed. Thus, rollover for trucks is of more concern at lower design speeds than at higher design speeds.
3. Based upon a review of the literature, the lowest rollover thresholds for tanker trucks (i.e., liquid-cargo tank trucks) are in the range of 0.28 to 0.30.

In later sections, multiaxle and multibody models are used to check individual axle and individual tire normal forces on passenger vehicles and trucks. These latter analyses supplement the steady-state analysis presented here to verify the results and to determine if transient maneuvers are sufficient to excite momentary wheel lift.

4.7 Step 6: Predict Skidding of Individual Axles during Steady-State Behavior on a Curve

The objective of Step 6 was to identify whether steady-state axle forces obtained based on the steady-state bicycle model violate the available friction supply. Using a bicycle model with the vehicles classes chosen for study, an analysis was performed based upon steady-state behavior to determine force requirements on each axle. From the force requirements, friction demand was inferred and compared to available friction supply (i.e., from Step 1).

4.7.1 Analysis Approach

In this step, a steady-state bicycle model was developed to predict skidding of individual axles accounting for the effects of vehicle type, grade, superelevation, and deceleration. A primary criticism of the point-mass model is that it does not account for the per-axle force generation capabilities of a vehicle. The point-mass model used currently by AASHTO to determine expected friction demand adds the front- and rear-axle lateral forces to determine if a vehicle can maneuver through a curve. It does not check if one of the axles requires more or less friction relative to the other. While the average of forces on each axle might not express skidding, one axle might be beyond the friction supply limit, while another is well below the limit.

Nearly all vehicles have different tire loads on the front and rear axles caused by the center of gravity of the vehicle not being located midway between the axles. For example, a typical passenger vehicle has an approximately 60/40 weight split from front to rear. When the vehicle is in a curve, this weight difference means that the lateral forces required on the front axle are usually much different than those on the rear axle. Indeed, the lateral forces required on each axle are proportional to the mass distributed over each axle; thus, on a flat road (i.e., one with no superelevation or grade), the weight distribution on the tires is exactly the same proportion as the lateral forces required from each axle. This is beneficial to curves on level roads: the vertical forces pushing down on each axle are pushing hardest on the axles that most need cornering forces. The net effect is that, for level roads, the weight differences are generally ignored for friction analysis without much error. However, on grades and in cases where there is deceleration, the weight shift from the

rear to the front of the vehicle may significantly change the relative amounts of vertical tire force on each axle. If there is a curve on a grade, the cornering forces required from each axle remain proportional to the mass above each axle, not the weight. This difference between the mass-related cornering forces and the weight-related friction supply illustrates why curves on grades may be problematic for ensuring sufficient lateral friction margins.

To calculate the effect of per-axle friction utilization, a common simplification in vehicle dynamics was assumed for this analysis: the vehicle is idealized as a rigid beam, and each axle is represented as a single tire situated at the midline of the vehicle. The resulting model is termed a "bicycle model" because of its appearance (see Figure 41). This classical bicycle model is typically used to study vehicle maneuvers on a flat road. One goal of this analysis was to expand this model to evaluate a steady turning maneuver taking into consideration the horizontal alignment, grade, and superelevation. The effects of constant braking were also included. This model was used to check the friction demand for each axle and to check if the friction supply generated by the tire–pavement is sufficient for cornering and/or braking.

A number of assumptions were made for the steady-state bicycle model as follows:

1. The velocity changes slowly relative to the forward and turning motions, such that the speed is approximately constant over the maneuver analysis window (generally a few seconds).
2. The vehicle is assumed to be steered only by the front tires.
3. There is no lateral load transfer.
4. The vehicle is right/left symmetric.
5. The roll and pitch of the vehicle and tires are ignored, other than the steady contributions due to grade and superelevation.
6. Aerodynamics and rolling resistance of the tires are ignored.
7. The vehicle's suspension is assumed to be stiff and non-moving throughout the curve.
8. The deceleration (if any) is assumed to be constant.
9. The vehicle is assumed to be driving forward down the road at a slip angle to the road that is small enough to ignore the sideways skidding of the vehicle.
10. The grade and superelevation angles are assumed to be small enough that small angle approximations can be used.

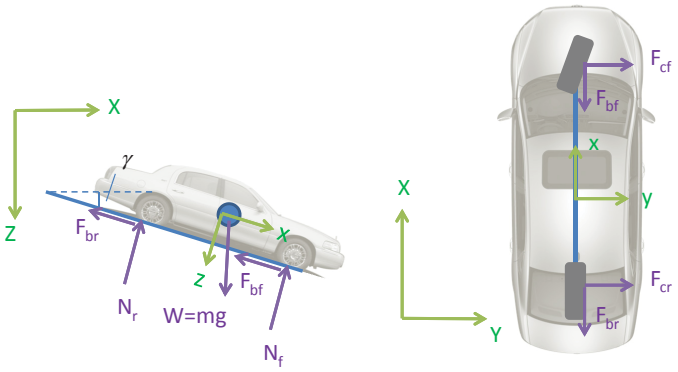

Figure 41. Forces acting on a vehicle in a steady turn on a superelevated curve with a downgrade.

In this and in later sections, the vehicle may be braking with a specified deceleration. This deceleration is specified in the vehicle's coordinate system, and hence the equations of motion are most conveniently written in this frame of reference. In previous sections, the equations of motion were written in a global frame of reference, and so to distinguish one reference frame from the other, lower-case x, y, and z are used hereafter to denote the vehicle's coordinate system, while the upper-case X, Y, and Z denote the earth-referenced coordinate system. Both designations are shown in Figure 41.

For a vehicle traveling steadily on a curve, the force balances can be conducted in the local longitudinal (x-axis), lateral (y-axis), and vertical (z-axis) directions separately, as the motions for each will be orthogonal. The forces acting along each axis are shown in Figure 41. Using this figure's force direction conventions, and small angle approximations where appropriate, in the longitudinal direction (braking), the governing equation is:

$$F_b = F_{bf} + F_{br} = ma_x - mg\frac{G}{100} \tag{35}$$

In the lateral direction (cornering), the governing equation is:

$$F_{cf} + F_{cr} = m\frac{V^2}{R} - mg\frac{e}{100} \tag{36}$$

Finally, the weight balance equation gives:

$$N_f + N_r \approx mg \tag{37}$$

Equations 35 to 37 are similar to Equations 21 to 23 derived earlier for the modified point-mass model. The only difference is that the steady-state bicycle model is derived from per-axle forces whereas the modified point-mass model uses only body-aggregated forces.

From Equations 35 to 37 some preliminary observations can be formulated. First, the longitudinal friction demand depends on the grade and deceleration levels as shown in the braking equation. Thus, the lateral friction margins should change with both grade and braking effort. While it would appear that the cornering equation depends on superelevation, in the case of steady-state driving on curves with the

AASHTO minimum curve radii, this is not the case. Equation 36 for the steady-state bicycle model can be rewritten as:

$$F_{cf} + F_{cr} = m\frac{V^2}{R_{\min}} - mg\frac{e}{100} \tag{38}$$

If Equation 38 is compared to the AASHTO design equation for minimum-radius curves, Equation 9, the two equations can be combined to obtain:

$$F_{cf} + F_{cr} = mg \cdot f_{\max} \tag{39}$$

This result shows that the side forces on the vehicle following a minimum-radius curve depend only on the maximum side friction, f_{max}. This factor, according to AASHTO design policy, depends only on the design speed, not on superelevation. Therefore, the only geometric design variable affecting cornering forces is the design speed. This makes the lateral friction demand independent of the superelevation for the steady-state analysis, e.g., the superelevation of the curve will not affect friction demand at all.

To calculate the friction supply available to each axle, the normal forces on each axle must be known. The individual axle forces are obtained by the moment balance about the *y*-axis and *z*-axis. Shown in Figure 42, a moment balance about the *y*-axis direction (at front and rear tire contact point) yields the normal force on the front and rear axles on a downgrade while the vehicle is braking:

$$N_f = mg\frac{b}{L} + \left(m\left(a_x - g\frac{G}{100}\right)\right)\frac{h}{L} \tag{40}$$

$$N_r = mg\frac{a}{L} - \left(m\left(a_x - g\frac{G}{100}\right)\right)\frac{h}{L} \tag{41}$$

The moment balance about the *z*-axis, shown in Figure 43, gives the ratio of front- and rear-axle cornering forces:

$$\frac{F_{cf}}{F_{cr}} = \frac{b}{a} \Rightarrow \frac{F_{cf}}{F_{cf} + F_{cr}} = \frac{b}{b+a} = \frac{b}{L} \tag{42}$$

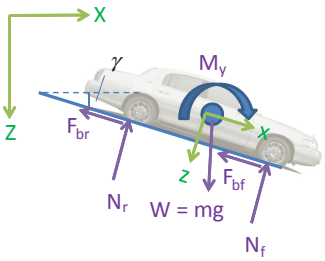

Figure 42. Moment balance about the y-axis for a vehicle braking on a downgrade.

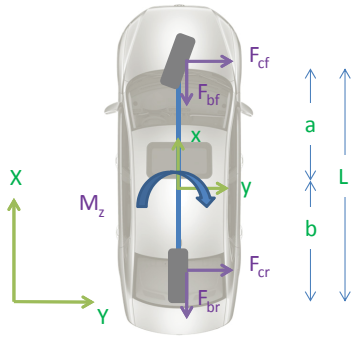

Figure 43. Moment balance about z-axis.

Therefore, the lateral (cornering) forces at the front and rear are given by:

$$F_{cf} = \frac{b}{L}\left(\frac{mV^2}{R} - mg\frac{e}{100}\right)$$

$$F_{cr} = \frac{a}{L}\left(\frac{mV^2}{R} - mg\frac{e}{100}\right) \tag{43}$$

Using the formulas for the cornering forces and weights on each axle, the lateral friction factor expressions for each axle are:

$$f_{yf} = \frac{F_{cf}}{N_f},\ f_{yr} = \frac{F_{cr}}{N_r} \tag{44}$$

Substituting the expressions for side forces and weights on each axle, and noting the weight of the vehicle, $W = mg$, the closed-form expressions for the side friction factors per axle are:

$$f_{yf} = \frac{F_{cf}}{N_f} = \frac{\frac{b}{L}\left(\frac{mV^2}{R} - W\frac{e}{100}\right)}{W\frac{b}{L} + \left(m\left(a_x - g\frac{G}{100}\right)\right)\frac{h}{L}}$$

$$f_{yf} = \frac{F_{cr}}{N_r} = \frac{\frac{a}{L}\left(\frac{mV^2}{R} - W\frac{e}{100}\right)}{W\frac{a}{L} - \left(m\left(a_x - g\frac{G}{100}\right)\right)\frac{h}{L}} \tag{45}$$

These represent the quasi-static friction demands on the front and rear axles. To determine whether these friction demands exceed the friction supply, the friction ellipse of the tire is used to modify the friction supply by the amount of friction used for braking.

To complete the analysis for the steady-state bicycle model, the prediction for the braking forces on each axle is required. A simple braking model is introduced to illustrate how brake forces are split between each axle. It is important to under-

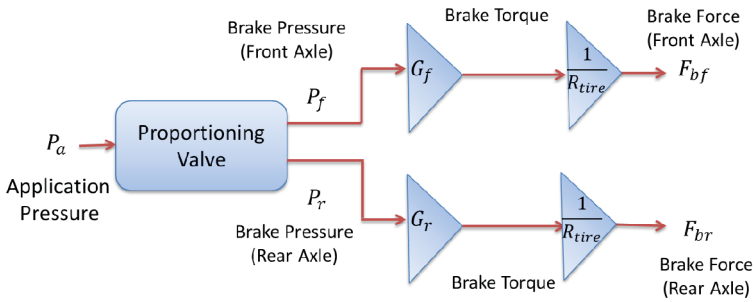

Figure 44. Brake-proportioning flowchart.

stand that braking is sometimes (and intentionally) not distributed equally between axles. Passenger vehicles typically use hydraulic brakes which transfer braking pressure from the controlling unit to the actual brake mechanism. Balancing the brake outputs on the front and rear axles is achieved by "proportioning" the brake pressure appropriately for the brakes installed on a vehicle (Limpart, 1999). The proportioning valve is a critical component in the brake system which acts to prevent rear tire skidding prior to the front tire skidding to avoid vehicle spin-out; at higher braking levels, it switches to cause more braking force to the front axle.

To maintain consistency in notation and presentation, the brake system is presented here. In the simple model used in this analysis (see Figure 44), the braking torque is the product of brake pressure and brake gain for each axle.

The brake force can be obtained by dividing the brake torque by the tire's rolling radius, R_{tire}.

$$F_{bf} = \frac{1}{R_{tire}} G_f \cdot P_f$$

$$F_{br} = \frac{1}{R_{tire}} G_r \cdot P_r \tag{46}$$

To avoid rear-axle lock-up that causes spin-out of a vehicle, the brake outputs are reduced at higher braking efforts by appropriately adjusting the braking pressures at the front and rear axles. In typical passenger vehicles, the brake pressure output for the rear axle is reduced to approximately 30% after a certain application pressure, P'_{a}. This reduction in brake pressure can be represented by the following equations:

$$P_{\text{f}} = P_{\text{r}} = P_{\text{a}} \qquad \text{for } P_{\text{a}} \le P'_{\text{a}} \tag{47}$$

and

$$P_{\text{f}} = P_{\text{a}} \qquad \text{for } P_{\text{a}} > P'_{\text{a}}$$

$$P_{\text{r}} = P'_{\text{a}} + 0.3(P_{\text{a}} - P'_{\text{a}})$$

The values of the parameters involved in this brake-proportioning model are listed for the passenger vehicle classes in Table 22. The truck models simulated in this study do not have brake-proportioning valves.

The above relationships relate to brake pressures, but not to brake forces. To be useful in the model, a relationship between brake force and brake pressure is needed. To derive this, first note that the net braking force, F_{b}, required for a decelerating vehicle is given by Equation 35, and the net braking force is $F_{\text{b}} = F_{\text{bf}} + F_{\text{br}}$. The braking force distribution for the front versus rear axle depends on whether the application pressure, P_{a}, is greater or less than P'_{a}, the pressure at which the brake-proportioning valve begins to prevent rear wheel lock. The corresponding braking force, F'_{b}, when $P_{\text{a}} = P'_{\text{a}}$ is given by:

$$F'_b = \frac{1}{R_{tire}} (G_f + G_r) \cdot P'_a \tag{48}$$

and the corresponding deceleration that initiates the brake-proportioning valve is given by:

$$a_{x,p} = \frac{F'_b}{m} + g\frac{G}{100} \tag{49}$$

Table 22. Per-axle brake-proportioning parameters for passenger vehicles.

Vehicle class	G_{f} (ft-lbf/psi)	G_{r} (ft-lbf/psi)	P_{a}' (psi)	R_{tire} (ft)
E-class sedan	4.07	3.05	363	1.19
E-class SUV	4.07	3.05	290	1.26
Full-size SUV	5.09	3.56	290	1.32

Table 23. Decelerations for passenger vehicles at which brake-proportioning valve activates.

Vehicle class	$a_{x,p}$, 0% grade	$a_{x,p}$, –9% grade
E-class sedan	–17.21 ft/s^2	–14.31 ft/s^2
E-class SUV	–12.82 ft/s^2	–9.92 ft/s^2
Full-size SUV	–10.92 ft/s^2	–8.02 ft/s^2

Table 23 shows the decelerations at which each vehicle's proportioning valve would initiate a reduction in rear tire braking force, for a level grade situation and for a 9% downgrade. Thus, of the four decelerations levels (0, –3, –11.2, and –15 ft/s^2) considered throughout these analyses, Table 23 indicates that the two highest decelerations may cause brake-force redistribution to the rear tires through activation of the brake-proportioning valve.

In general the stopping sight distance (–11.2 ft/s^2) and emergency braking (–15 ft/s^2) decelerations would not be considered "steady-state" driving situations, as the vehicles' speed is changing too abruptly to satisfy the model assumptions. However, the equations in this analysis are "steady" in that they assume constant terms in the equations, including decelerations, and thus they will give good estimates of necessary tire forces at the onset of the maneuver before speed changes significantly. These results are therefore included here despite the fact that they are not steady-state or constant-speed maneuvers. Additional discussion of emergency, transient maneuvers is presented in Section 4.9.

To relate brake pressure to brake-force distribution per axle, two cases have to be considered:

1. $F_b \le F_b'$
2. $F_b > F_b'$

In the case of $F_b \le F_b'$, the brakes are lightly used and the brake-proportioning valve is not reducing the rear brakes to prevent lock-up. In this case the braking forces per axle are simply:

$$F_{bf} = \frac{1}{R_{tire}} G_f \cdot P_a \tag{50}$$

and

$$F_{br} = \frac{1}{R_{tire}} G_r \cdot P_a .$$

And hence, the braking forces are distributed according to the brake gain on each axle:

$$F_{bf} = \frac{G_f}{G_f + G_r} \cdot F_b$$

and

$$F_{br} = \frac{G_r}{G_f + G_r} \cdot F_b \tag{51}$$

In the second case, when the brake-proportioning valve is acting to reduce rear lock-up, the brake force is $F_b > F_b'$. In this case, the braking forces per axle must be determined by two different brake pressures, e.g., $F_{bf} = \frac{1}{R_{tire}} G_f \cdot P_f$ and $F_{br} = \frac{1}{R_{tire}} G_r \cdot P_r$. The values of P_f and P_r are different and can be found by first obtaining the value of the application brake pressure, P_a. The net braking force for this case is given by:

$$F_b = F_{bf} + F_{br} = \frac{1}{R_{tire}} \left(G_f \cdot P_f + G_r \cdot P_r \right) \tag{52}$$

Substituting the equation for the brake-proportioning valve:

$$F_b = F_{bf} + F_{br} = \frac{1}{R_{tire}} \left(G_f \cdot P_a + G_r \cdot \left(P_a' + 0.3 \left(P_a - P_a' \right) \right) \right) \tag{53}$$

Rearranging:

$$F_b = \frac{1}{R_{tire}} \left(\left(G_f + 0.3 G_r \right) \cdot P_a + 0.7 G_r \cdot P_a' \right) \tag{54}$$

which can be rearranged to solve for the brake pressure:

$$P_a = \frac{R_{tire} \cdot F_b - 0.7 G_r \cdot P_a'}{G_f + 0.3 G_r} \tag{55}$$

Once P_a is known, the per-axle braking forces can be found by using an equation for the brake-proportioning valve. Using the per-axle braking forces, the longitudinal friction factors can be found using their basic definitions:

$$f_{xf} = \frac{F_{bf}}{N_f}, \; f_{xr} = \frac{F_{br}}{N_r} \tag{56}$$

Using the equations for the brake forces, the reduction in friction supply can be determined. The lateral friction supply factors are defined per axle in the same manner as described previously for the point-mass model in Equation 17:

Front Axle:

$$f_{yf,supply} = f_{y,max} \sqrt{1 - \left(\frac{f_{xf}}{f_{x,max}} \right)^2} \tag{57}$$

Rear Axle:

$$f_{yr,supply} = f_{y,max} \sqrt{1 - \left(\frac{f_{xr}}{f_{x,max}} \right)^2} \tag{58}$$

When the longitudinal friction factor exceeds the longitudinal friction supply, $f_{x,max}$, the lateral friction supply is assumed to be zero.

Using the above equations for the steady-state bicycle model, the friction demand and friction supply analysis is performed for each individual axle. If the lateral friction supply for the rear axle, $f_{yr,supply}$, is less than the lateral friction demand, f_{yr}, then the rear axle is likely to skid. This individual axle skidding may not be noticed in the point-mass model, and is the advantage of using the bicycle model over the point-mass model.

4.7.2 Analysis Results

Figure 45 shows a comparison of the per-axle friction demand for a steady-state E-class sedan assuming −11.2 ft/s^2 deceleration on the curve, for a road with no superelevation and a 9% downgrade. The three lines at the top of the figure represent friction supply, and the four lines at the bottom of the figure represent friction demand. As expected, the point-mass friction demand agrees exactly with the AASHTO design friction curves, which agrees with intuition because they both utilize the same vehicle model.

In Figure 45 two effects are occurring simultaneously that cause the steady-state model to have lower friction margins than the point-mass model: the rear demand is increasing while the rear supply is decreasing. Both are caused by braking which causes a rear-to-front weight shift as predicted by Equations 40 and 41. The change in f_x as predicted by Equation 44 explains the reduction in the friction supply on the rear axle and increase in the supply on the front axle. The same weight shift changes the normal forces in the f_y calculation in Equation 44, with the result that the lateral demand is increasing. Thus, on the rear axle, braking and downgrades cause the friction supply to go down, while simultaneously increasing friction demand.

Because load transfer depends on the mass properties of the vehicle, different vehicle setups will result in different per-axle friction demand. In the case of an E-class SUV, for example, the load-transfer effect is more pronounced for exactly the same conditions (Figure 46) due to higher CG height, *h*. Also, these figures are identical across different superelevations; like the modified point-mass model, the steady-state bicycle model results are independent of the grade when stopping sight deceleration is considered.

While Figures 45 and 46 illustrate the simultaneous change in demand and supply, the most important information is the difference between lateral friction supply per axle and lateral friction demand per axle which provides the lateral friction margin. Consistent with how the lateral friction margins are calculated for the point-mass model in Equation 16, the lateral friction margins for the bicycle model can be defined per axle as follows, for the front tire:

$$f_{margin,f} = f_{yf,supply} - f_{yf} \tag{59}$$

And for the rear tire:

$$f_{margin,r} = f_{yr,supply} - f_{yr} \tag{60}$$

In practice, however, the lateral friction demand can have both positive and negative values; hence, the absolute value

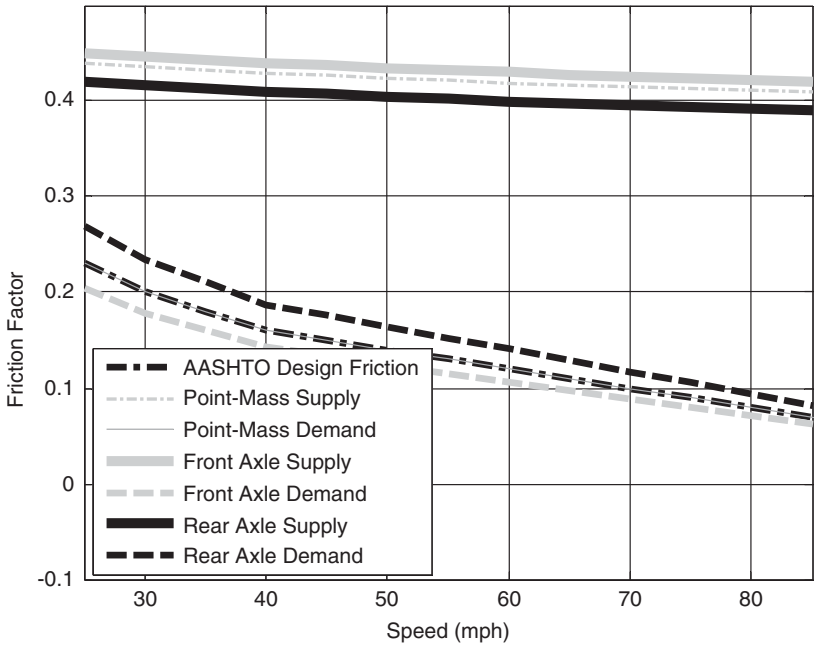

Figure 45. Friction factors for E-class sedan (G = −9%, e = 0%) (a_x = −11.2 ft/s^2).

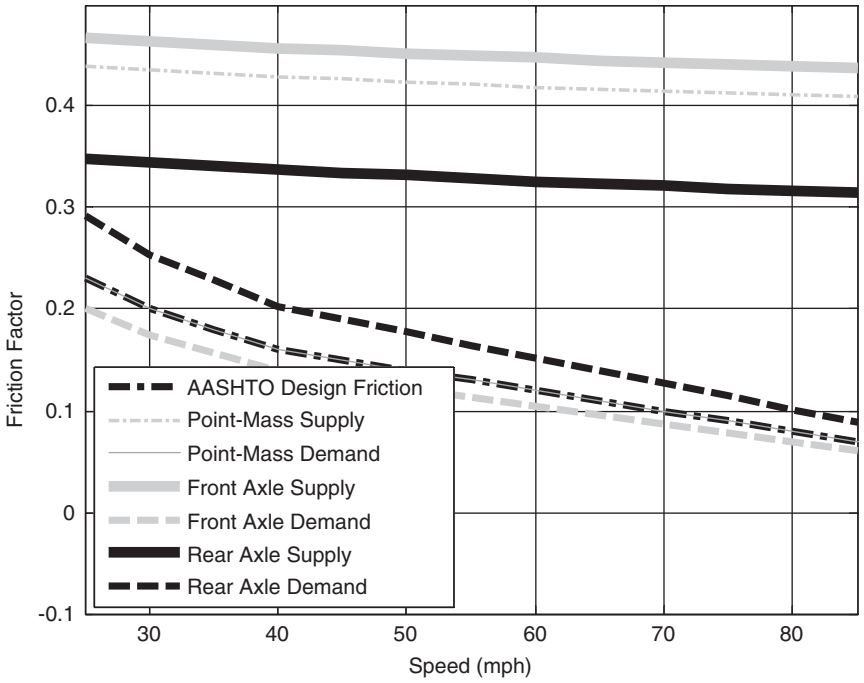

Figure 46. Friction factors for E-class SUV (G = −9%, e = 0%) (a_x = −11.2 ft/s²).

of the demand is more appropriate. Thus, the lateral friction margins are formulated as:

$$f_{margin,f} = f_{yf,supply} - |f_{yf}|$$

$$f_{margin,r} = f_{yr,supply} - |f_{yr}| \quad (61)$$

To illustrate how both grade and braking effort change the friction margins, Figure 47 shows the lateral friction margins for an E-class sedan and an E-class SUV. For both vehicles, the effect of grade is to decrease lateral friction margins at each braking level, except for the stopping sight distance decelerations (−11.2 ft/s²) as these decelerations reduce with increasing grade per AASHTO guidelines. The largest factor, however, is the level of braking effort applied. As the braking effort increases, the friction margins drop to where, for emergency braking levels (decelerations of −15 ft/s²), they can become negative.

Figure 47 shows that, for the E-class sedan, the use of braking increases the detrimental effects of grade. For example, with no braking (a_x = 0 ft/s²), each percent change in grade

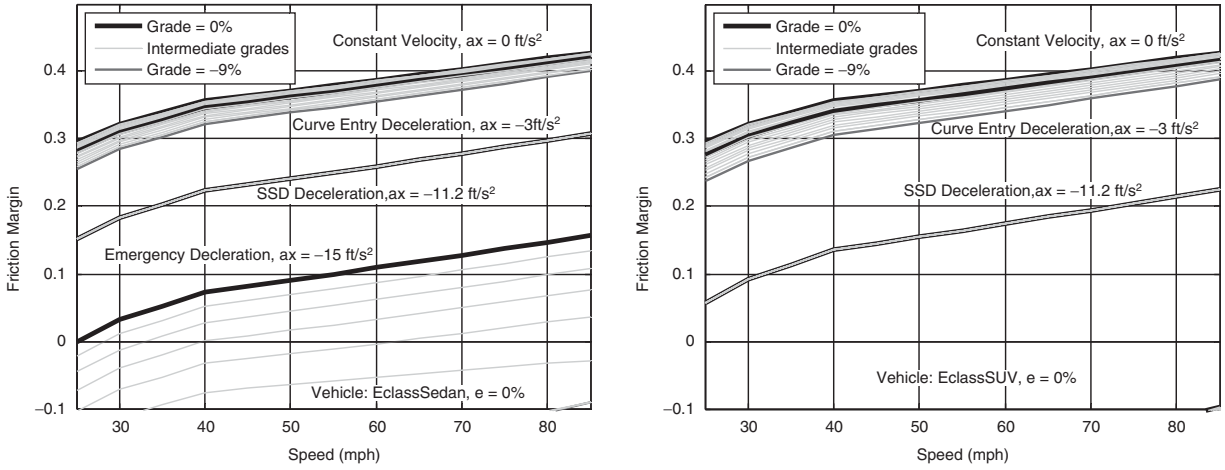

Figure 47. Lateral friction margins for E-class sedan and E-class SUV (G = 0% to −9%, e = 0%) (a_x = 0, −3, −11.2, and −15 ft/s²).

decreases the lateral friction margin by approximately 0.001. For curve-entry deceleration ($a_x = -3$ ft/s^2), the effect of grade is to decrease lateral friction margin by 0.002 per percent of grade, approximately. For emergency braking deceleration ($a_x = -15$ ft/s^2), the lateral friction margin decreases by 0.02 per percent of grade decrease. Note that stopping sight distance (SSD) decelerations are not affected by grade, but this is because the actual decelerations vary by grade per AASHTO policy.

Figure 47 also illustrates that individual vehicles experience different lateral friction margins. For example, the E-class sedan is able to maintain much higher lateral friction margins, even positive margins for much of the grade situations, whereas the E-class SUV has emergency braking friction margins that are all negative (below –0.1).

In the sections that follow, the steady-state bicycle model results are compared to results from more complex models. These comparisons include additional vehicles not shown here, for example the full-size SUV and trucks.

4.7.3 Summary of Key Results from Step 6

In summary, the following findings were obtained from the analysis in Step 6 that examined the steady-state bicycle model predictions of friction margins:

1. If AASHTO design policy is used for curvature design, and the vehicle is following the curve at the design speed, the equations of motion predict per-axle tire forces will change only with design speed, not with changes in superelevation or grade. Thus, superelevation- and grade-induced changes in lateral friction margin will occur only due to changes in the tire's normal force and braking inputs.
2. The effects of the brake-proportioning valve built into most passenger vehicles do not activate at the curve-entry deceleration rates considered in this study. However, the valve does activate at much lower levels on downgrades than on level roads and may in fact activate during stopping sight distance decelerations as well as emergency braking.
3. The steady-state bicycle model predicts friction supply and demand that are very similar to the point-mass model in that the lateral friction margins increase with design speed, namely because the demand at higher speeds drops faster than the supply at higher speeds.
4. Due to weight shift on downgrades and decelerations, the steady-state bicycle model predicts that the front-axle supply is always higher than the point-mass model and the demand is lower. The reverse is seen on the rear axle. Thus, the front-axle margins are nearly always better than predicted by the point-mass model, and the rear tire is nearly always less. Thus, the rear axle of passenger vehicles nearly always has the lowest lateral friction margin.
5. Different vehicles have different lateral friction margins from the steady-state bicycle model.
6. The use of braking increases the detrimental effects of grade. For example, with no braking ($a_x = 0$ ft/s^2), each percent change in grade decreases the lateral friction margin by approximately 0.001 for the E-class sedan. For curve-entry deceleration ($a_x = -3$ ft/s^2), the effect of grade is to decrease the lateral friction margin by 0.002 per percent of grade, approximately. For emergency braking deceleration ($a_x = -15$ ft/s^2), the lateral friction margin decreases by 0.02 per percent of grade decrease. Stopping sight distance decelerations are not affected by grade because the actual decelerations vary by grade per AASHTO policy.
7. The steady-state bicycle model predicts that high braking situations are likely to cause negative friction margins resulting in vehicles skidding while traversing horizontal curves on downgrades.

4.8 Step 7: Predict Skidding of Individual Axles during Braking and Lane-Change Maneuvers on a Curve

The objective of Step 7 was to identify whether braking, lane changes, and other non-steady steering maneuvers affect the ability of a vehicle to traverse a sharp horizontal curve without skidding, taking into consideration horizontal curvature, grade, and superelevation. Using the bicycle model inclusive of non-steady effects, simulations were run modifying the transient steering inputs for each vehicle class of interest in this study to determine cornering forces and friction factors. The results of these simulations are compared to results from previous steps. Data from the speed and vehicle maneuver studies (Section 3.2) and instrumented vehicle studies (Section 3.3) were used as inputs for this analysis.

4.8.1 Analysis Approach

The basis of this transient analysis is to determine whether the driver's change in braking or steering inputs to the vehicle might introduce temporarily changes in the vehicle motion (transient behavior) that could affect the friction demand of each axle. For this analysis, a bicycle model suitable for transient maneuver analysis is developed taking into consideration the horizontal curvature, grade, and superelevation. Like the model in Section 4.7, this formulation of the classical bicycle model assumes a two-wheel vehicle whose behavior is similar to a beam; but unlike in Section 4.7, the equations of motion are not solved in static force balance but in differential equation form by finding numerical solutions. One of the simplest differential equations for vehicle motion inclusive of per-axle tire forces is a 2 degree-of-freedom differential equation model

with yaw rate and lateral velocity as the motion variables. The input variables in this model—the steering input, δ, and velocity of the vehicle—are assumed to be under the driver's control. This same model is commonly employed in vehicle stability systems, such as electronic stability control, to confirm that the measured vehicle behavior agrees with model predictions.

The derivation of this modified transient bicycle model is much more involved than previous models, so only the salient points are presented here. Additional details on the model formulation can be found in Varunjikar (2011). Several assumptions are used in the derivation of the transient bicycle model, and most of the assumptions are similar to the steady-state bicycle model assumptions. The additional assumptions are as follows:

1. The moments acting on the vehicle about the vertical z-axis are not always balanced and hence give a differential equation for the spin motion of the vehicle.
2. The road grade and superelevation angles are constant within the curve.
3. The tire forces are linear (i.e., the angle between the tire and the roadway is small enough that a doubling of the relative angle doubles the tire forces).
4. The steer angle is small enough that coordinate transforms from the tire angle to the vehicle's body angle can be simplified using small angle approximations.
5. Braking forces per axle are obtained from the steady-state results.

The resulting equations of motion are obtained by a force and moment balance on the vehicle. The results are similar to the previous bicycle model except that the lateral and spin motions of the vehicle are governed by a dynamic force balance, instead of a static force balance. On a typical vehicle, the lateral and spin motions most affect the vehicle side forces; hence, the added detail of the differential equation solution is intended to yield more insight into the lateral forces acting on the vehicle in a curve on grade. From Section 4.7, Equation 37 remains the same, describing the normal force on the tires. Equation 35, for longitudinal dynamics (braking), must be modified to include the rotation of the coordinate system attached to the vehicle:

$$m(-a_x - rV) = -F_{bf} - F_{br} - mg\frac{G}{100} \tag{62}$$

Here the variables are defined as in Section 4.7, except that a new variable, the spin rate of the vehicle, r, is introduced. This is the rotational rate of the vehicle about the z-axis of the vehicle (through the vehicle's CG). Equation 36, for the lateral dynamics of the vehicle (cornering), becomes:

$$m\left(\frac{dV_y}{dt} + rV\right) = F_{cf} + F_{cr} + mg\frac{e}{100} \tag{63}$$

Here again the variables are defined as before, except that the lateral sliding velocity of the vehicle is introduced, V_y. This is the sideways speed of the vehicle as it moves across the road surface, as measured at the CG of the vehicle (for trucks, it is measured at the tractor's CG). This velocity is usually very small, but it is non-zero and generates appreciable errors if ignored for high-speed dynamic motion.

Finally, the yaw dynamics equation is introduced, which does not appear in Section 4.7:

$$I_{zz}\frac{dr}{dt} = a \cdot F_{cf} - b \cdot F_{cr} \tag{64}$$

This equation predicts how the vehicle's spin rate, r, will speed up or slow down depending on the unbalanced moments produced at the front and rear axles. I_{zz} is the moment of inertia of the vehicle (or tractor in the case of articulated trucks) about the z-axis of the vehicle.

In the models in this section and Section 4.9, it is assumed that the brakes, when applied, are done so using a constant value of net braking force, F_b. The brake-proportioning model described in Section 4.7 is again used to find the per-axle braking forces, F_{bf} and F_{br}, per Equation 35. The values of normal loads acting on the front (W_f) and rear axles (W_r) are found also using the formulations given earlier in Equations 40 and 41.

A major difference between the transient and steady-state formulation of the bicycle model is that with the transient model in this step, the tire forces change with the dynamic angle of the vehicle to the road surface. For this reason, a simple explanation of tire modeling is provided that focuses on topics that may affect lateral friction margins.

Tires experience very small amounts of sideways skidding, called lateral slip, as they roll under cornering conditions for normal driving. This well-known phenomenon is used to accurately predict how a tire will develop a lateral force, F_c (Gillespie, 1992). The slip angle of the tire is measured from the tire's orientation (x′-axis) to the tire's direction of travel (i.e., tire's velocity vector relative to the road directly underneath). A diagram of the tire's slip angle, α_i, is shown in Figure 48. In contrast, the tire's steer angle, δ, is the angle measured from

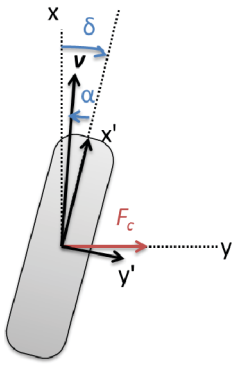

Figure 48. Transient bicycle model.

the vehicle's longitudinal orientation (vehicle's x-axis) to the tire's direction of heading (i.e., tire's x'-axis). The tire's slip angle is rarely the same as the steering angle; however, the purpose of the steering angle is to influence the tire's skid angle to obtain the desired vehicle trajectory.

For small tire slip angles (5° or less) that are typical of normal driving, the cornering force for an ordinary tire under a fixed normal load increases linearly with the tire slip angle (i.e., if the slip angle of the tire is doubled, the lateral force from the tire doubles). This proportionality constant for the cornering force to α is called the "cornering stiffness," C_α. This linear tire model is used in this section and Section 4.9 to find cornering forces, F_{cf} and F_{cr}, in Equations 63 and 64. The cornering forces on the front and rear axles are:

$$F_{cf} = C_{\alpha f} \cdot \alpha_f$$
$$F_{cr} = C_{\alpha r} \cdot \alpha_r \quad (65)$$

where $C_{\alpha f}$ and $C_{\alpha r}$ are the cornering stiffness values for the front and rear axles, respectively. Like a friction force, the cornering stiffness strongly depends on normal load and is assumed to change proportionally to normal load, as a first approximation (Gillespie, 1992). The cornering coefficient, CC, is defined as the ratio of the cornering stiffness to the normal load (F_z), such that one can calculate the cornering stiffness given a normal load on the tire:

$$C_\alpha = CC \cdot F_z + CC_{offset} \quad (66)$$

Figure 49 shows the cornering stiffness at four different loads for a passenger vehicle tire, and a linear curve-fit using the least-square method. These cornering stiffness values were obtained from tire curves, which are taken from data sets for passenger vehicle and truck tires (see CarSim and TruckSim documentation for example data sets). The slope of the linear curve-fit is the cornering coefficient of a tire. For most tires this value is in the range of 10 to 25 [1/rad]. Table 24 shows the cornering coefficients assumed for vehicles in this analysis.

To use the cornering stiffnesses for tire force calculations, the tire's slip angle (i.e., the angle of the tire with respect to the road) must be known. The slip angle of the tire can be found using geometry as described by Bundorf (1968) and Pacejka (2006). For the front axle, the tire's slip angle is:

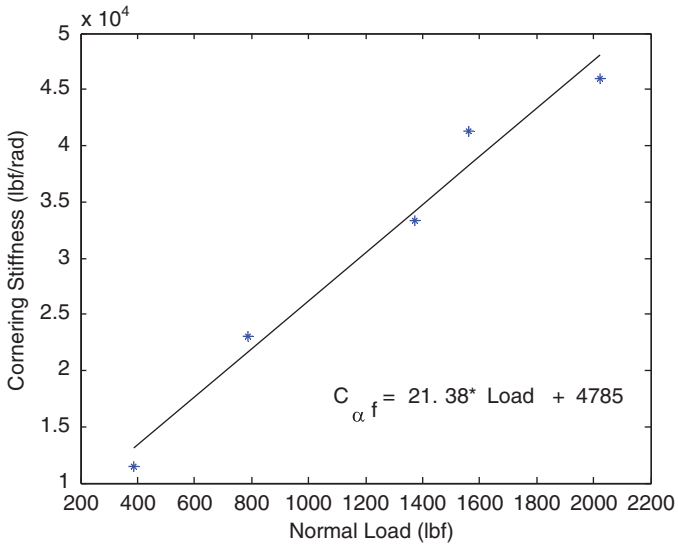

Figure 49. Tire cornering stiffness for normal loads on passenger vehicle tire.

$$\alpha_f = \tan^{-1}\left(\frac{V_y + a \cdot r}{V}\right) - \delta \quad (67)$$

And for the rear tire:

$$\alpha_r = \tan^{-1}\left(\frac{V_y - b \cdot r}{V}\right) \quad (68)$$

Using small angle approximations, Equations 67 and 68 can be rewritten as:

$$\alpha_f = \frac{V_y + a \cdot r}{V} - \delta$$
$$\alpha_r = \frac{V_y - b \cdot r}{V} \quad (69)$$

Table 24. Cornering coefficients for vehicles used in this research.

Vehicle	*CC* (1/rad)	*CC* offset (lbf/rad)
E-class sedan	21.38	4,785
E-class SUV	10.55	6,848
Full-size SUV	10.55	6,848
Single-unit truck	7.08	7,336
Tractor semi-trailer truck	7.08	7,336
Tractor semi-trailer/full-trailer truck	7.08	7,336

Substituting these expressions into the equations of motion given earlier, Equations 63 to 69, the lateral dynamics (cornering) equation becomes:

$$m\left(\frac{dV_y}{dt}+rV\right)=\cdots$$

$$(CC\cdot N_f+CC_{offset})\left(\frac{V_y+a\cdot r}{V}-\delta\right)$$

$$+(CC\cdot N_r+CC_{offset})\left(\frac{V_y-b\cdot r}{V}\right)+mg\frac{e}{100} \quad (70)$$

And the yaw dynamics equation, Equation 64, can be found through similar substitutions:

$$I_{zz}\frac{dr}{dt}=a\cdot(CC\cdot N_f+CC_{offset})\left(\frac{V_y+a\cdot r}{V}-\delta\right)$$

$$-b\cdot(CC\cdot N_r+CC_{offset})\left(\frac{V_y-b\cdot r}{V}\right) \quad (71)$$

These two coupled differential equations are solved for each vehicle trajectory using a built-in numerical ordinary differential equation (ODE) solver, the fixed-step Runge-Kutta method, using a time step of 0.01 s. The Simulink® software within MATLAB was used to solve these differential equations.

4.8.1.1 Definition of Maneuvers

This analysis considers a vehicle entering a simple horizontal curve with constant radius, varying the horizontal curvature, grade, and superelevation. This allows for the analysis of both the transient dynamics of the vehicle due to a sudden change in steering input, and also the steady-state tire forces for a given scenario as described in Step 6. The vehicle is assumed to be traveling at a constant speed up until the point that brakes are applied. The curve approach and pre-braking speed is assumed to be the same as the design speed for the curve. Depending on the situation, the vehicle applies brakes, steers into the curve, steers into the curve and performs a lane change, or combinations thereof.

To calculate the steady steering for the vehicle entering the curve, the level-road steering equation was first used. This equation, shown below, predicts the steer angle, δ, necessary for a vehicle of length L between the front and rear axles to traverse a curve of radius R' in steady state. If the front and rear tire slip angles, α_f and α_r, are known, the equation is given by:

$$\delta=\frac{L}{R'}+\alpha_f-\alpha_r \quad (72)$$

The rotation radius, R', in Equation 72 represents the effective radius of the vehicle maneuver path. For a superelevated curve, the rotation radius is greater than the curve's radius, R,

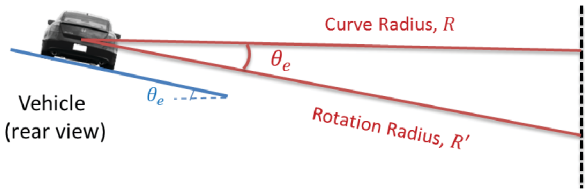

Figure 50. Rotation radius and curve radius for superelevated curve.

as seen in Figure 50. The rotation radius can be found using geometry, which results in the following equation:

$$R'=\frac{R}{\cos\theta}=R\sec\theta \quad (73)$$

The final steering angle in a curve on a superelevated roadway, δ, can be found by combining the steady turning equation, Equation 72, with the equation for the cornering stiffness, Equation 66, to obtain:

$$\delta=\frac{L}{R'}-\left(\frac{b}{C_{\alpha f}}-\frac{a}{C_{\alpha r}}\right)\cdot\frac{m}{L}\left(\frac{V^2}{R}-g\frac{e}{100}\right) \quad (74)$$

In the simulation of the transient bicycle model, the steering inputs are done "open-loop," where the steering values are fed into the simulation as inputs with no corrections if the vehicle does not follow the correct trajectory. On the curves and on tangents, the steering inputs required are readily calculated using Equation 74—for tangents, the radius is set to infinity. However, it is especially difficult to predict the steering inputs required for the transitions on the tangent approach to a curve. This is because the superelevation is changing from a normal crown to full superelevation. To simplify the analysis and to produce "worst-case" results, it is assumed in the simulations that the tangent approach is fully developed prior to entry into the curve. This gives the worst-case friction margins for the entire trajectory, because the steering change from tangent to curve keeping is the most abrupt with fully developed superelevation on the tangent.

The steering input is assumed to transition quickly from the tangent steering value to the curve value, to provide worst-case responses. The worst-case situation would be to model the steering change as a step steering input; however, this is equivalent to instantaneously turning the front tires on the road and such an unrealistic steering change will automatically induce front tire skidding. To represent a fast but reasonable transition from tangent to curve steering, the transition from one to the other was assumed to take at least 2 s. Comparisons are presented later between the multibody simulations in Sections 4.10 and 4.11 (which include

a feedback-driver model), and it is seen that the transient bicycle model is noticeably more conservative in predicting lateral friction margins on entry to the curve because of these assumptions of fully developed superelevation on the tangent approach.

Similar to the steering inputs, the braking inputs are defined as step inputs. The magnitudes of the deceleration values are calculated prior to the simulation to ensure that rates correspond with the braking situations appropriate for this analysis, per braking Equations 50 to 55. Representative inputs into the simulation are plotted versus time in Figure 51 for a vehicle that is first steering into a curve at $t = 3$ s and then braking at $t = 6.75$ s. The top plot shows the application of the brake input, the middle plot shows the steady decrease in vehicle speed during the maneuver, and the bottom plot shows the change in steering input applied over a 1 s duration from driving the tangent to driving the curve. Note vehicle speeds are limited to a minimum of 5 mph.

Since the deceleration, a_x, is assumed to be constant, the braking inputs are found using the brake-proportioning model described in Step 6 (Section 4.7). This analysis assumes that the weight shift due to deceleration is instantaneous since suspension dynamics are being ignored. A comparison of lateral friction margins for a suspension-less vehicle and for a simulation inclusive of suspension was performed, and both models gave nearly identical results for the predicted maximum lateral forces and minimum lateral friction margins. Thus, for purposes of simplicity and clarity, the suspension-free model is used in this analysis.

With the simulation equations and parameters now defined, a trajectory can be simulated. At each time step, the numerical solver calculates a solution to the differential equation, and then moves incrementally to the next time instant using the previous solution as an initial condition for the current step. This is repeated until an entire time trajectory is produced. Each trajectory is simulated for at least 10 s and more as necessary to ensure a sufficient duration to capture both the transient and the steady responses to the curves. The forces on the tires during each simulated trajectory are saved and used to calculate the friction margins throughout the maneuver, and the worst-case friction margins are saved for plotting purposes.

For many of the plots of friction margin that follow, each data point in each margin curve represents one simulation. When multiple curves are presented for various situations, some trends become evident.

4.8.2 Analysis Results

4.8.2.1 Effects of Curve Keeping at Constant Speed

The first set of simulations performed using the transient bicycle model were used to study the differences between the point-mass model, the steady-state bicycle model from Section 4.7, and the transient bicycle model in Section 4.8. To simplify the analysis and to choose a situation where all models should nominally agree, these first sets of analyses consider vehicles traveling at constant speed on the curves. There are

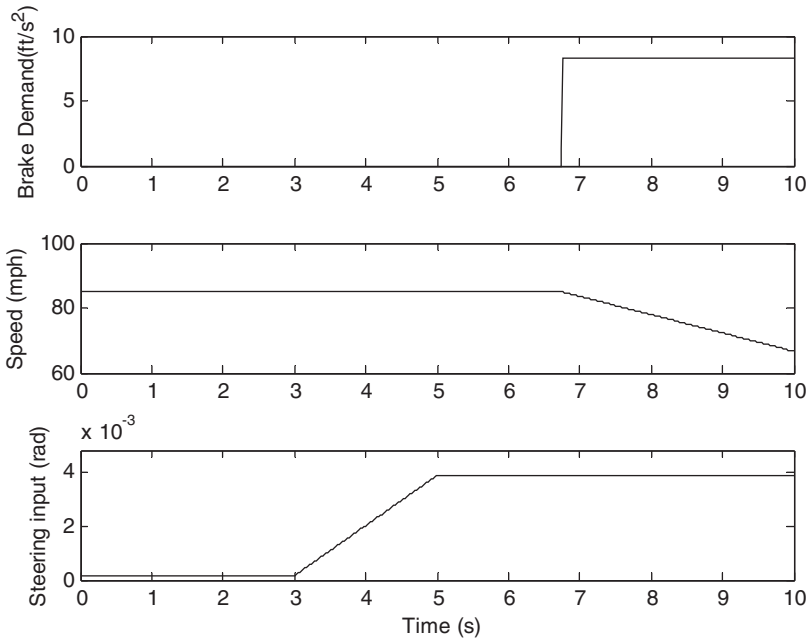

Figure 51. Simulation inputs for E-class sedan (V = 85 mph, G = −9%, e = 12%) ($a_x = -11.2$ ft/s²).

no steering inputs other than those to maintain the vehicle within the lane, and no braking inputs other than those to prevent the vehicle from accelerating on a downgrade.

When analyzing the simulation results, there were effects at high and low speeds that caused disagreement between the transient model and the other models. One of these effects only occurs at larger superelevations, while the other only occurs on the front tires. Figure 52 shows the lateral friction margins for the front and rear tires versus speed for two different superelevations, where the differences between the models, particularly the transient bicycle model and the steady-state bicycle model, can be observed.

To understand the high-speed model disagreements, these situations are plotted showing the normalized forces, the friction supply, and the resulting friction margins for both the front and rear tires in Figure 53. In the margin plots for high superelevations (i.e., 12%), the minimum margins are seen to occur immediately prior to entry to the curve, not on the curve itself. This behavior is not seen in the low superelevation case. This indicates that the superelevated road on entry to the curve is requiring more friction utilization than the curve itself. However, recall that for the simulations, the superelevation is assumed to be fully developed prior to entry into the curve. This is not typical design practice. AASHTO policy indicates that the proportion of the superelevation runoff length [i.e., the length of roadway needed to accomplish a change in outside-lane cross-slope from zero (flat) to full superelevation] on the tangent should be in the range of 0.6 to 0.9 (60% to 90%) for all speeds and rotated widths. Therefore, these results should be interpreted carefully.

To assist with design of superelevation, it is possible to derive conditions for which the superelevation on the tangent approach will give worse margins than the curve, at least for steady driving. In Section 4.7, the steady-state front and rear friction factors are given by Equation 45. For the situation with no braking, $a_x = 0$, this set of equations simplifies to:

$$f_{yf} = \frac{b\left(\frac{m}{W}\frac{V^2}{R} - \frac{e}{100}\right)}{b - h\frac{G}{100}}$$

$$f_{yr} = \frac{a\left(\frac{m}{W}\frac{V^2}{R} - \frac{e}{100}\right)}{a + h\frac{G}{100}} \tag{75}$$

On the approach tangent, the radius is infinite, and so the radius term can be simplified. Additionally, the superelevation may only be developed by some fraction, p_{tangent}, which is the proportion of the design or maximum superelevation that is attained at the point of curvature for a simple curve.

$$f_{yf,tangent} = p_{tangent}\frac{-\frac{be}{100}}{b - h\frac{G}{100}}$$

$$f_{yr,tangent} = p_{tangent}\frac{-\frac{ae}{100}}{a + h\frac{G}{100}} \tag{76}$$

For the front friction margin on the approach to be less than within the curve, the friction factor on the tangent must be less than the friction factor in the curve:

$$p_{tangent}\frac{-\frac{be}{100}}{b - h\frac{G}{100}} < \frac{b\left(\frac{m}{W}\frac{V^2}{R} - \frac{e}{100}\right)}{b - h\frac{G}{100}} \tag{77}$$

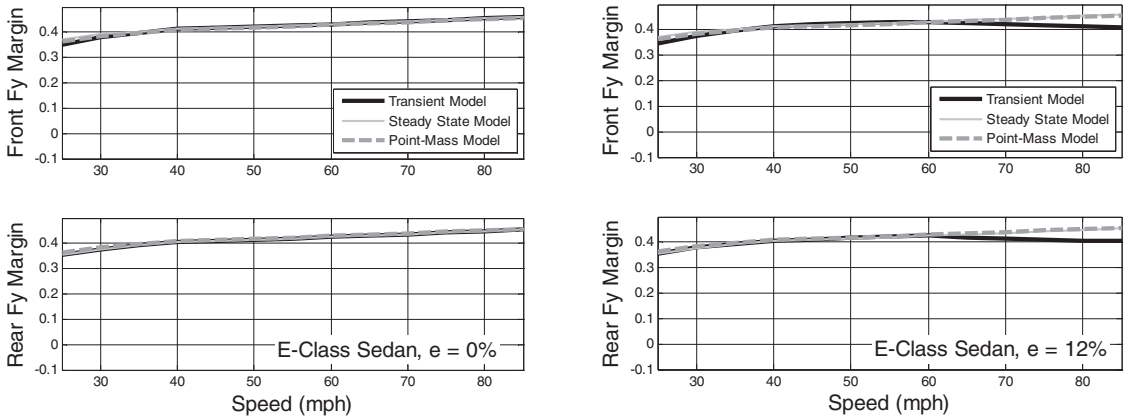

Figure 52. Front (top plots) and rear (bottom plots) lateral friction margins from point-mass, steady-state bicycle, and transient bicycle models for E-class sedan (G = −9%, e = 0% and 12%) (a_x = 0 ft/s²).

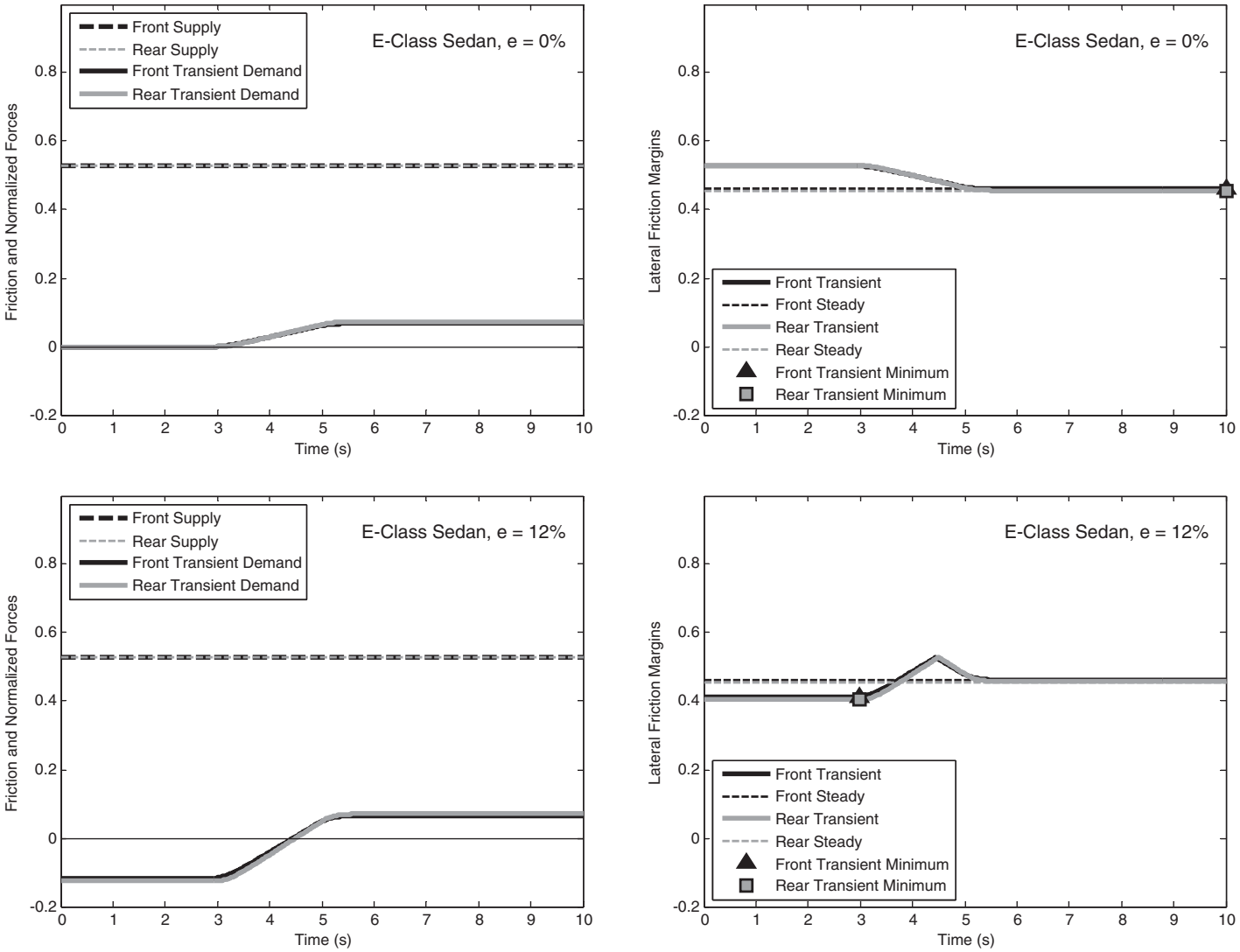

Figure 53. Friction supply and normalized forces (left plots) and resulting lateral friction margins (right plots) from transient bicycle model for E-class sedan (V = 85 mph, G = −9%, e = 0% and 12%) (a_x = 0 ft/s²).

$$p_{tangent}\frac{e}{100} < \frac{V^2}{gR} - \frac{e}{100} \tag{78}$$

$$\frac{e}{100} < \frac{1}{1+p_{tangent}}\frac{V^2}{gR} \tag{79}$$

The same result is obtained for the rear friction margin.

This result indicates that, if the superelevation at the PC entry is larger than this value, then the lateral friction margin on entry to the curve is likely to be less than the lateral friction margin on the curve. Further, Equation 79 does not depend on the road grade, the road friction levels, or the vehicle type.

The example shown in Figure 53 was simulated at 85 mph for e = 12%, with a design radius of 2,542 ft. For the simulation, the road is fully superelevated at curve entry, and so $p_{\text{tangent}} = 1$. For these values, Equation 79 predicts that the largest superelevation that should be used is 9.5%. Above this value, the superelevation on the approach tangent reduces friction values prior to the beginning of the curve (i.e., PC) more than it helps within the curve. Similarly, at 55 mph for e = 12%, with an AASHTO design radius of 807 ft, and $p_{\text{tangent}} = 1$, the maximum superelevation is 12.5%. As shown in Figure 52, the lateral friction margin for the transient model begins to diverge from the steady-state model at 55 mph, as predicted. Thus, the disagreement between the transient model and the steady-state model at high speeds and superelevations is due to the transient model identifying lateral friction margin reductions on the tangent approach, whereas the steady-state model ignores this.

To understand the low-speed model disagreements, again plots are made of these specific situations. The top plots in Figure 54 show the friction forces and normalized margins for a 25 mph curve with 0% superelevation. The steering

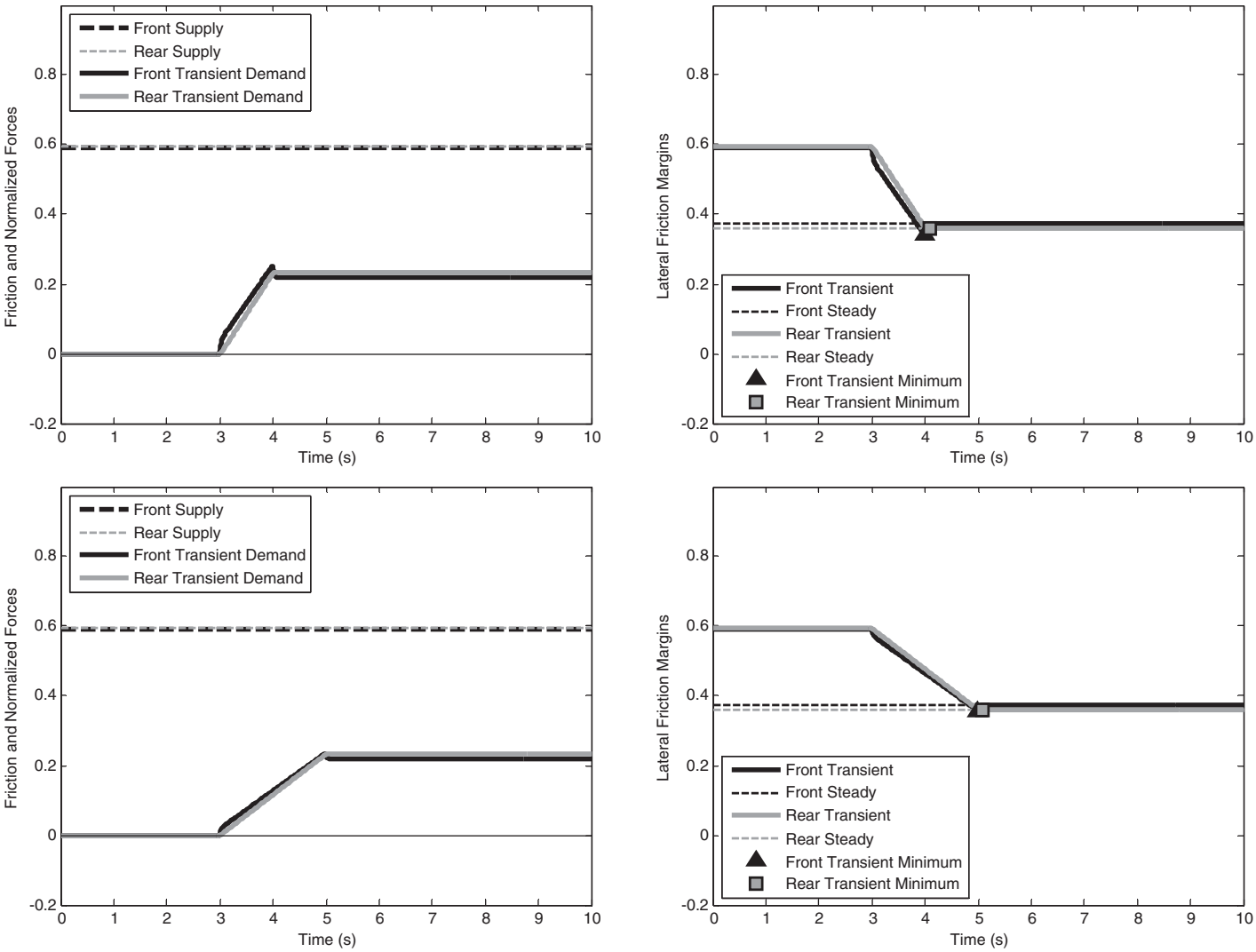

Figure 54. Friction supply and normalized forces (*left plots*) and resulting lateral friction margins (*right plots*) from transient bicycle model with a 1 s transition (*top plot*) and a 2 s transition (*bottom plots*) for E-class sedan (V = 25 mph, G = −9%, e = 0%) (a_x = 0 ft/s²).

input in this case is a 1 s transition from the tangent steering value to the curve-keeping steering value, but the resulting tire forces show a small peak at the end of the steering transition. This peak is due to the additional forces necessary to accelerate the vehicle in rotation versus the steady forces necessary for maintaining the vehicle's spin and tire forces within the curve. Because the acceleration depends on how quickly the vehicle transitions from driving the tangent (i.e., straight-line driving) to driving the curve, this peak should decrease if the transition is spread out over a longer interval. The bottom plots in Figure 54 show the friction forces and normalized margins for a 25 mph curve following a 2 s transition. These plots show a reduced overshoot of tire forces versus the 1 s transition case, and thus hereafter the 2 s transition is used.

Once the curve entry friction margins were understood, simulations were repeated to study the differences between the point-mass model, the steady-state model from Section 4.7, and the transient bicycle model within the curve for simple curve-keeping steering inputs (i.e., the intended trajectory of the vehicle is within the same lane on the approach tangent and through the curve). The results are shown in Figure 55. The first observation is that all of the models predict more lateral friction margin at high speeds than low speeds, except for the case with high superelevation (i.e., $e = 16$) where, due to the entry approach issues mentioned previously, the friction margins are similar at very low and very high speeds.

The next observation is that at all speed ranges for lower superelevations (i.e., 4% and 8%), all three models largely agree. The point-mass model and steady-state bicycle model also largely agree at all speed ranges for higher superelevations (i.e., 12% and 16%) as well. However, at higher speeds

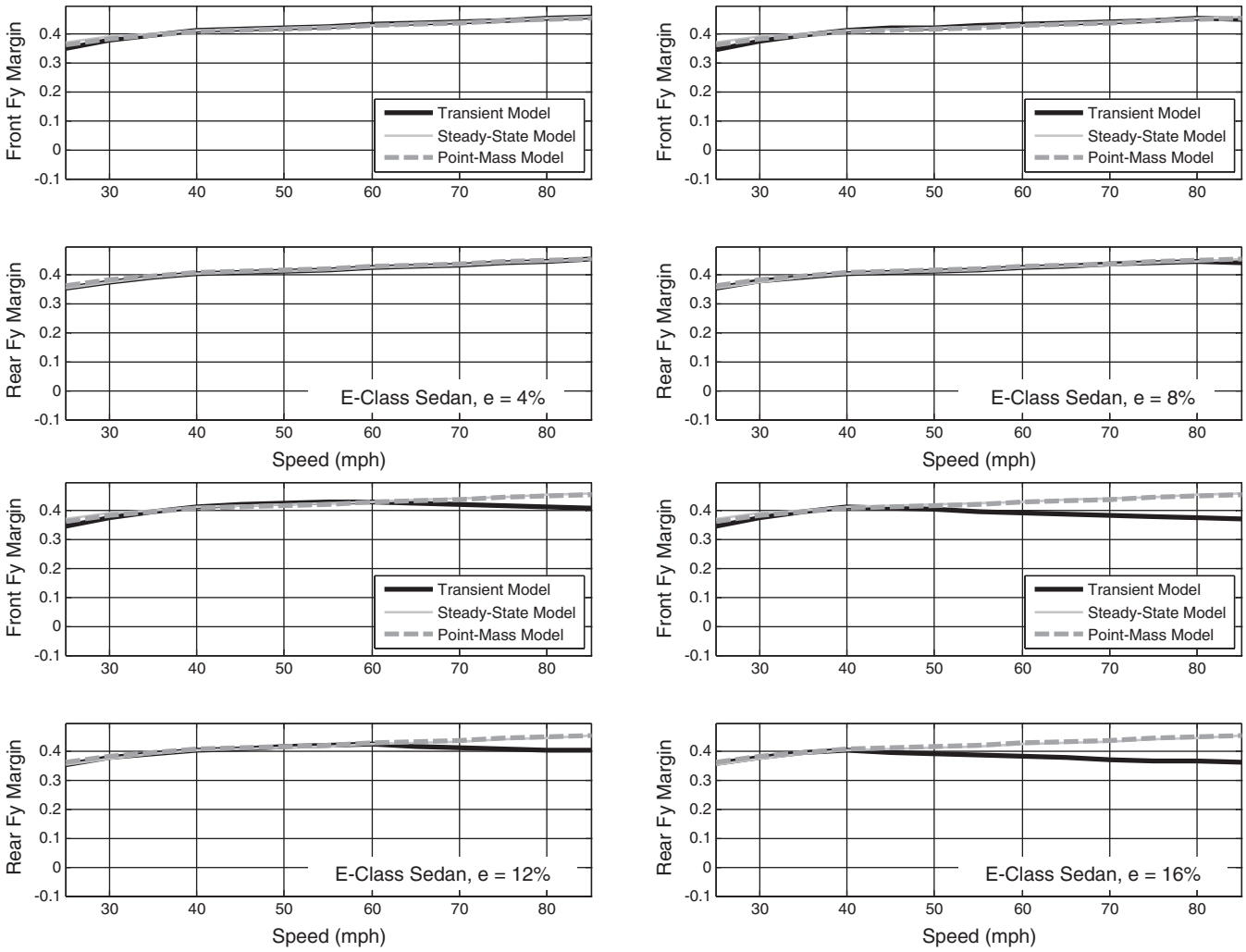

Figure 55. lateral friction margins from point-mass, steady-state bicycle, and transient bicycle models for E-class sedan (G = −9%, e = 4% to 16%) (a_x = 0 ft/s²).

and higher superelevations, the transient bicycle model estimates lower friction margins than the other models.

Comparing the steady-state bicycle model and the point-mass model, the point-mass model predicts a rear-axle friction margin that is 0.006 higher than predicted by the steady-state model. The front lateral friction margin is similarly underpredicted by the point-mass model. This very minor difference is observed over all speeds, and across all grades, and is due to the weight shift caused by grade.

While there remains some disagreement between the models for the front-axle friction margins, the rear tire predictions for the steady-state and transient bicycle models are in agreement for the lower speeds for the rear tire. This is important because the rear tire margins appear to be the limiting case, e.g., the rear tires appear to be the first to lose friction at the higher speeds expected of high-speed downgrades. In the plots that follow hereafter, only the minimum lateral friction margins between the front and rear axles are presented. This minimum is calculated at each speed by taking the minimum of the front- and rear-axle friction values. A dividing line is shown in the plot where the minimum margins occur at the front tires versus rear tires; in general this line is at 30 mph.

Figure 56 shows the minimum lateral friction margins for cornering plotted versus speed for grades from 0% to −9%, for four superelevations (4% to 16% in 4% increments), for an E-class sedan. There is a minor but consistent influence of grade seen across superelevations: increasing grade decreases the friction margins available. Specifically, the approximate 10% of grade change in each plot (from 0% to −9%) spans a margin of 0.01, so each percentage increase of grade (i.e., a steeper downgrade) reduces the friction margins by about 0.001 at speeds higher than 40 mph. This consistent effect is due to the rear tire saturation and is relatively minor compared to the lateral friction margin variations due to speed.

Below 40 mph, the change in behavior was analyzed by examining the simulation trajectories one-by-one. It was

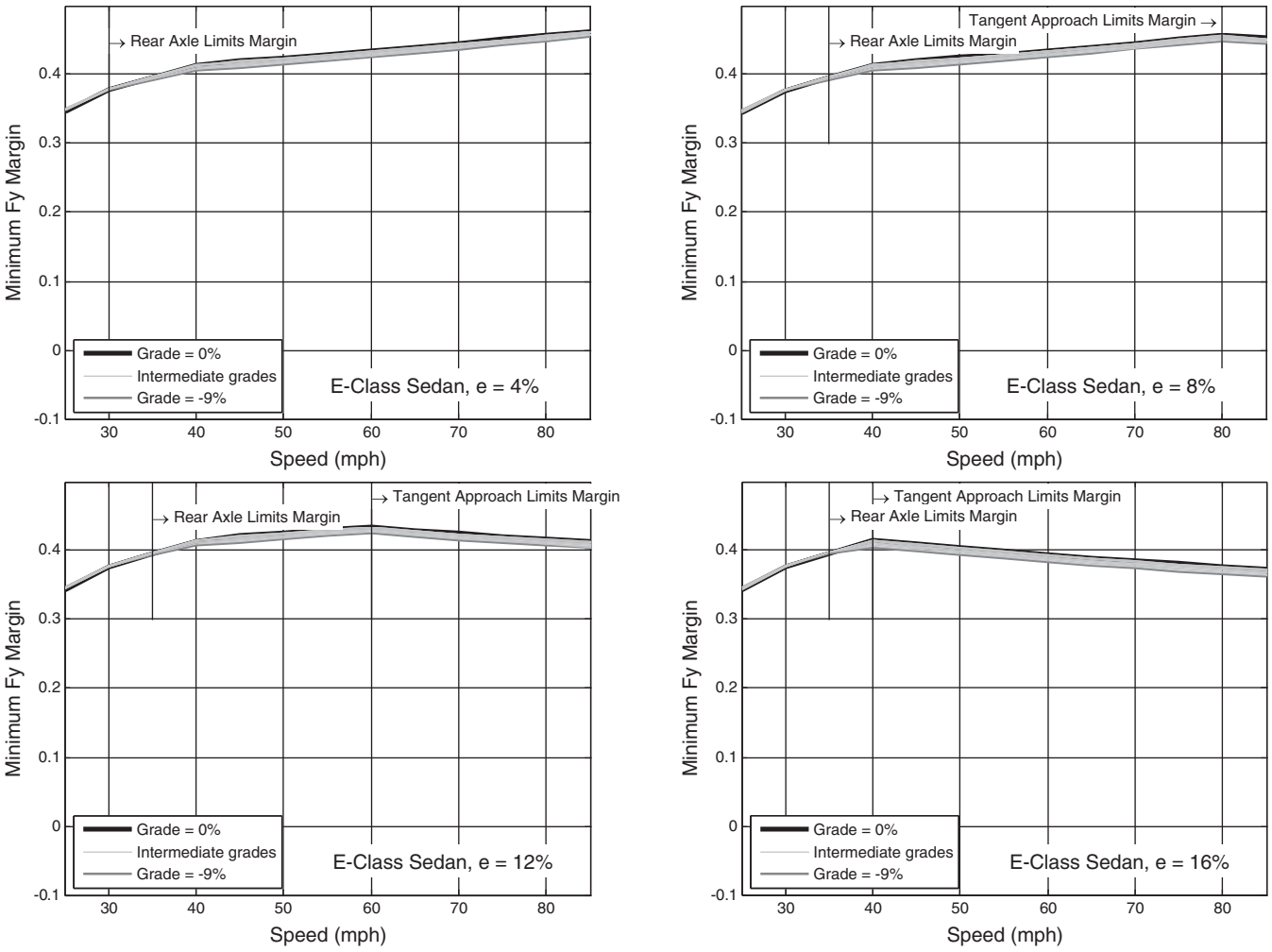

Figure 56. Lateral friction margins from transient bicycle model for E-class sedan (G = 0% to −9%, e = 4% to 16%) (a_x = 0 ft/s²).

found that the minimum friction margins occur at the front axle for all these cases and is caused by the front tires requiring additional friction during the transition from the tangent to the curve steering levels. This transition becomes increasingly abrupt with increasing superelevation. For a very high superelevation (e.g., 16%), the vehicle has to steer significantly to the outside of the curve immediately before the curve. In the curve, the steering effort must reverse to produce force to the inside of the curve.

To confirm that this curve entry effect occurs consistently across different vehicles, Figure 57 shows the minimum lateral friction margins for a fixed grade of –9%, for superelevations ranging from 0% to 16%, for four vehicles. At lower speeds, all vehicles have lower lateral friction margins across the range of superelevations. At higher speeds, the higher superelevation curves have lower lateral friction margins because the superelevation on the tangent approach is actually requiring more friction utilization than within the curve.

To summarize the above constant-speed plots, they illustrate that grade and superelevation have very little effect on the friction margins for these maneuvers. The biggest insight offered is that the point-mass model slightly over-predicts available margin on the rear tires, and slightly under-predicts margin on the front tires. Without braking, however, the difference between the models is minimal. Note that vehicle designs vary widely, and the effects of weight distribution on individual axle friction margins could be more significant for some vehicles. This can be seen in Figure 57 where the different vehicles yield slightly different margin predictions. These vehicle-to-vehicle differences are minor among passenger vehicles. However, the figure shows that the lateral friction margin for the truck is approximately 0.1 lower than the passenger vehicles across all speeds. This is largely due to the lower friction available to truck tires versus passenger tires.

The results in Figure 57 suggest that, at low speeds, the steering adjustment from tangent to curve keeping can cause

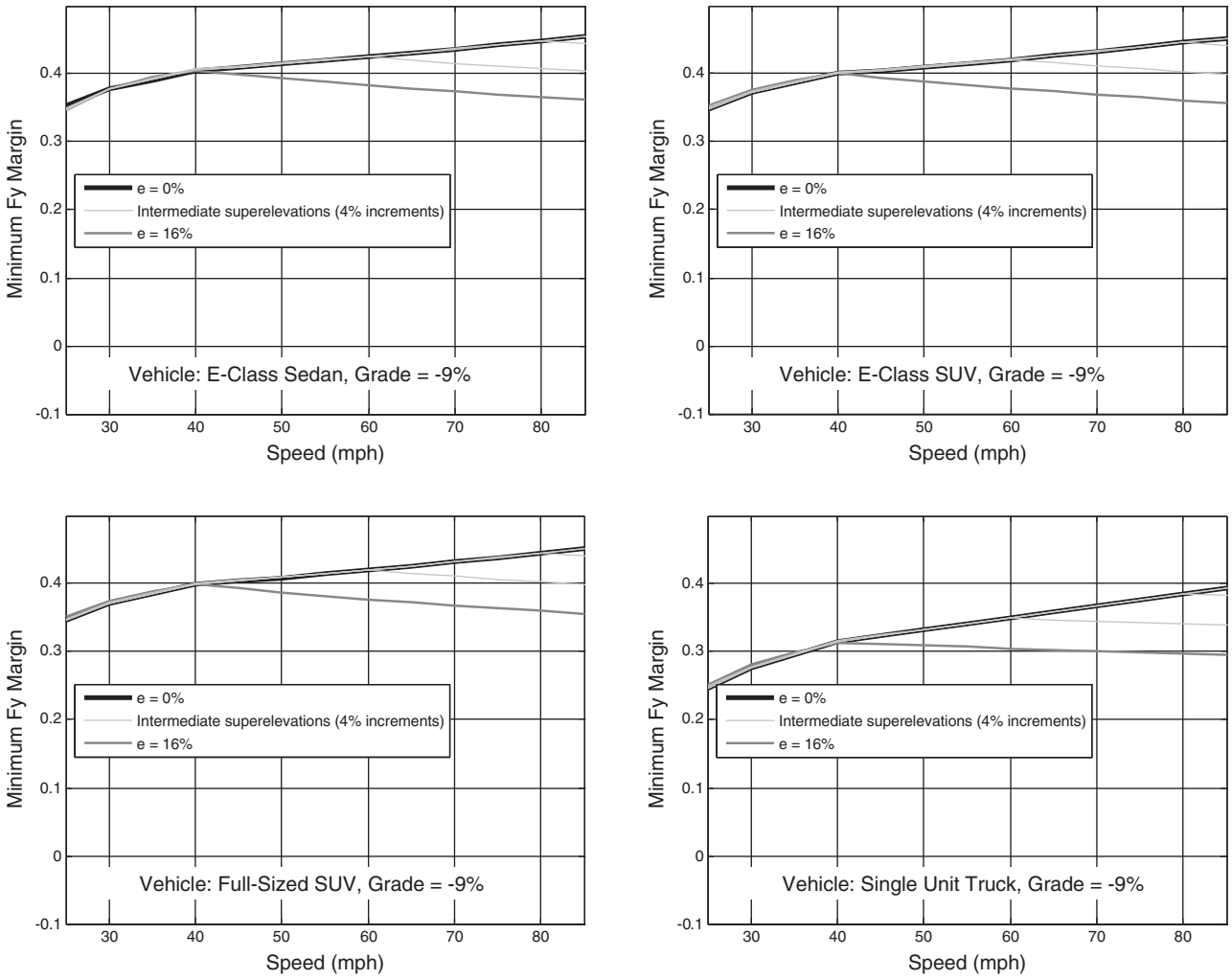

Figure 57. Lateral friction margins from transient bicycle model for E-class sedan, E-class SUV, full-size SUV, and single-unit truck (G = −9%, e = 4% to 16%) (a_x = 0 ft/s²).

reduction in lateral friction margins if transitioned too quickly.

4.8.2.2 Effect of Curve-Entry Deceleration

Another set of simulations were conducted to represent a mild deceleration within a curve. Specifically, a constant deceleration value of −3 ft/s² was initiated 3.75 s after curve entry. (This choice of timing is discussed in later sections.) This deceleration value was not adjusted for grade, so to maintain the same deceleration, the net braking friction demand increases slightly as grade becomes steeper.

Figure 58 compares the results of the modified point-mass model, the steady-state bicycle model, and the transient bicycle model for this curve-entry deceleration case. As before, all models predict increasing lateral friction margin with increasing design speed. And again, the transient model agrees closely with the steady-state model for speeds above 35 mph and as long as the superelevation on approach is not higher than the thresholds given by Equation 79.

Figure 59 shows the same situation as Figure 58 to illustrate the effects of grade. Only the transient model is presented for grades from 0% to −9%. Again, there is a distinct transition in margins at around 35 mph, representing the transition from front-axle skidding-dominated behavior at low speeds to rear-axle skidding at higher speeds.

The minimum friction margins of the constant-speed case (a_x = 0 ft/s²) in Figure 56 and the curve-entry deceleration case (a_x = −3 ft/s²) in Figure 59 have very similar minimum margins at lower speeds (around 0.34 to 0.35), but at higher speeds, the (a_x = −3 ft/s²) braking case has larger changes in the margin with increasing grade. Specifically, each of the "bands" of 10 grades in each deceleration plot of Figure 59 spans a friction margin of approximately 0.02. This mean that each 1% increase in the downgrade slope results in a 0.002 decrease in friction margin on that downgrade during

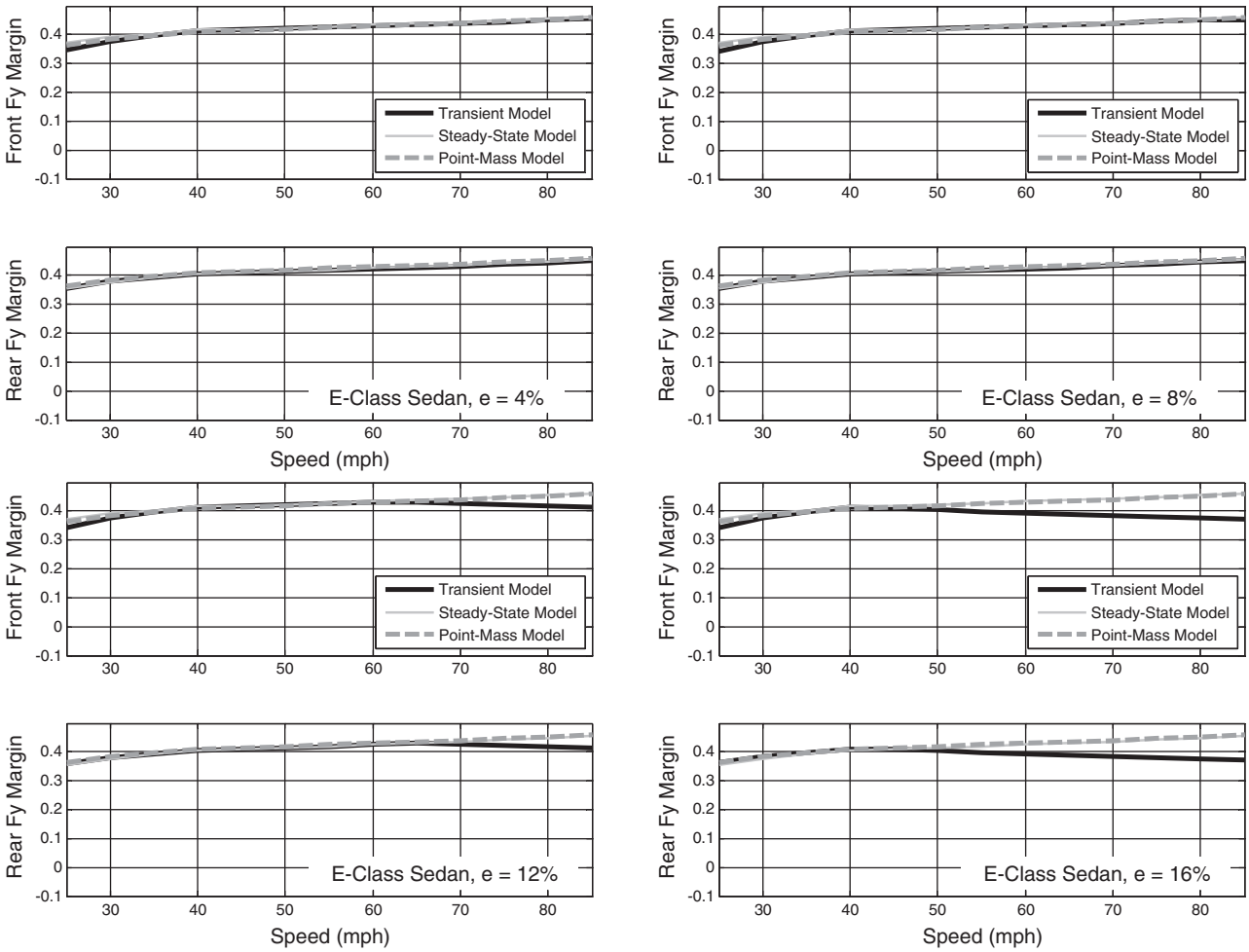

Figure 58. Lateral friction margins from point-mass, steady-state bicycle, and transient bicycle models for E-class sedan (G = −9%, e = 4% to 16%) (a_x = −3 ft/s²).

the same levels of deceleration. As before, this level is particularly small and dwarfed by the change in friction margins versus speed. However, this value is 1.5 to 2 times that of the case when there is no braking present (Figure 56). Thus, the results suggest that braking inputs to the vehicle magnify grade-related reductions in friction margin.

In Figure 60, the minimum lateral friction margins are plotted for different vehicles across the entire range of superelevations. Finally, and most importantly, the figure shows that there is still some amount of friction in reserve with curve-entry deceleration ($a_x = -3$ ft/s²) while the vehicle is following the curve. One can see that increasing superelevation has a very slight effect on the lateral friction margin, and more specifically the 16% superelevation improves the friction margin by 0.01 versus the 0% case. Thus, this effect is very minor compared to the changes in margin with respect to speed, or with respect to differences between vehicles.

For passenger vehicles above 55 mph for the 16% superelevation case, or above 75 mph for the 12% superelevation case, Figure 60 shows that the additional superelevation does not benefit the passenger vehicles (due to the thresholds given by Equation 79). But for trucks, the curve-entry deceleration results in Figure 60 are quite different than the constant-speed case plotted in Figure 57. Even this small difference in deceleration drops the margin by 0.1, enough that the margin is lowest in the curve rather than on the approach, a result that of course would be different if braking were applied on the entry to the curve. Comparing the truck to the passenger vehicles, the truck has a margin 0.2 lower than the passenger vehicles. Previously, for the constant-speed case, the truck's margin was 0.1 lower than the passenger vehicles. Thus, braking inputs tend to reduce lateral friction margins for trucks much more severely than for passenger vehicles.

4.8.2.3 Analysis of Friction Margins When Curve Radius Is 80% of AASHTO Minimum Design Radius

One goal of this study was to understand how modifications to the existing AASHTO roadway design policy might affect

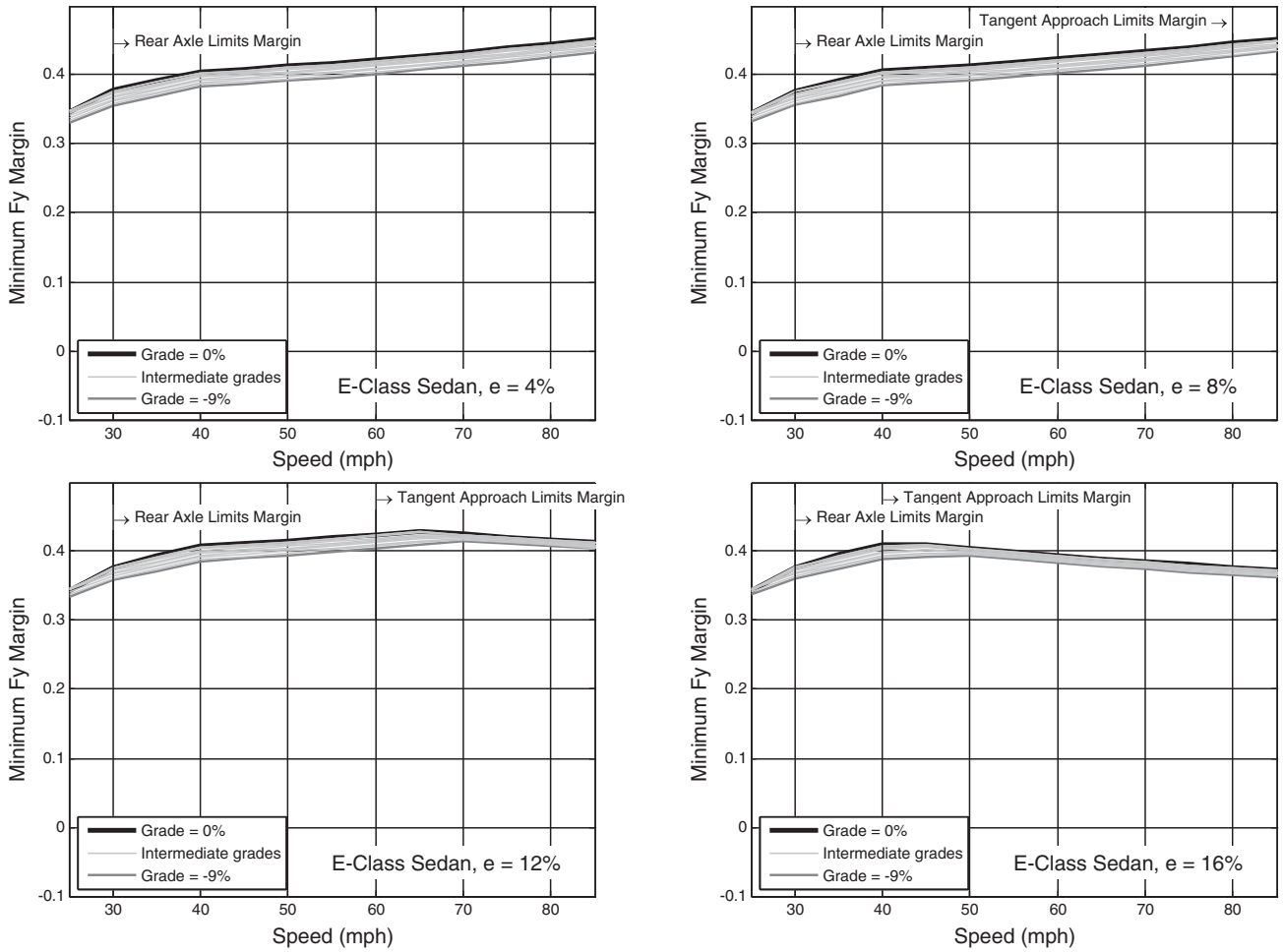

Figure 59. Lateral friction margins from transient bicycle model for E-class sedan (G = 0% to −9%, e = 4% to 16%) (a_x = −3 ft/s²).

vehicle behavior on curves with steep grades. To investigate how tighter curve geometries might affect friction margin, the friction margins were evaluated for curves with radii that were 80% of the AASHTO minimum-radius curves. To keep the analysis simple, no braking inputs were added for this analysis.

For purposes of comparing the effects of the reduced design radius, Figure 61 shows lateral friction margins for a –9% grade, for superelevations ranging from 0% to 16%, for an E-class sedan, E-class SUV, full-size SUV, and single-unit truck. The figure shows the nominal radius case side-by-side with the low-radius case. The reduced design radius situations reduce the lateral friction margins at low speeds by about 0.1 to 0.14, and by about 0.02 at high speeds. Thus, the effect of radius reduction appears to be more significant at lower design speeds than for higher design speeds. In the low-radius case, the addition of superelevation appears to reduce the margin across all speeds. Further, for the lower-radius design, the margins change much more with changes in superelevation, i.e., the sensitivity of the design to changes in superelevation is much higher.

4.8.2.4 Effect of Lane-Change Maneuver at Constant Speed

The effects of a lane-change maneuver within the curve were also studied. This subsection is organized to first introduce how the lane changes were modeled. Next, the worst-case timing for lane-change inputs is investigated. These worst-case lane changes are then simulated for a variety of geometric and vehicle situations to understand the influence of lane changes on lateral friction margins at constant speed.

To begin, it was assumed that for a lane-change maneuver, the vehicle travels from a low-speed lane to a high-speed lane at a constant speed. This assumption was made as lane changes are often made to avoid slower-moving traffic in the right lane. For the analysis, it was assumed that the curve was to the left, and therefore the lane change was toward the inside of the curve. This was chosen to require higher tire forces, since this type of lane change effectively tightens the turning radius of the vehicle.

For most driving, the steering input used for the lane-change simulations can be approximated by one period of

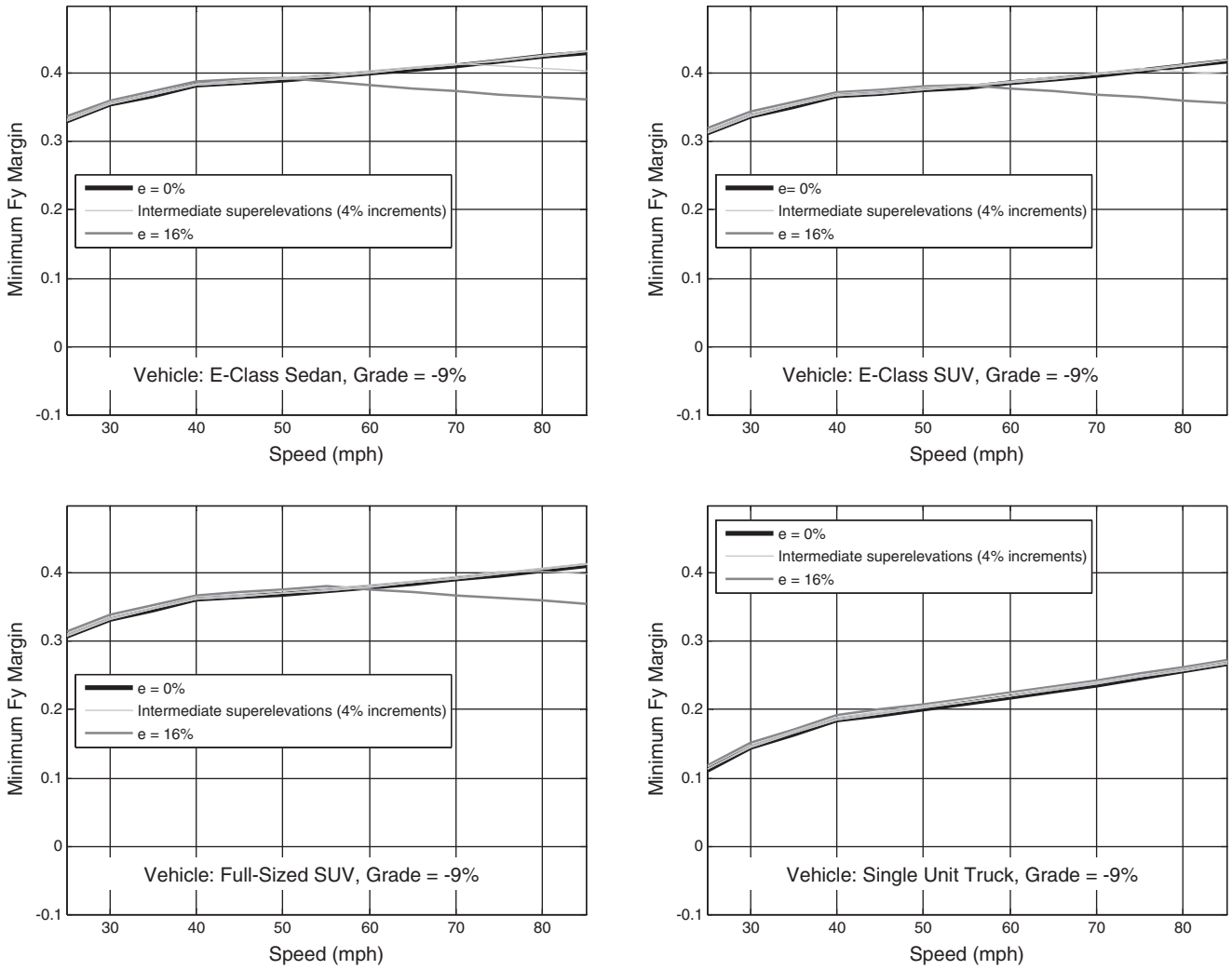

Figure 60. Lateral friction margins from transient bicycle model for E-class sedan, E-class SUV, full-size SUV, and single-unit truck (G = −9%, e = 4% to 16%) (a_x = −3 ft/s²).

a sine wave, and so this steering waveform was used as an idealization of the driver's input. To determine the appropriate duration of the lane-change portion of the steering input, field data were used for guidance. Based upon lane-change duration data collected in the field (see Section 3.2.3), most lane changes are completed within approximately 3 s for passenger vehicles and 4 s for trucks. Thus, the period of the sine wave steering input was limited to 3 s for passenger vehicles and 4 s for trucks. This sine wave steering input is applied in addition to the nominal steering required for traveling on a curve.

A challenge in simulating lane-change maneuvers is that the steering amplitude of the single sine wave required for a lane change depends on the vehicle and on speed. At low speeds, larger steering inputs are required to obtain the same lateral motion of small-amplitude, high-speed steering inputs. To calculate how the lane-change steering amplitude changes with speed, the vehicles were simulated on a tangent section of roadway and given increasingly larger steering amplitudes. The assumption is that the steering inputs are additive: e.g., one can add a curve-keeping steering input to a straight-road lane-change steering input to obtain the steering input for changing lanes on a curve. This addition of steering inputs assumes that the superposition principle is valid for the vehicle system, which is generally true as long as the steering inputs are small and the vehicle behavior is linear (e.g., it is not near skidding). In the cases where the vehicle is actually near skidding, this will be discerned in the friction analysis and in the comparison of steering inputs between this transient model and in the multibody simulations in later sections.

The simulated road was made infinitely wide and uniform in friction to avoid roadway departure effects. Also the steering inputs specified a lane-change maneuver of 12 ft.

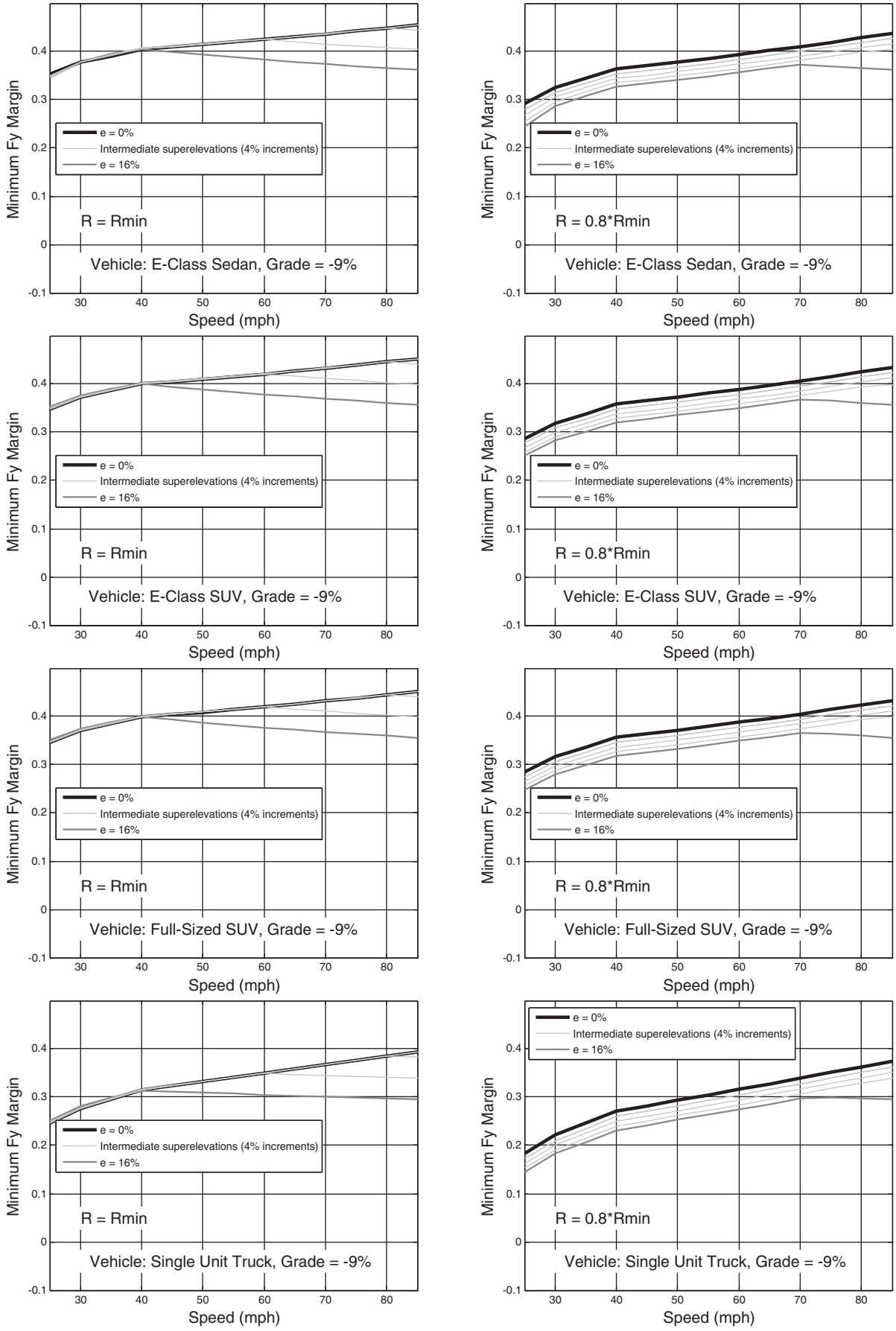

Figure 61. Lateral friction margins for AASHTO minimum-radius curves and 80% of minimum radius for E-class sedan, E-class SUV, full-size SUV, and single-unit truck (G = −9%, e = 0% to 16%) (a_x = 0 ft/s²).

Sensitivity analyses of the steering input assumptions revealed several important points. Lane-change-steering amplitudes strongly depend on speed. However, the effect of grade is quite small, so small that it can be ignored in calculating the lane-change-steering inputs. Additionally all vehicles reach steady curve-keeping tire forces within several seconds of curve entry. This allows the simulations to be simplified in several ways. First, they do not have to be simulated for long durations: in this study, 10 s was seen to be more than sufficient to understand the resulting vehicle motions and friction margins. Second, the lane-change maneuvers can be simulated within several seconds before and after entry of the curve, and the resulting analyses allow understanding of the entire curve behavior as long as the speed conditions are similar. For this reason, most of the analysis that follows focuses on curve entry conditions and maneuvers near curve entry, yet the insights apply throughout the curve.

It was unclear at the start of the study whether the "worst-case" tire forces and friction margins would occur if the lane change happened immediately before curve entry, during curve entry, or after the curve entry when curve-keeping tire forces were fully developed. The reason for this uncertainty is because, unlike curve-keeping steering inputs, the shape of the lane-change steering input changes directions in time. A sample steering profile is summarized in Figure 62.

To understand the lane-change effects in more detail, simulations were conducted to find the worst time to initiate a lane-change maneuver within a curve. The vehicle simulations were set up to stagger the lane-change initiation time relative to the curve entry time. For each simulation, the minimum lateral friction margin was recorded across both front and rear axles. The results of these simulations indicated that, except for low-speed turns, the worst location to perform a lane change is well within a curve. For low speeds (i.e., speeds below 35 mph), the lowest lateral friction margins occur when the lane change occurs only a second or so after curve entry. This is because the tire forces overshoot in low-speed cases because the vehicle is much more responsive to steering changes and steering amplitudes must be much larger at these lower speeds for the same maneuver. However, these represent very aggressive curve entry conditions at low speed. Therefore, hereafter, the worst-case lane-change inputs are simulated well after the curve-entry point, at least 2 s or more after entering the curve.

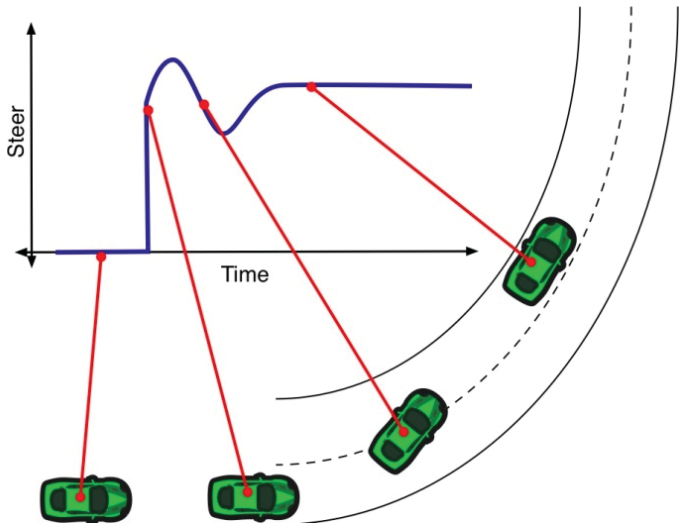

Figure 62. Steering inputs for lane-change simulations.

To analyze and quantify lateral friction margins further, a series of simulations were conducted studying whether lane-change maneuvers affect the agreement between the different models. Note that neither the point-mass model nor the steady-state bicycle model can predict friction margins for lane changes because these maneuvers violate the assumptions of steady behavior in both of the models. For the transient model, the lane-change event was initiated 3 s after curve entry, and thus the lateral tire forces for steady curve keeping are fully developed prior to the start of the lane-change maneuver.

Figure 63 shows a comparison of the lateral friction margins for the transient model, the steady-state model, and the point-mass model for the lane-change maneuver for an E-class sedan on –9% grade, and for 4%, 8%, 12%, and 16% superelevations. In earlier sections examining steady maneuvers, the point-mass and steady-state models agreed very well with the transient model. In contrast, for the lane-change situations, the transient model predicts friction margins that are lower than the other models by 0.25. This is because the steady-state and point-mass models are unable to predict tire forces for situations where the steering inputs are changing, such as during a lane change. Additionally, this decrease in friction margin does not appear to occur at one particular speed range, but rather appears to be a uniform decrease in margin across all speeds. Figure 63 shows some variation in the minimum friction margins with changing superelevation.

A comparison specifically focusing on the effects of grade and speed is shown in Figure 64. The plots indicate that several effects are consistent across vehicles and superelevations. First, the margins increase by 0.062 from 40 to 85 mph, or about 0.0015 margin increase with each 1 mph increase in design speed; this is due to the AASHTO design policy, which decreases the design friction with increasing speeds. Further, as grades change from 0% to –9%, the margins reduce by approximately 0.015, or a margin reduction of 0.0015 per degree of grade.

Figure 65 shows the effect of speed, superelevation, and vehicle type on friction margins. For all vehicles and all speeds, as superelevation increases, there is a very slight increase in friction margins across all speeds (i.e., a 0.02 increase in margin across 16% of superelevation change, or about 0.001 in margin increase per degree of superelevation added). The

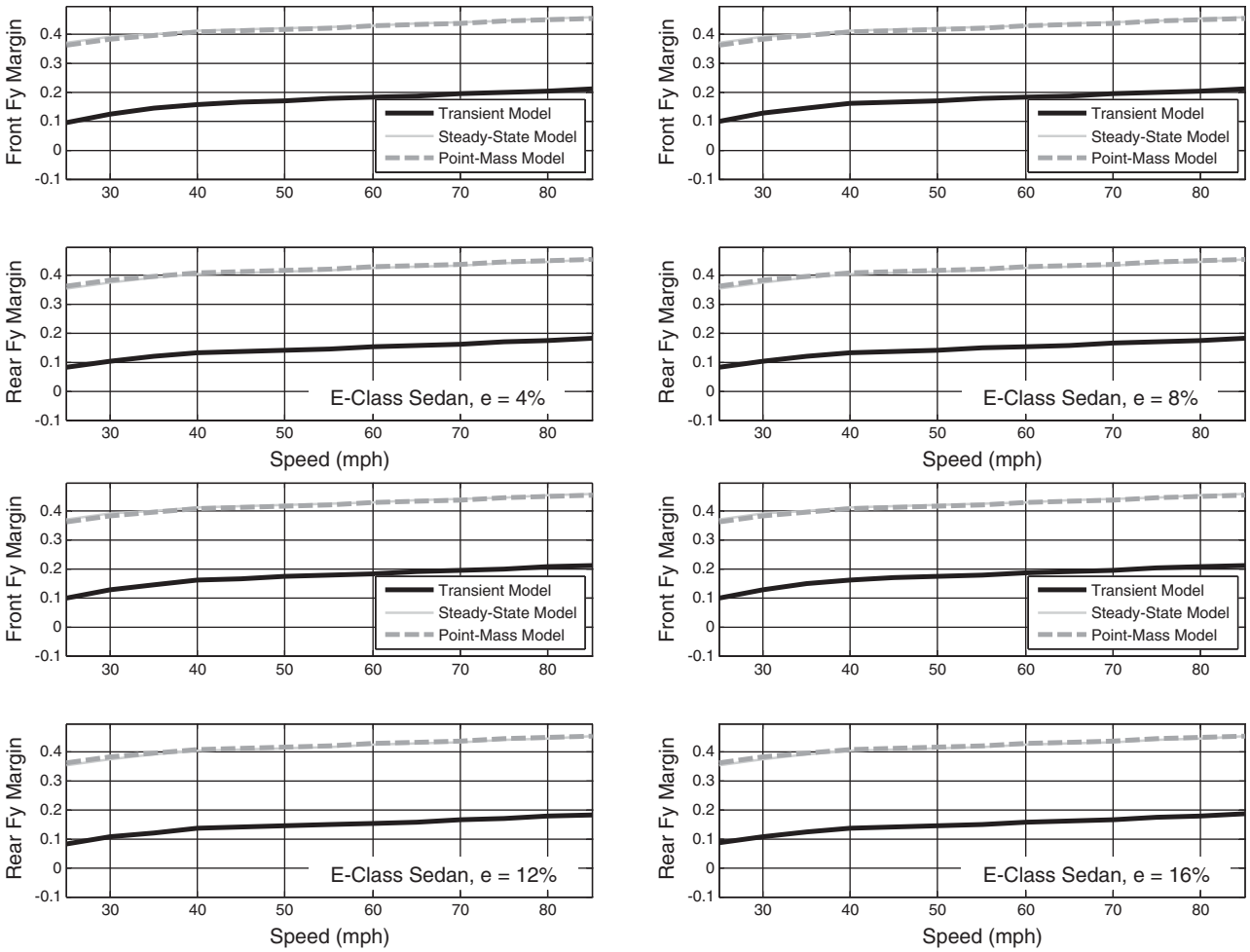

Figure 63. Lateral friction margins from point-mass, steady-state bicycle, and transient bicycle models for E-class sedan (G = −9%, e = 4% to 16%) (a_x = 0 ft/s² and lane change).

vehicle-to-vehicle differences amount to approximately 0.06 in margins. The full-size SUV had the worst margins among the two-axle vehicles simulated here (articulated vehicles are studied in later sections).

4.8.2.5 Effect of Lane-Change Maneuver at Curve-Entry Deceleration

In addition to analyzing the effects of lane changes at constant speed, the effect of minor decelerations during lane changes was also studied. As before, it was unclear when the worst time would be to apply brakes within a curve, particularly if a lane change was also occurring in the curve.

To investigate the worst time for braking in combination with a lane change, a range of braking inputs were applied, with the braking application time measured relative to the start of the lane change. The lane-change maneuver was defined using the worst-case situation found earlier: occurring 3 s after curve entry. As the stagger time between brake application and lane-change initiation was changed, the margins for each simulation were noted. The brake times were varied substantially, from 2 s before the lane change to 4 s after the lane-change maneuver was completed. It was determined that the worst time to initiate a brake input was approximately 0.75 s after the lane change starts (e.g., when the vehicle is just beginning to spin toward the target lane). The simulations hereafter for combined lane-changing, braking, and curve-keeping inputs are set up so that the lane change initiates 3 s after curve entry and the brake inputs occur 0.75 s after the lane change starts. Both situations correspond to the worst-case conditions for each situation.

Figure 66 compares the lateral friction margins for the point-mass model, steady-state bicycle model, and the transient bicycle model for an E-class sedan. The resulting margins from this non-steady situation are significantly lower than the steady-state model and the point-mass model predicted margins.

To study the effect of grade, superelevation, and vehicle type in lane-change and braking situations, another series of simulations was conducted. The results are shown in

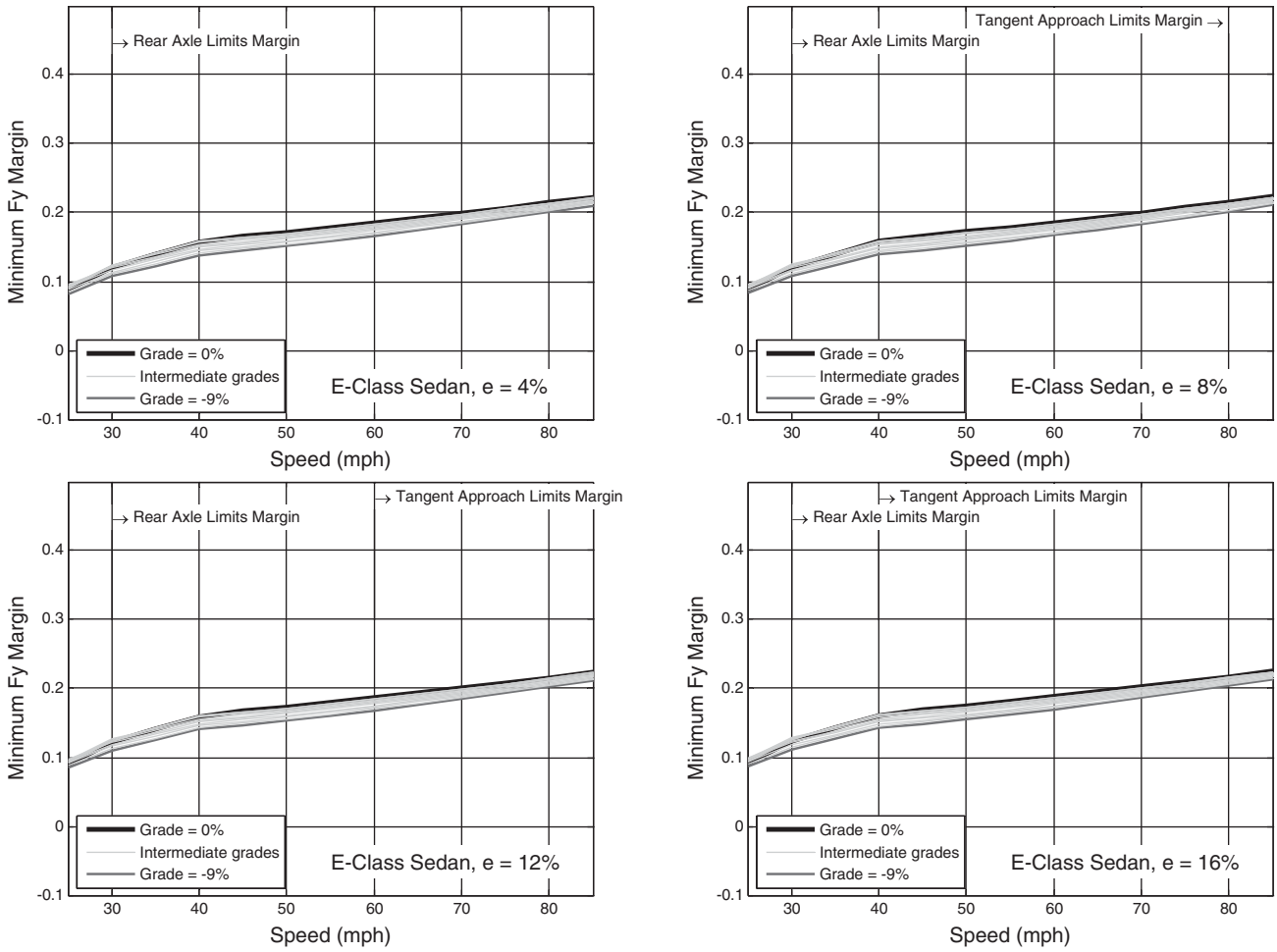

Figure 64. Lateral friction margins from transient bicycle model for E-class sedan (G = 0 to −9%, e = 4% to 16%) (a_x = 0 ft/s² and lane change).

Figure 67 for an E-class sedan, in Figure 68 for an E-class SUV, in Figure 69 for a full-size SUV, and in Figure 70 for a single-unit truck. As observed before, for passenger vehicles, each percentage decrease in grade appears to reduce friction margin by approximately 0.001. However, for the truck, the lateral friction margin decreases by 0.002. This is due to many factors: a higher center of gravity that causes more weight shift, different tire type, and greater tire force magnitudes required for braking. Across all vehicle types, the margins are worse at low speeds. At low speeds and on high grades, the margins are particularly low. For the single-unit truck, the combination of low speeds on high grades results in negative lateral friction margins. Considering the effect of superelevation on lateral friction margins, the addition of superelevation does increase the lateral friction margins slightly, but this effect is consistently very small across all the vehicles considered in this study.

When lane changes combined with braking (−3 ft/s²; see Figures 67 to 70) are compared to the no-braking (0 ft/s²) lane-change case (see Figures 64 and 65), the addition of braking reduced the lateral friction margins for constant-speed lane changes by an additional 0.05 for passenger vehicles and by 0.15 for the single-unit truck. For grades of −8% and −9%, the single-unit truck has negative friction margins in this case for design speeds less than 40 mph. Thus, the effects of braking and lane changes on lateral friction margins can accumulate to ultimately give very low or negative lateral friction margin situations.

With the negative friction margins observed in Figure 70, it is worthwhile to review how these margins are physically obtained and what they signify. As noted in Section 3.4, the minimum friction supplies are obtained from the statistical distribution of friction values obtained from field measurements for wet pavement conditions. To calculate the friction supply, the statistical distribution of supply friction is calculated at two standard deviations below the mean; as reference, these 2nd percentile friction values are generally 0.1 to 0.15 below the mean values. To calculate the friction demand, the simulations are conducted on dry roads as these will generally not excite skidding (which is difficult to simulate) and also generally demand the most tire forces. Further, the simulation procedure above is intentionally seeking out the lowest friction margins (i.e., the worst-case maneuver combinations). Thus, the negative friction margins do not imply that the roadway design will cause skidding for a particular vehicle; rather, it indicates that if the road conditions are wet, if the road condition is at the 2nd-percentile friction

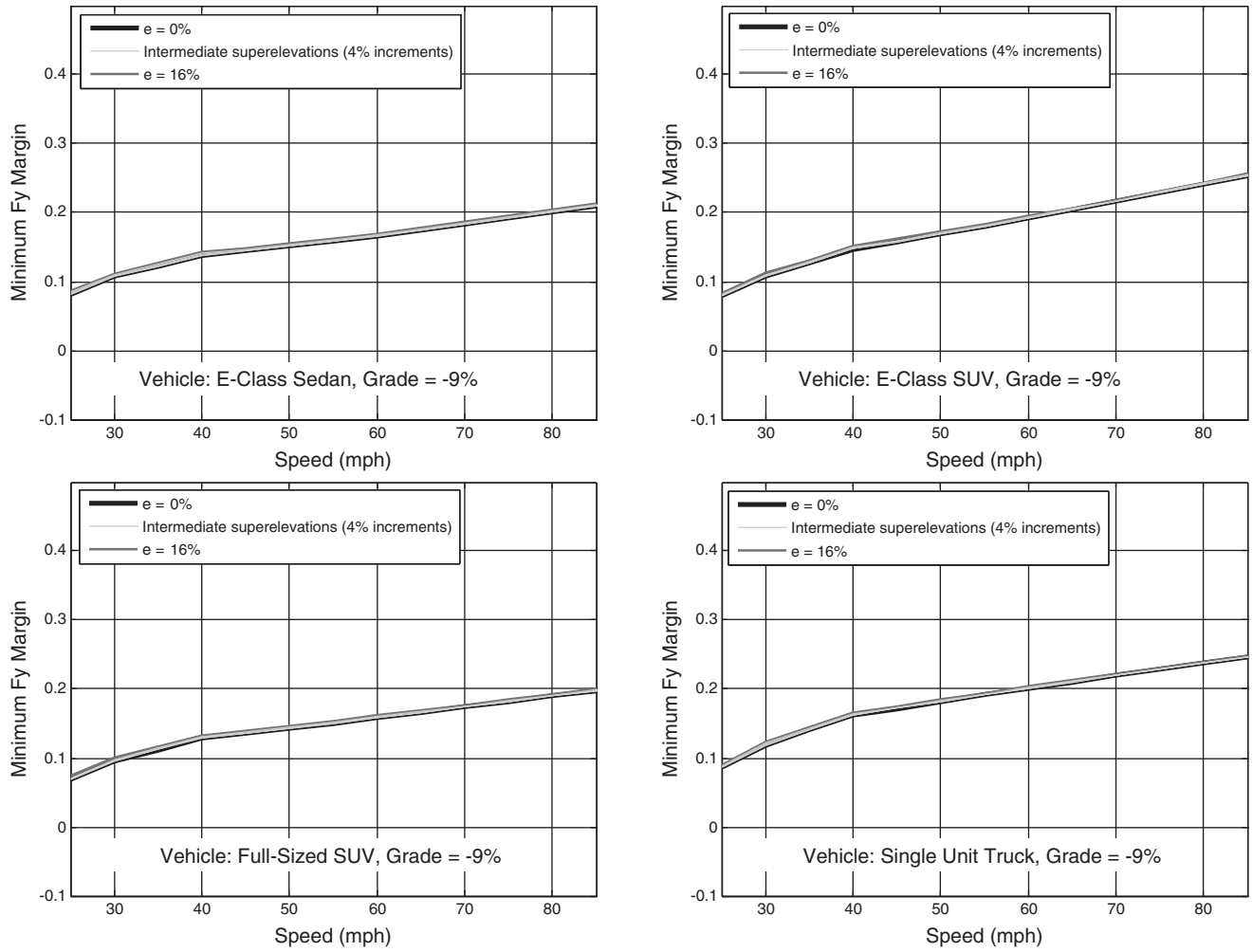

Figure 65. Lateral friction margins from transient bicycle model for E-class sedan, E-class SUV, full-size SUV, and single-unit truck (G = −9%, e = 4% to 16%) (a_x = 0 ft/s² and lane change).

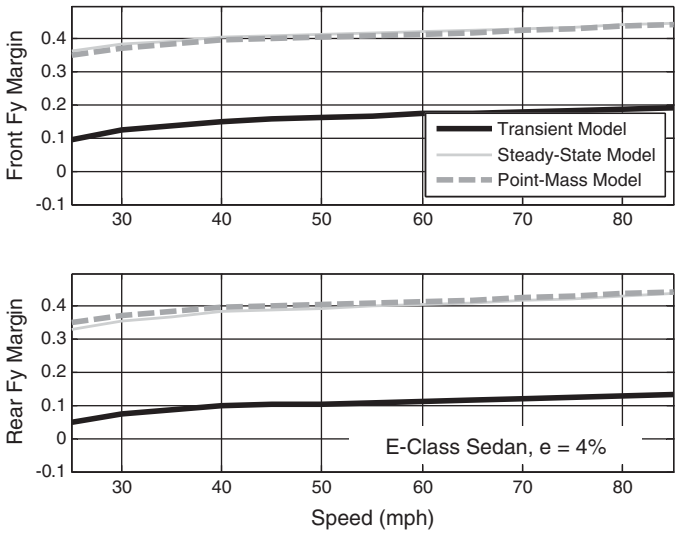

Figure 66. Lateral friction margins from point-mass, steady-state bicycle, and transient bicycle models for E-class sedan (G = −9%, e = 4%) (a_x = −3 ft/s² and lane change).

values of all roads, and if the maneuver combination is at the worst timing and location within the curve, then skidding may occur. Thus, the results do not provide absolute pass/fail criteria for a road design; instead they serve as indicators of trends and identify combinations of designs and operational conditions that might cause concern.

Because several of the simulation results above show very low margins, the more complex simulation models' accountings of horizontal curvature, grade, and superelevation are used to simulate these maneuvers in later steps (see Section 4.11) to confirm whether this transient model is accurately predicting the possibility of skidding during a lane-change maneuver combined with braking inputs.

4.8.2.6 Tractor Semi-Trailers

Tractor semi-trailer behavior was also considered for the same geometry and the same maneuver types. The model used in the following tractor semi-trailer simulations was developed with the same assumptions as the passenger vehicle bicycle model. One key difference, however, is that since tractor

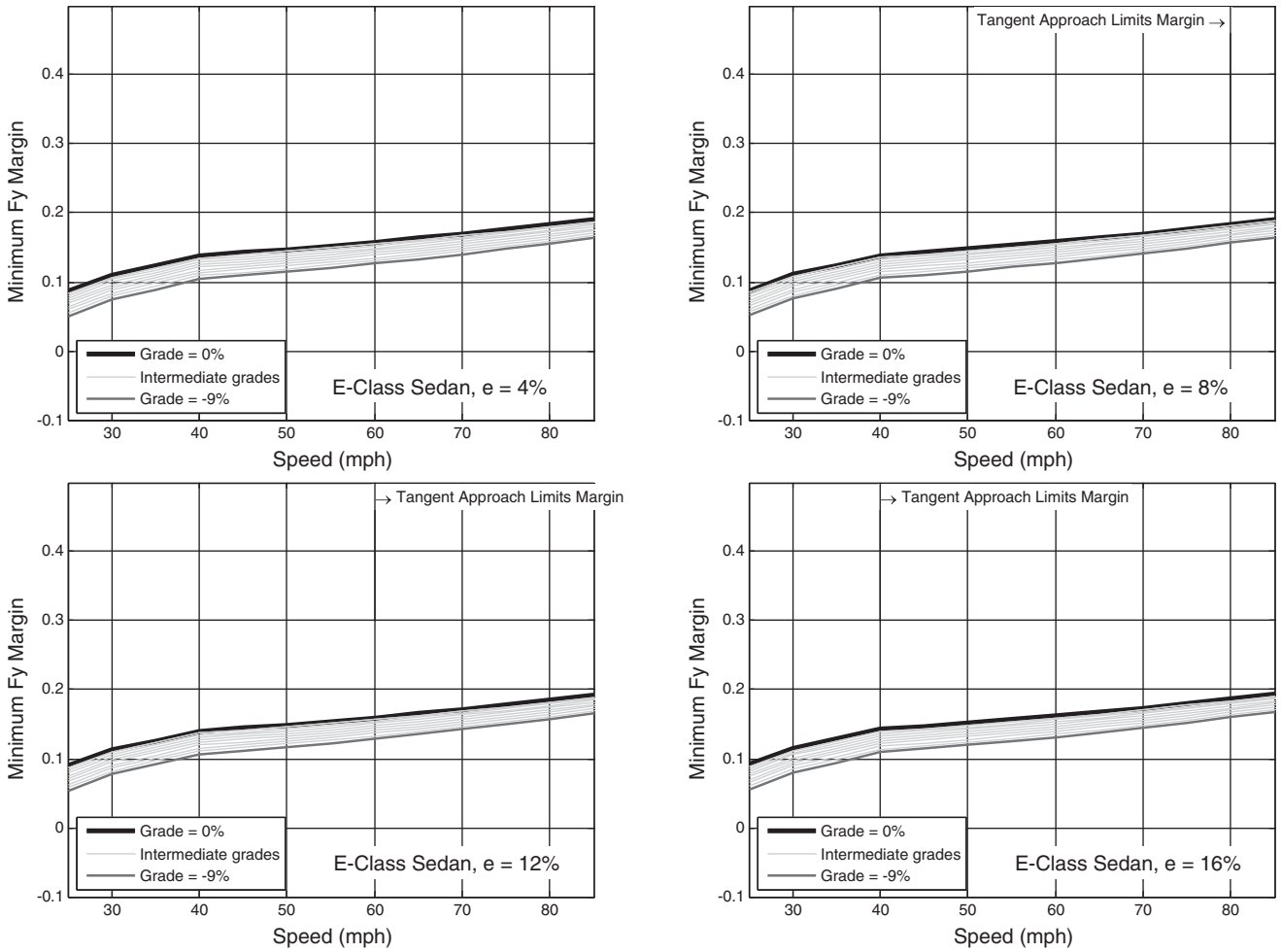

Figure 67. Lateral friction margins from transient bicycle model for E-class sedan (G = 0% to −9%, e = 4% to 16%) (a_x = −3 ft/s² and lane change).

semi-trailers typically have multiple axles spaced close together longitudinally at the back of the cab and at the back of the trailer unit, these axles were each lumped into single representative axles for the simulations. A diagram outlining the model structure for the low-order tractor semi-trailer dynamic equations is presented in Figure 71.

To explain the equations that follow, Table 25 defines the symbols used in the equations in addition to those symbols previously defined. Key measurements are labeled in Figure 71. The tractor semi-trailer has three wheel clusters: the front of the tractor, the back of the tractor, and the back of the trailer. These are referred to as the "front," "rear," and "trailer" axles in the plots and discussion that follow.

To calculate the tire forces, the analysis of the tractor semi-trailer is more complex than a passenger vehicle because the hitch point transmits braking forces between the tractor and trailer. To solve for each axle's normal force, the braking forces on each axle must be known. In this analysis they are assumed to be distributed according to their normal loads. Since the total braking force on the combined tractor semi-trailer is given by the requested deceleration, ma_x, the braking forces for the trailer are:

$$F_{bt} = \frac{N_t}{mg} \cdot a_x m = N_t \frac{a_x}{g} \tag{80}$$

Similarly,

$$F_{bf} = N_f \frac{a_x}{g}$$

$$F_{br} = N_r \frac{a_x}{g} \tag{81}$$

For the trailer, the normal force on the trailer axle is found by moment balance around the hitch point:

$$N_t = m_2 g \cdot \frac{f_t}{g_t + h_h \frac{a_x}{g}} - \left(m_2 \left(a_x - g\frac{G}{100}\right)\right) \frac{h_2 - h_h}{g_t + h_h \frac{a_x}{g}} \tag{82}$$

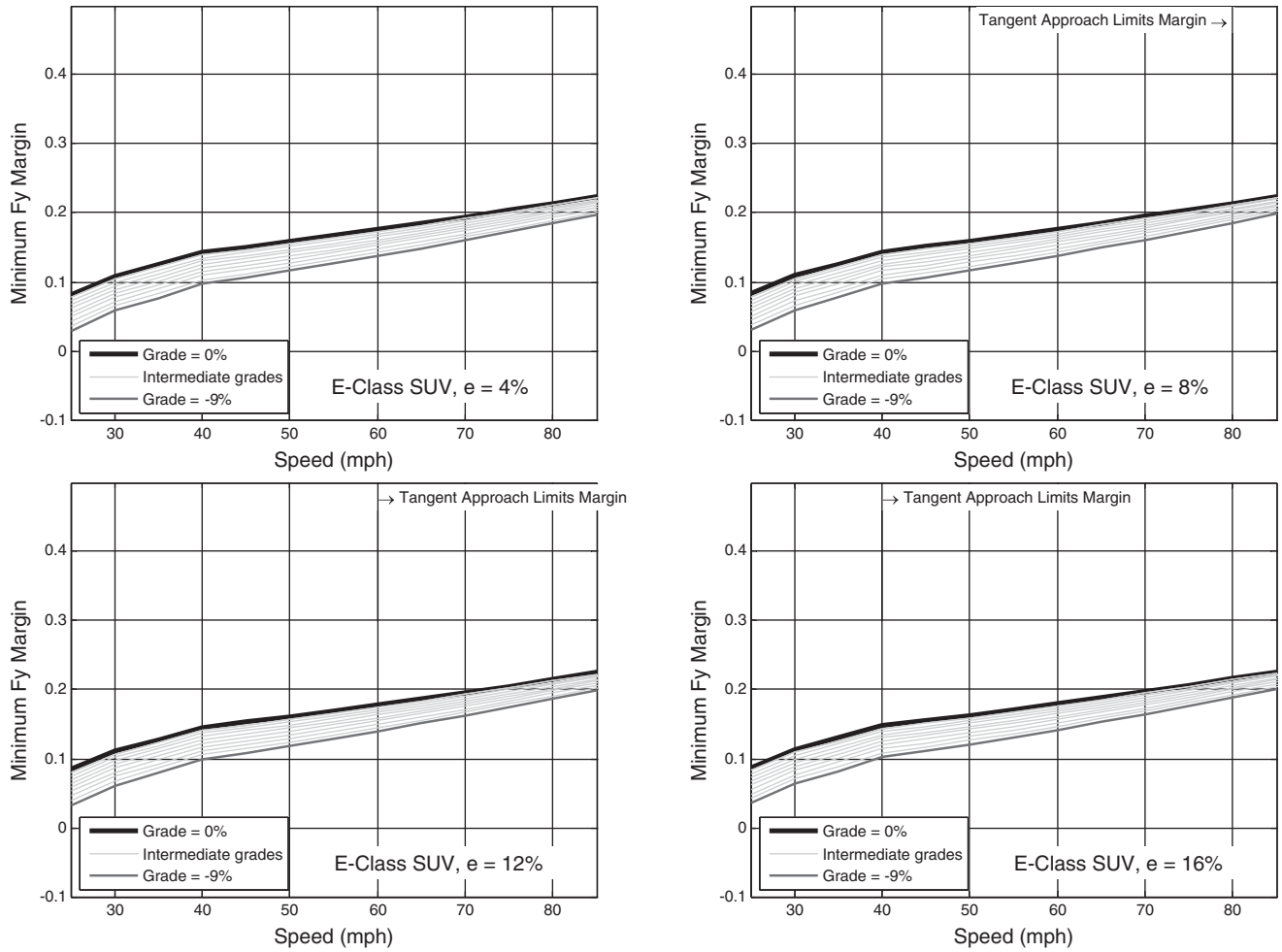

Figure 68. Lateral friction margins from transient bicycle model for E-class SUV (G = 0% to −9%, e = 4% to 16%) (a_x = −3 ft/s² and lane change).

And the sum of vertical forces on the trailer gives the vertical load at the hitch point to be:

$$N_h = m_2 g - N_t$$

$$= m_2 g \cdot \frac{1 - f_t}{g_t + h_h \frac{a_x}{g}} - \left(m_2 \left(a_x - g \frac{G}{100} \right) \right) \frac{h_2 - h_h}{g_t + h_h \frac{a_x}{g}} \qquad (83)$$

The braking force passed through the hitch is given by the amount of deceleration force necessary for the trailer that is not compensated by the trailer axle:

$$F_{bh} = \left(m_2 g - N_t \right) \cdot \frac{a_x}{g} \qquad (84)$$

The moment balance about the rear axle of the tractor gives:

$$N_f = m_1 g \frac{b}{L} + \frac{b - d_h}{L} N_h + \left(\frac{h_h}{L} N_h + m_1 g \frac{h_1}{L} \right) \left(\frac{a_x}{g} - \frac{G}{100} \right) \qquad (85)$$

And the front gives:

$$N_r = m_1 g \frac{a}{L} + \left(1 - \frac{b - d_h}{L} \right) N_h - \left(\frac{h_h}{L} N_h + m_1 g \frac{h_1}{L} \right) \left(\frac{a_x}{g} - \frac{G}{100} \right) \qquad (86)$$

The above equations often have to be used to calculate axle forces on flat surfaces (G = 0%, e = 0%) with no acceleration. These equations simplify in this case to the following:

$$N_{to} = m_2 g \cdot \frac{f_t}{g_t}$$

$$N_f = m_1 g \frac{b}{L} + m_2 g \left(\frac{b - d_h}{L} \right) \left(1 - \frac{f_t}{g_t} \right)$$

$$N_r = m_1 g \frac{a}{L} + m_2 g \left(\frac{a + d_h}{L} \right) \left(1 - \frac{f_t}{g_t} \right) \qquad (87)$$

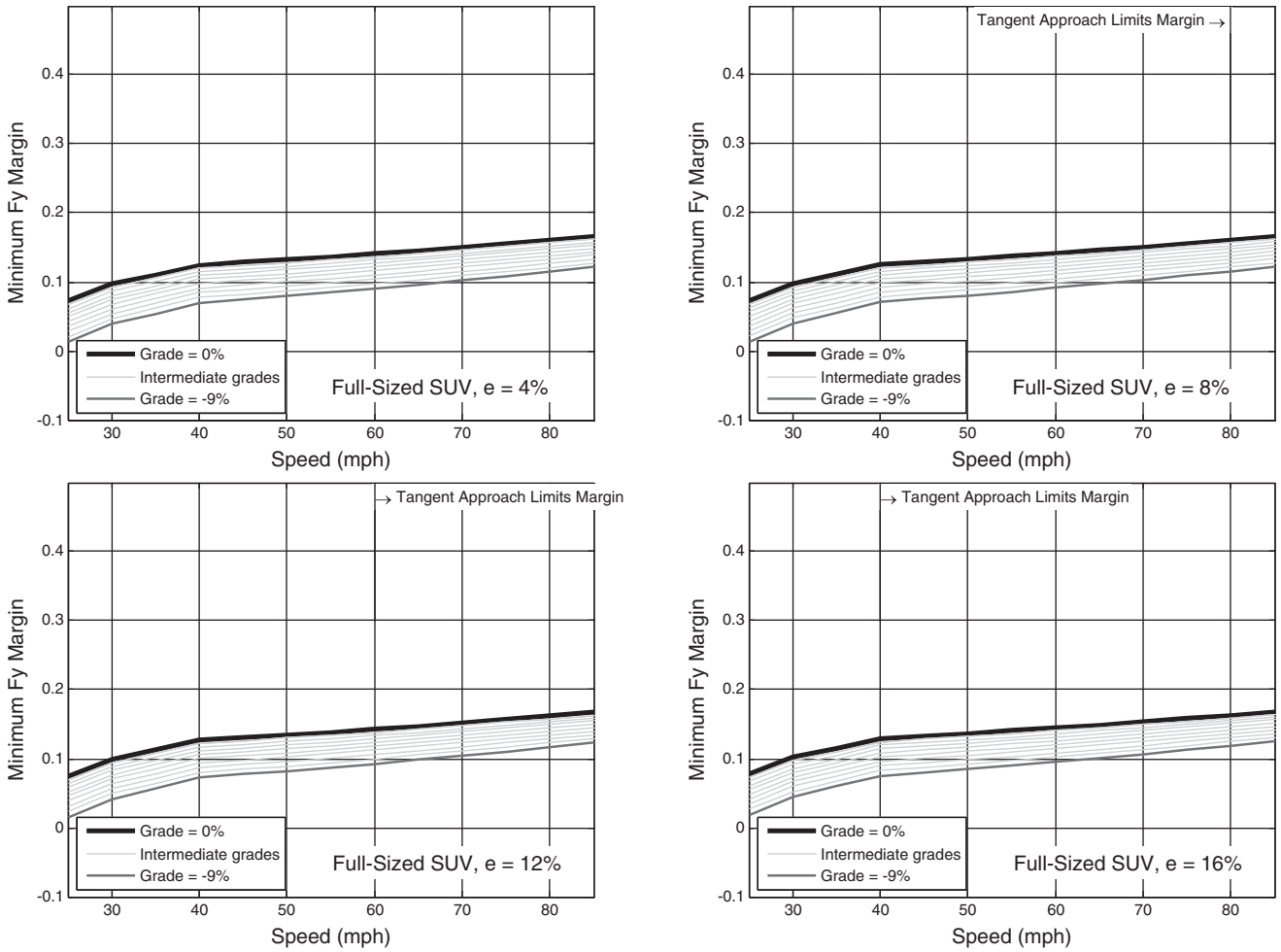

Figure 69. Lateral friction margins from transient bicycle model for full-size SUV (G = 0% to −9%, e = 4% to 16%) (a_x = −3 ft/s² and lane change).

The full equations of motion for the tractor semi-trailer are extensive and significantly more complicated than the bicycle model presented here (Pacejka, 2006).

Effect of Curve Keeping at Constant Speed for Tractor Semi-Trailers. A set of simulations for tractor semi-trailers was run to investigate situations where the vehicle transitions from a straight tangent to a constant-radius curve at a constant speed. As before, it was assumed that the superelevation is fully developed on the approach to the curve and thus is constant throughout the maneuver.

A comparison of the point-mass, steady-state bicycle, and transient bicycle models for the tractor semi-trailer for a constant-speed curve entry did not show appreciable differences between the three model predictions. This is expected, as the constant-speed, curve-keeping driving situation is the least likely to excite transient motions that might favor one axle or another. As with the passenger vehicle situations discussed earlier, the lateral friction margin increases with speed from 0.29 at 25 mph up to 0.41 at 85 mph. Additionally, the transient model predicts slightly less margin at low speeds. Again, this is due to the change in steering input necessary at the beginning of the curve. Because the agreement between the models was quite good across all grades, superelevations, and speeds for this driving situation, only one example plot comparing the models is shown in Figure 72.

Shown in Figure 73 are the minimum lateral friction margins for grades from 0% to –9%, and for four superelevations (4% to 16% in 4% increments), for the tractor semi-trailer. As noted with passenger vehicles, there is a minor but consistent influence of grade seen across all superelevations. For speeds above 35 mph, the 10% change in grade reduces the friction margin by about 0.01 to 0.02, or about 0.001 to 0.002 margin reduction per each 1% change in grade. These numbers are consistent with those observed for two-axle vehicles noted earlier. Like passenger vehicles, tractor semi-trailers are limited at low speeds (35 mph and lower) by the margins available on the front tires, and thus the steering change at the onset of the curve causes the lowest friction margins. At high speeds and high superelevations, the friction margins are limited by

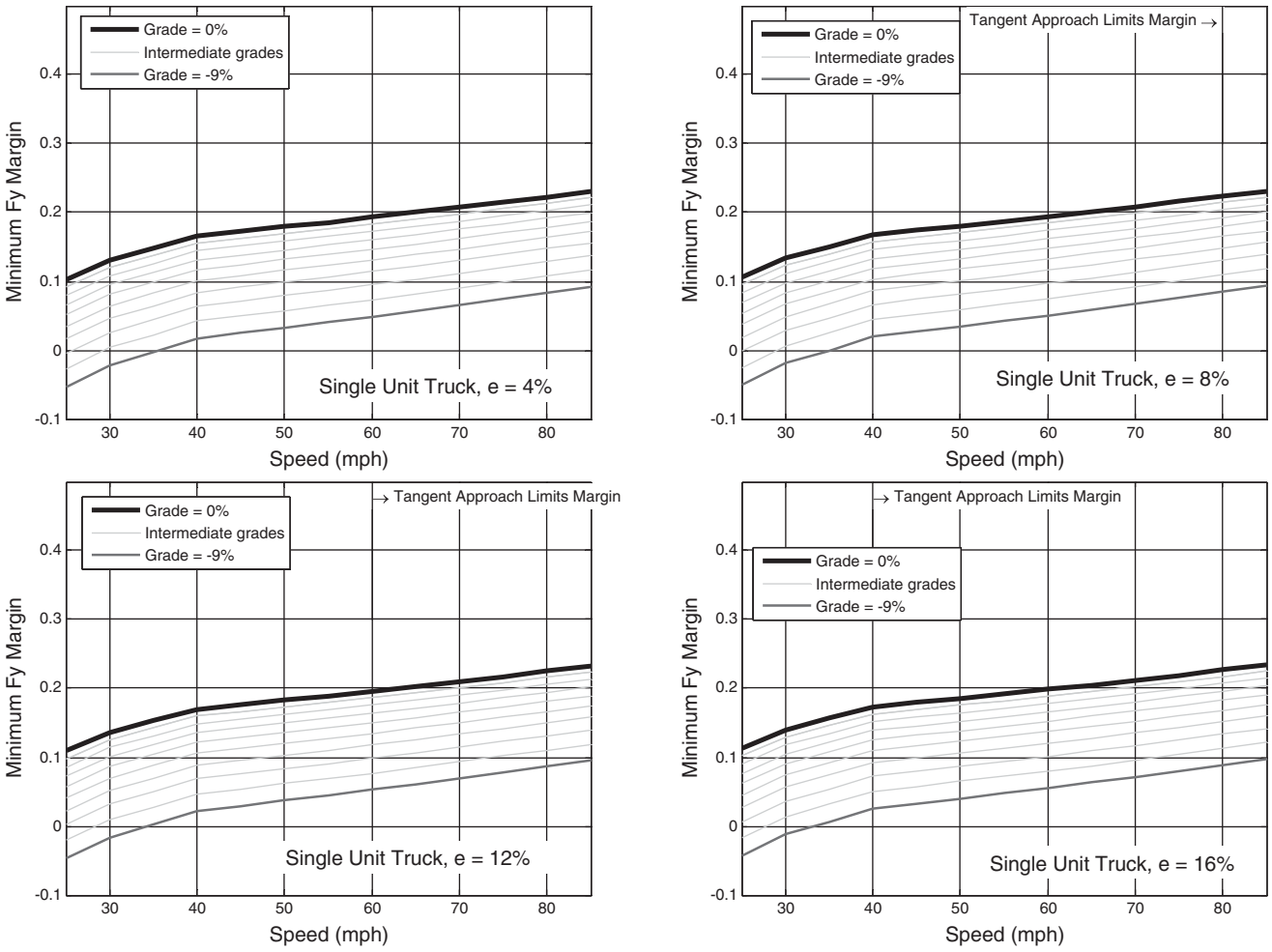

Figure 70. Lateral friction margins from transient bicycle model for single-unit truck (G = 0% to −9%, e = 4% to 16%) (a_x = −3 ft/s² and lane change).

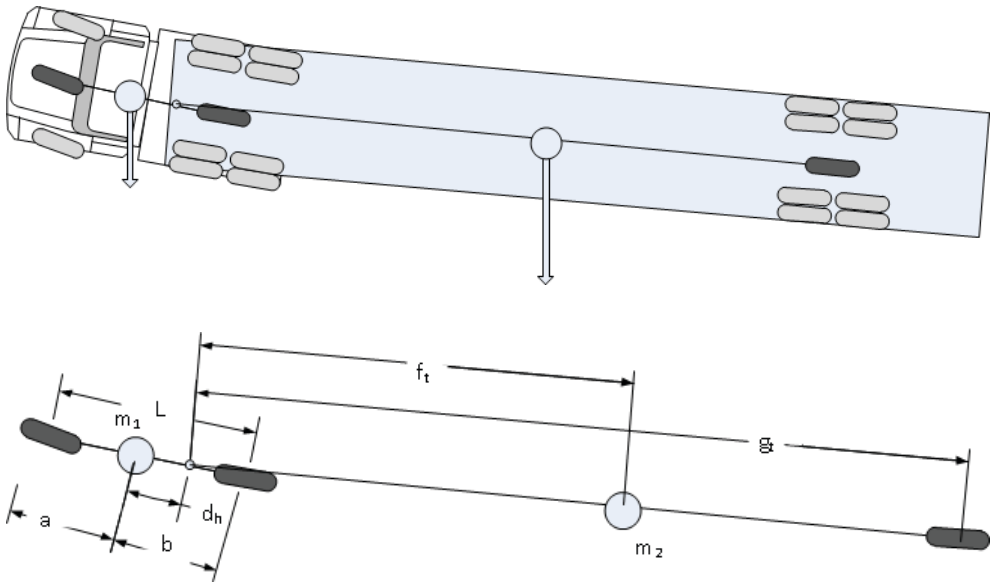

Figure 71. Bicycle model representation of tractor semi-trailer, each set of tires is represented by a single axle.

Table 25. Variables used to extend bicycle model to tractor semi-trailer.

Symbol	Meaning
m_1	Mass of tractor
m_2	Mass of loaded trailer
m	Mass of tractor and trailer together
g_t	Distance from hitch to trailer axle
f_t	Distance from hitch to trailer CG
a_x	Deceleration along x-axis
F_{bf}, F_{br}, F_{bt}	Braking force (front, rear, trailer axle)
F_{cf}, F_{cr}, F_{ct}	Cornering force (front, rear, trailer axle)
N_f, N_r, N_t, N_h	Normal loads (front, rear, trailer axle, hitch)
W	Vehicle weight ($m \cdot g$)
a, b	Tractor CG to front- and rear-axle distance
d_h	Tractor CG to hitch distance
L	Wheelbase of tractor (i.e., a + b)
h_1, h_2, h_h	Height of tractor CG, trailer CG, and hitch point

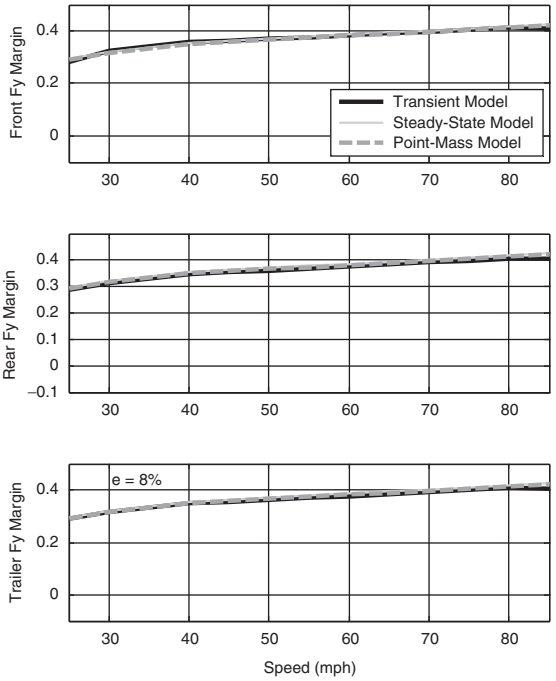

Figure 72. Lateral friction margins from point-mass, steady-state bicycle, and transient bicycle models for tractor semi-trailer (G = −9%, e = 8%) (a_x = 0 ft/s²).

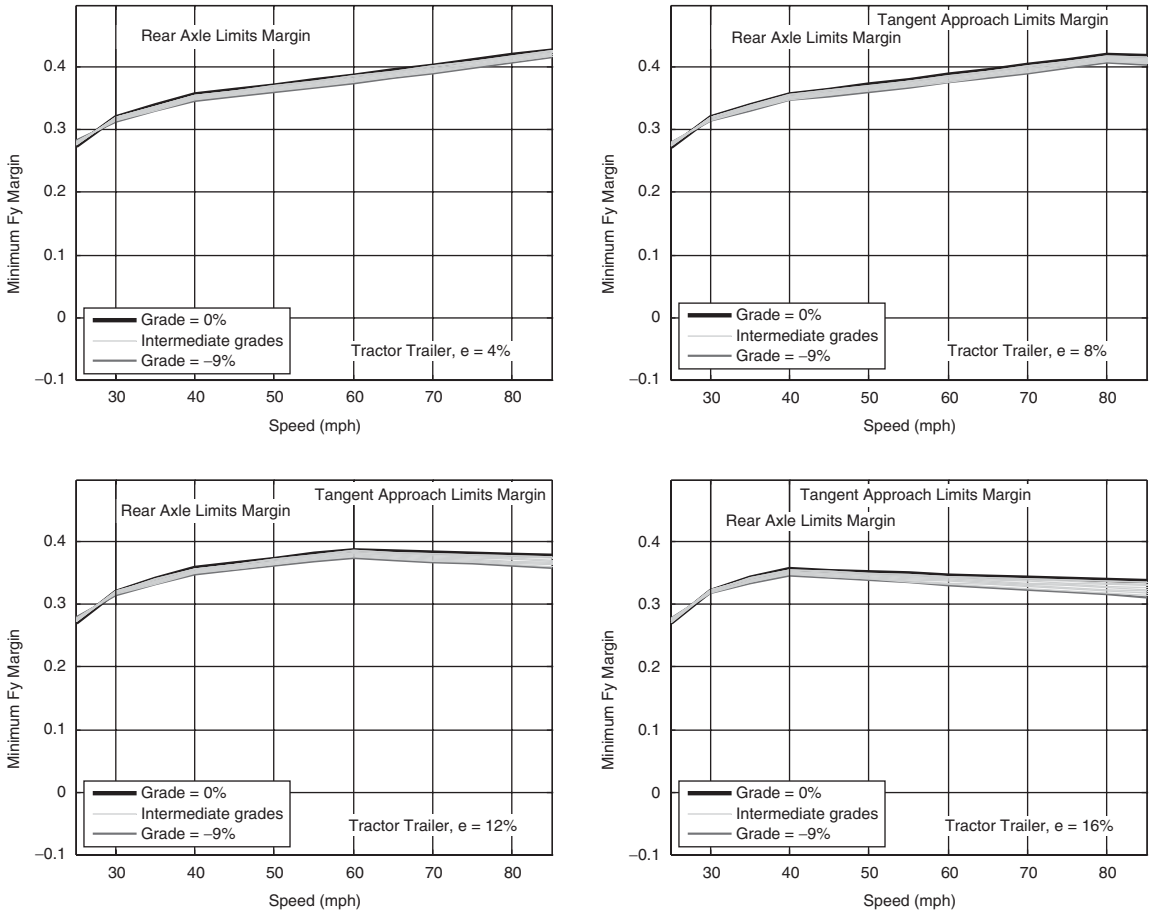

Figure 73. Lateral friction margins from transient bicycle model for tractor semi-trailer (G = 0% to −9%, e = 4% to 16%) (a_x = 0 ft/s²).

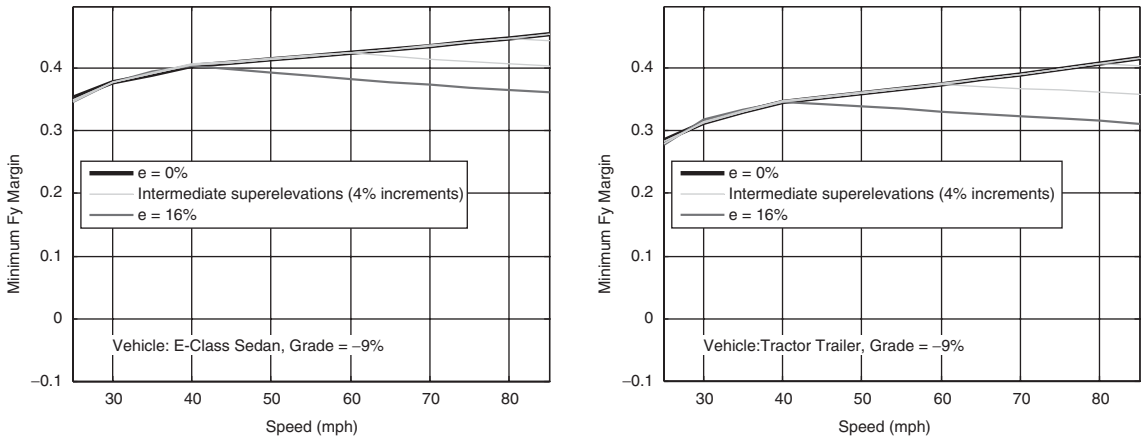

Figure 74. Lateral friction margins from transient bicycle model for E-class sedan and tractor semi-trailer (G = −9%, e = 0% to 16%) (a_x = 0 ft/s²).

the approach tangent rather than the curve itself. Again, this is consistent with observations made from passenger vehicles.

To further illustrate the similarities and differences between passenger vehicles and tractor semi-trailers, Figure 74 shows the minimum lateral friction margins for cornering for a fixed grade of –9%, and for five superelevations (0% to 16% in 4% increments), for both the tractor semi-trailer and an E-class sedan. As noted before, while grade and superelevation have some visible influence on the friction margins, overall these effects are minor compared to the influence of speed and maneuvers on the road. For this configuration of a tractor semi-trailer, the superelevation influenced the friction margin by a maximum of approximately 0.10 when comparing 0% superelevation margins to 16% superelevation margins at 85 mph, but the effect of superelevation decreases with speed. Thus, as observed with passenger vehicles, the primary benefit of superelevation appears to be to allow designers to decrease the radius of curvature. And like passenger vehicles, the tractor semi-trailer also exhibits lower friction margins on the curve approach for high superelevations, at higher design speeds. Thus, as noted before, superelevations above 12% cause decreasing friction margins at high speeds compared to roads with lower superelevations.

Effect of Curve-Entry Deceleration for Tractor Semi-Trailers. To consider the curve-entry deceleration case, another set of simulations were conducted to represent a mild deceleration on the curve. Specifically, a constant deceleration value of –3 ft/s² was initiated 6.75 s after curve entry. (This choice of timing is discussed in later sections.) As with passenger vehicles, this deceleration value was not adjusted for grade, so the net braking friction demand increases slightly as grade becomes steeper and steeper.

Figure 75 compares the results of the transient model to the steady-state model and the point-mass model for the curve-entry deceleration case. As with passenger vehicles, all models predict increasing friction margin with increasing design speed. Again, the transient model agrees closely with the steady-state model and point-mass models, with a very slightly lower predicted margin on the rear and trailer axles. These predictions agree as long as the superelevation on the approach is not too high, as mentioned in previous sections. Because the agreements between the models are so close for this maneuver, only one example is shown.

Figure 76 shows the effect of grade and superelevation on the tractor semi-trailer's lateral friction margins for curve-entry

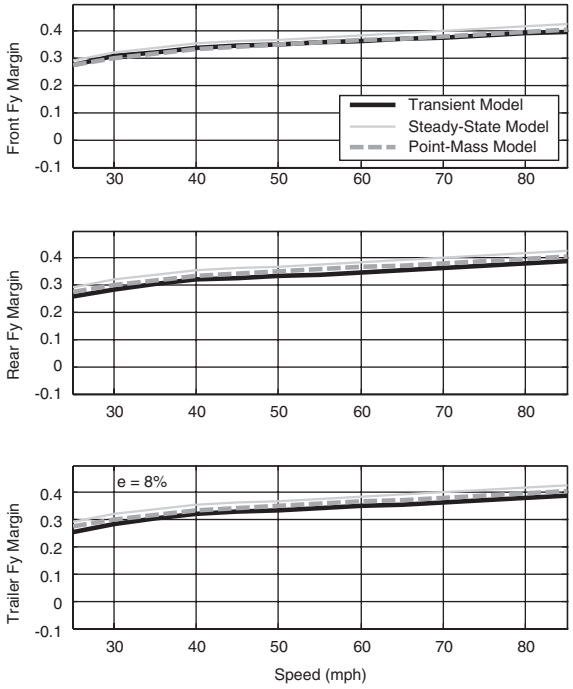

Figure 75. Lateral friction margins from point-mass, steady-state bicycle, and transient bicycle models for tractor semi-trailer (G = −9%, e = 8%) (a_x = −3 ft/s²).

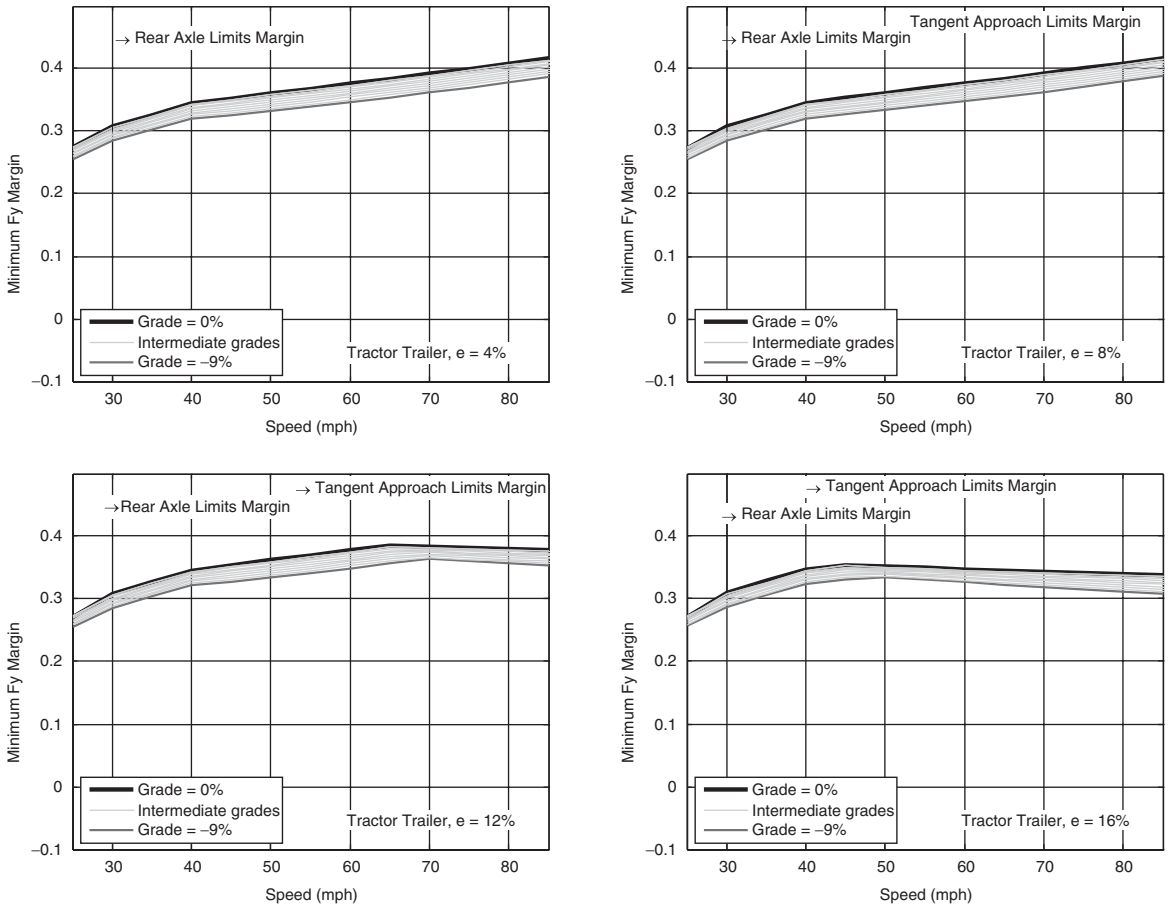

Figure 76. Lateral friction margins from transient bicycle model for tractor semi-trailer (G = 0% to −9%, e = 4% to 16%) ($a_x = -3$ ft/s²).

deceleration. Again, there is a distinct transition in margins at around 35 mph, representing the transition from front-axle skidding-dominated behavior at low speeds, to rear-axle skidding at higher speeds. This same behavior is observed in passenger vehicles, as seen in Figure 59; however, the friction margin for a tractor semi-trailer is approximately 0.08 to 0.1 lower. This is most likely due to differences in the tires between passenger vehicles and trucks.

The constant-speed case ($a_x = 0$ ft/s²) in Figure 73 and the curve-entry deceleration case ($a_x = -3$ ft/s²) in Figure 76 have very similar minimum friction margins at lower speeds. In other words, the minor decelerations observed on the approach and within the curve do not appear to significantly affect the lateral friction margins.

In Figure 77 the effects of superelevation are plotted for the tractor semi-trailer case and compared to the closest passenger vehicle case. Specifically, the minimum friction margins are plotted for the tractor semi-trailer across the entire range of superelevations and compared to the E-class sedan. Comparing the tractor semi-trailer to the E-class sedan, the truck has a friction margin that is 0.08 to 0.1 lower across all speeds. While this could be significant, it reveals that the tractor semi-trailer is not the most sensitive to braking situations. In comparison, the single-unit truck had a friction margin in the same situations that was 0.2 lower than the passenger vehicles. But even considering supply frictions two standard deviations below the mean measured friction across all sites, there is still some amount of friction in reserve for normal driving maneuvers with curve-entry deceleration ($a_x = -3$ ft/s²).

Effect of Lane-Change Maneuver at Constant Speed for Tractor Semi-Trailers. Like the studies done for passenger vehicles, the effects of lane-change maneuvers on a tractor semi-trailer were also studied. As before, it was assumed that for a lane-change maneuver, the vehicle travels from a low-speed lane to a high-speed lane at a constant speed, the curve was to the left, and therefore the lane change was toward the inside of the curve. The sine wave steering input was used for the tractor semi-trailer with a 4 s period as noted for the single-unit truck. One large difference in the simulation of a tractor semi-trailer is that the lane-change maneuver was performed further in the curve than with other vehicles, at 5 s into the curve rather than the 3 s for other vehicles. Again, this represents the worst-case time to initiate a lane-change maneuver. This time difference is

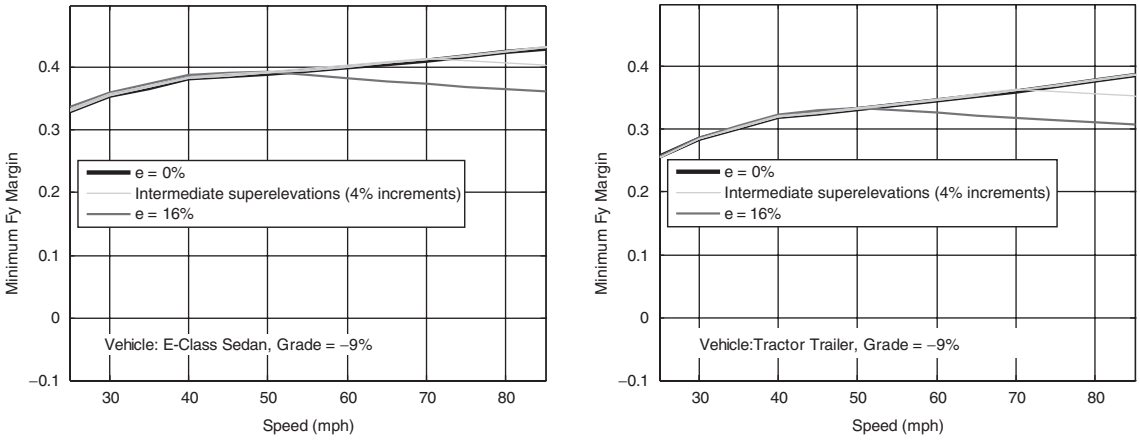

Figure 77. Lateral friction margins from transient bicycle model for E-class sedan and tractor semi-trailer (G = −9%, e = 0% to 16%) (a_x = −3 ft/s²).

because tractor semi-trailers were seen to take longer to reach steady-state after the curve entry than other vehicles, due to the trailer dynamics and the vehicle's larger mass.

Figure 78 shows a comparison of the lateral friction margins for the transient model, the steady-state model, and the point-mass model for the lane-change maneuver for the tractor semi-trailer for 8% superelevation. Other superelevations were also simulated (0% to 16% in 4% intervals), and the results were nearly identical. As expected, the lane-change event reduces friction margin noticeably versus the steady-state bicycle model and the point-mass model. This is seen across all three axles. This reduction in friction values ranges from 0.1 to 0.15. However, comparing the tractor semi-trailer results to the passenger vehicle results in Figure 63, the friction margin reductions for tractor trailers are actually much less than the passenger vehicle case. In other words, passenger vehicles are far more sensitive to lane-change maneuvers than are tractor semi-trailers. This is primarily due to the slower response of the tractor semi-trailers relative to passenger vehicles; the lane changes for the larger vehicles are not only initiated over a longer interval, but it takes longer to complete even when the intervals are kept the same.

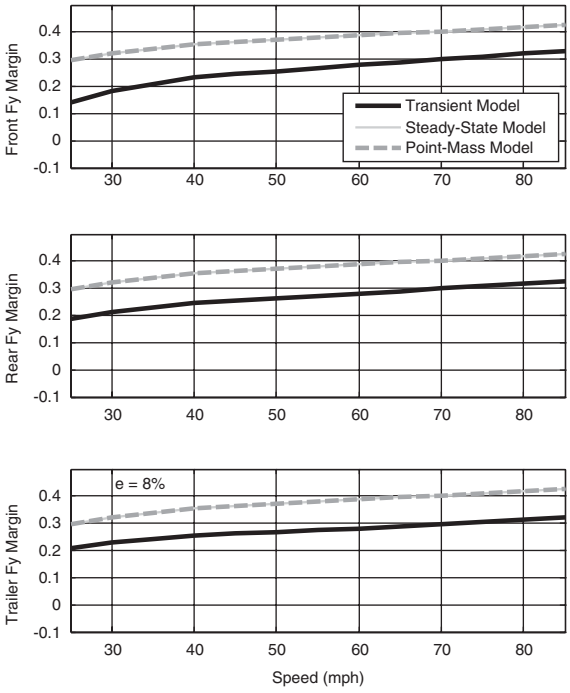

Figure 78. Lateral friction margins from point-mass, steady-state bicycle, and transient bicycle models for tractor semi-trailer (G = −9%, e = 8%) (a_x = 0 ft/s² and lane change).

To determine the effects of grade, superelevation, and speed on friction margin, a series of plots are shown in Figure 79. Several effects are consistently observed across superelevations. First, the lateral friction margins increased from approximately 0.15 to 0.30 as speeds increase from 25 to 85 mph. Second, the effects of superelevation on lateral friction margins appear to be small, as the plots are nearly indistinguishable from each other between the 4%, 8%, 12%, and 16% superelevation cases. As grade changes from 0% to –9%, the margin changes by approximately 0.02, and thus the grade's influence on margin is about 0.002 per each 1% change in grade. Interestingly, for a tractor semi-trailer, the lateral friction margins improve for increasing grade at speeds less than 40 mph, and above 60 mph the margins are worse for increasing grade. Between 40 and 60 mph, the effect of grade has mixed impacts on the resulting margin. Overall, the effects of grade and superelevation are small compared to the effects of speed, vehicle type, and maneuvers.

Figure 80 shows the effect of superelevation and vehicle type on friction margins, comparing a tractor semi-trailer to the worst-performing passenger vehicle, the full-size SUV. The plots show a slight increase in lateral friction margins across all speeds. However, the influence of superelevation is

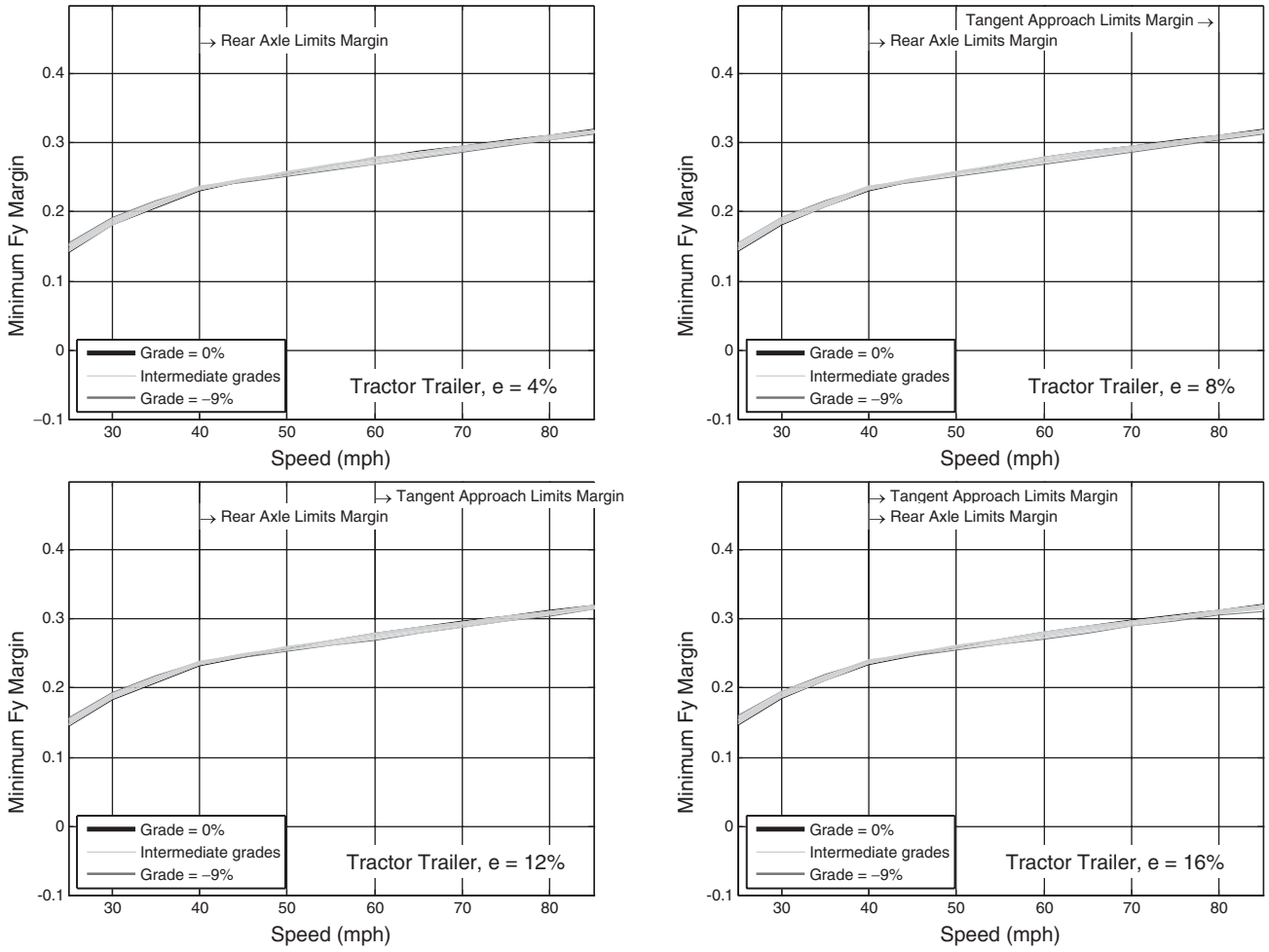

Figure 79. Lateral friction margins from transient bicycle model for tractor semi-trailer (G = 0% to −9%, e = 4% to 16%) (a_x = 0 ft/s² and lane change).

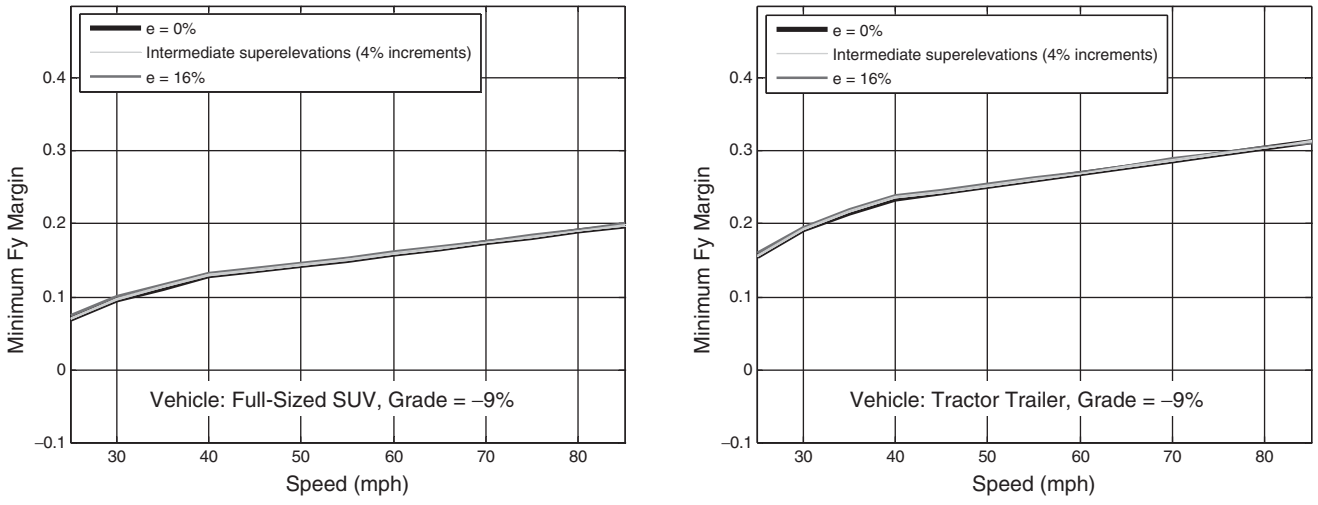

Figure 80. Lateral friction margins from transient bicycle model for full-size SUV and tractor semi-trailer (G = −9%, e = 0% to 16%) (a_x = 0 ft/s² and lane change).

small: a 0.02 increase in margin occurs across a 16% superelevation change, or about 0.001 increase in margin increase per 1% of superelevation added. This, as observed earlier, is almost negligible. Thus, the effect of superelevation appears mainly to allow designers to reduce road curvature. Compared to passenger vehicles, the tractor semi-trailer has higher lateral friction margins across all speeds by a factor of about 0.08 to 0.1. Again, this is due to the more gradual lane changes that these vehicles perform versus passenger vehicles.

Effect of Lane-Change Maneuver at Curve-Entry Deceleration for Tractor Semi-Trailers. The effect of minor decelerations during lane changes was also studied for the tractor semi-trailer. As in the passenger vehicle case, it was unclear when the worst time would be to apply brakes within a curve, particularly if a lane change was also occurring on the curve. To investigate the worst time for braking, a sensitivity analysis was performed varying braking inputs for the tractor semi-trailer. Through this analysis it was determined that the worst time to initiate a brake input for a tractor semi-trailer is approximately 0.75 s after the lane change starts (e.g., when the vehicle is just beginning to spin toward the target lane). This is nearly identical to the passenger vehicle case as shown with the sedan. From the results of the worst-case braking time, the simulations hereafter have the brake inputs occur 0.75 s after the lane change starts.

From the same sensitivity analysis, it was also determined that the limiting axle on tractor semi-trailers changes with speed. At low speeds, the front axle has the lowest margin. At intermediate speeds, the tractor's rear axle has the lowest margin, and at high speeds, the trailer's axle has the lowest margin.

To analyze model-specific effects for a tractor semi-trailer, Figure 81 provides a comparison of the point-mass model, steady-state bicycle model, and transient bicycle model with the additional effects of brake inputs included with the lane change. Note that only the transient model includes the lane-change effects, and the margins from this model are significantly lower than the others, as expected. The results shown here are consistent with the results discussed earlier for passenger vehicles.

To study the effect of grade, superelevation, and speed in lane-change and braking situations, another series of simulations was conducted, the results of which are plotted in Figure 82. Comparing these results to the two-axle vehicle cases shown in Figures 67 through 70, the plots show that a tractor semi-trailer has much higher margins than other vehicles for combined braking and lane-change situations. While all other vehicles had margins below 0.1 (and sometimes below zero), the tractor semi-trailer margins were all above 0.15. As observed for passenger vehicles, each percentage decrease in grade appears to reduce the lateral friction margin by approximately 0.001. When compared to other vehicles, tractor semi-trailers are relatively insensitive to lane-change inputs.

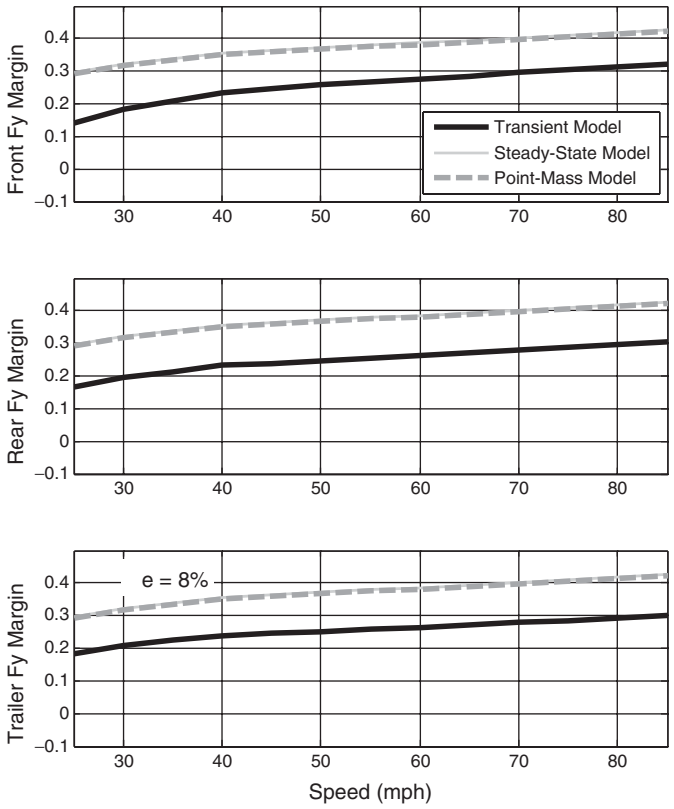

Figure 81. Lateral friction margins from point-mass, steady-state bicycle, and transient bicycle models for tractor semi-trailer (G = −9%, e = 8%) (a_x = −3 ft/s² and lane change).

Finally, Figure 83 presents the effect of superelevation on lateral friction margins, comparing a tractor semi-trailer to the worst-case two-axle vehicle for this situation (i.e., the single-unit truck). As noted earlier for the combined curve-entry deceleration and simple lane-change scenarios, the tractor semi-trailer has much higher lateral friction margins than other vehicles. This is due to the very long length, which results in much lower rear-to-front weight shift.

Effect of Loading for Tractor Semi-Trailers. A series of simulations was conducted to vary the loading conditions to understand these effects. In the previous simulations, the trailer load was set to 22,050 lb, situated 19.7 ft to the rear of the hitch. This results in 14,053 lb on the front axle, 24,778 lb on the rear (tractor) axle, and 18,378 lb on the trailer axle. The total load is 57,209 lb. This is considered the "standard" load in TruckSim, a common commercial truck simulation software tool. However, this is not a worst-case load.

To simulate a truck near the overload condition, the payload of the trailer was increased to 44,841 lb. At this load, if the position of the load is kept at the default (19.7 ft from the hitch), the rear axle of the tractor carries a weight in excess of 37,000 lb, which exceeds the per-axle limit of most

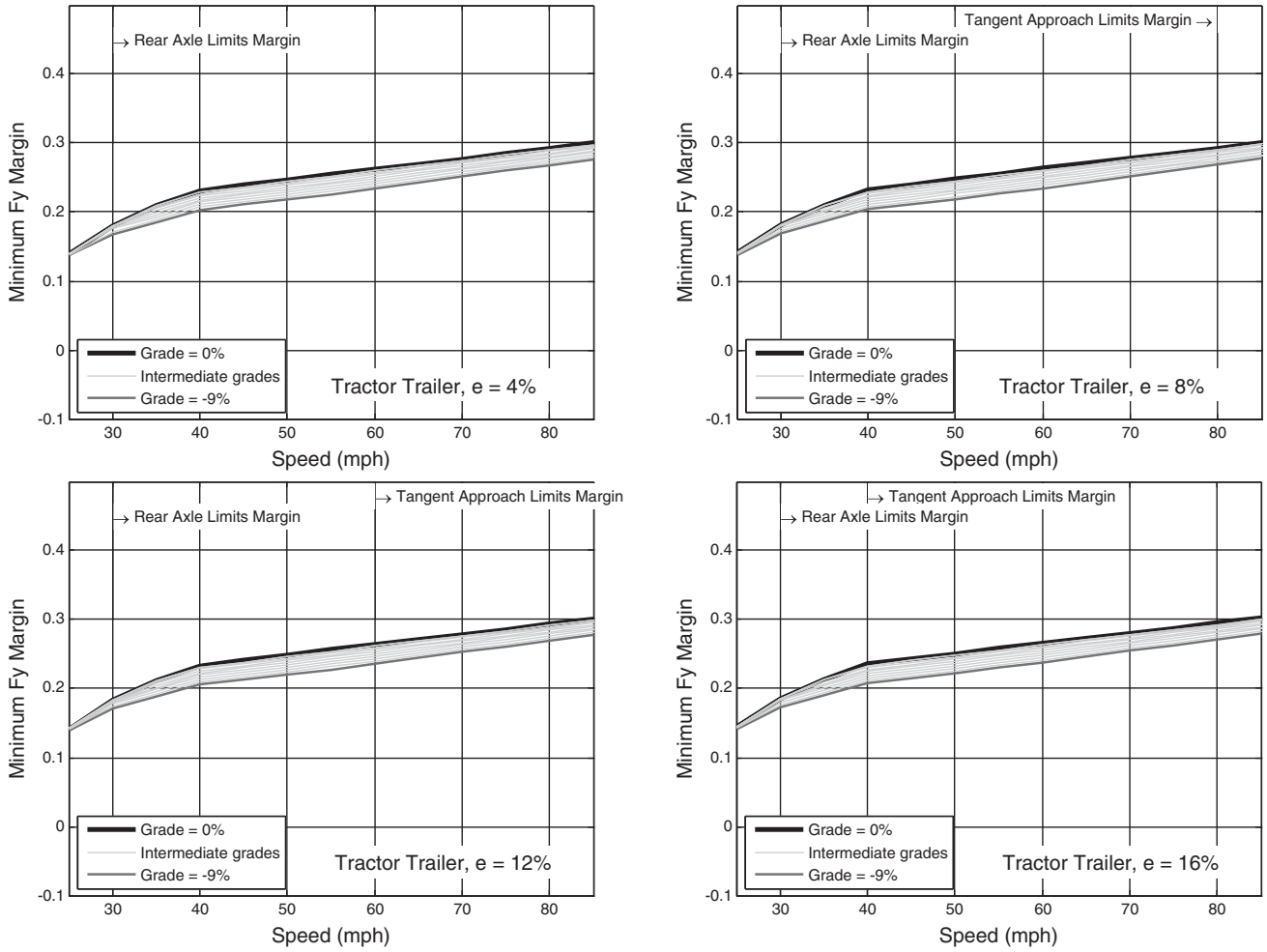

Figure 82. Lateral friction margins from transient bicycle model for tractor semi-trailer (G = 0 to −9%, e = 4 to 16%) (a_x = −3 ft/s² and lane change).

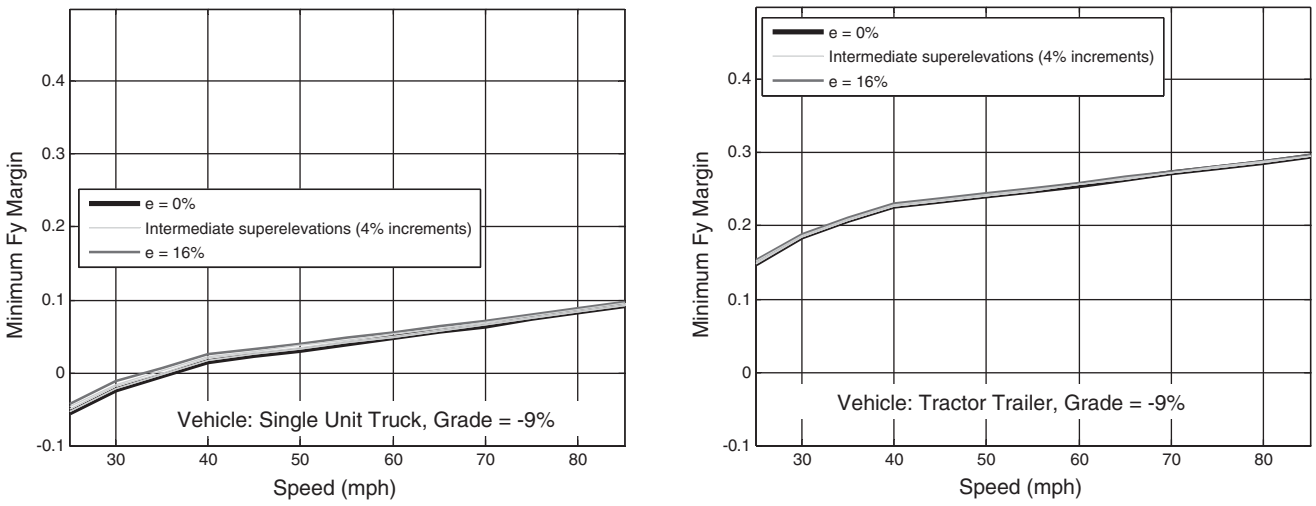

Figure 83. Lateral friction margins from transient bicycle model for single-unit truck and tractor semi-trailer (G = −9%, e = 0% to 16%) (a_x = −3 ft/s² and lane change).

departments of transportation (DOTs) of 34,000 lb. However, if the weight is shifted rearward to 24.0 ft behind the hitch, this results in the per-axle weights becoming 14,053 lb on the front axle, 33,393 lb on the rear (tractor) axle, and 32,554 lb on the trailer axle. Note that the front tire load does not change; this is because the hitch for tractor semi-trailers is generally designed to lie exactly on the rear axle of the vehicle. This provides much greater steering repeatability since the front tire loads are not changing. The total load in this case is 80,000 lb (i.e., the maximum weight limit for this vehicle per most DOT specifications). Additionally, the per-axle loads do not violate DOT limits of 34,000 lb. This vehicle hereafter is considered the fully loaded tractor semi-trailer case.

Figure 84 shows the difference between the normally loaded and fully loaded tractor semi-trailer situations. The additional loading has a small influence on margins, and indeed the lateral friction margins for the fully loaded case are slightly higher (by 0.03) than the normally loaded case. The limiting axle for each case, however, is notably different. As the trailer becomes more fully loaded, it appears that the trailer axle margins decrease relative to the other axles. Above 55 to 60 mph, it is the trailer's rear axles that generally have the lowest margins for the fully loaded trailer situation.

Effect of Brake Variation for Tractor Semi-Trailers. In the previous tractor semi-trailer simulations, brake forces were assumed to be distributed proportional to the static load on each axle; this results in the most repeatable behavior of the vehicle. However this also assumes that the braking forces are correctly distributed between the tractor and the trailer. In the case of design differences between the two different brake systems, several cases were considered where the braking force on the tractor was 25% higher than the nominal values and 25% lower. To calculate the trailer-tire forces, these are increased or decreased to maintain the requested deceleration.

Results of the brake variation simulation analysis are shown in Figure 85. The variation in braking in both cases resulted in a slight decrease in lateral friction margins around 0.01, but the

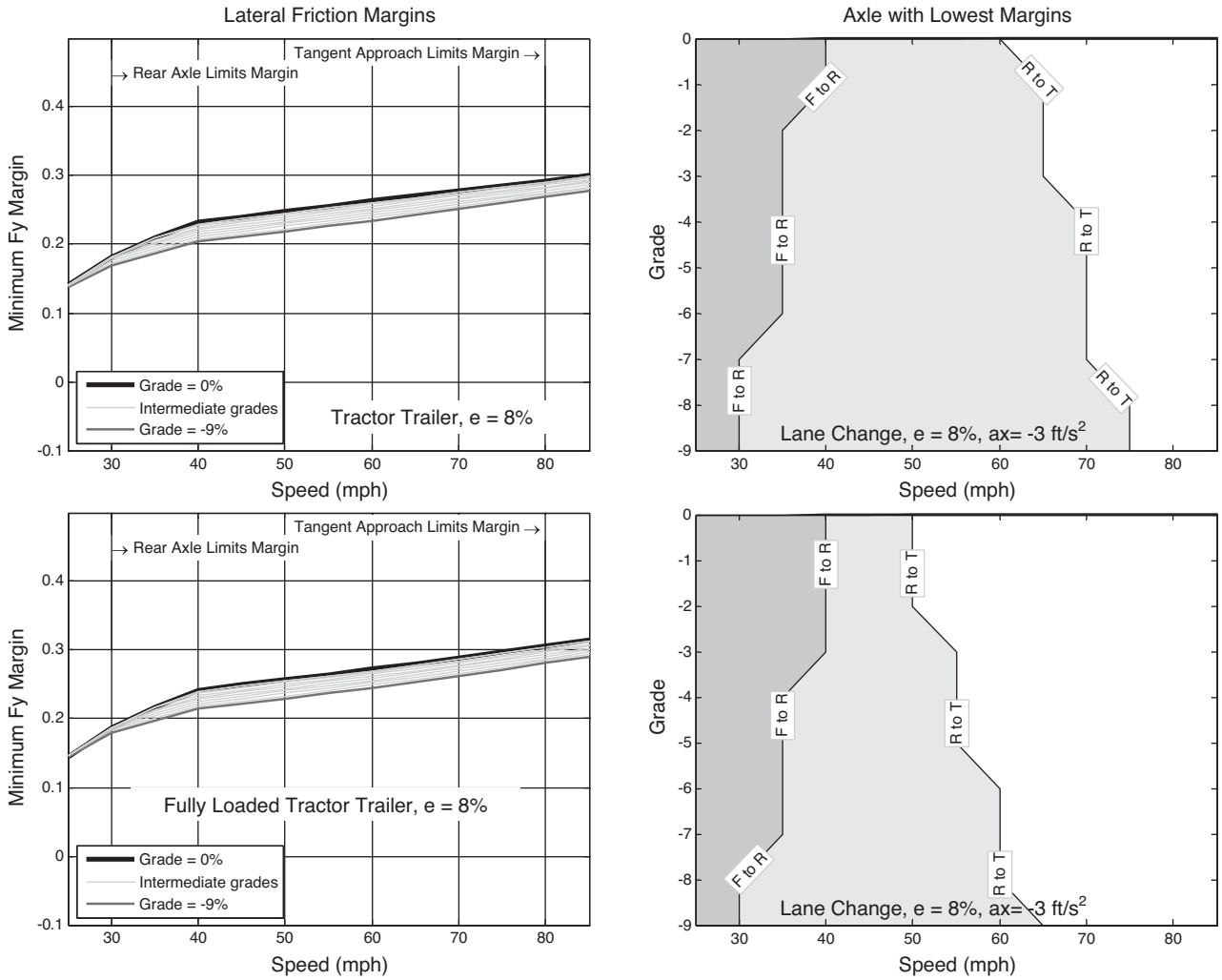

Figure 84. Comparison of normally loaded (*top plots*) and fully loaded (*bottom plots*) tractor semi-trailers (G = −9%, e = 8%) (a_x = −3 ft/s² and lane change).

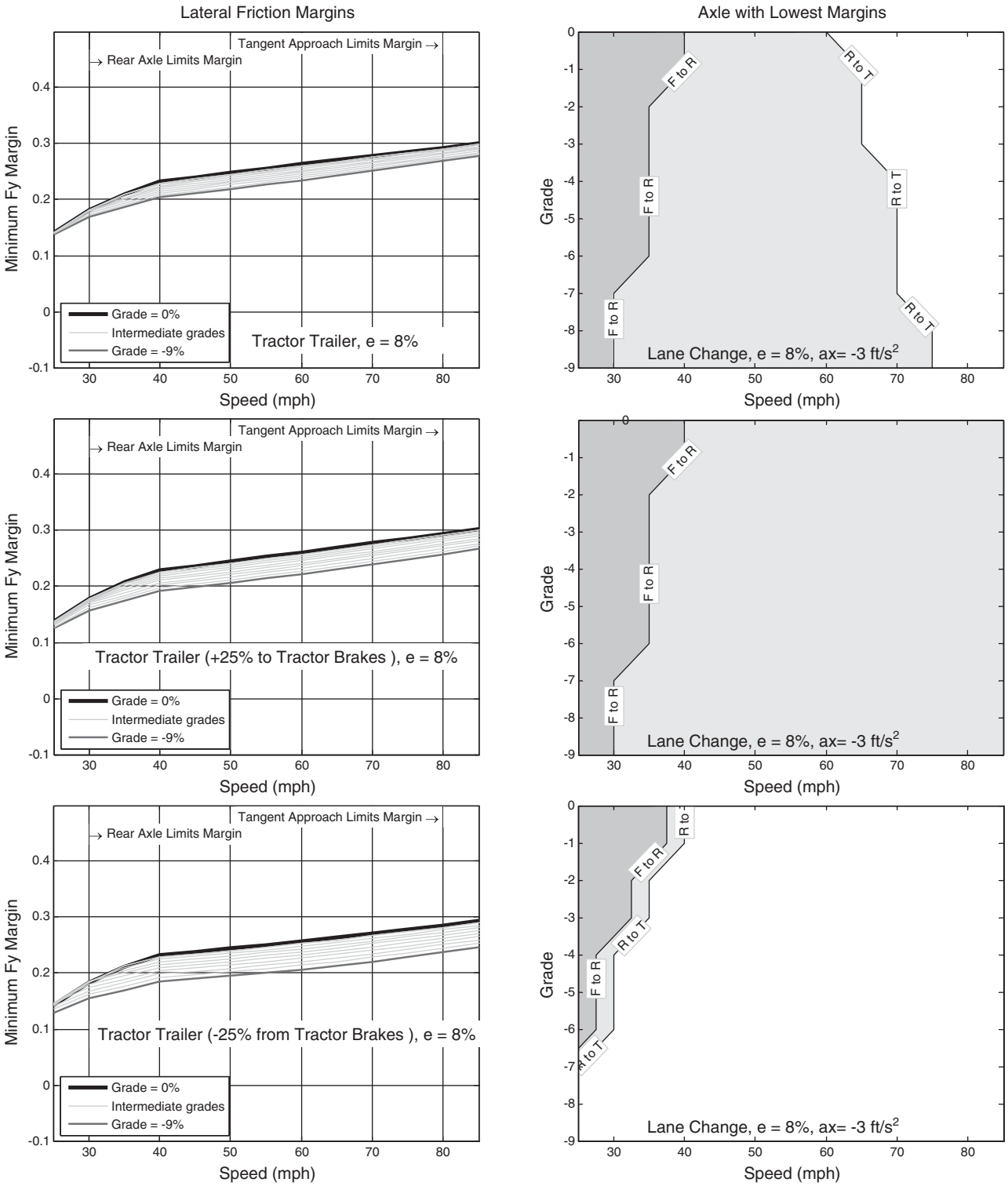

Figure 85. Comparison of ordinary braking (top plots), 25% higher braking on tractor (*middle plots*), and 25% less braking on tractor (*bottom plots*) (G = −9%, e = 8%) (a_x = −3 ft/s² and lane change).

overall shape of the margin curves and trends are unchanged. The biggest effect of the brake variations is to change the axle with the minimum force in the speeds from 45 to 60 mph to be the trailer axle instead of the rear axle of the tractor.

4.8.3 Summary of Key Results from Step 7

In summary, the following findings were obtained from the analysis in Step 7:

1. In transitioning from the tangent approach to a curve, if the steering transition is faster than 2 s, the front tires will often skid, particularly at lower design speed curves.
2. The vehicle's suspension has a negligible impact on lateral friction margins.
3. The worst-case lateral friction margins for situations with braking and steering changes appear to occur when lane changes or other steering inputs occur well into the curve, after the tire forces have built up after curve entry. The worst-case braking situation was found to be when brakes are activated shortly after the steering maneuver has started, by 0.75 s. This is because the lateral tire forces take some duration to build up, whereas the braking forces act nearly instantly in comparison.
4. The transient bicycle model agrees very closely with the steady-state bicycle model and the point-mass model except in the situations that only the transient model can study: for example, curve-entry steering transitions and lane-change maneuvers.
5. On curve entry at speeds lower than 35 mph, the lateral friction margins predicted by the transient bicycle model are 0.05 lower than predicted by the point-mass model or the steady-state bicycle model.
6. For roads with superelevations higher than 12%, vehicles often exhibited the lowest friction margins on the approach to the curve rather than within the curve. This is due to the vehicle steering up the superelevated roadway on the approach, then reversing steering inputs toward the inside of the curve. For roadways with 12% superelevation, the tangent began to reduce lateral friction margins for design speeds above 65 mph. For roads with 16% superelevation, the tangent began to reduce margins for design speeds above 45 mph. In general, the tangents will reduce margins when the superelevation is larger than:

$$\frac{e}{100} < \frac{1}{1 + p_{tangent}} \frac{V^2}{gR}$$

   This result is independent of grade. In practical terms, this suggests that superelevations larger than 12% should be avoided. Also, the above condition should be used to check that the superelevation achieved at the PC of a simple horizontal curve is less than the threshold value computed based on the given design speed–curve radius combination. Based upon further analyses, the condition above is satisfied for maximum-superelevation/minimum-radius curves for all design speeds. However, the condition above may be violated when using greater than minimum horizontal curve radii.
7. The effect of grade is to decrease the lateral friction margin by 0.001 for each percent grade decrease for situations with no braking ($a_x = 0$ ft/s^2) and, like the observations earlier for the steady-state model, the effect of grade increases with increased deceleration, to about 0.002 / grade percent when $a_x = -3$ ft/s^2.
8. Compared to the influence of the design speed, the effects of grade and superelevation on the resulting friction margins are relatively minor, as long as vehicles travel at the design speed.
9. The worst-case vehicle in terms of lateral friction margins was the single-unit truck, which has friction margins 0.2 less than other vehicles for the same maneuvers for curve-entry deceleration cases. This is due to the much larger weight shift of this particular vehicle relative to other vehicles. The difference of this vehicle to other passenger vehicles (which also have two axles) is only 0.1 when maintaining the same speed from the approach through the curve; thus, the addition of braking inputs increases the relative differences between vehicles.
10. If curves are designed with tighter radii than present AASHTO design policy, this will reduce the friction margin but this reduction depends on design speed. Specifically, for curves that are 80% of the design radius, yet used at the same design speed, vehicles will undergo a 0.1 to 0.15 reduction in friction margin at low speeds (25 mph) and 0.02 margin reduction at high speeds (85 mph).
11. Lane-change maneuvers within a curve reduce the lateral friction margins by 0.2 to 0.25 for two-axle vehicles. This reduction appears consistent across all speeds, vehicles, grades, and superelevations. The tractor semi-trailer was less sensitive to lane changes, with the margins reduced by approximately 0.15 across all speeds.
12. In lane-change situations, the full-size SUV had the most substantial reduction in margins among all vehicles.
13. When lane changes were combined with braking, the addition of braking reduced the margins for constant-speed lane changes by an additional 0.05 for passenger vehicles and by 0.15 for the single-unit truck. The single-unit truck will have negative friction margins in this case for design speeds less than 45 mph.
14. A tractor semi-trailer is much less sensitive to braking inputs and lane changes than passenger vehicles, and thus the lateral friction margins for a tractor semi-trailer do

not change as significantly as do passenger vehicles for combined lane changes and braking. This is primarily due to the longer length, slower response, and tires that are less sensitive to changes in loading conditions.

15. There were minimal differences in friction margins between a normally loaded tractor semi-trailer and fully loaded tractor semi-trailer.
16. Unlike passenger vehicles, it is difficult to predict which axle on the tractor semi-trailer will experience the minimum lateral friction margins. The lowest-margin axle changes depending on the maneuver, the loading condition, and braking situation.

4.9 Step 8: Predict Skidding of Individual Axles during Transient Steering Maneuvers and Severe Braking

The objective of Step 8 was to identify whether severe braking while traversing a sharp horizontal curve affects the ability of a vehicle to traverse the curve without skidding, taking into consideration the horizontal curvature, grade, and superelevation. Using the transient bicycle model from Section 4.8, additional braking inputs were simulated to determine cornering forces and friction factors for the same vehicle/maneuver sets as used earlier. These simulations were used to check whether the acceptable road geometries in previous steps are still suitable for decelerations rates assumed in calculating stopping sight distance design criteria and emergency braking maneuvers. Further, the results of the transient and steady-state bicycle models were compared to determine whether the steady-state models of Section 4.7 agree with the transient models of Section 4.8 for severe braking events. Finally, for situations where the margins become zero or negative, the lateral skid distances were calculated, assuming the vehicle is skidding during the duration of negative margins. These lateral distances represent approximations of how far a skidding vehicle will deviate out of the lane, and thus give some means of comparing severity of skid events that may occur in extreme situations.

4.9.1 Analysis Approach

The aim of this step was to further utilize the transient bicycle model described in Step 7 to consider severe braking conditions. The equations of motion from the previous model still apply; however, they are used under some assumptions that must be clear to understand the results that follow.

First, the vehicles are simulated under high-friction conditions, and the lateral friction margins are calculated by comparing the resulting tire forces with the friction supply assuming low-friction situations (i.e., wet-road, 2nd-percentile road conditions). This means that the high-friction road simulations will usually not exhibit skidding-related effects that would otherwise occur in low-friction roads, such as spin-out, skid-reduced steering, and longer deceleration times. As an example, consider a vehicle that is braking in two scenarios: for 5 s at 10 ft/s^2 and for 10 s at 5 ft/s^2. Assume also that the high-friction road can maintain these deceleration braking levels, but that the low-friction road will cause skidding in both cases. If the durations of skidding are calculated from the two maneuvers using a high-friction road simulation, then the lower deceleration braking situation would appear to skid longer, despite a lower applied braking level. This result would not occur in practice, and thus the results are erroneous. One way to prevent these types of errors is to simulate the skidding event on low-friction roads; however, this is quite difficult because the model complexity vastly increases for skidding cases due to many factors including the additional fidelity necessary in the tire model, the presence of ABS, and the need for a well-defined driver model. Further, the transition between road types becomes a critical factor. An actual vehicle can drive from a high-friction surface onto a low-friction surface, and thus the friction demand generated at the onset of a maneuver (e.g., on dry pavement) might not be met by the roadway further within the maneuver (e.g., on wet pavement). For this analysis, most of the maneuvers of interest should have no skidding, or often very short-duration skidding when it does occur. For simulation results presented in Section 4.9.2 where there are long-duration skidding events (i.e., more than a few seconds), the results should be interpreted with caution.

The lateral friction margins alone can also be deceptive, as a negative margin during a maneuver does not indicate the severity of the low-friction behavior. For example, consider two vehicles that have the same minimum margins of –0.1 for a particular maneuver. However, one vehicle may have a 10 s skidding event, while the other a skid duration of 0.01 s. Thus, the margin alone does not indicate how long a vehicle is operating within that margin, and thus it is sometimes not a sufficient indicator of road condition. This is particularly true for transient situations like lane changes where only short durations of high friction supply are needed, and thus only very short durations of skidding would be expected.

To differentiate between skidding events, the duration of the skidding event can be noted in each simulation of the transient vehicle model. Indeed, this is a key benefit of this model versus the point-mass and steady-state models. If the skid duration is known, then one can calculate how much the vehicle is expected to deviate laterally from its lane (i.e., intended path) during the skid. This can be done for each skidding event to classify the severity of the skid. For short-duration skids (i.e., fractions of a second), these estimates should be fairly accurate. For long-duration skidding events,

these lateral deviation estimates will be less accurate due to the assumptions mentioned previously as well as due to approximations used in the derivation of the lateral deviation distance.

To calculate the lateral deviation distance, some basic assumptions must be made about the vehicle within the skid. First, the lateral deviation is measured from the center of the original lane, and the distance is obtained by simple integration of the lateral acceleration to obtain lateral distance. For this integration, the velocity of the vehicle is assumed to be constant during the skid event, at a value equal to the speed at the onset of the skid (usually the design speed of the road). It is also assumed that the driver does have the capability of steering back into the lane, which implies that there is no ABS or other stability systems on the vehicle. Under these assumptions, the lateral deviation distance is given by:

$$y_{\text{Lat Dev}} = \frac{1}{2}\left(\frac{V^2}{R} - \frac{g \cdot e}{100}\right) t_{\text{skid}}^2 \qquad (88)$$

Where $y_{\text{Lat Dev}}$ is the lateral deviation distance, V is the forward velocity of the vehicle at the onset of the skid, R is the curve radius, g is the gravitational constant, e is the superelevation, and t_{skid} is the time duration of the skid event. While the constant-speed assumption is quite good for short-duration skid events, it will be a very poor assumption if the skid lasts long enough for speed to change appreciably, generally more than a second or two, or if the vehicle departs the high-friction driving lane into a low-friction shoulder, for example. Thus, for lateral deviation distances of more than half a lane width, the lateral deviation estimates rapidly become erroneous. Further, vehicles with ABS or other stability systems will generally be able to steer in a manner to maintain position on the road; however, their braking forces will be limited to the peak friction values of the road and thus the actual deceleration and lateral motion of the vehicle are likely to not match driver expectations. Figure 86 provides a sample illustration of lateral deviation distances experienced by a vehicle during a skidding event.

In presenting the results of this analysis, comparisons of lateral friction margins are provided for four deceleration levels (a_x = 0, −3, −11.2, and −15 ft/s²) at 10 different grades (0% to −9%) at each speed. Each deceleration level, simulated across the 10 grades, tends to produce a "ribbon" of margins, and thus there are four different "ribbons" of margins in each plot. Each ribbon is plotted so that the 0% grade case is the thick black line, the −9% case is a darker grey line, and intermediate grades are light grey lines between these high/low levels. For some situations, the plots of lateral friction margins are so far below zero that it is not practical to extend the axes lower without making them much more different than the other plots and thus making comparisons quite difficult.

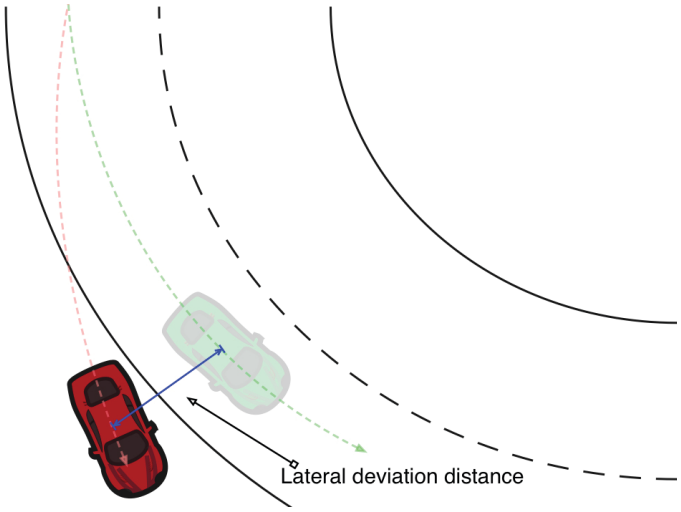

Figure 86. Diagram showing lateral deviation distance for skidding vehicle.

In cases where the margins do not appear on the plot, the highest and lowest margins are noted via text near the bottom of the figure.

4.9.2 Analysis Results

The first set of simulation results compare the predictions of the steady-state bicycle model to the transient bicycle model, for situations where there was only braking on the curve (i.e., no lane-change maneuvers). The results for the E-class sedan, E-class SUV, full-size SUV, single-unit truck, and tractor semi-trailer are shown in Figures 87 to 91. These figures show that the overall agreement between the two models is quite good. Both models show similar trends across all vehicles and braking conditions, and the numerical values for the lateral friction margins are within acceptable error levels, generally with ± 0.04 differences in margins.

In comparing the results from the steady-state bicycle models with the results from the transient bicycle models in Figures 87 to 91, the areas of disagreement between the two models are important to mention. First, for the higher braking levels, for a_x = −15 ft/s² in particular, the lateral friction margins appear to increase slightly with increasing speed for the steady-state models, but they are often flat or decrease with increasing speed for the transient models. This is because the transient models, unlike the steady-state models, include the additional forces necessary to initiate rotation into the curve. These "turn-in" forces are apparently small; hence, the general agreement between the models. However, the forces appear to increase with speed; hence, the reason that the transient models have slightly different trends than the steady-state models.

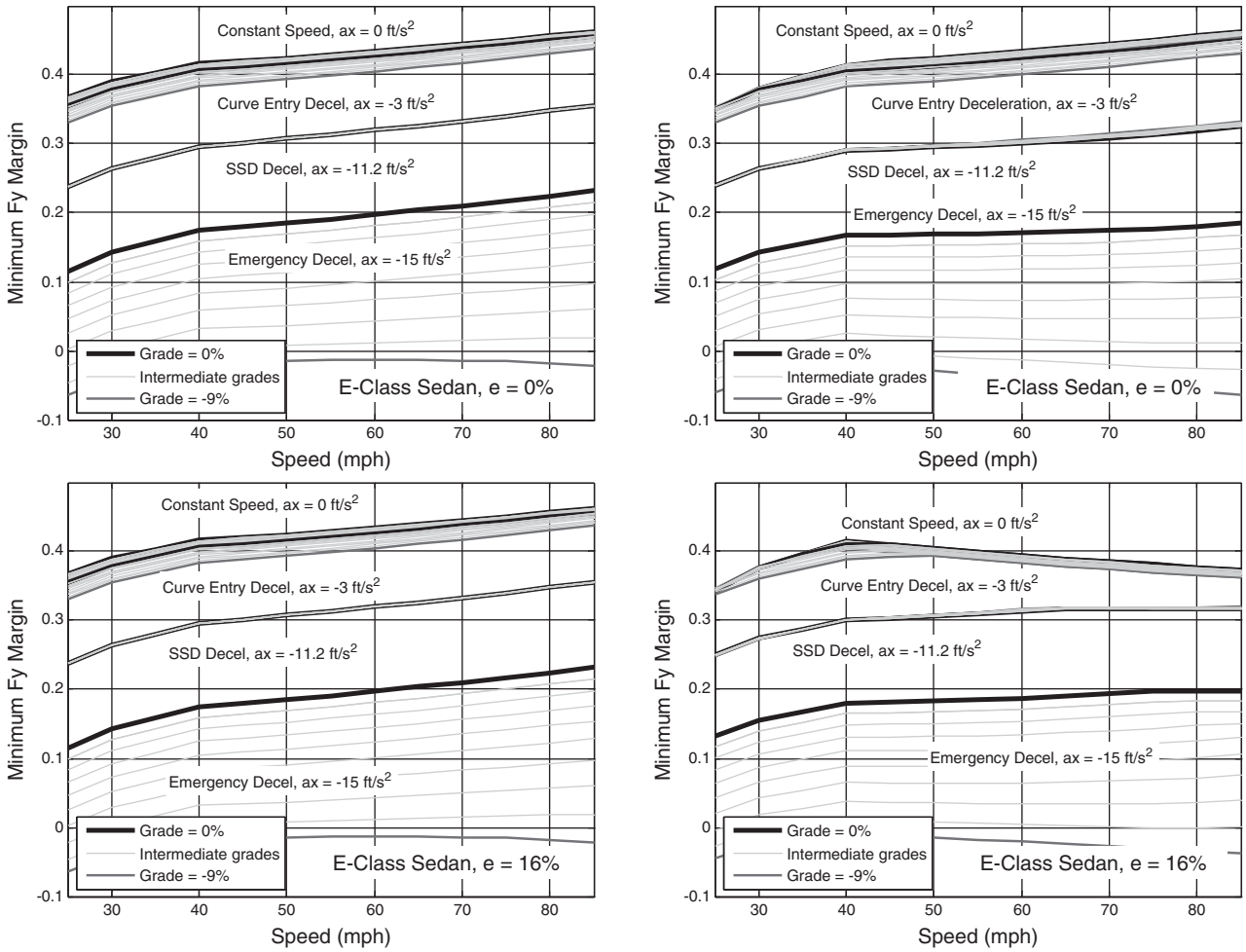

Figure 87. Lateral friction margins from steady-state bicycle (*left plots*) and transient bicycle (*right plots*) models for E-class sedan (G = 0% to −9%, e = 0% and 16%) (a_x = 0, −3, −11.2, and −15 ft/s²).

The second area of disagreement between the model results is seen by comparing the 0% superelevation case (top plots) to the 16% superelevation case (bottom plots). In the transient models, for the high superelevation cases (the bottom right plots for each vehicle), the lateral friction margins under mild braking conditions appear to drop, whereas the margins for the steady-state model appear to rise, with increasing speeds. This is due to the situation noted in Section 4.8 where the vehicles in very high superelevation cases are actually experiencing their lowest margins on the tangent approach to the curve, rather than within the curve itself. This situation, explained earlier, manifests itself as decreasing margins with increasing speeds for normal driving, but disappears when brakes are being applied because the braking events happen within the curve. And, this situation is only of concern on curves with high superelevation (greater than 12%).

The situations considered in Figures 87 to 91 are aggressive enough that lateral friction margins approach zero or become negative. In both models, this generally occurs at the 0% grade situation, for the emergency braking situation. Further, for the transient models, the margin curves at this level are generally "flat" across all passenger vehicles (e.g., this boundary, averaged over all passenger vehicles, neither rises nor drops with respect to speed). The flatness and location of this specific lateral friction margin is important. If a friction demand curve is zero and flat, this means that the AASHTO maximum side friction curve exactly matches the difference between supply and demand for this situation. Thus, the plots indicate that the present AASHTO policy, in general, supplies enough friction for all non-emergency maneuvers on wet roads, as long as the friction levels on those roads are no less than two standard deviations below the mean. Thus, the present AASHTO policy curves appear to form a good estimate of the curve-keeping margins necessary for all non-emergency maneuvers for passenger vehicles.

The limiting vehicle, as noted in Section 4.8, appears to be the single-unit truck, shown in Figure 90. This vehicle has particularly low lateral friction margins, indeed so low that the fric-

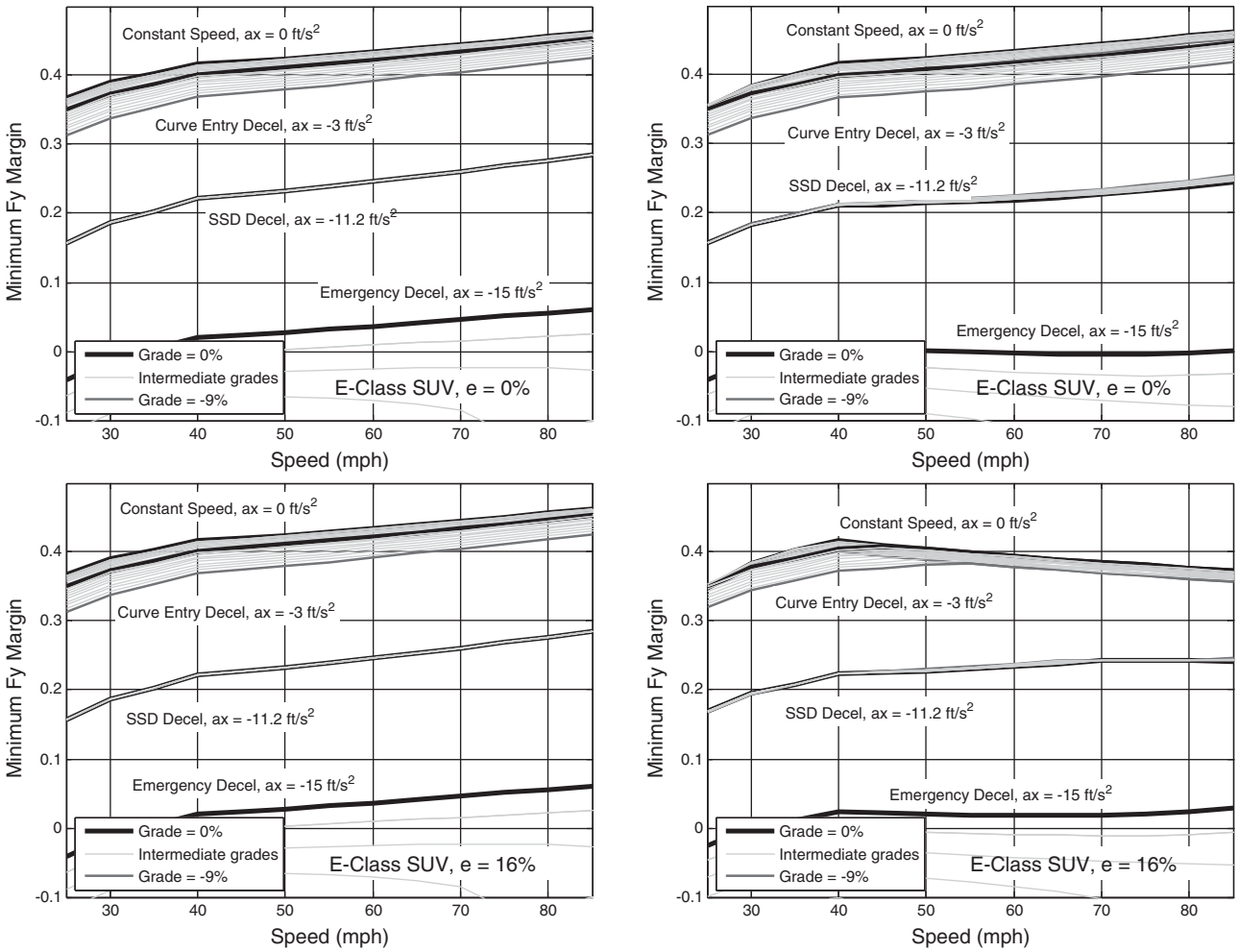

Figure 88. Lateral friction margins from steady-state bicycle (left plots) and transient bicycle (right plots) models for E-class SUV (G = 0% to −9%, e = 0% and 16%) (a_x = 0, −3, −11.2, and −15 ft/s²).

tion margins for the stopping sight deceleration and emergency braking deceleration situations are all below zero. This is true even for the 0% grade case. Additionally, the sensitivity of this vehicle to grade is quite high, as evidenced by the very "thick" bands for each situation, as compared to the other vehicles. The reason this vehicle is such an anomaly versus the others is best understood by noting that it has a center of gravity, roughly twice as high (3.85 ft) as the E-class sedan's (1.93 ft), yet its distance from the front to rear axles is only 64% longer (16.4 ft for the truck versus 10.0 ft for the sedan). Thus, there is a much larger rear-to-front weight shift on this vehicle than for other vehicles. This results in the rear tires having much lower normal force, which means that the friction ellipse, the size of which is roughly proportional to normal load on the tire, shrinks considerably. However, the braking and cornering forces necessary for a maneuver are governed by the vehicle's mass, and thus do not change significantly. Thus, the friction ellipse is shrinking on the rear tires for this vehicle precisely when the demanded forces are growing. The result is very low lateral friction margins.

In contrast to the single-unit truck, the tractor semi-trailer (Figure 91) exhibits very little change in lateral friction margin relative to different braking conditions, at least compared to other vehicles. This is likely because the situation for the tractor semi-trailer is nearly opposite that of the single-unit truck. Its CG height (5.45 ft) is 2.8 times that of the E-class sedan, but the length of the semi-trailer alone is 4.5 times longer. If the semi-trailer and tractor are included together, the tractor semi-trailer is 6.4 times longer than the sedan. Thus, the braking and grade sensitivity of the tractor semi-trailer is expected to be ⅓ that of the sedan, whereas the sensitivity of the single-unit truck would be roughly 25% higher.

The next set of simulations compared the lateral friction margins for normal curve-following maneuvers (i.e., the intended trajectory of the vehicle is within the same lane on the approach tangent and through the curve) to the margins that are observed during lane-change maneuvers within the curve. In both cases, the transient bicycle model was used. The results for the E-class sedan, E-class SUV, full-size SUV,

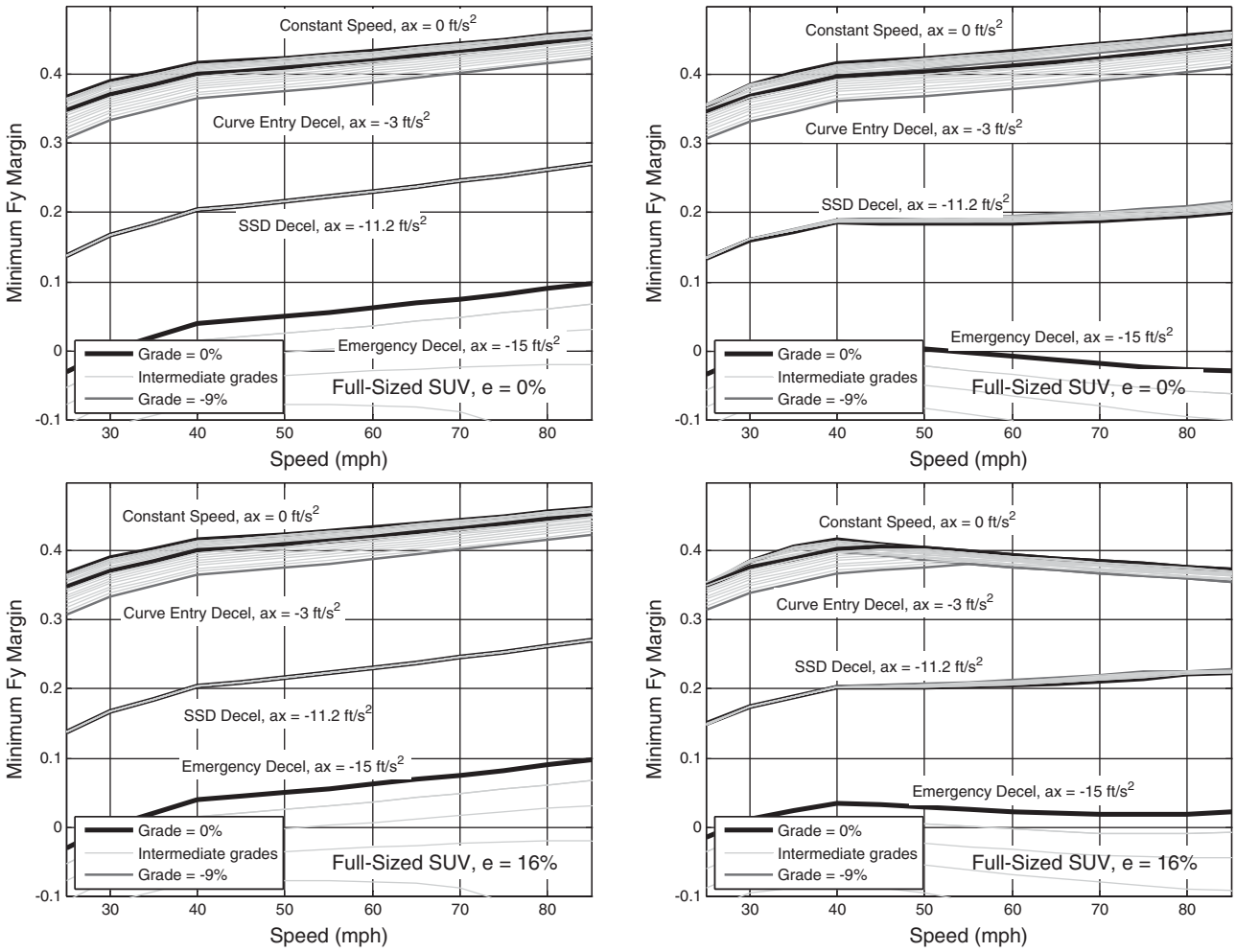

Figure 89. Lateral friction margins from steady-state bicycle (*left plots*) and transient bicycle (*right plots*) models for full-size SUV (G = 0% to −9%, e = 0% and 16%) (a_x = 0, −3, −11.2, and −15 ft/s²).

single-unit truck, and tractor semi-trailer are shown in Figures 92 to 96, respectively. For passenger vehicles, the lane-change maneuver reduces the margins by approximately 0.25 across all speeds. Interestingly, the single-unit truck and tractor semi-trailer margins are reduced by only 0.1 to 0.15; as noted before, this is due to the larger mass of these vehicles and their slower lane-change durations. In the passenger vehicles and in the single-unit truck, the presence of a lane-change maneuver magnifies the effect of grades on margins, as seen by the thicker "ribbons" associated with each situation. Additionally, with lane changes, the margins for the stopping sight distance deceleration situations generate wider "ribbons" with increasing speed.

Most notably, with lane-change maneuvers combined with stopping sight distance decelerations or emergency braking decelerations, all vehicles except the tractor semi-trailer exhibit negative margins. For the E-class sedan (Figure 92), the stopping sight distance deceleration is only slightly negative (with margins around −0.05) and relatively "flat" with little change with speed. In contrast, the SUVs (Figures 93 and 94) and single-unit truck (Figure 95) exhibit stopping sight distance and emergency braking deceleration lateral friction margins that are well below zero when lane changes are required during these maneuvers. Because these negative margins occur during a lane change, it is appropriate to consider how "severe" these events are by analyzing the corresponding lateral deviation distance.

Shown in Figures 97 to 101 are the lateral deviation distances for all cases of grades 0% to −9% and zero superelevation where negative lateral friction margins were observed in the combined lane-change and deceleration cases. Note, for the large superelevation case (i.e., e = 16%), the lateral deviation distances were roughly within 5% of the 0% superelevation case. For the passenger vehicles (Figures 97 to 99), the stopping sight distance deceleration cases (a_x = −11.2 ft/s²) show very little lateral deviation in general, as all values are less

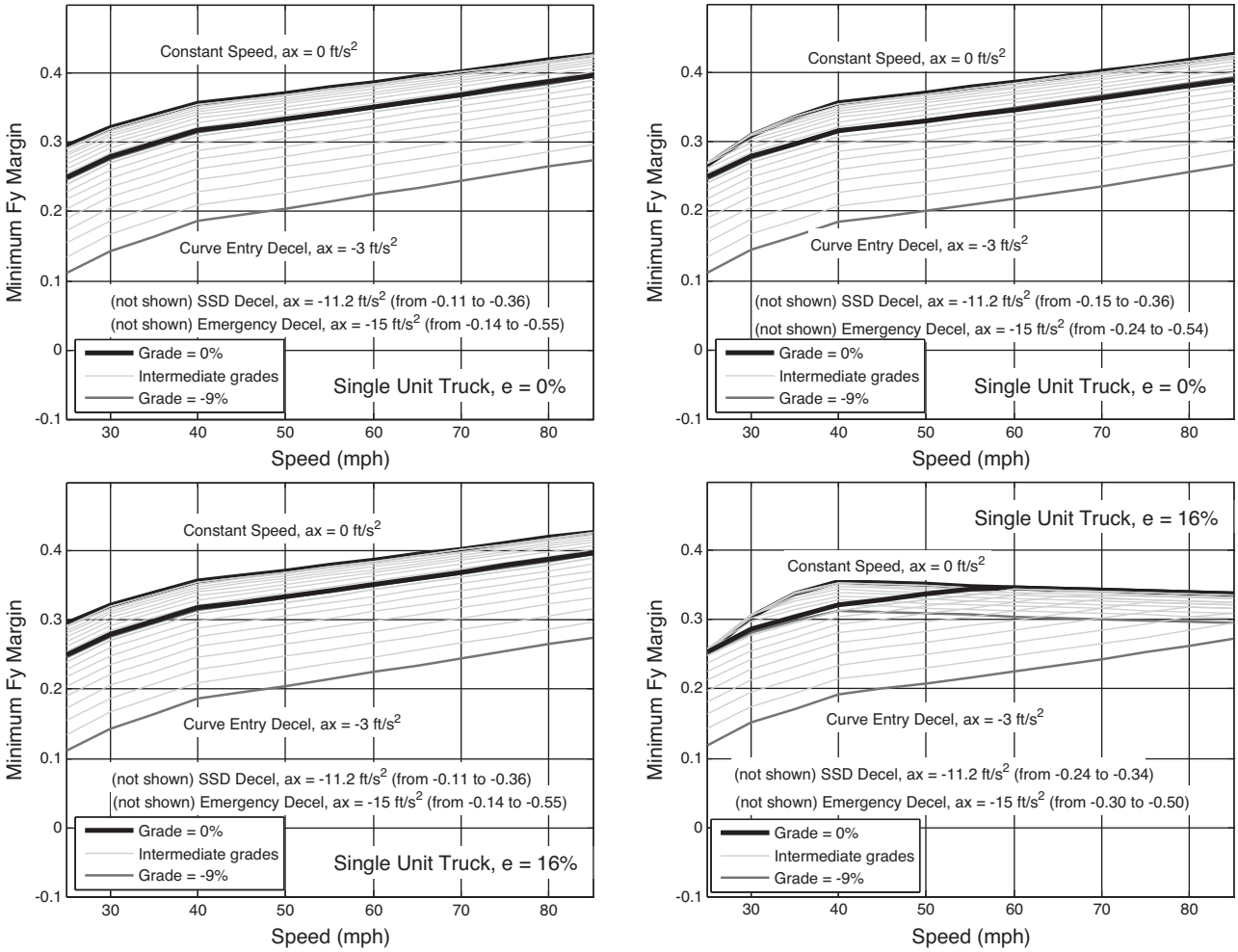

Figure 90. Lateral friction margins from steady-state bicycle (left plots) and transient bicycle (right plots) models for single-unit truck (G = 0% to −9%, e = 0% and 16%) (a_x = 0, −3, −11.2, and −15 ft/s²).

than 1.5 ft. The worst-case situations are for 0% grades, and for design speeds between 55 and 75 mph. For most of these situations, the durations of the potential skid are so small that it is questionable whether it would affect the driver's ability to maintain the vehicle on the road. In contrast, the situations with emergency braking decelerations ($a_x = -15$ ft/s²) show much larger lateral deviation distances. Particularly for the SUV cases in Figures 98 and 99, the lateral deviation distances become particularly severe at −4% grade for high speeds (85 mph) and at all speeds for grades larger than −7%. The 12 ft contour that extends from 85 mph/−4% grade to 25 mph/−7% grade is an important dividing line, as this lateral deviation distance represents one full lane width.

For the single-unit truck lane-change situations shown in Figure 100, the lateral deviation distances are particularly severe. However, some anomalies are evident in that the lower deceleration appears to give larger lateral deviation distances; as noted earlier, this is due to the methodology to calculate lateral deviation distance from simulations that do not include skidding dynamics. Because the deceleration is lower, the vehicle will be operating for a longer duration in simulation. In reality, the skidding vehicle will likely be unable to achieve the higher emergency braking deceleration levels of $a_x = -15$ ft/s², and thus the vehicle will actually skid longer than predicted by simulations. Therefore, the very large lateral deviation distances in this plot are likely low estimates due to the over-estimation of available deceleration, but they are also likely to be high estimates due to the assumption that the speed is constant during the skid and equal to the skid-onset speed. In any case, the magnitude of the lateral deviation distance indicates that the single-unit truck experiences lateral friction margins low enough to be of concern.

Just as in the lane-change situations, lateral deviation distances can be calculated for the negative lateral friction margin situations where there are no lane changes, just simple curve keeping (i.e., the intended trajectory of the vehicle is within

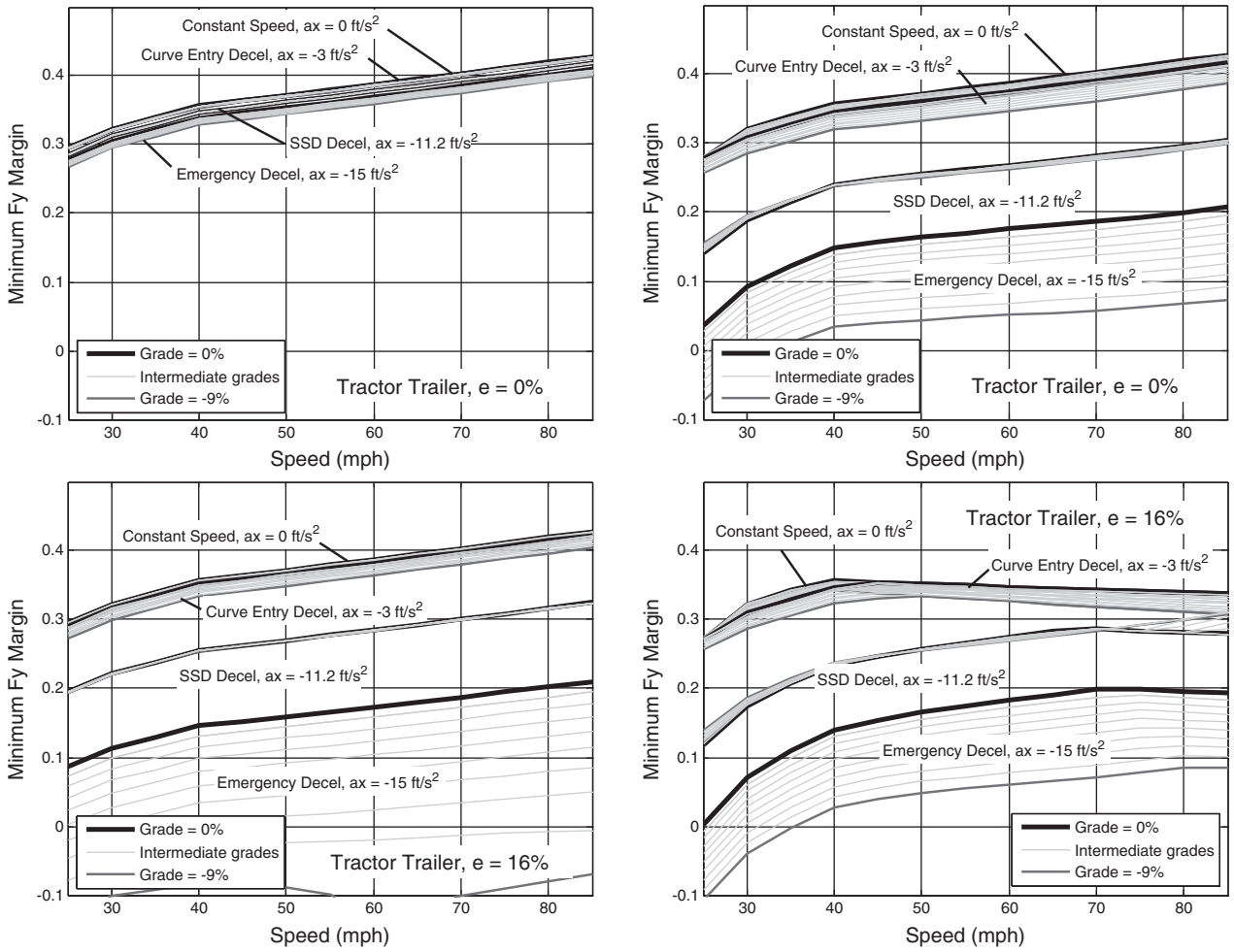

Figure 91. Lateral friction margins from steady-state bicycle (*left plots*) and transient bicycle (*right plots*) models for tractor semi-trailer (G = 0% to −9%, e = 0% and 16%) (a_x = 0, −3, −11.2, and −15 ft/s²).

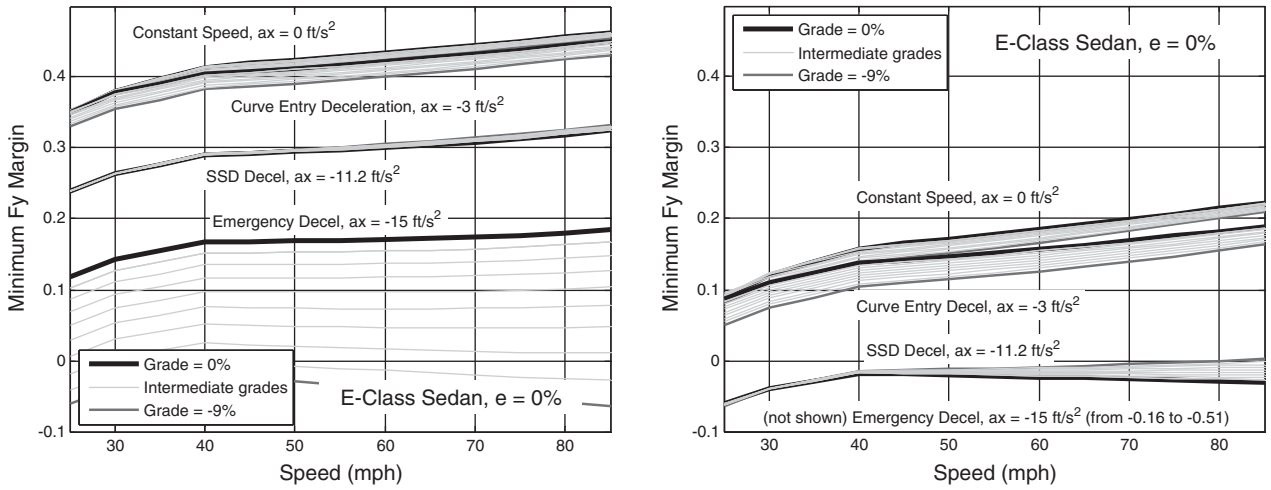

Figure 92. Lateral friction margins while maintaining the same lane (*left plots*) and with a lane change (*right plots*) for E-class sedan (G = 0% to −9%, e = 0%) (a_x = 0, −3, −11.2, and −15 ft/s²).

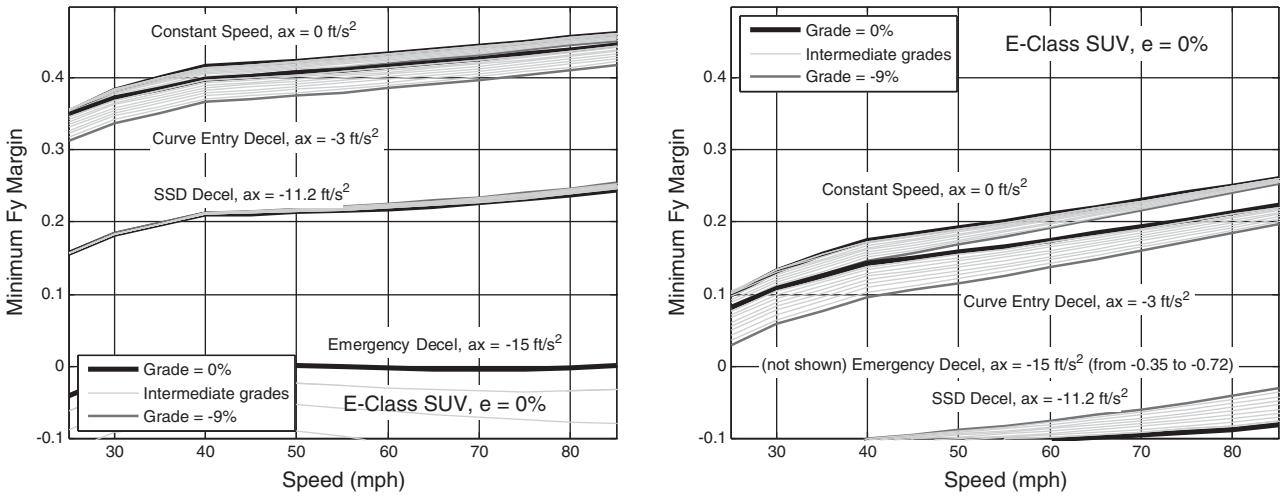

Figure 93. Lateral friction margins while maintaining the same lane (left plots) and with a lane change (right plots) for E-class SUV (G = 0% to −9%, e = 0%) (a_x = 0, −3, −11.2, and −15 ft/s²).

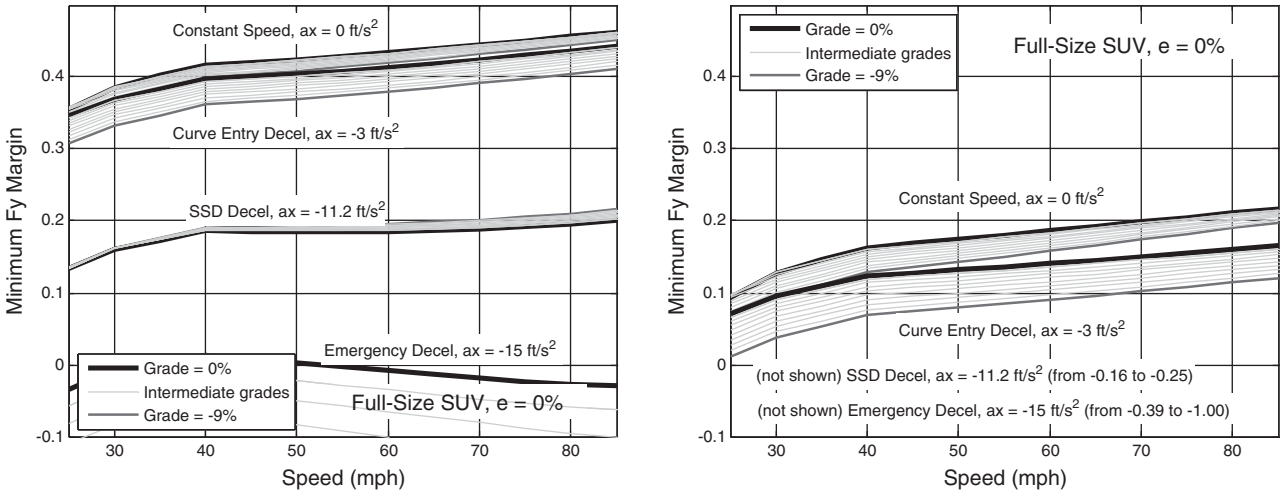

Figure 94. Lateral friction margins while maintaining the same lane (left plots) and with a lane change (right plots) for full-size SUV (G = 0% to −9%, e = 0%) (a_x = 0, −3, −11.2, and −15 ft/s²).

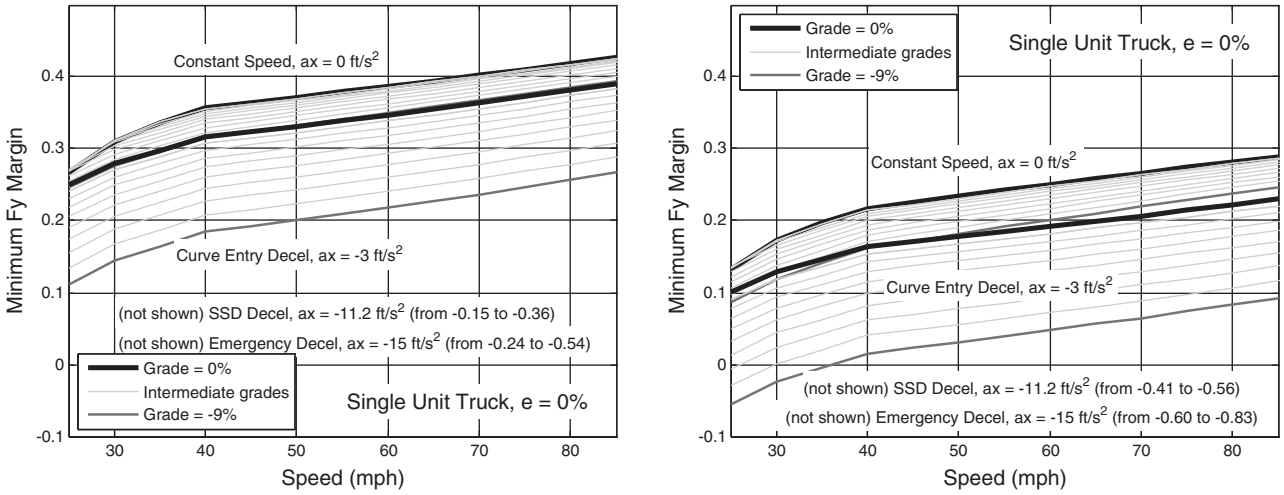

Figure 95. Lateral friction margins while maintaining the same lane (left plots) and with a lane change (right plots) for single-unit truck (G = 0% to −9%, e = 0%) (a_x = 0, −3, −11.2, and −15 ft/s²).

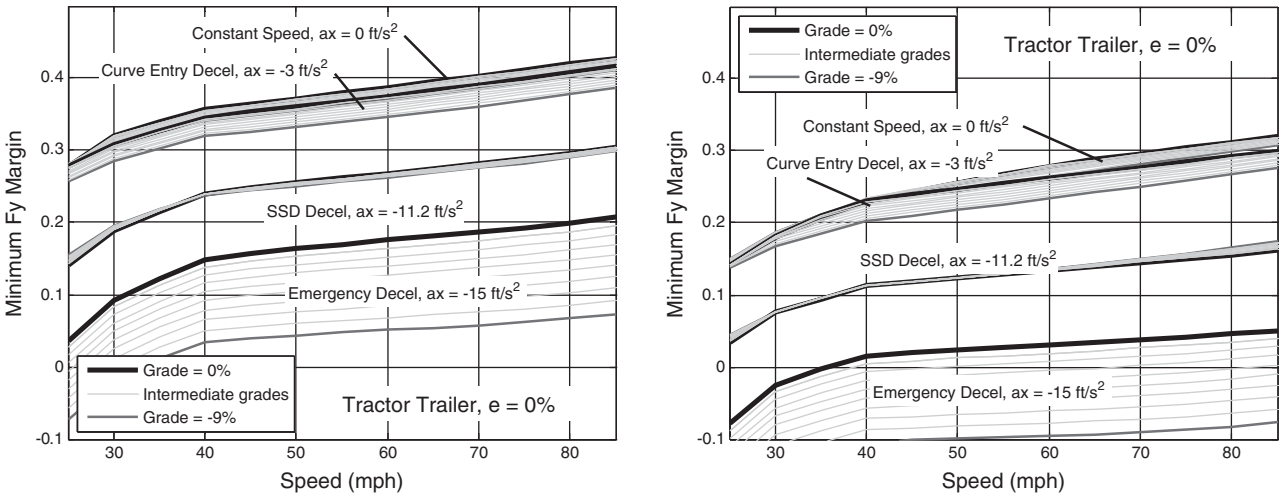

Figure 96. Lateral friction margins while maintaining the same lane (left plots) and with a lane change (right plots) for tractor semi-trailer (G = 0% to −9%, e = 0%) (a_x = 0, −3, −11.2, and −15 ft/s²).

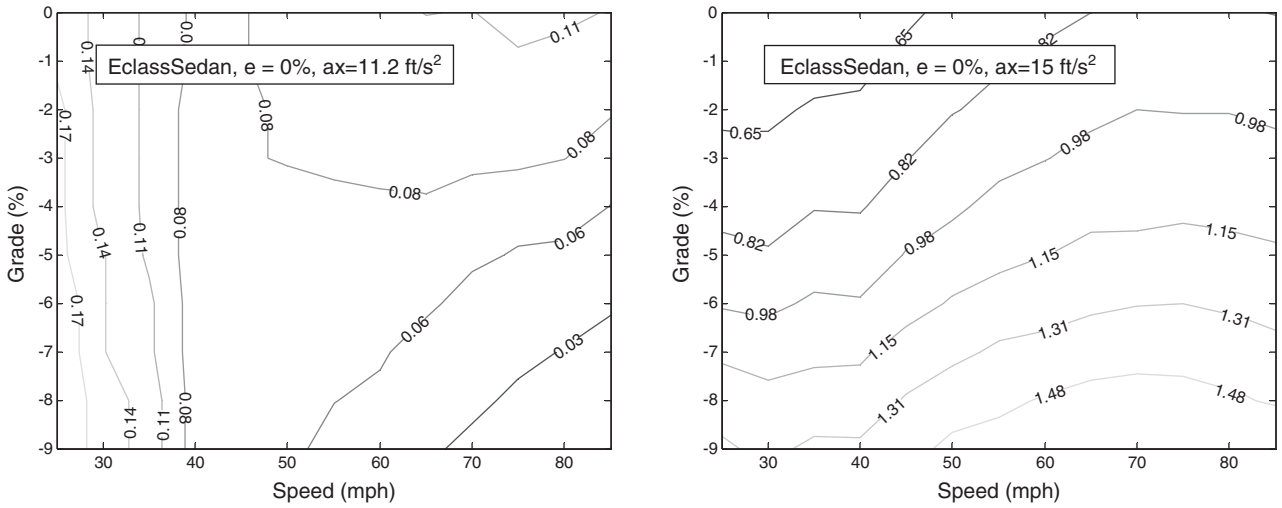

Figure 97. Lateral deviation distances (ft) for all situations with negative margins for E-class sedan (G = 0% to −9%, e = 0%) (a_x = −11.2 and −15 ft/s² and lane change).

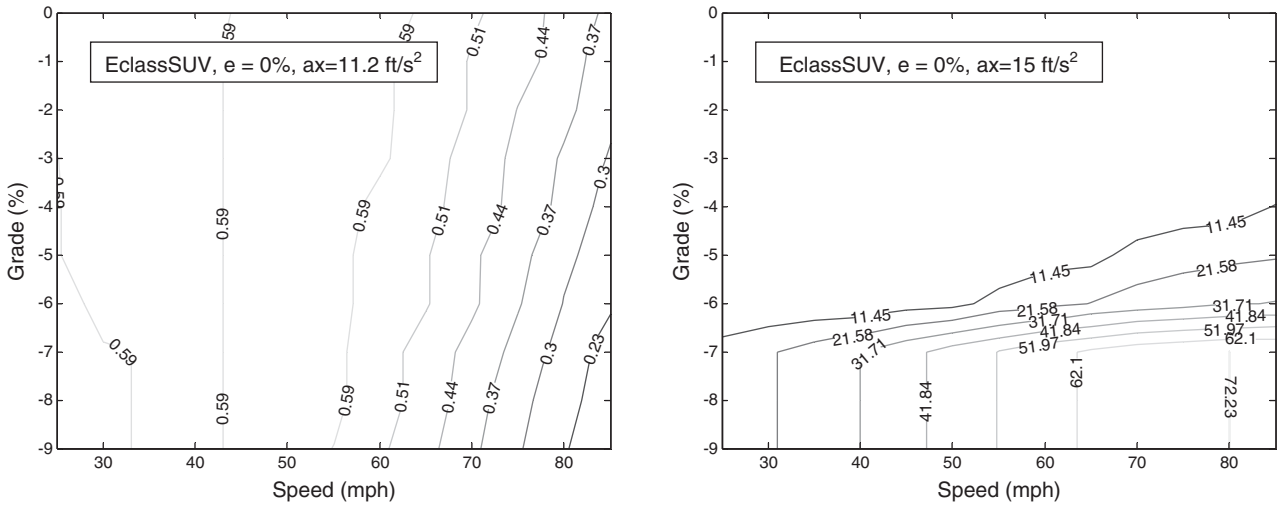

Figure 98. Lateral deviation distances (ft) for all situations with negative margins for E-class SUV (G = 0% to −9%, e = 0%) (a_x = −11.2 and −15 ft/s² and lane change).

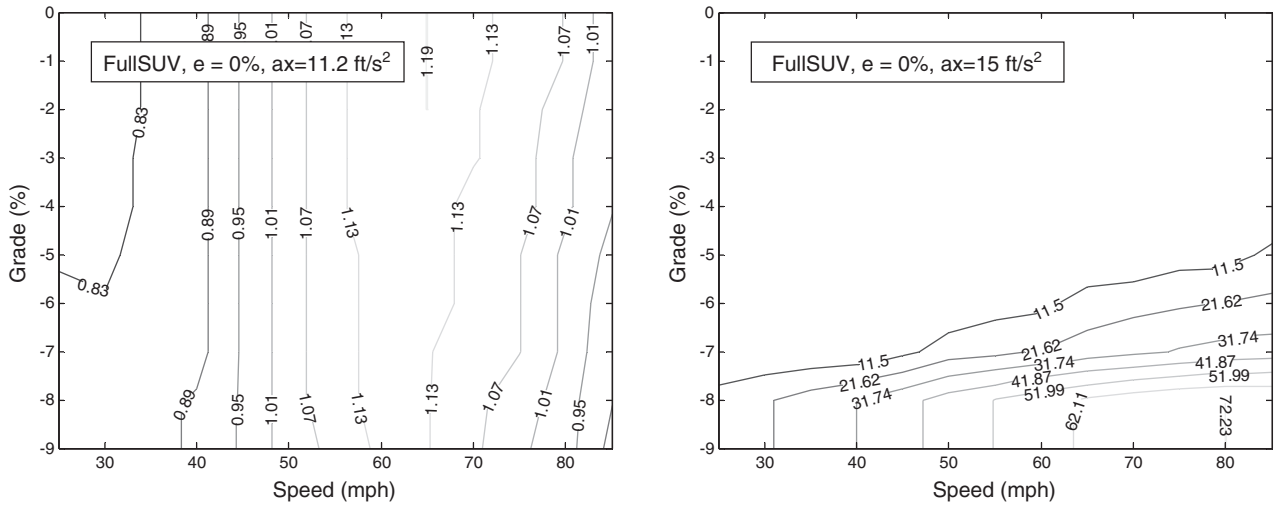

Figure 99. Lateral deviation distances (ft) for all situations with negative margins for full-size SUV (G = 0% to −9%, e = 0%) (a_x = −11.2 and −15 ft/s² and lane change).

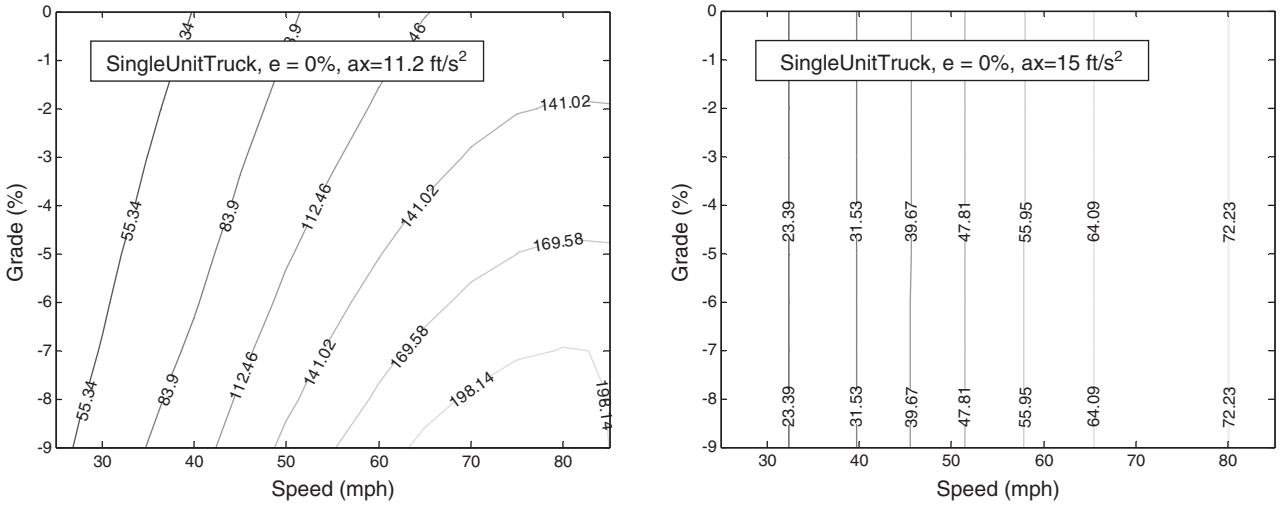

Figure 100. Lateral deviation distances (ft) for all situations with negative margins for single-unit truck (G = 0% to −9%, e = 0%) (a_x = −11.2 and −15 ft/s² and lane change).

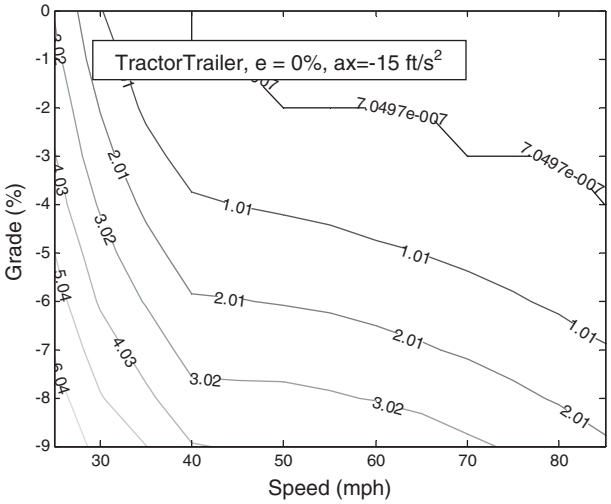

Figure 101. Lateral deviation distances (ft) for all situations with negative margins for tractor semi-trailer (G = 0% to −9%, e = 0%) (a_x = −15 ft/s² and lane change).

the same lane on the approach tangent and through the curve). These results are shown in Figure 102 for all vehicles, for the zero superelevation case. Again, there was very little difference in lateral deviation distances versus changes in superelevation, and hence these plots are not repeated here. The plots indicate that, again, the single-unit truck is of particular concern. For passenger vehicles, the E-class sedan undergoes large lateral deviation for grades steeper than −7% to −8%, and for speeds faster than 50 to 60 mph. The SUV cases again start to exhibit large lateral deviations during emergency braking situations defined by a line connecting the 25 mph/−7% grade situation to the 85 mph/−4% grade situation.

4.9.3 Summary of Key Results from Step 8

In summary, the following findings were obtained from the analysis in Step 8:

1. For situations without lane-change maneuvers, the lateral friction margins from the steady-state bicycle models agreed quite closely with those from the transient bicycle models, except in situations with high superelevation and high speeds.
2. The disagreement between the models becomes more pronounced with increasing braking levels, and with increasing CG height of the vehicle. For the most severe braking levels for the single-unit truck, the transient bicycle model estimates lateral friction margins 0.15 lower than the steady-state bicycle model.
3. For passenger vehicles, lateral friction margins generally are above 0.15 for stopping sight distance decelerations when a vehicle stays within the same lane from the tangent approach through the curve. Lateral friction margins are near zero or become negative when passenger vehicles undergo stopping sight distance deceleration combined with a lane change, and when they undergo emergency braking maneuvers in the curve.
4. Even when the intended trajectory of the vehicle is within the same lane on the approach tangent and through the curve (i.e., no lane change), most vehicles will exhibit near-zero lateral friction margins when experiencing emergency braking decelerations.
5. For all decelerations except stopping sight distance deceleration, the addition of grade reduces the lateral friction margins. This effect is relatively minor except for emergency braking where each percentage drop in grade corresponds to a large drop in margin, by about 0.03 per each 1% change in grade for full-size SUVs.
6. For transient models with severe braking, the lateral friction margins do not necessarily increase with speed and may often drop slightly with increasing speed.
7. The worst-case vehicle for the transient bicycle model with severe braking is the single-unit truck with lateral friction margins as low as −0.50 for emergency braking and −0.34 for stopping sight distance decelerations. All margins for both braking types, for all speeds, are negative, even for the 0% grade.
8. The tractor semi-trailer is predicted to have relatively high lateral friction margins and, for all the maneuvers evaluated, the lateral friction margins were positive. The tractor semi-trailer was also less sensitive to the effects of grade compared to other vehicles.
9. The presence of a lane-change maneuver within a curve reduces lateral friction margins by approximately 0.25 across all speeds for passenger vehicles and by approximately 0.1 to 0.15 for single-unit trucks and tractor semi-trailers. For passenger vehicles and single-unit trucks, steeper downgrades cause more decrease in margins during lane changes.
10. When lane-change maneuvers are combined with stopping sight distance or emergency braking decelerations, all vehicles except the tractor semi-trailer exhibit negative lateral friction margins.
11. Examining the lateral motion of vehicles during a potential skid, in many situations the vehicles are skidding only a short duration (and distance) when lateral friction margins are potentially negative, for example less than a foot for stopping sight decelerations with lane changes for the E-class vehicles. The duration and level of lateral motion did not change noticeably with increasing superelevation.
12. For the worst-case skidding situations, the lateral motion of vehicles—particularly the single-unit truck—is potentially quite severe (more than two lanes of lateral motion).

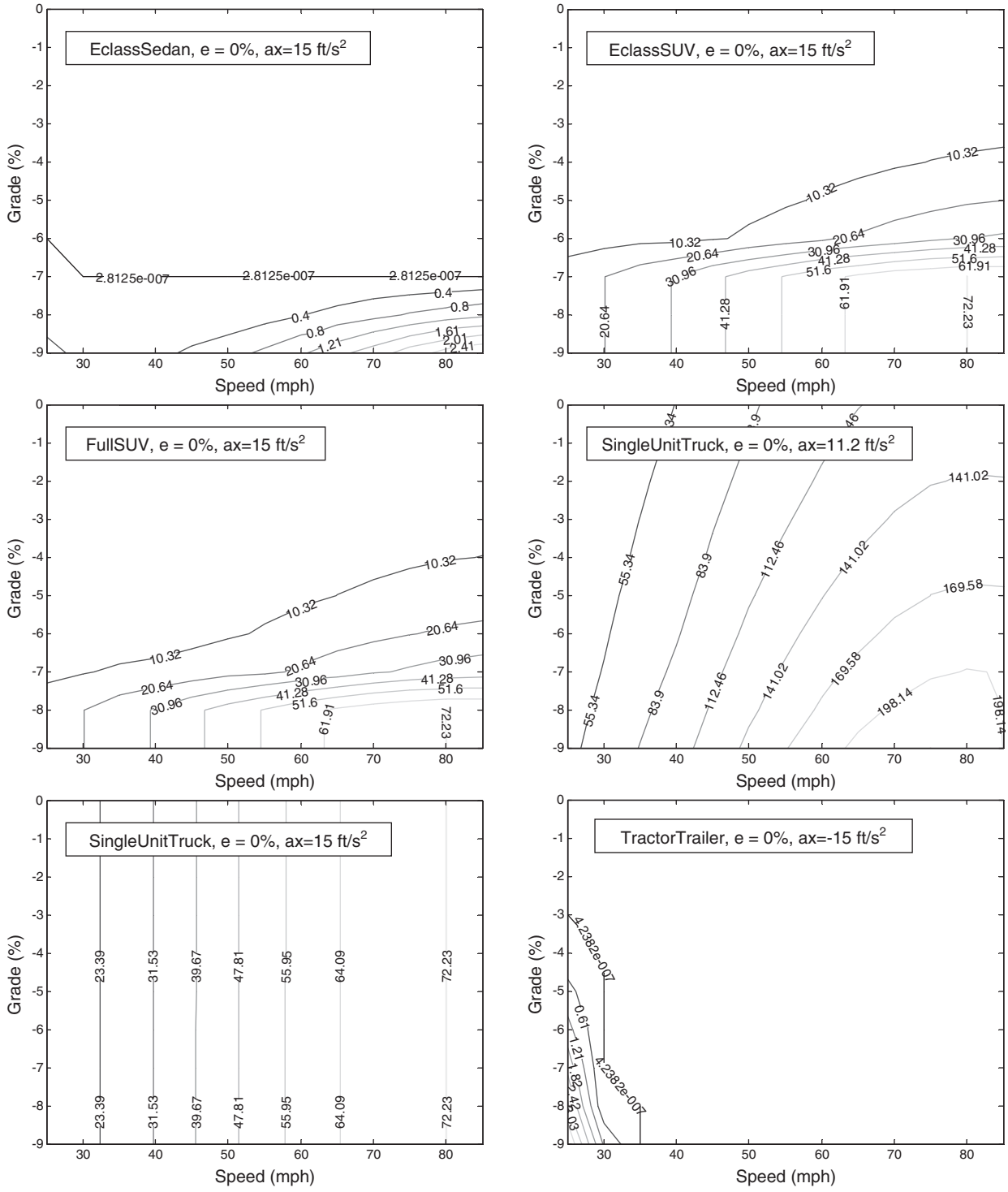

Figure 102. Lateral deviation distances (ft) for all situations with negative margins for vehicles of interest (G = 0% to −9%, e = 0%) (a_x = −11.2 and −15 ft/s²).

Without ABS, the transient bicycle model predicts that this vehicle may not be able to maintain its position in the lane on a curve while undergoing stopping sight distance or emergency braking decelerations.

13. For SUVs, there appears to be a boundary for skidding during lane-change maneuvers and stopping sight distance decelerations that extends from grades steeper than –4% at design speeds of 85 mph to grades steeper than –7% at design speeds of 25 mph.

4.10 Step 9: Predict Skidding of Individual Wheels

The objective of Step 9 was to use high-order multibody models to predict skidding of individual wheels as a vehicle traverses a sharp horizontal curve on a steep grade. Using commercially available vehicle dynamic simulation software (i.e., CarSim and TruckSim), high-order multibody models were used to predict skidding of individual wheels as a vehicle traverses a sharp horizontal curve, taking into consideration a range of conditions such as the horizontal curvature, grade, and superelevation. Rather than simulating the full range of hypothetical geometries considered throughout this research, this analysis focused on those situations identified in previous steps as areas of concern.

4.10.1 Analysis Approach

In this step, the commercial vehicle simulation package CarSim and the similar truck-oriented software package TruckSim were used to perform nearly full-fidelity simulations of vehicle behavior during traversals of simulated curves. The focus of the simulations is on situations identified in previous sections as areas of concern. These software packages were chosen primarily because they are the most widely used in industry for similar studies. They also allow direct import of known road geometries, or relatively easy specification of hypothetical geometries. Further, there is a comprehensive library of vehicles to choose from that cover all the vehicle types in this research.

To simulate a vehicle driving down a road with a particular geometric profile in CarSim and TruckSim, the software requires a three-dimensional model of the road. CarSim and TruckSim represent the three-dimensional road on which the virtual vehicle is to be driven based on the following parametric specifications:

1. Plan-view (XY) geometry of the lane centerline
2. Global road centerline height
3. Local height offset of each lane edge

In short, for each of the roadway geometries simulated within CarSim and TruckSim (i.e., either hypothetical curves or the actual curves included in the speed and vehicle maneuver studies), the research team created global X,Y,Z coordinates describing the roadway geometry for import into CarSim and TruckSim. After constructing the lists of X,Y,Z points describing the road geometry, these lists were compiled into CarSim/TruckSim for use in simulation. Portions of these procedures were performed using MATLAB. A rendering of a hypothetical roadway geometry used within the CarSim and TruckSim simulations is shown in Figure 103. Note, unlike the analyses in Sections 4.9 and earlier, in the multibody models the superelevation transition is simulated (i.e., designed) according to the *Green Book* policy.

For these simulations, the roadway possesses a very high coefficient of friction, higher than any friction supply value used in the preceding sections. This allows for calculations of lateral friction margins according to the method used throughout the analyses by subtracting demand from supply, and taking the tire forces provided by the simulation software as demand only. Again, this is primarily beneficial in that it decouples the simulation results from a specific tire–pavement interaction model used in the simulation that might change for the range of friction values (which change with speed) as measured from field data, as noted in Section 3.4.

The implications of the high-friction assumption in simulation are important. If the vehicle was simulated on a road with a friction margin as low as the supply values calculated in Section 4.2, the Force vs. Slip curves would differ drastically from those in Section 4.8, because of the difference in tire model type between CarSim and the transient bicycle model. CarSim uses a Pacejka-type tire model, which has slightly different behavior than the modified linear tire model used in Sections 4.8 and 4.9, and different yet from the LuGre tire model used to derive friction supply values in Section 4.2. To minimize discrepancies between models as much as possible, the high-friction road was used to help ensure that the friction demand reported by the multibody model matched the friction demand reported by the transient bicycle model as much as possible.

CarSim requires that certain driver and vehicle parameters be specified. Vehicle inertial, tire, and suspension properties were input according to the representative vehicle families discussed earlier. The CarSim driver model is based on a human-like preview controller developed by MacAdam (1981). It requires little user interaction and follows the road centerline by default. When specifying a lane-change maneuver during the traversal of a curve, the plan-view geometry of the lane-change maneuver with respect to the road centerline is specified. If the vehicle should depart from the trajectory, the driver model changes the steering input to correct accordingly. This differs from the methodology employed in Section 4.8, where the vehicle inputs (steering and braking) were specified for a particular lane change directly. This allows the software to more realistically simulate human behavior and driver response.

Figure 103. Three-dimensional rendering of simulated road within CarSim/TruckSim; situation shows an E-class SUV skidding while changing lanes and emergency braking.

CarSim also requests a desired speed profile for each simulation. Speed profiles for vehicles were generated using MATLAB for input into CarSim. Where there are instances of braking, the speed profiles were determined by piece-wise integration of the decelerations starting at the time and distance locations where braking is first applied.

Comparison of vehicle inputs such as steering angle, vehicle speed, and deceleration assumed for the transient bicycle models in Section 4.8 and for the multibody models in this step showed close agreement. Agreement between the models indicated that the input assumptions used for specifying the CarSim simulations were reasonable; and thus, results of the CarSim simulations could be viewed with a high level of confidence.

4.10.2 Analysis Results

4.10.2.1 Validation of Transient Bicycle Models in Step 7 at Constant Speed and Curve-Entry Deceleration

To check the fidelity of the transient bicycle models developed in Section 4.8 with a minimum of confounding variables, the most modest situation was first analyzed: a constant-speed traversal of a horizontal curve while maintaining the same lane. This very simple situation was selected as it is important to compare lateral friction margins obtained from CarSim/TruckSim to the transient bicycle model. Once agreement between the transient bicycle model and the multibody model is confirmed for mild maneuvers, boundary or questionable cases can be evaluated using CarSim/TruckSim to gain a better understanding of which highway design and maneuver scenarios are most concerning.

Section 4.8 showed that the overall effects of grade and superelevation, for minimum-radius curves, were far less significant than vehicle speed, vehicle maneuver type, and vehicle type when determining the lateral friction margins. Thus, most of the simulations that follow are conducted using a moderate combination of superelevation and grade, while the focus is on the three factors that showed the most effects in previous sections: vehicle speed, vehicle maneuver type, and vehicle type.

Because the full-size SUV was determined to be the worst-case passenger vehicle for friction margins in Section 4.8 and for rollover propensity in Section 4.6, this vehicle is a focus for many of the following analyses. Figure 104 shows inputs and outputs for both the transient bicycle model and multibody model for a full-size SUV assuming a 55 mph design speed,

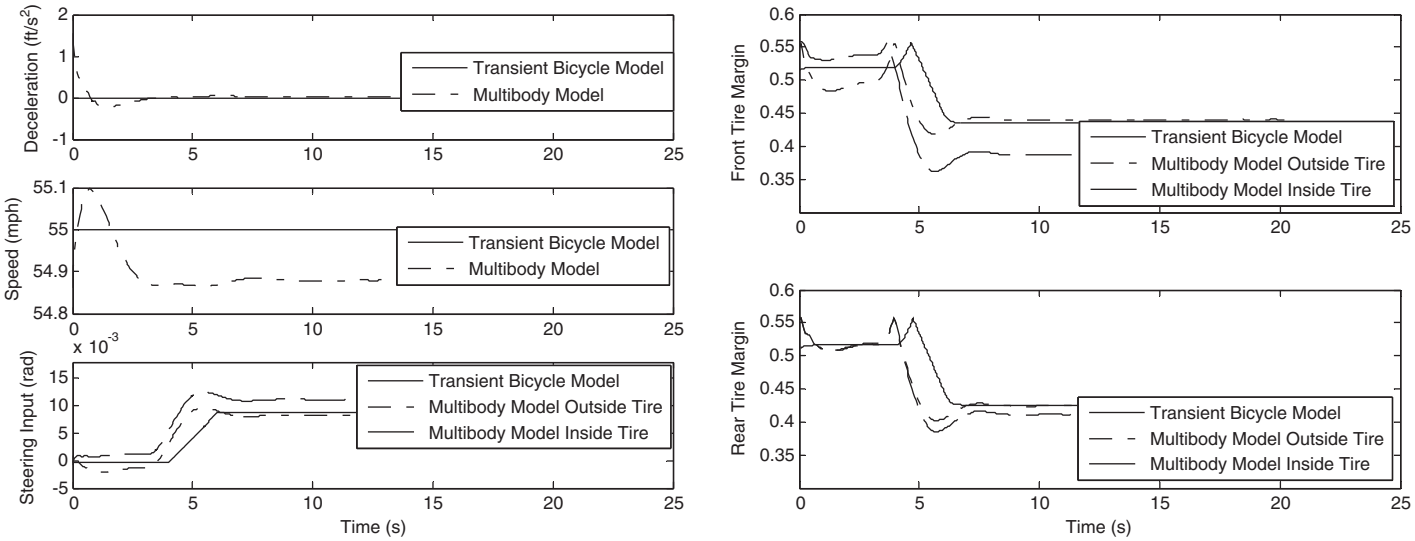

Figure 104. Inputs and outputs from transient bicycle and multibody models for full-size SUV (V = 55 mph, G = −6%, e = 4%) (a_x = 0 ft/s²).

grade of −6%, and superelevation of 4% and assuming a constant speed throughout the maneuver and the intended trajectory of the vehicle is within the same lane on the approach tangent and through the curve. The resulting lateral friction margins match fairly well between these two models for this mild, steady maneuver. When the multibody model was run for an entire range of speeds, there remained good agreement between the transient bicycle model and multibody model, as shown in Figure 105.

In Figure 105, the lateral friction margins for the front and rear axles for the CarSim simulations were determined by taking the minimum margin experienced by the inside and outside wheels on each axle, respectively. The agreement between multibody and transient bicycle models is excellent for this scenario.

For trucks, the single-unit truck was determined in previous sections to be the worst-case vehicle for many scenarios, so this vehicle type is given attention here. Lateral friction margins from the transient bicycle model and multibody

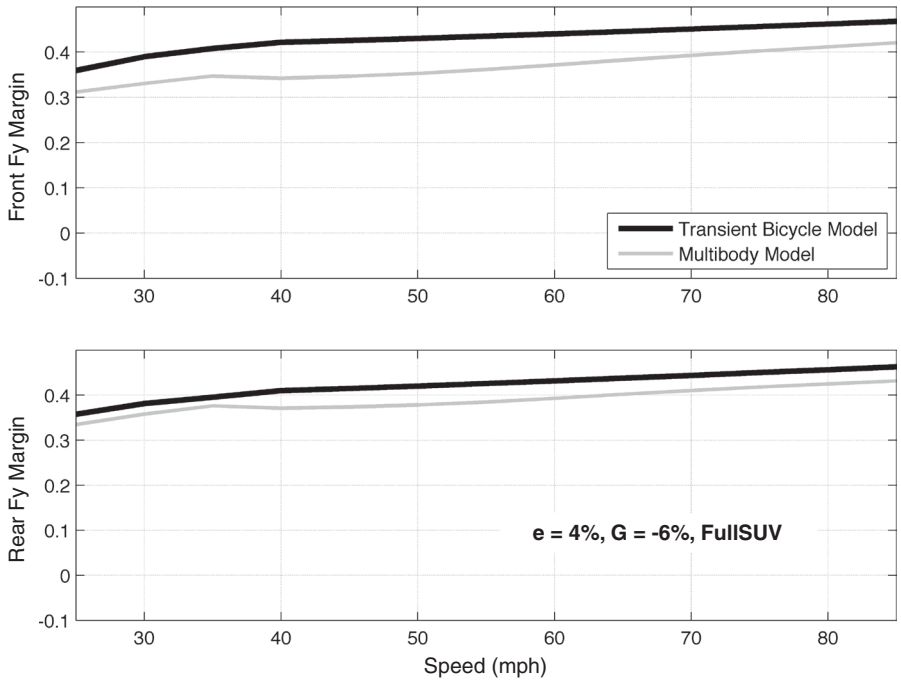

Figure 105. Lateral friction margins from transient bicycle and multibody models for full-size SUV (G = −6%, e = 4%) (a_x = 0 ft/s²).

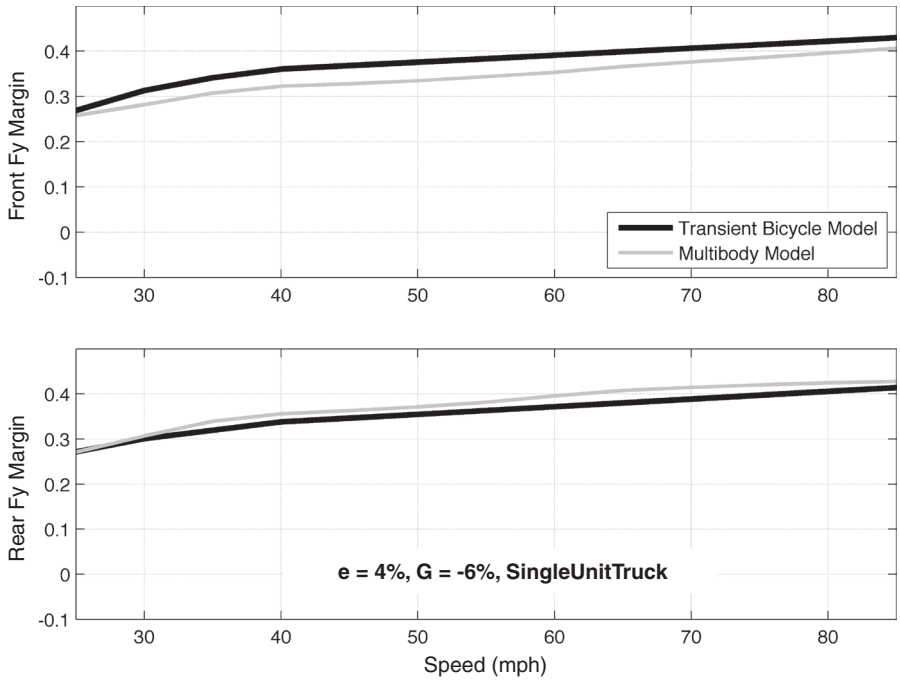

Figure 106. Lateral friction margins from transient bicycle and multibody models for single-unit truck (G = −6%, e = 4%) (a_x = 0 ft/s²).

model are shown in Figure 106 for a −6% grade and a 4% superelevation, assuming constant speed. The rear-margin minimums of the transient model agree with the front-margin minimums from the multibody model. The rear margins are most important, as these must prevent vehicle spin-out; the transient model gives lower margins and thus is slightly more conservative than the multibody model for this vehicle. This has many potential causes, not the least significant of which is likely air resistance. This is an interesting result, as it suggests that the transient bicycle model of the single-unit truck may be the worst-case vehicle choice for highway design. The recognition of the worst-case vehicle for the most conservative low-order model, in general, is useful; a roadway design that works with this vehicle in this simulation model may ensure a roadway design that is suited for all vehicles.

In Figure 107, the lateral friction margins of the transient bicycle model and the multibody model for the tractor semi-trailer are compared. This comparison is important as the transient bicycle model for the tractor semi-trailer has an added level of complexity versus the same type of model for a two-axle vehicle, and thus there are additional potential sources of error. Again, the match between the transient bicycle model and the multibody model is quite good, but the picture is a little less clear with the tractor semi-trailer than with the full-size SUV or the single-unit truck. There are larger discrepancies visible on all of the axles, particularly on the rear axle of the tractor and the trailer axle. One reason for these discrepancies for the tractor semi-trailer, as mentioned in Section 4.8, is that the transient bicycle model for the tractor semi-trailer "lumps" the tires in each axle group and represents them by one, effective tire. Thus, in the transient bicycle model, eight tires in an axle group might be represented by only one tire. The multibody model for the tractor semi-trailer models five axles and 18 wheels: axle 1 has one tire on each side, while axles 2, 3, 4, and 5 (working toward the back of the loaded combination) have four tires per axle. In summary, Figure 107 shows the minimum lateral friction margins experienced by the inside and outside tires on each axle for the multibody model. It is clear that there is some disparity between the margins predicted for axles 2 and 3, and again between axles 4 and 5. Still, the "average" margins between the two axles in the "rear" axle group and the "trailer" axle group are in agreement with the transient bicycle model, which is really all one can expect from a model that, by definition, averages tire forces from the two axles in the group.

Interestingly, the disparity between the two axles at the rear of the tractor and the two axles at the rear of the trailer can be quite large. They appear to handicap the tractor semi-trailer even at constant speed when speeds are low. For low-speed curves, the trailer articulation angle is high, the steering angle required to navigate the curve is relatively high, and the lateral acceleration required to negotiate the curve is relatively high. Still, care must be taken when jumping to the conclusion that this apparent handicap will cause loss of control of a tractor semi-trailer. Axles 2 and 3 at the rear of the tractor are closely spaced and fixed, as are axles 4 and 5 at the rear of the trailer. These closely spaced axles cannot steer around the same turn center; therefore, turning requires that at least

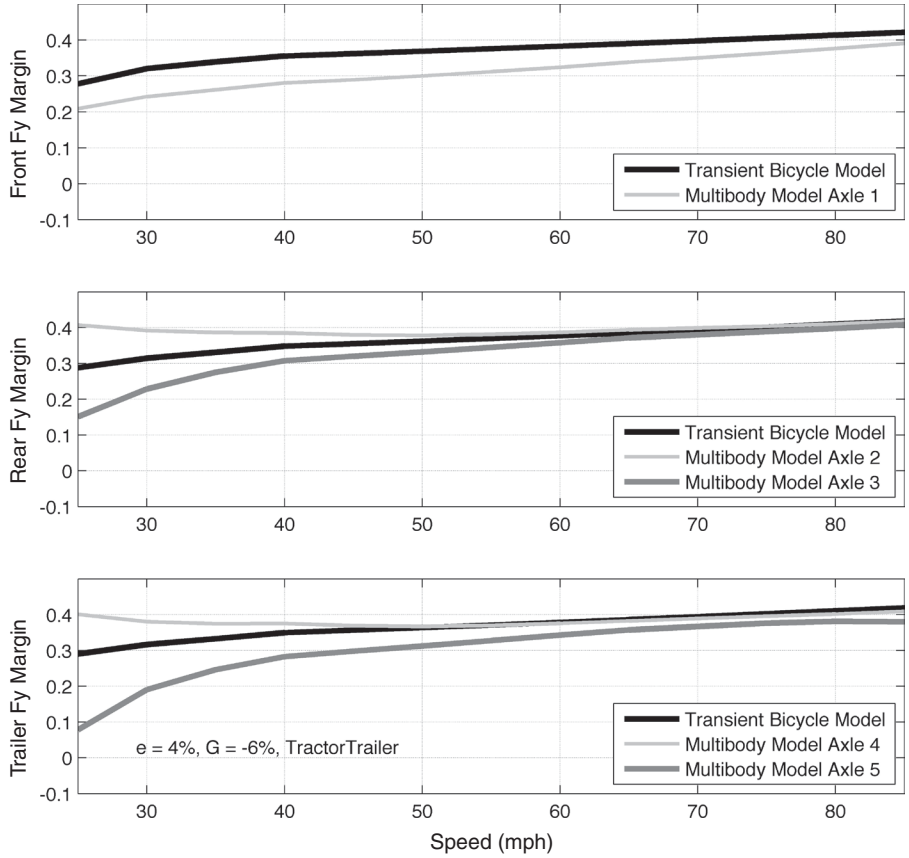

Figure 107. Lateral friction margins from transient bicycle and multibody models for tractor semi-trailer (G = −6%, e = 4%) (a_x = 0 ft/s²).

one axle exhibits slip. This can result in low margins for one axle of a closely spaced pair. This behavior will be particularly pronounced for low-speed turns, since the turn radii are generally much smaller for lower speeds. Thus, at low speeds, alternating low and high margins for adjacent, closely spaced axles can be expected and do not necessarily constitute a safety concern. To illustrate this phenomenon, consider Figure 108, which shows the margin trajectories for a tractor semi-trailer navigating a 500 ft radius curve at 25 mph. In this low-speed, large-radius turn, the lateral acceleration is so low as to be negligible, but even so, the rear axle on the tractor unit and the rear axle on the trailer unit exhibit different, "split" margins than their "partner axles," located just forward of each, respectively. The split is in the opposite sense for this low-speed turn (i.e., the rearward axle in each group has a higher lateral friction margin than the forward axle in each group). This occurrence happens because the axle that "skids" depends heavily on tire slip and weight shift, and both of these factors are affected by the specifics of each driving maneuver.

To investigate this "splitting" phenomenon among the tires in each tractor semi-trailer axle group further, and examine its pervasiveness across maneuver types, consider the comparison between the transient bicycle model and multibody model for the curve-entry deceleration traversal shown in Figure 109. The "splitting" of margins between the axle groups still occurs, but the transient bicycle model seems to over-predict lateral friction margins for the trailer axle group. This is a potential problem when using the transient bicycle model to evaluate the dynamics of a tractor semi-trailer for geometric design purposes. Assuming that the multibody model is more representative of real-world situations, this disagreement shows that the transient bicycle model is predicting higher lateral friction margins than they likely are in reality and therefore may miss the occurrence of negative friction margins. Thus, for tractor semi-trailers or other vehicles with multiple adjacent axles, a multibody simulation should be run to confirm whether negative margins result or not.

To investigate why the transient bicycle model does not predict the trailer margins correctly, consider Figure 110, in which the 30 mph input and margin trajectories for a tractor semi-trailer, assuming curve-entry deceleration and curve-keeping steering, are shown. Comparing the time trajectory of inputs and margins for this scenario, the reason for the discrepancy between the low-order model and the multibody model is

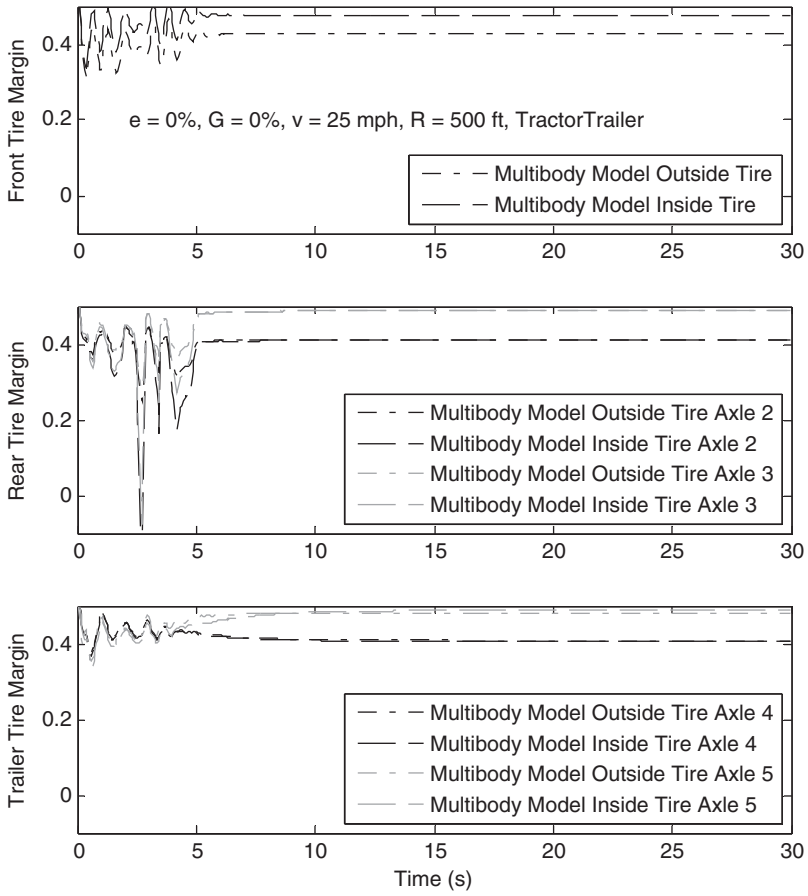

Figure 108. Lateral friction margins from multibody model for all five axles of a tractor semi-trailer (V = 25 mph, G = 0%, e = 0%, R = 500 ft).

apparent. At around 14.5 s, the deceleration rate overshoots the desired curve-entry deceleration value of −3 ft/s^2. This is due to the simulated driver's braking model employed by the multibody software, which represents the TruckSim simulated driver's efforts to maintain a particular deceleration rate by modulating the brakes. The spike in deceleration (resulting from a spike in brake force) at the trailer axle group corresponds exactly with the downward spike in trailer lateral friction margin at 14.5 s. This suggests that, while the mean lateral friction margin of each axle group matches well between the transient bicycle model and the multibody model, the driver-influenced braking dynamics of the tractor semi-trailer are especially significant for the trailer axle (e.g., there are oscillations in the braking systems of trailers that cause spikes in braking to occur when brakes are suddenly applied). The spike at 14.5 s in Figure 110 corresponds with the minimum reported margin in Figure 109 for 30 mph but should not really be seen as cause for concern, as the spike to a lateral friction margin of nearly zero on the trailer axle is momentary, and an artifact of the simulated driver control of the braking system.

4.10.2.2 Investigation of Weight-Transfer Effects on Lateral Friction Margins

In examining the results in the preceding subsections, it becomes apparent that the multibody model, in its prediction of the forces present at each tire on the vehicle, predicts slightly different lateral friction margins for the inside and outside tires. This phenomenon has a few contributing factors, like steering geometry (for the front tires), as well as longitudinal and lateral weight transfer during the maneuver (especially on the rear tractor and trailer axles). Tire behavior changes as a function of vertical loading, so the forces contributed by each tire are coupled not only to the tire's slip angle, but also to the way load shifts from the inside to the outside tire during cornering. This behavior is assumed to be nearly negligible for most driving scenarios and is ignored in the assumptions used to derive the transient bicycle model of Section 4.8.

To confirm that lateral weight shift has a relatively small influence on the overall lateral friction margin predictions for

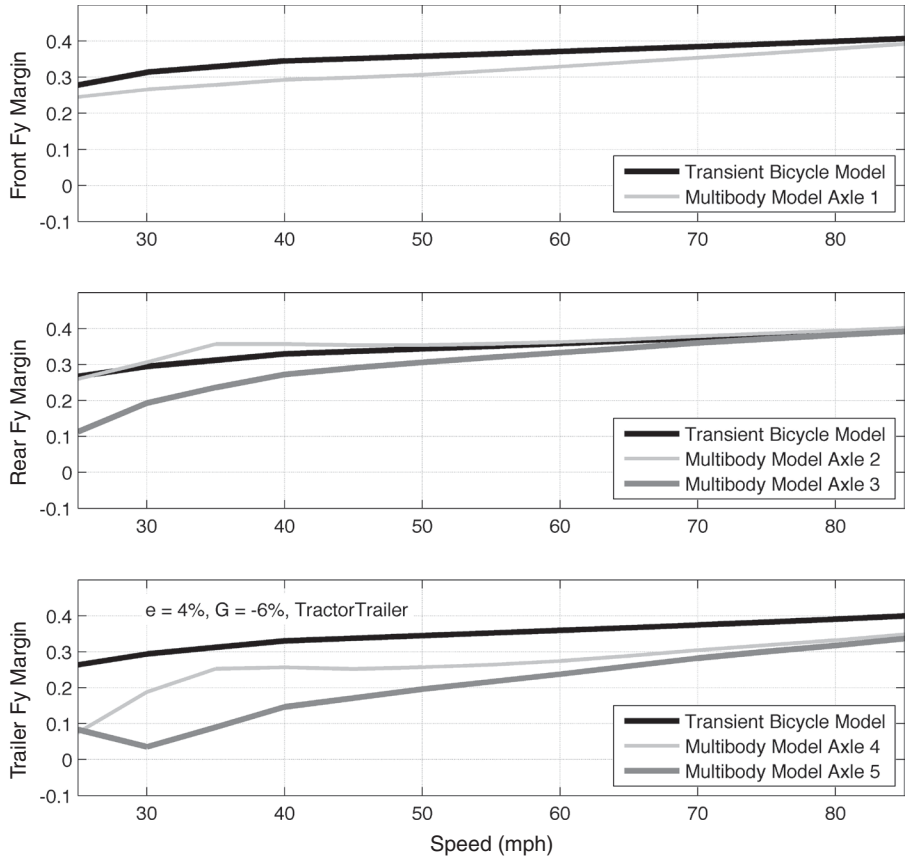

Figure 109. Lateral friction margins from transient bicycle and multibody models for tractor semi-trailer (G = −6%, e = 4%) (a_x = −3 ft/s²).

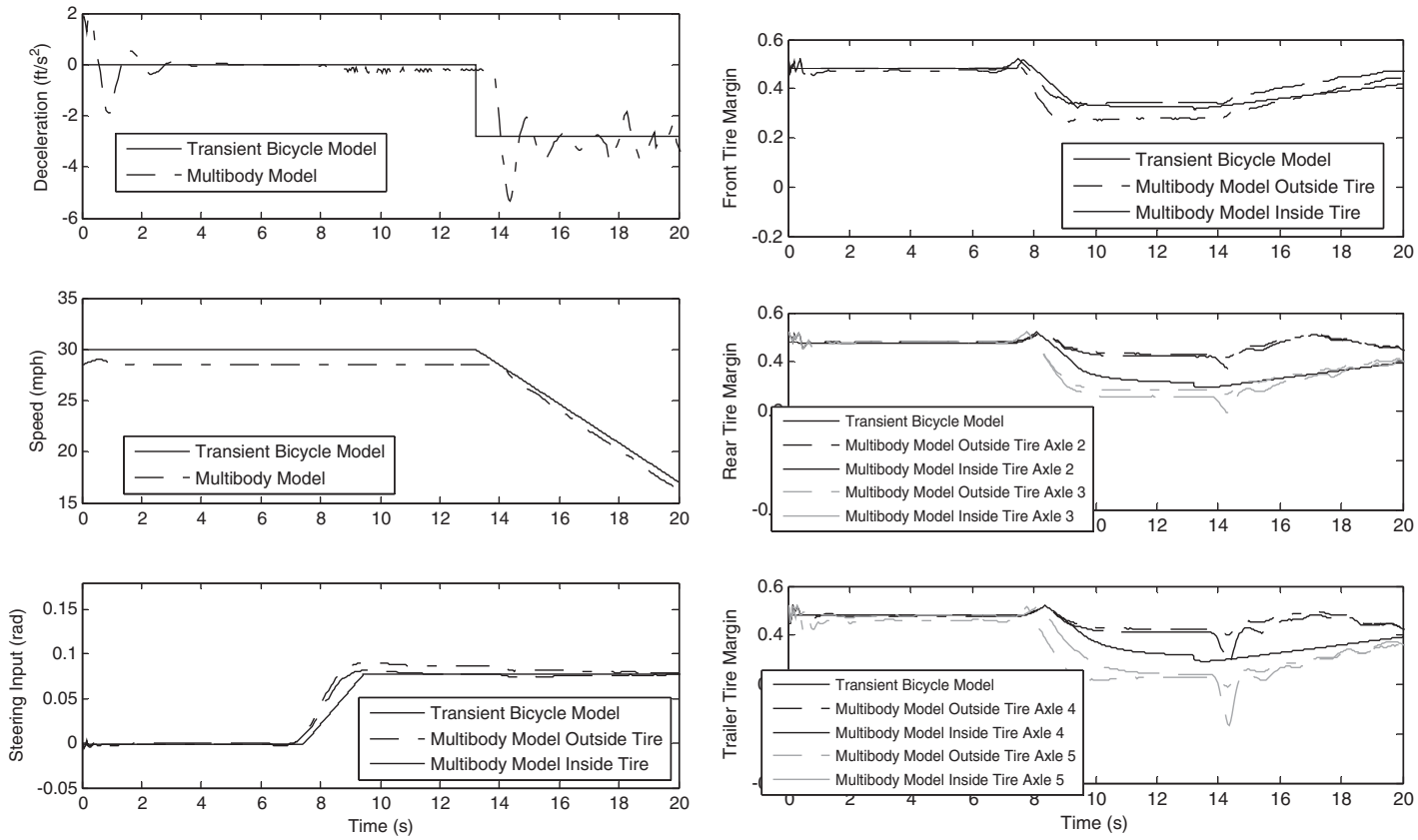

Figure 110. Inputs and outputs from transient bicycle and multibody models for tractor semi-trailer (V = 30 mph, G = −6%, e = 4%) (a_x = −3 ft/s²).

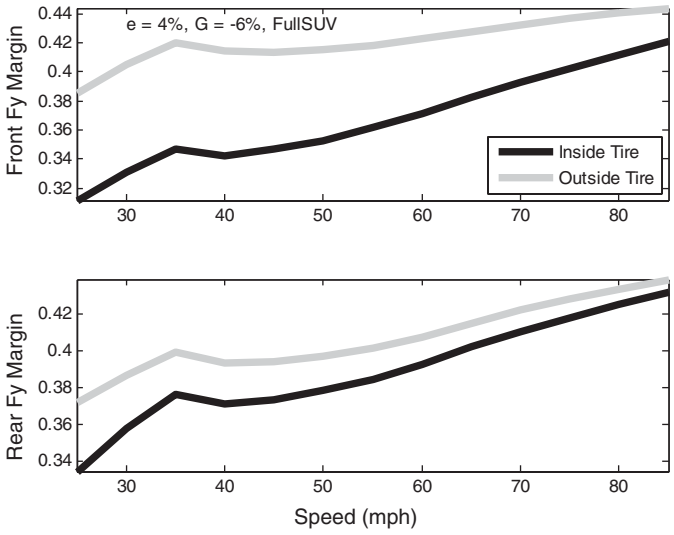

Figure 111. Effect of lateral weight shift on lateral friction margins for full-size SUV (G = −6%, e = 4%) (a_x = 0 ft/s²).

normal driving, Figure 111 compares the inside versus outside tire lateral friction margins for a full-size SUV. The overall differences between the inside and outside tire margins are only a maximum of about 0.06. The front tires experience more disparity than the rear tires mainly due to steering geometry issues (i.e., the vehicle does not possess so-called "Pure Ackermann" steering geometry, which means that the act of steering at moderate to high speeds will, in itself, induce a small relative amount of slip in either the inside or outside tires). This effect may seem detrimental to performance, but it does have design advantages as it can be used to design and tune chassis behavior (e.g., to ensure that vehicles skid prior to rollover). This effect is often present in passenger vehicles. The Ackermann disparity is magnified at low speeds, since the smaller radii of curves with lower design speeds will, by definition, require higher steering amplitudes.

Figure 112 shows that the effects of lateral weight shift on friction margins remains small for normal maneuvers, even for a tractor semi-trailer. The TruckSim model predicts lateral, longitudinal, and vertical forces for all five axles (and all 18 tires) on a tractor semi-trailer, while the transient bicycle model used in Section 4.8 provides estimates for three representative "lumped" axles. Again, the differences between inside and outside lateral friction margins are small across the range of speeds for normal driving cases.

In summary, the lateral friction margin plots illustrate that Ackermann geometry errors, combined with weight-transfer effects, are together probably small contributors to overall lateral friction margins. Both likely only play a role in the lateral friction margin estimates in extreme cases where the margins predicted by the transient bicycle model are already close to zero due to other factors. While this is certainly supportive of the modeling assumptions made in Section 4.8, there is the possibility that under some of the more extreme driving conditions considered, lateral weight-transfer effects could have a more severe effect. Some of these cases are discussed in the sections that follow.

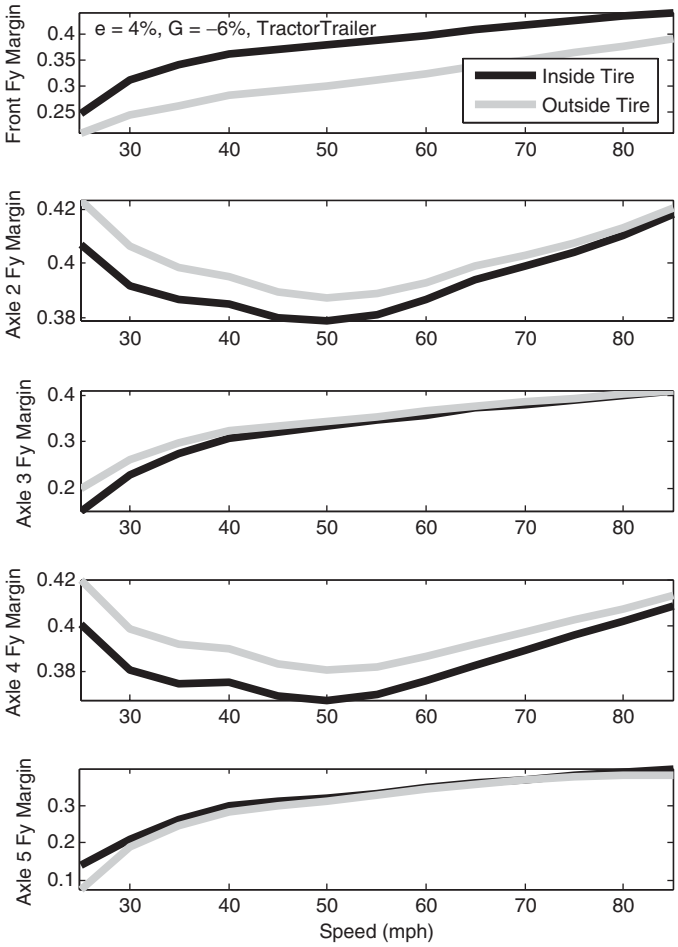

Figure 112. Effect of lateral weight shift on lateral friction margins for tractor semi-trailer (G = −6%, e = 4%) (a_x = 0 ft/s²).

4.10.2.3 Effect of Lane-Change Maneuver at Curve-Entry Deceleration

One of the situations of concern identified in Section 4.8 dealt with combined lane-change and braking maneuvers while traversing a horizontal curve. When assuming a lane-change maneuver combined with curve-entry deceleration, the transient bicycle models for the E-class sedan, E-class SUV, and tractor semi-trailer estimated relatively high lateral friction margins, but for the full-size SUV and the single-unit truck, the transient bicycle model estimated relatively low lateral friction margins for these cases. To determine whether this situation is actually of concern for the full-size SUV and the single-unit truck, the worst-case horizontal curves (i.e., curves on –9%

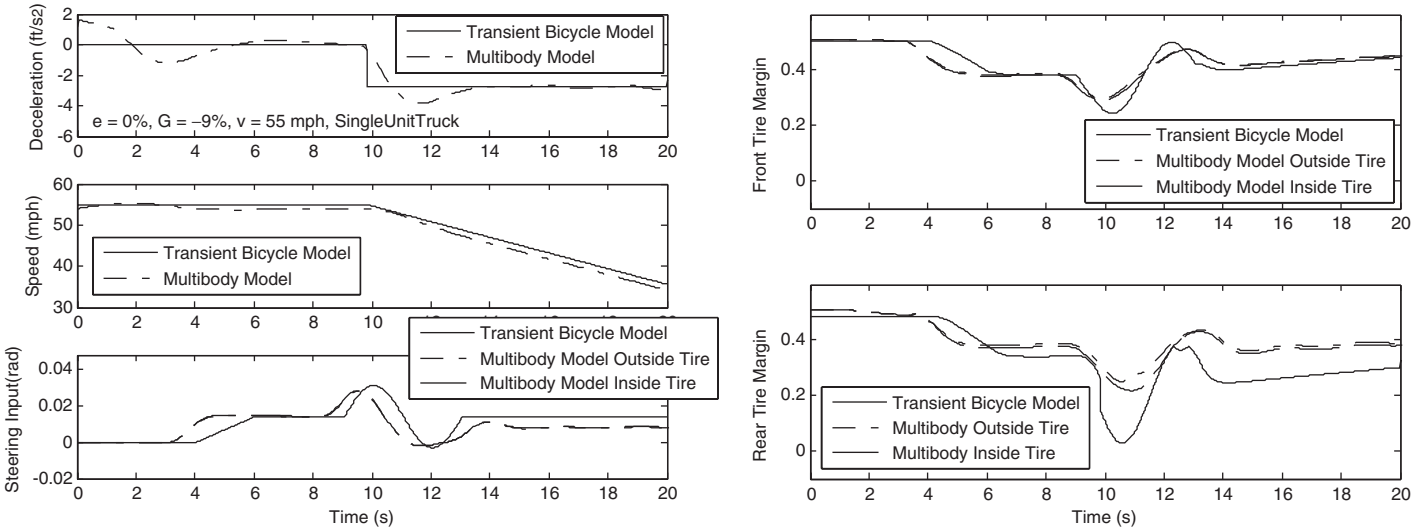

Figure 113. Inputs and outputs from transient bicycle and multibody models for single-unit truck (V = 55 mph, G = −9%, e = 0%) (a_x = −3 ft/s² and lane change).

grade with 0% superelevation) as determined by the simulations in Section 4.8 were further evaluated. Some matching scenarios with curves on –9% grade with 8% superelevation are also shown for comparison. Recall, previous results from the transient bicycle model and the multibody model show that the effect of superelevation is quite small overall.

A comparison of inputs and outputs is shown in Figure 113 for the transient bicycle model and the multibody model for the single-unit truck and for a 55 mph constant-speed curve traversal on a –9% grade and 0% superelevation. Figure 114 shows the same situation, except for 8% superelevation. The results are nearly identical. Both figures show that the multibody model predicts higher lateral friction margins than the transient bicycle model. This may be due to extra factors considered in the multibody simulation that are neglected in the transient model, including air resistance, tire lag, roll dynamics, and chassis stiffness. Each of these factors has the potential to "soften" the response of the vehicle to control inputs. Additionally, there are slight differences in the simulation inputs (brake, steering). Notably, the steering amplitude is smaller in the multibody model, and the peak of the sinusoid no longer aligns perfectly with the onset of braking. Both effects are due to the multibody simulation's use of a more human-like driver model.

To further examine the differences between the transient bicycle model and the multibody model across speeds, Figure 115 shows lateral friction margins for the front and rear axles for a single-unit truck assuming a lane-change maneuver combined with curve-entry deceleration. Both 0% and 8% superelevation cases are shown, and again these cases are quite similar to each other. The multibody model predicts

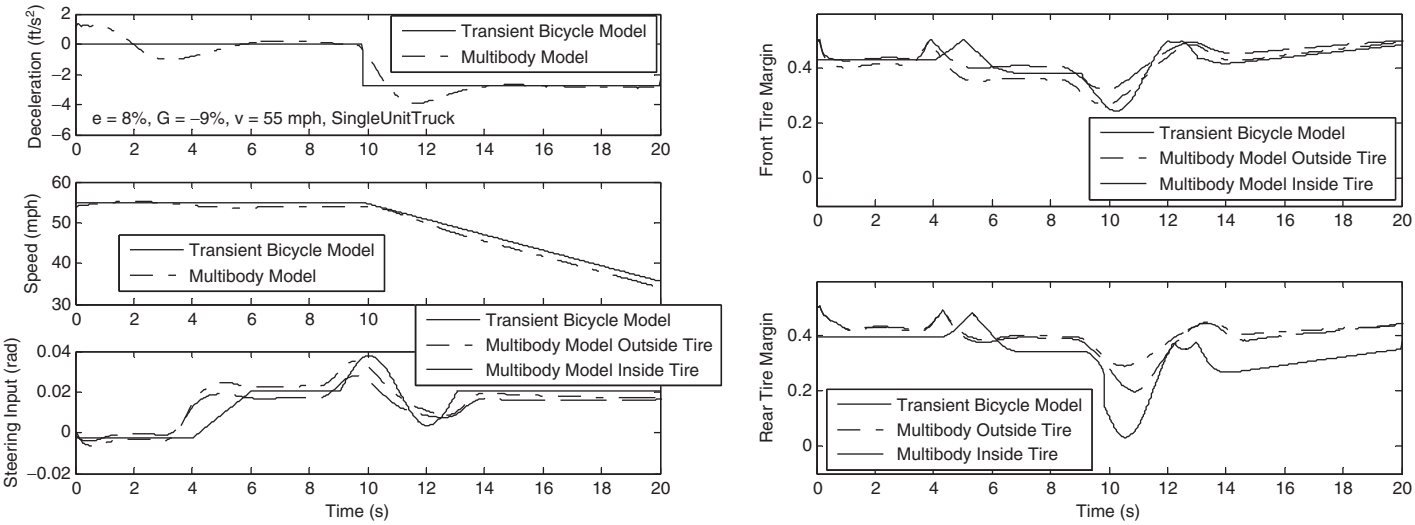

Figure 114. Inputs and outputs from transient bicycle and multibody models for single-unit truck (V = 55 mph, G = −9%, e = 8%) (a_x = −3 ft/s² and lane change).

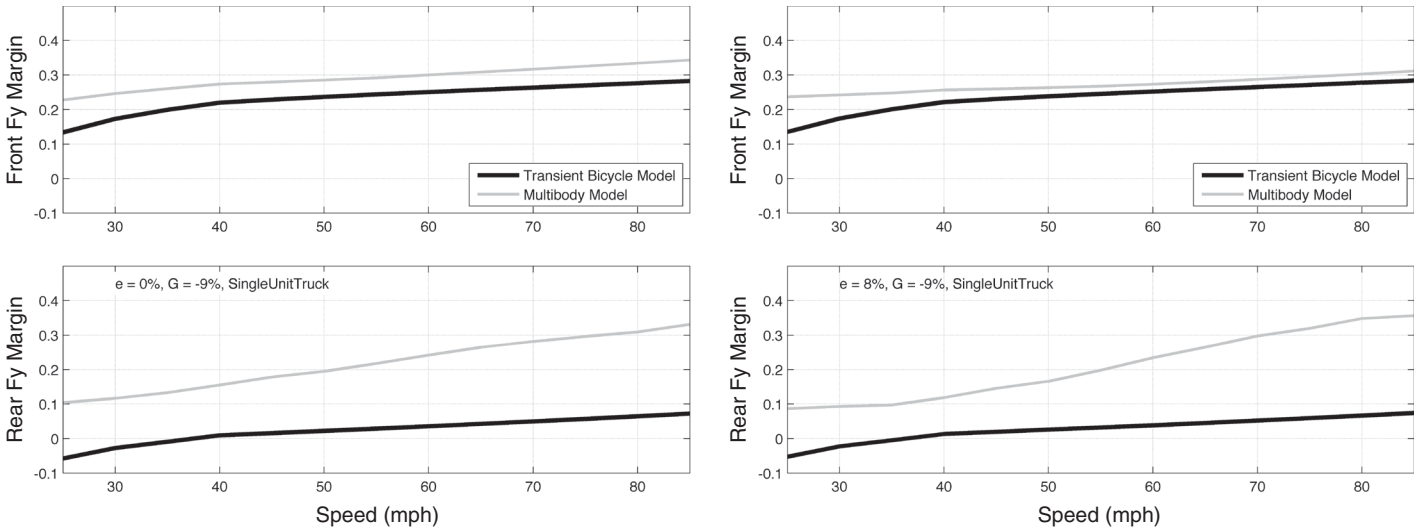

Figure 115. Lateral friction margins from transient bicycle and multibody models for single-unit truck (G = −9%, e = 0% and 8%) (a_x = −3 ft/s² and lane change).

low margins but predicts that there will be no skidding across the range of speeds. In contrast, the transient bicycle model predicts that the rear axle could skid or be close to skidding for nearly all speeds. This suggests some conservatism on the part of the transient bicycle model for two-axle vehicles.

To determine whether the difference in lateral friction margins is an effect strictly seen on the single-unit truck, Figures 116 and 117 compare the transient bicycle model to the multibody model for the full-size SUV assuming a lane-change maneuver combined with curve-entry deceleration. Again, the multibody model predicts much higher rear-axle margins than the transient bicycle model. And again, this is likely due to the differences in inputs. This should not necessarily be taken as an indication that all lane-change maneuvers combined with curve-entry deceleration result in lateral friction margins greater than zero; rather, it suggests that using the transient bicycle model to evaluate the dynamics of two-axle vehicles for geometric design purposes is a conservative approach. Additionally, Figures 116 and 117 indicate that certain higher-order braking effects have the potential to obscure the fundamental trends in margin calculations for certain cases. While this may be the case for two-axle vehicles, the possibility of disagreement between the transient bicycle model and the multibody model for a tractor semi-trailer has already been discussed for curve-entry deceleration without the addition of a lane change.

When a lane-change maneuver is superimposed onto the curve-entry deceleration for a tractor semi-trailer, the results of a comparison between models is even more revealing. Consider the comparison between models for a 55 mph horizontal curve (Figure 118) and across design speeds (Figure 119).

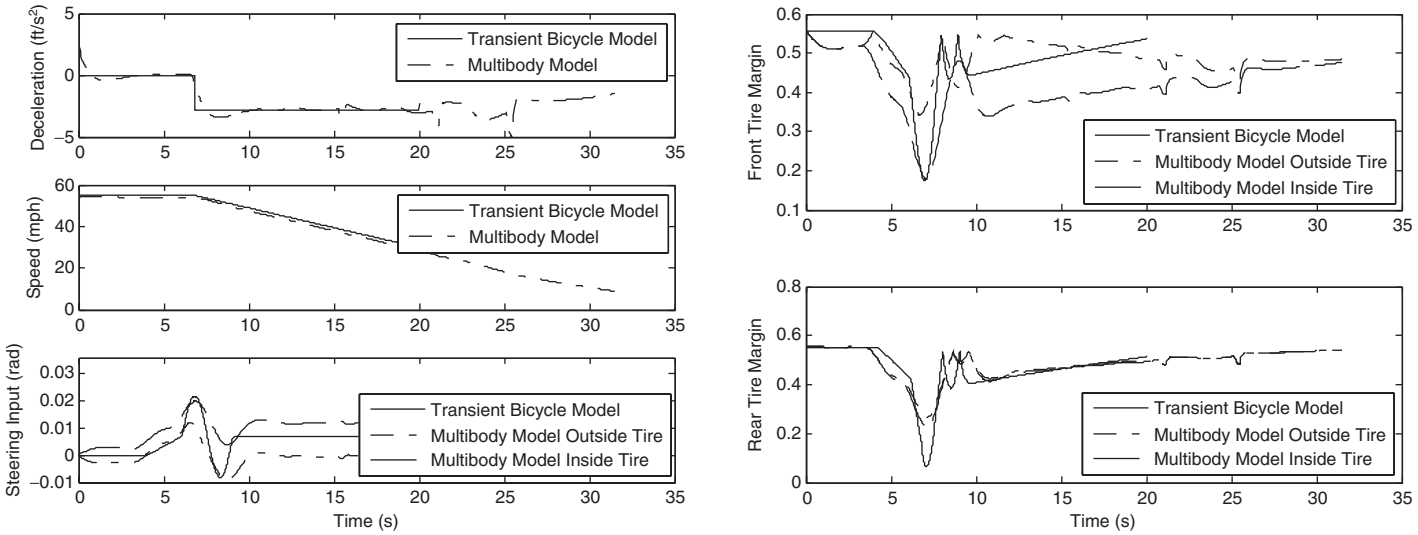

Figure 116. Inputs and outputs from transient bicycle and multibody models for full-size SUV (V = 55 mph, G = −9%, e = 0%) (a_x = −3 ft/s² and lane change).

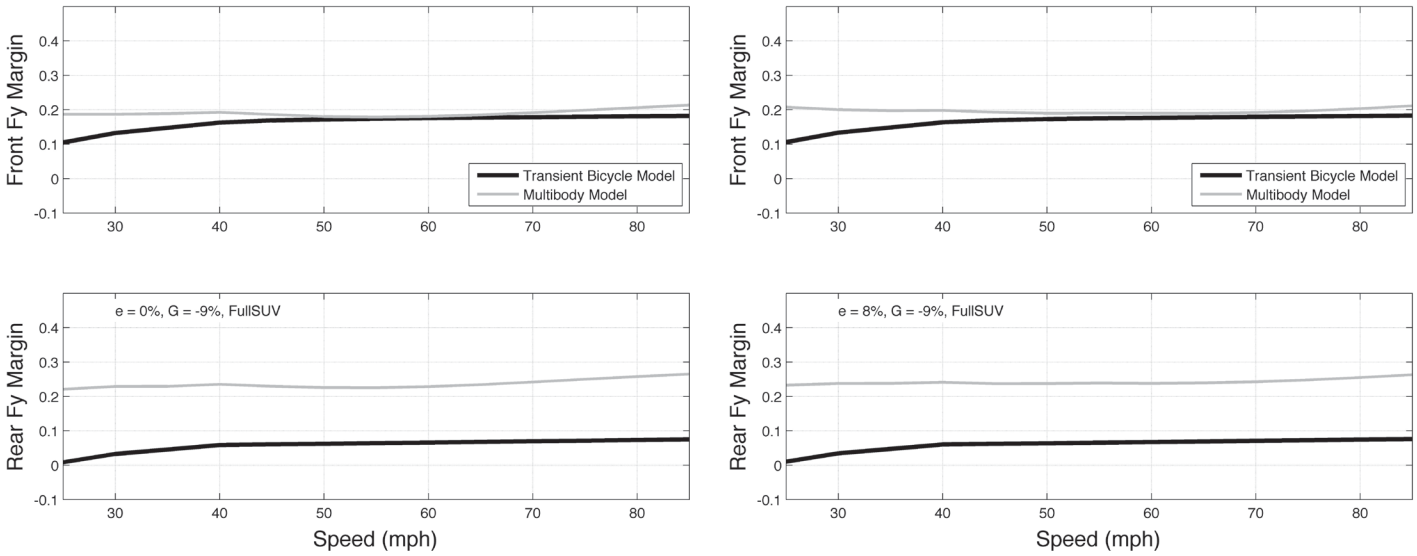

Figure 117. Lateral friction margins from transient bicycle and multibody models for full-size SUV (G = −9%, e = 0% and 8%) (a_x = −3 ft/s² and lane change).

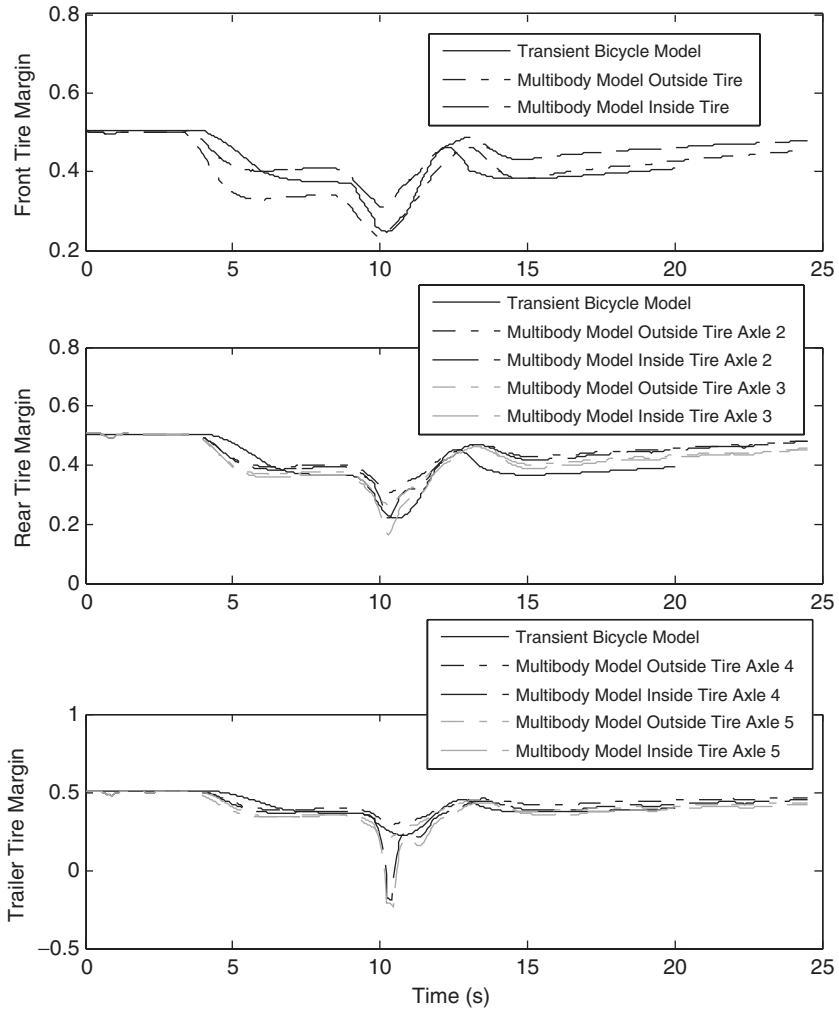

Figure 118. Lateral friction margins from transient bicycle and multibody models for tractor semi-trailer (V = 55 mph, G = −9%, e = 0%) (a_x = −3 ft/s² and lane change).

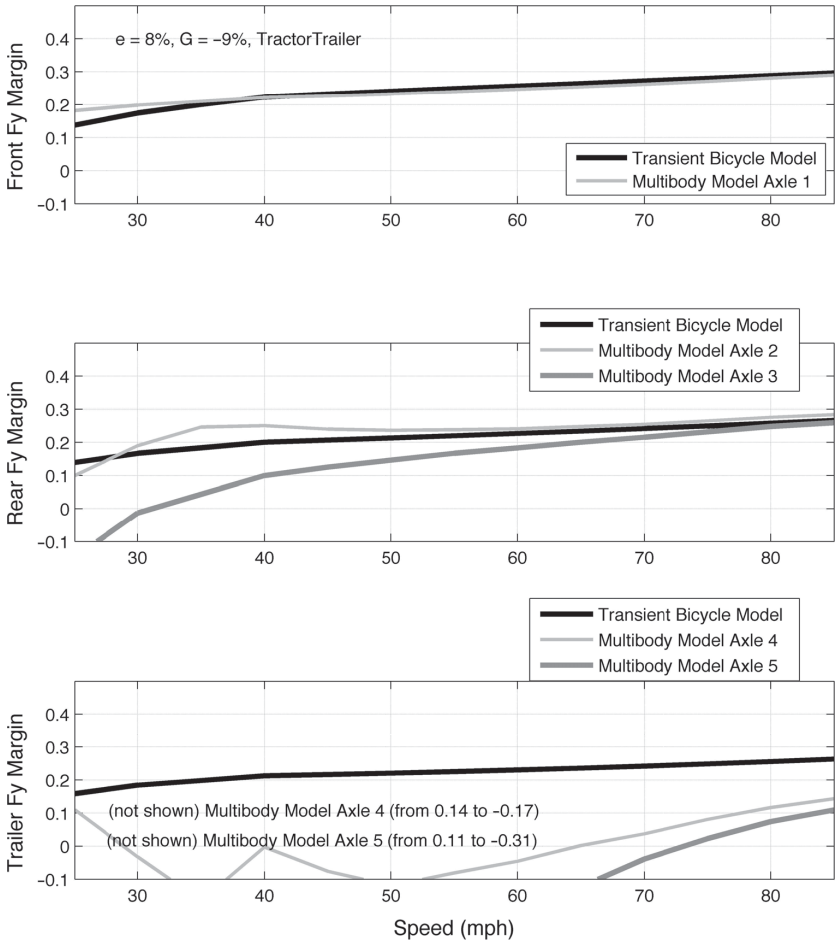

Figure 119. Lateral friction margins from transient bicycle and multibody models for tractor semi-trailer (G = −9%, e = 8%) (a_x = −3 ft/s² and lane change).

As Figure 119 shows, the transient bicycle model for a tractor semi-trailer does not capture an apparently significant effect that leads to trailer-tire saturation between 30 to 65 mph design speeds.

Part of this phenomenon can be explained by looking at the simulation inputs, specifically braking, shown in Figure 120. These inputs correspond to the same 55 mph truck simulation shown in Figure 118. The braking deceleration is oscillatory, because the simulation attempts to achieve curve-entry deceleration by mimicking a human driver applying and releasing the brakes in an unsteady manner. For this same situation, the brake's master cylinder "control" pressure is shown in Figure 121. This master cylinder pressure corresponds directly with foot pressure on the brake pedal by the driver model, and it exhibits the oscillatory behavior seen in the deceleration plot of Figure 120. Each axle's individual brakes lag behind the master cylinder pressure due to their own dynamic properties, which are related in part to the distance of the axle from the master cylinder. To illustrate this, Figure 121 also shows the brake pressure in axle 5 (i.e., the last axle on the trailer of the tractor semi-trailer). The peaks in this axle's pressure oscillations lag behind the master cylinder pressure significantly, which is the likely cause of the excessive spiking specifically seen in the trailer margins as predicted by the multibody model. As a result of the oscillations resulting from simulated driver control of deceleration in the multibody model, Figure 120 shows the deceleration value predicted by the multibody model momentarily spike higher than −3 ft/s², which contributes to the low margins. Additionally, as mentioned in the previous section, while weight-transfer effects on lateral friction margins are small for most driving, the tractor semi-trailer has a high center of gravity, which amplifies weight-transfer effects.

The high CG of the tractor semi-trailer, combined with the relative severity of the lane-change maneuver, indicates the possibility of weight transfer playing a role in the negative margins. To examine this possibility, the individual lateral

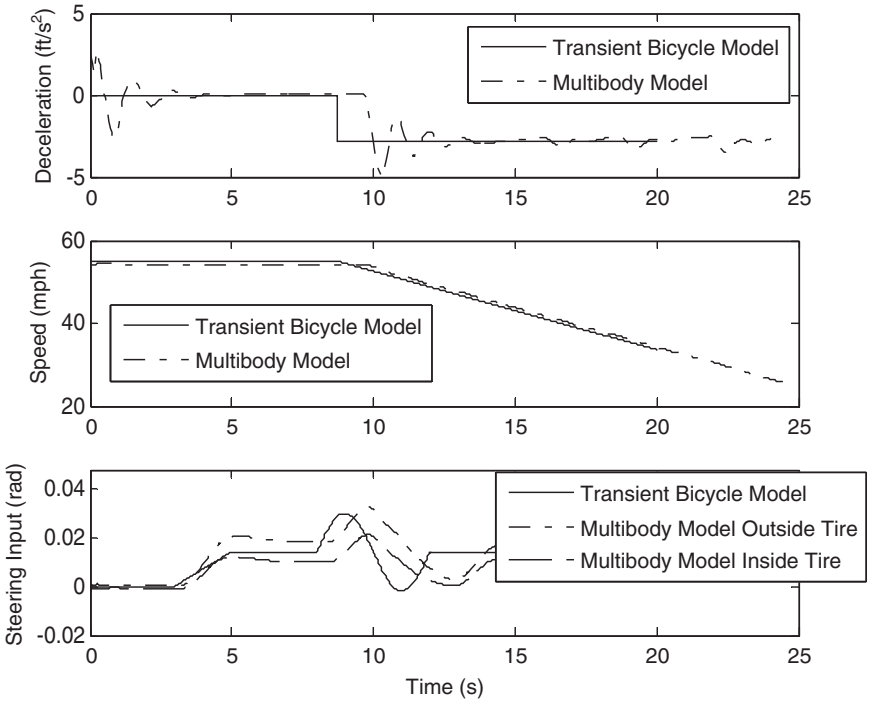

Figure 120. Inputs for multibody model for tractor semi-trailer (V = 55 mph, G = −9%, e = 0%) (a_x = −3 ft/s² and lane change).

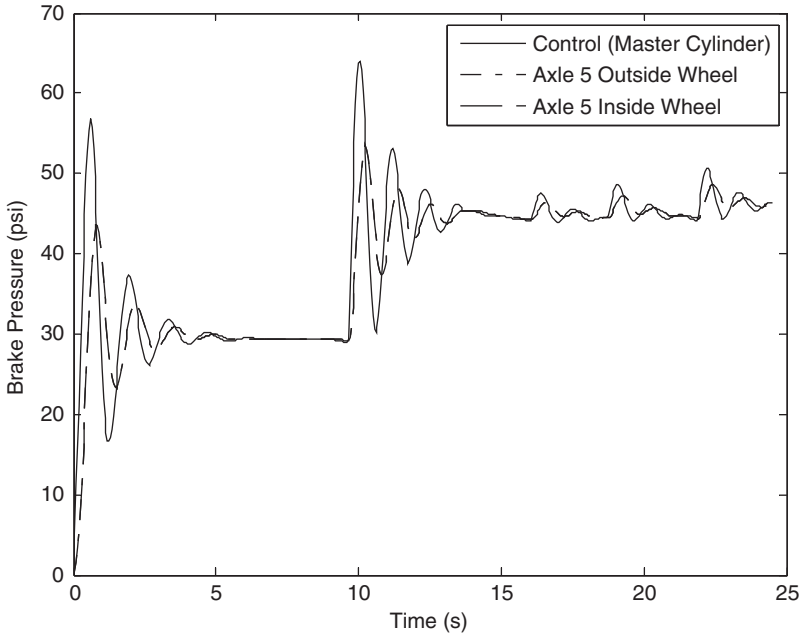

Figure 121. Braking pressures for multibody model for tractor semi-trailer (V = 55, G = −9%, e = 0%) (a_x = −3 ft/s² and lane change).

friction margins are shown for the inside and outside tires in Figure 122 for the 0% superelevation case and in Figure 123 for the 8% superelevation case. As anticipated, the figures indicate that the weight transfer effects on lateral friction margins are higher for this maneuver than for a steady-curve traversal. Both axles 4 and 5 have positive friction margins on the inside tire, but negative friction margins are estimated for the outside tire. This further supports the conclusion from the previous section that the transient bicycle model for a tractor semi-trailer should be used with extreme caution when predicting behavior for aggressive maneuvers.

Although the multibody model predicts negative lateral friction margins for a tractor semi-trailer for the case of a lane-change maneuver combined with curve-entry deceleration, the question of severity remains (i.e., how severe is the tire saturation and/or how far from its intended path does the tractor semi-trailer skid?). These questions were answered in Section 4.8 using the transient bicycle model by examining time-of-skidding for various speeds. Figure 118 shows the time trajectory of a tractor semi-trailer for a 55 mph traversal with a lane change and curve-entry deceleration. And although the lateral friction margins are

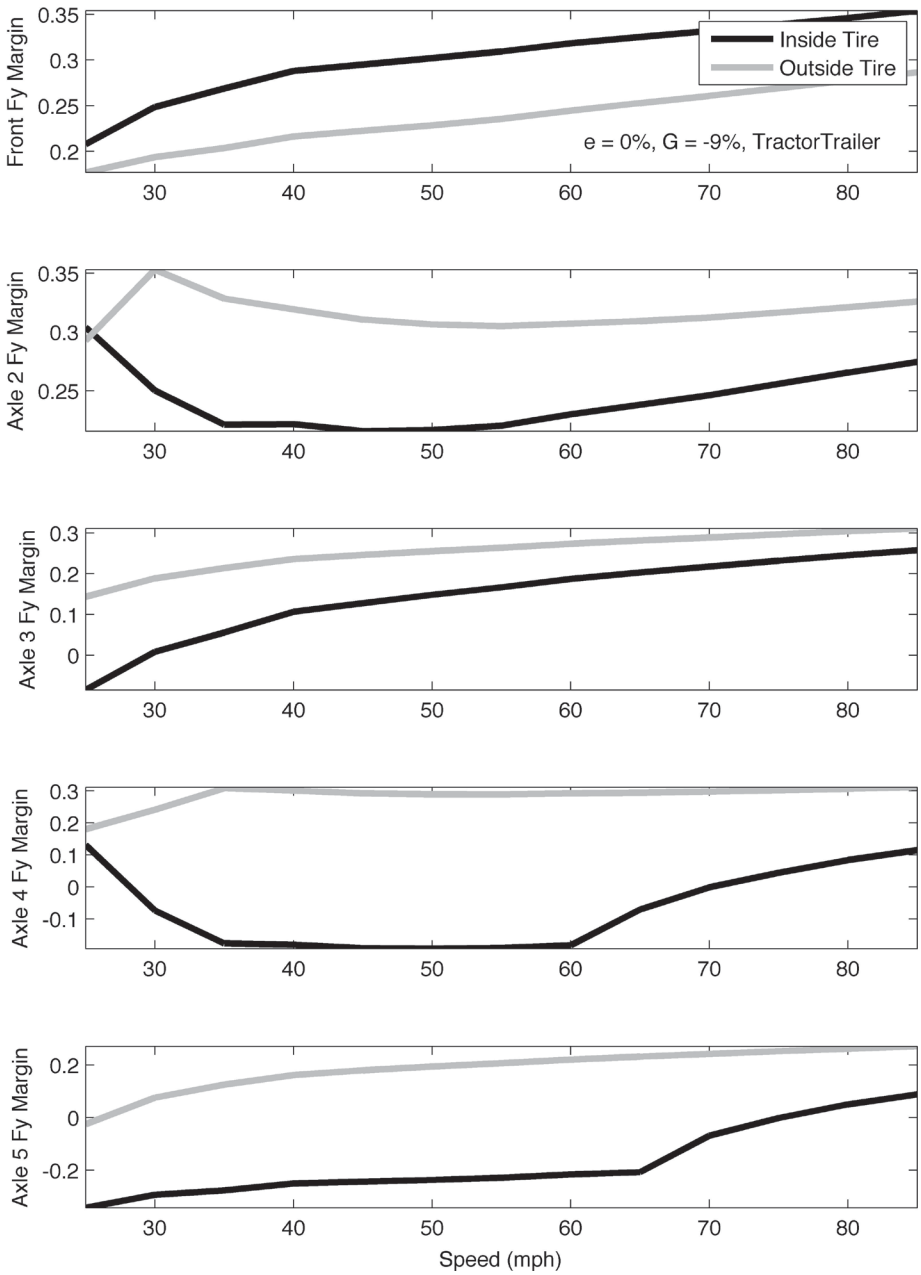

Figure 122. Effect of lateral weight shift for tractor semi-trailer (G = −9%, e = 0%) (a_x = −3 ft/s² and lane change).

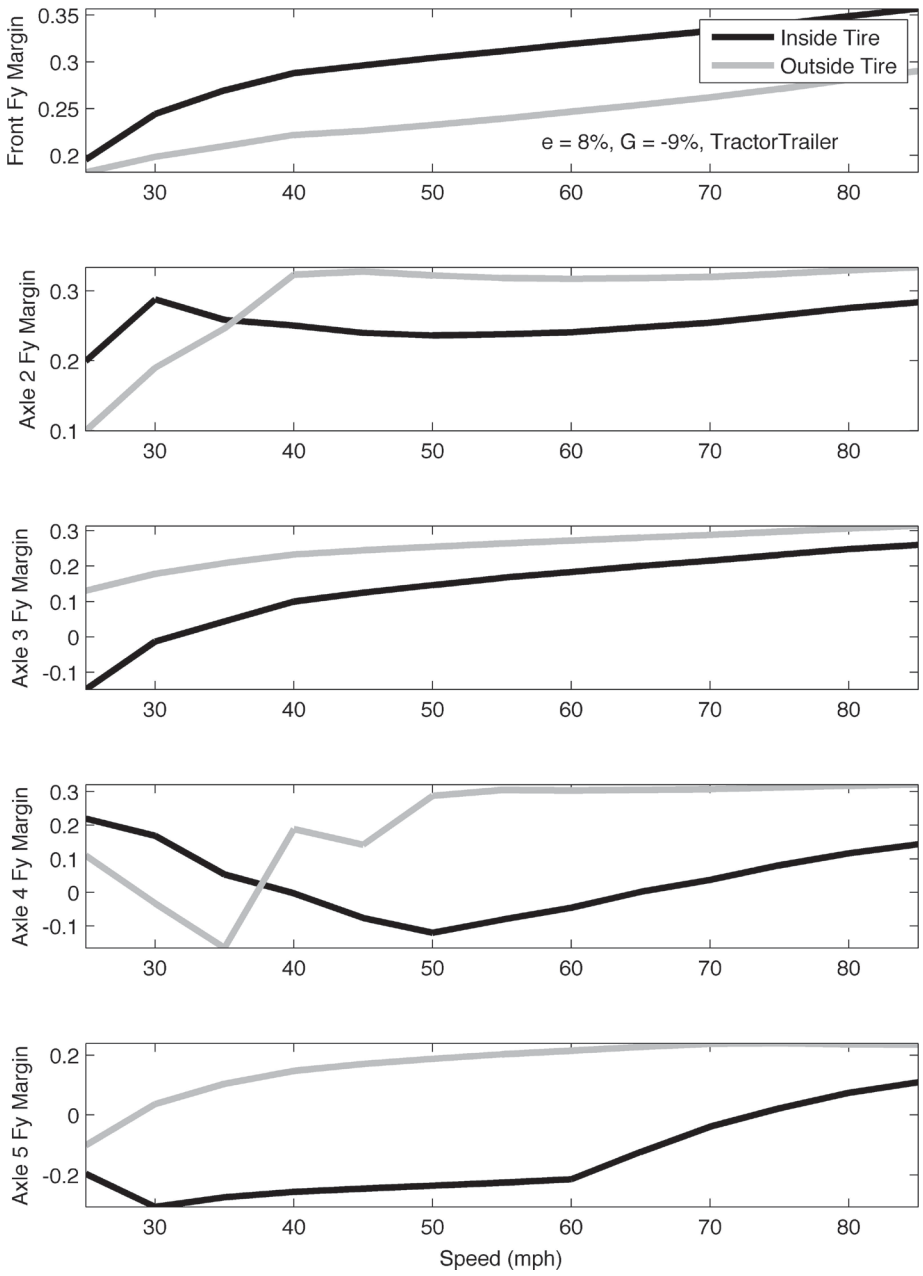

Figure 123. Effect of lateral weight shift for tractor semi-trailer (G = −9%, e = 8%) (a_x = −3 ft/s² and lane change).

zero or negative, the vehicle only skids for a short period of time (i.e., less than 1 s).

Simulations were next conducted to determine whether a short period of skidding affects the ability of the vehicle to continue to navigate the curve. Figure 124 shows the lateral position of the vehicle on the road for the 55 mph traversal, and the desired and actual positions agree quite closely. This suggests that, while the margins on certain individual tires become negative for a short period of time while traversing the curve, the vehicle is still able to negotiate the curve and perform the lane change as desired. Recall that the road surface in the multibody software has a higher coefficient of friction than the assumed friction supply for the margin calculation—this is to help ensure that the friction demand reported by the multibody software does not reflect premature tire saturation to maintain consistency with the transient bicycle model simulations. While this means that vehicles simulated in the multibody software have a slightly better ability to maintain tracking with "negative margins," some of the more aggressive maneuvers simulated still produced tire saturation and activation of ABS. These cases are discussed in the subsections that follow.

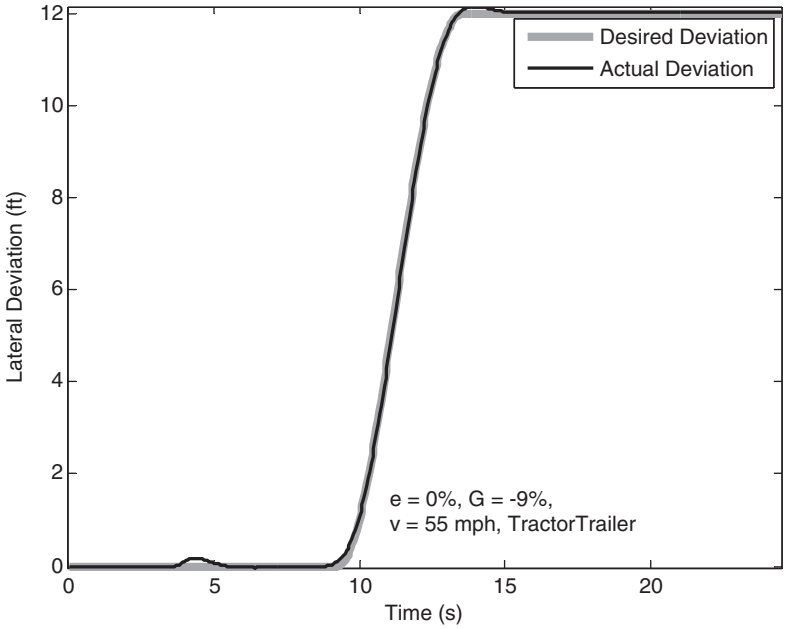

Figure 124. Lateral position of tractor semi-trailer with respect to road centerline (V = 55 mph, G = −9%, e = 0%) (a_x = −3 ft/s² and lane change).

For the sake of completeness in the analysis of trucks, this same maneuver on the same geometry of Figure 124 was simulated with the standard STAA Double twin-trailer truck (i.e., tractor semi-trailer/full-trailer). The standard model of the STAA Double in TruckSim comprises a two-axle lead unit (tractor), a loaded semi-trailer with one rear axle, and a second full-trailer with two total axles (one in front, one in rear). This vehicle configuration has five axles, like the tractor semi-trailer considered in this research, but the axles are in different locations and perform different functions. Therefore, the equations of motion derived for the transient bicycle model for the tractor semi-trailer do not apply. Figure 125 shows the margins on each axle of the STAA Double for the curve-entry deceleration with lane-change maneuver. The plots show that the STAA Double seems to have negative margins at speeds less than 55 mph for this configuration.

To investigate the severity of these low margin predictions for low design speeds, a plot of the margin trajectories at 25 mph is shown in Figure 126. This 25 mph situation represents the worst-case speed for the STAA Double, and the time traces show that margins on any one axle are negative for a short time duration. Additionally, the outside tire on each axle, the one carrying more load and generating more cornering force on each axle, maintains positive lateral friction margins throughout the maneuver. The inside tire, which is lighter, exhibits temporary negative margin spikes. Though the inputs are not shown, the lateral friction margin spikes are due to brake activation. Like the tractor semi-trailer, the pneumatic braking system dynamics combined with the multibody model's simulated driver model are responsible for the negative margins here.

Comparing the tractor semi-trailer in Figure 119 with the STAA Double in Figure 126, the trends exhibited by the STAA Double are similar to those exhibited by the tractor semi-trailer. The STAA Double, in fact, shows margins that are, in general, either comparable or higher than those exhibited by the tractor semi-trailer. In both situations, the rearmost axles on each vehicle exhibit the lowest margins, but the tractor semi-trailer exhibits lower margins on this axle. With this in mind, the results from the tractor semi-trailer simulations will be considered the worst-case articulated vehicle for the primary analysis of roadway design.

4.10.2.4 Effect of Stopping Sight Distance Deceleration

In Section 4.9 stopping sight distance deceleration (a_x = −11.2 ft/s²) scenarios were considered for all of the vehicles. Only the single-unit truck produced negative lateral friction margins for curve-keeping steering inputs alone. However, care must be taken when considering the tractor semi-trailer dynamics for this type of traversal as well. Previously, the transient bicycle model for the tractor semi-trailer was shown to be overly optimistic in predicting lateral friction margins when any but gentle steering and braking inputs were considered. Therefore, the multibody models for a single-unit truck and a tractor semi-trailer were used to analyze the stopping

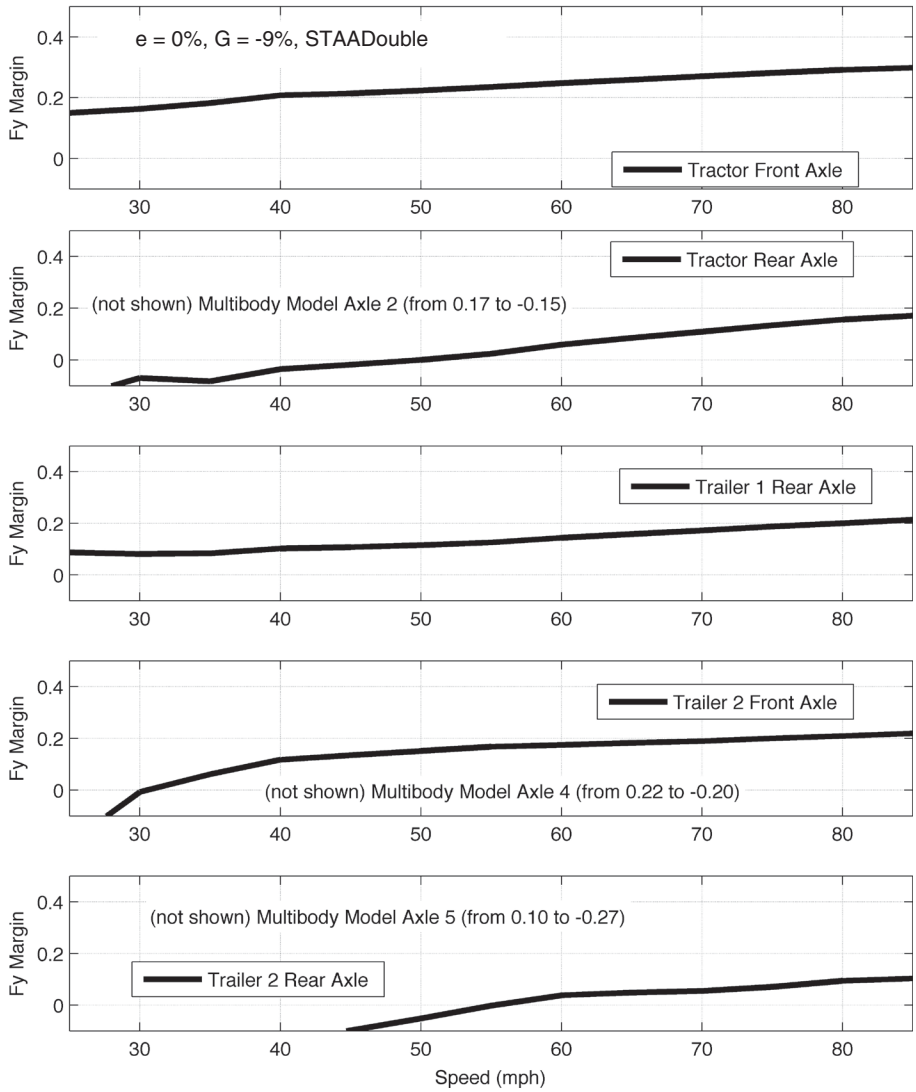

Figure 125. Lateral friction margins from multibody model for tractor semi-trailer/full-trailer truck (Double) (G = −9%, e = 0%) (a_x = −3 ft/s² and lane change).

sight distance deceleration case without the lane-change maneuver. Figure 127 compares the results of the transient bicycle and multibody models for the single-unit truck traversing a curve while undergoing stopping sight distance deceleration while maintaining the same lane. The transient bicycle and multibody models agree well, with the multibody model offering slightly less-negative margin predictions.

For the tractor semi-trailer, Figure 128 shows that at 55 mph both the trailer and rear tractor axles exhibit negative lateral friction margins on all tires for the stopping sight distance deceleration case. This is, again, a relatively small spike and the lateral friction margins are negative for a relatively short period of time, but these two axle groups exhibit skidding for this maneuver across all speeds (Figure 129). This provides further support for the previous claim that the transient bicycle model for a tractor semi-trailer should not be relied upon to estimate lateral friction margins when combined cornering and braking inputs are involved. Again, the low-frequency oscillatory behavior of the simulated driver's braking inputs also contributes to lower margins for the multibody model, as does the high-frequency oscillation caused by activation of the multibody simulation's ABS system. This effect has to be expected for real driving scenarios as well, since human drivers will also exhibit a range in variation in the applied brake pressure.

To emphasize the significance of the braking system in determining lateral friction margins, and the significance of the driver model in determining whether a tire will skid, consider the following curve-keeping, stopping sight distance deceleration traversal of an E-class sedan at 65 mph. This vehicle, which consistently produced the highest lateral friction margins in Sections 4.8 and 4.9, exhibits negative margins for several seconds during stopping sight distance

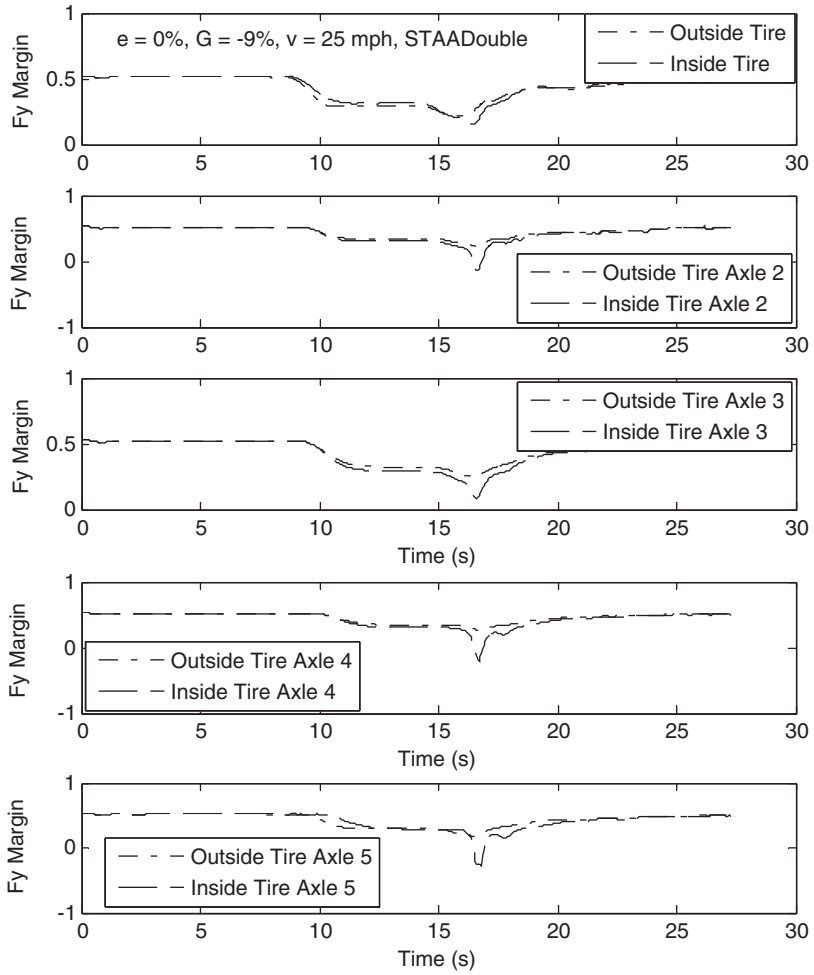

Figure 126. Margin trajectories for tractor semi-trailer/full-trailer truck (Double) (V = 25 mph, G = −9%, e = 0%) (a_x = −3 ft/s² and lane change).

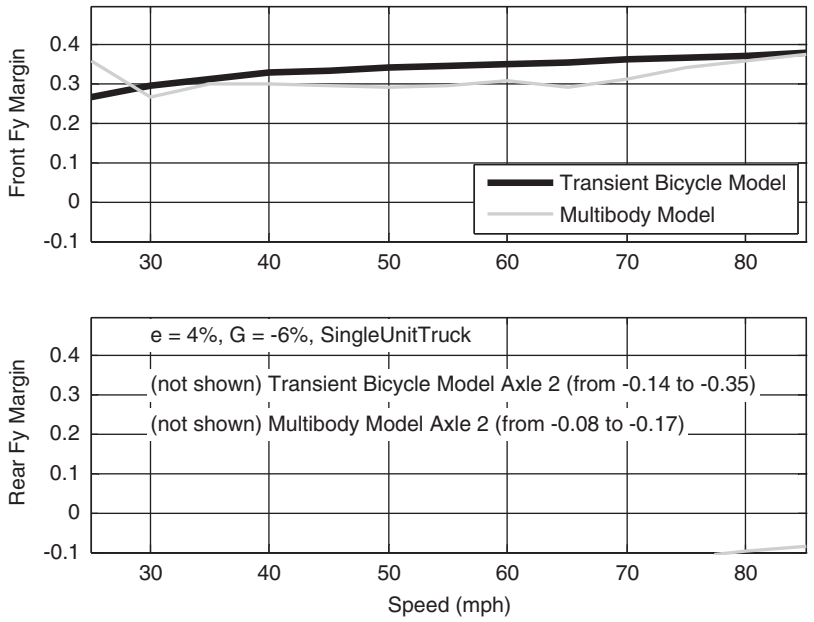

Figure 127. Lateral friction margins from transient bicycle and multibody models for single-unit truck (G = −6%, e = 4%) (a_x = −11.2 ft/s²).

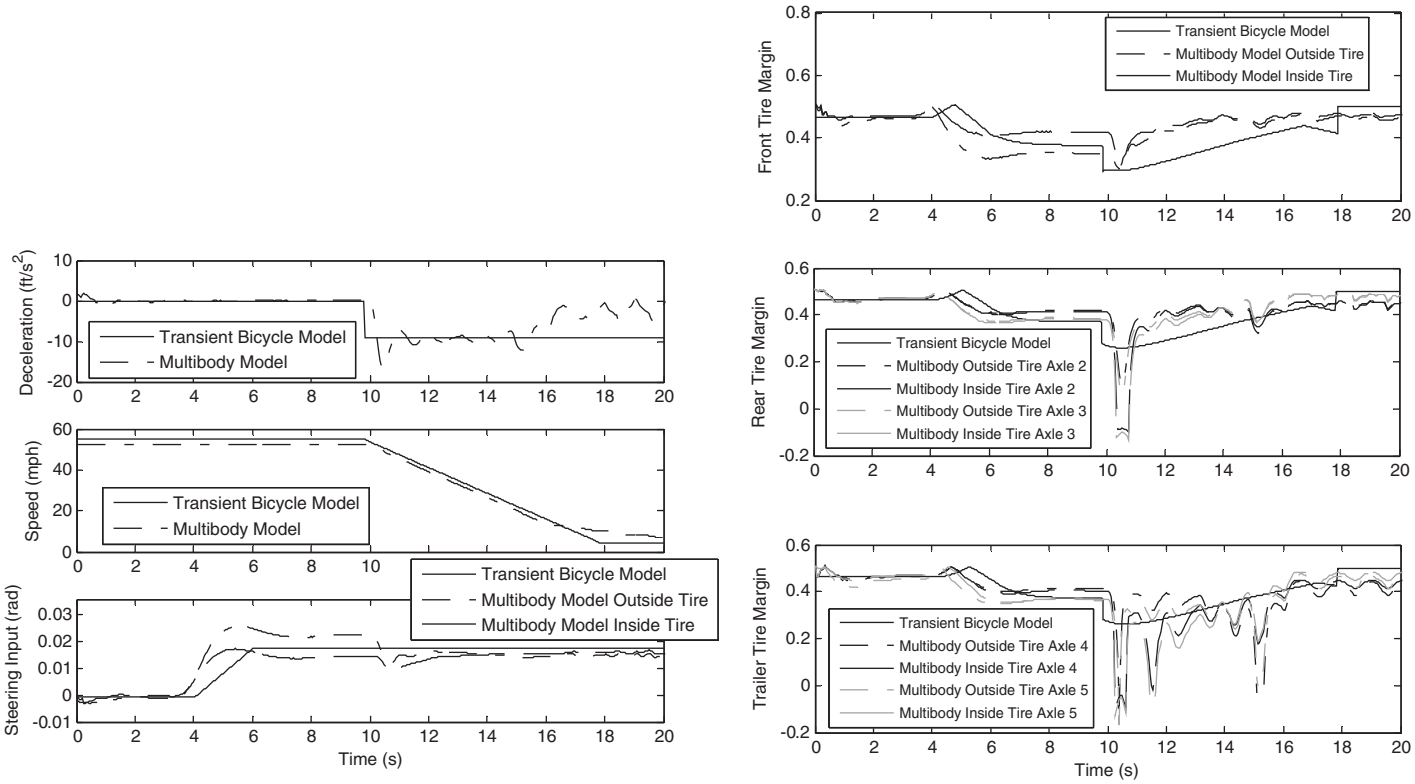

Figure 128. Inputs and outputs from transient bicycle and multibody models for tractor semi-trailer (V = 55 mph, G = −6%, e = 4%) (a_x = −11.2 ft/s²).

deceleration based upon a multibody simulation. The results of this traversal are shown in Figure 130.

It is unclear from the plots of the lateral friction margins in Figure 130 why the margins are estimated to be lower for the multibody model than for the transient bicycle model. However, upon close inspection of the simulation inputs (Figure 131) to simulation outputs (Figure 130), the minimum lateral friction margins occur precisely when the most aggressive braking is activated. This braking maximum is due to an oscillation caused when the multibody simulation software's driver model attempts to maintain not only the desired deceleration of −11.2 ft/s², but also the vehicle's position in the center of the lane. The result is that both the brake pressure (and thus deceleration) and the steering input oscillate together. This causes the two peaks in deceleration observed at approximately 7.5 and 11 s during the trajectory. These spikes correspond with the downward spikes in lateral friction margin in Figure 130. This behavior occurs again later with higher deceleration values. In Section 4.9 it was assumed that the required deceleration value was reached immediately and without error, which is not realistic for a human driver (or a computer approximation of a human driver) that is simply trying to match a deceleration profile. Thus, the transient bicycle model is better than the multibody model in that it more readily illustrates the effects of severe braking, but the transient model is deficient in that it neglects variations expected of human driving. Variations are simulated within the multibody model. Thus, the outputs of each model have to be compared judiciously. The transient model provides a simplified prediction of worst-case lateral friction margins, and the multibody model modifies these margins due to human variability.

At the very least, the consistent behavior of the transient bicycle model provides a more reasonable and predictable approach to assess lateral friction margins under these cases than a multibody simulation making use of a driver model. The transient bicycle model has no driver dynamics, and so only tests the vehicle dynamics themselves to determine lateral friction margins. The same model ignores the potential for variability on the part of a driver or an ABS system, and these results show that this variability can actually lead to negative friction margins.

Although negative lateral friction margins are estimated from multibody models for single-unit trucks and tractor semi-trailers for the stopping sight distance deceleration case while the desired trajectory is to maintain position in the same lane, in both vehicles the ABS system is initiated, and both vehicles are able to main their desired trajectory. The ability for a single-unit truck and tractor semi-trailer as predicted from multibody models to maintain their desired trajectory through a curve for stopping sight distance deceleration while maintaining position in the same lane is made more evident in the following section, which shows that both vehicles are able to maintain their desired trajectory through a curve while undergoing stopping sight distance deceleration with

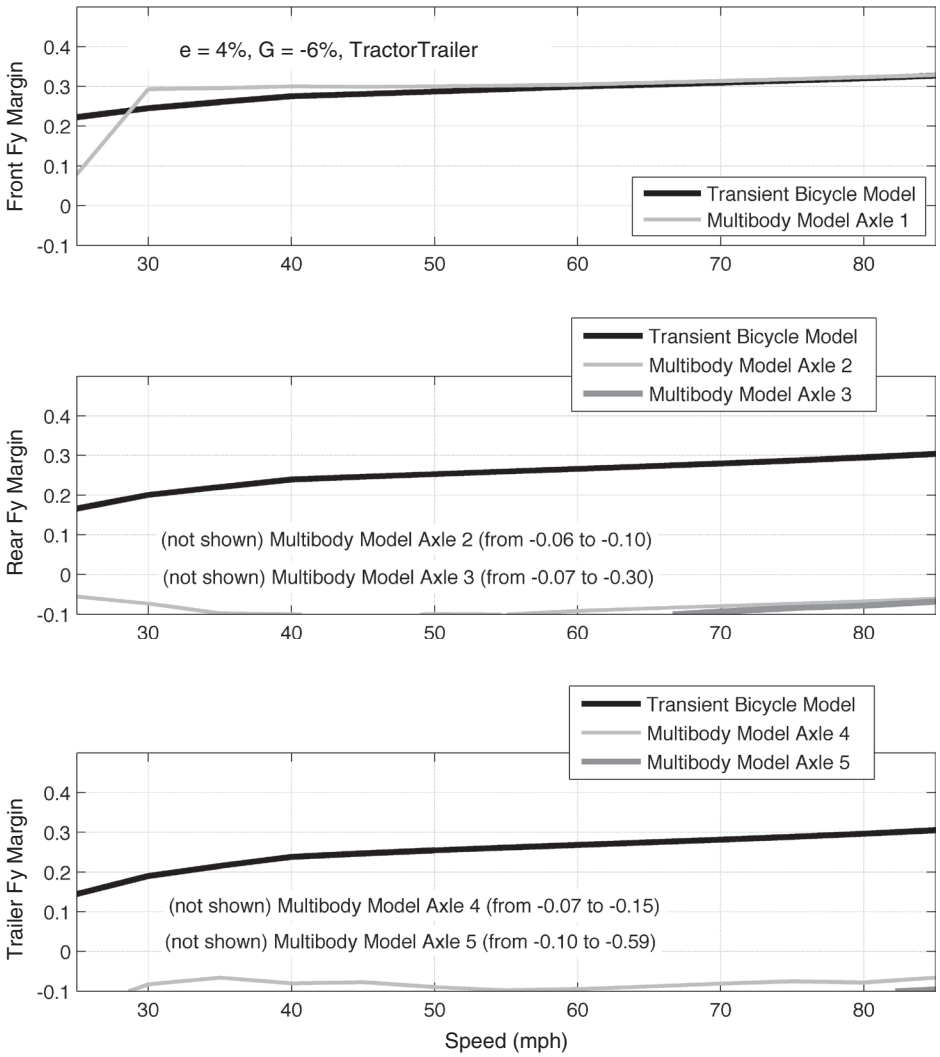

Figure 129. Lateral friction margins from transient bicycle and multibody models for tractor semi-trailer (G = −6%, e = 4%) (a_x = −11.2 ft/s²).

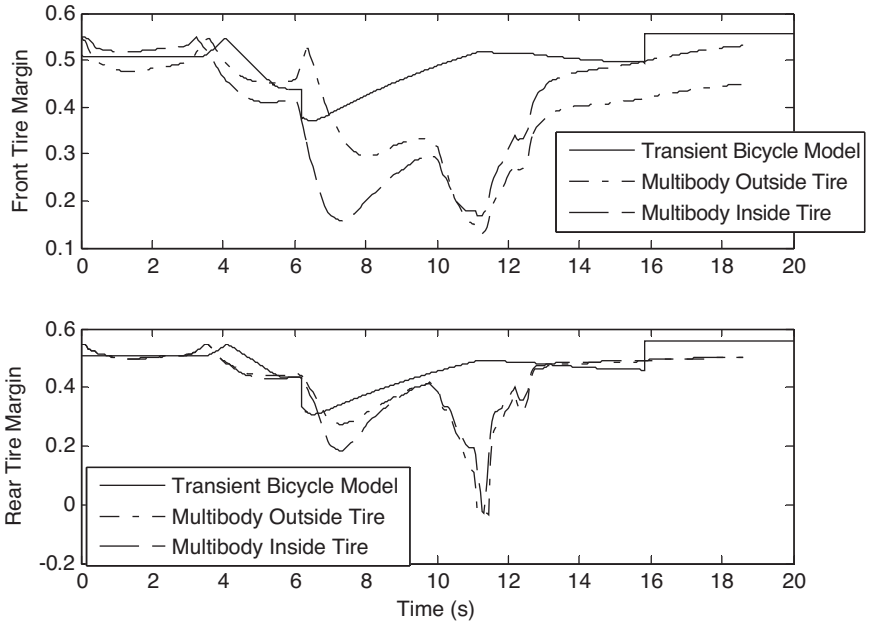

Figure 130. Trajectory of lateral friction margins for E-class sedan (V = 65 mph, G = −6%, e = 4%) (a_x = −11.2 ft/s²).

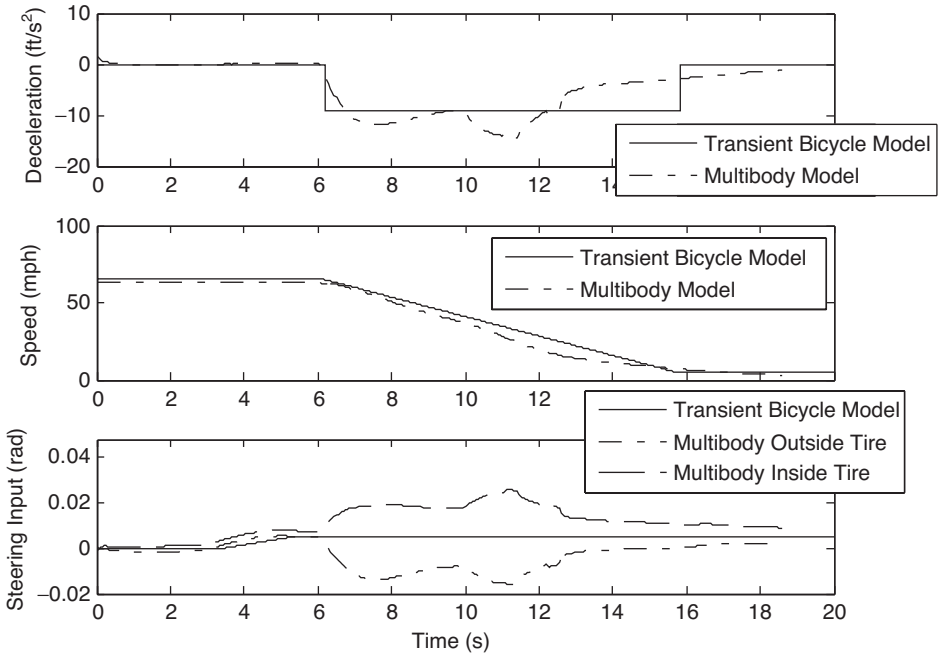

Figure 131. Trajectory of simulation inputs for transient bicycle and multibody models for E-class sedan (V = 65 mph, G = −6%, e = 4%) (a_x = −11.2 ft/s²).

a lane change (i.e., an even more aggressive maneuver). In both cases, the ABS system enables both vehicles to traverse the curve without experiencing a skidding event.

4.10.2.5 Effect of Lane-Change Maneuver at Stopping Sight Distance Deceleration

While several of the vehicle types considered maintained positive lateral friction margins for stopping sight distance deceleration while maintaining position in the same lane, all of the vehicles considered in Section 4.9 using the transient bicycle models exhibited negative lateral friction margins when a lane change was combined with a stopping sight distance deceleration event. To check whether the same is true using the multibody model, consider the lateral friction margin plots for the E-class sedan (Figures 132 to 134), the full-size SUV (Figures 135 to 137), single-unit truck (Figures 138 to 140), and tractor semi-trailer (Figures 141 to 143). These figures show the margins during traversals at three speeds (25, 55, and 85 mph), at a grade of −9% and superelevations of 0% and 8%.

Comparing the effects between 0% and 8% superelevations in Figures 132 to 143, the minimum lateral margins are found

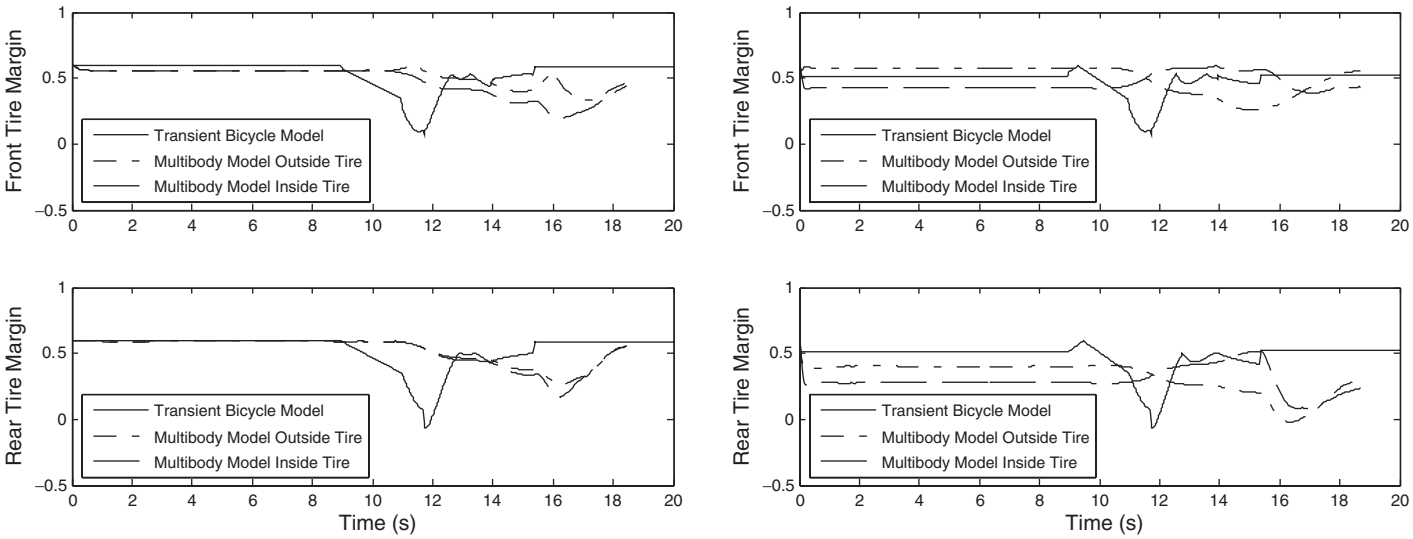

Figure 132. Lateral friction margin trajectories from transient bicycle and multibody models for E-class sedan [V = 25 mph, G = −9%, e = 0% (left plots) and 8% (right plots)] (a_x = −11.2 ft/s² and lane change).

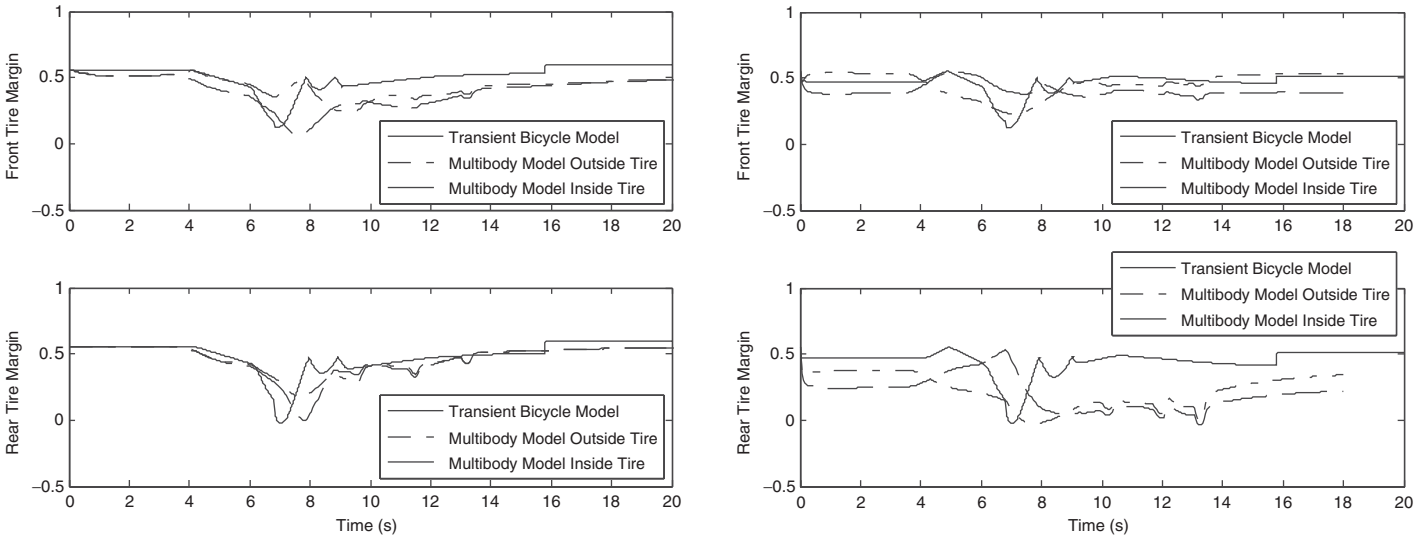

Figure 133. Lateral friction margin trajectories from transient bicycle and multibody models for E-class sedan [V = 55 mph, G = −9%, e = 0% (left plots) and 8% (right plots)] (a_x = −11.2 ft/s² and lane change).

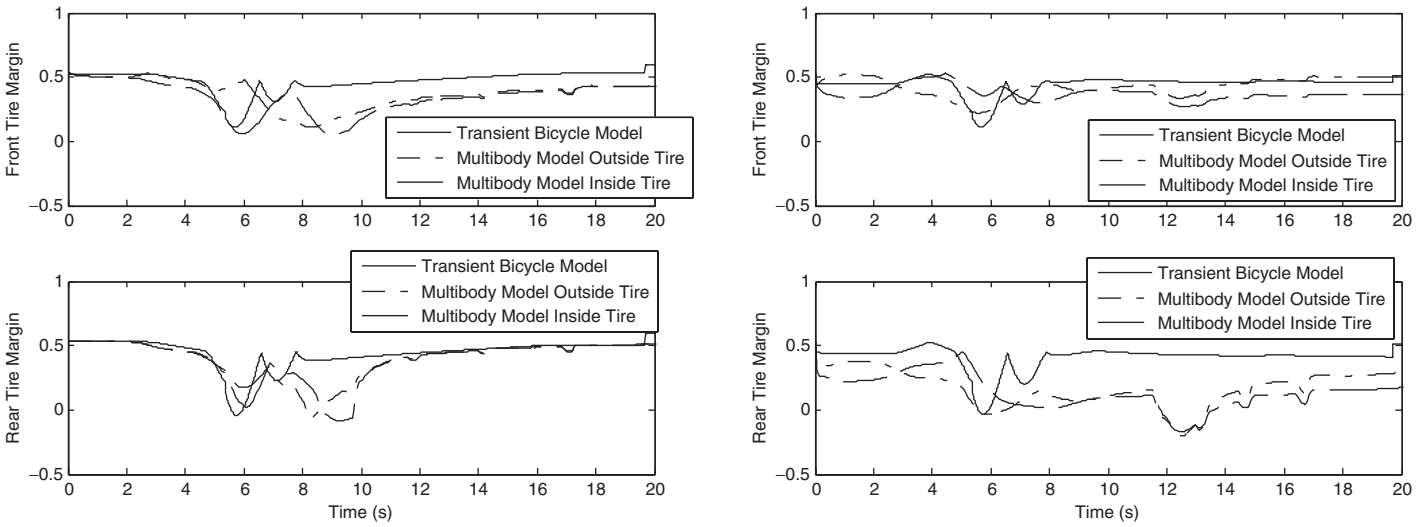

Figure 134. Lateral friction margin trajectories from transient bicycle and multibody models for E-class sedan [V = 85 mph, G = −9%, e = 0% (left plots) and 8% (right plots)] (a_x = −11.2 ft/s² and lane change).

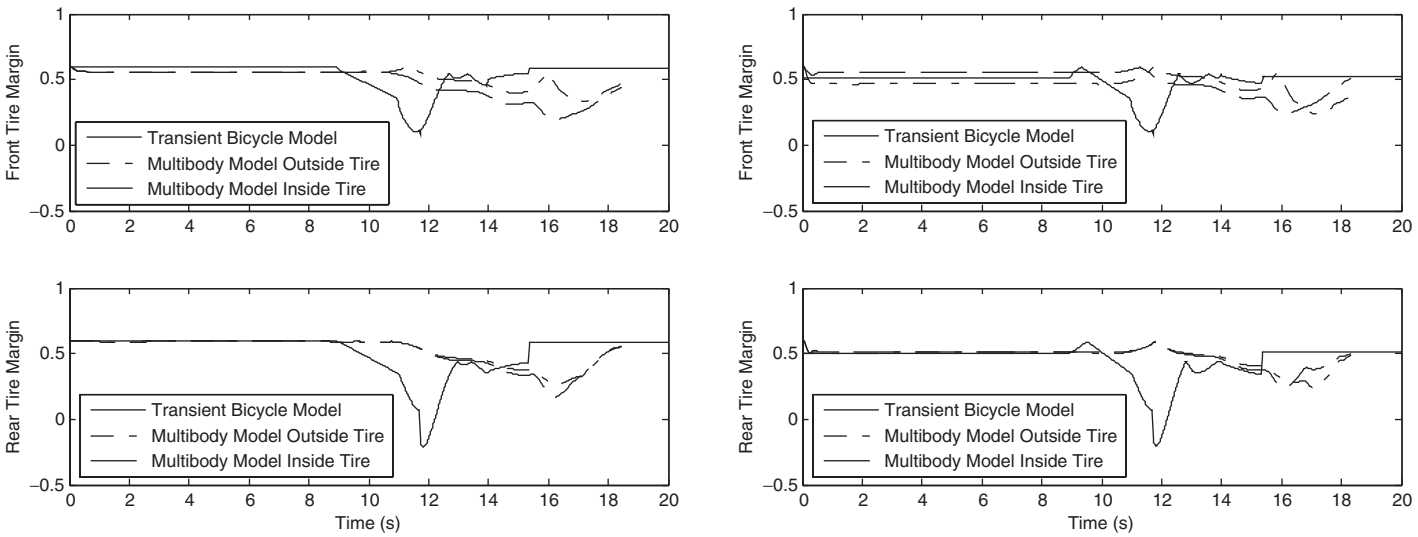

Figure 135. Lateral friction margin trajectories from transient bicycle and multibody models for full-size SUV [V = 25 mph, G = −9%, e = 0% (left plots) and 8% (right plots)] (a_x = −11.2 ft/s² and lane change).

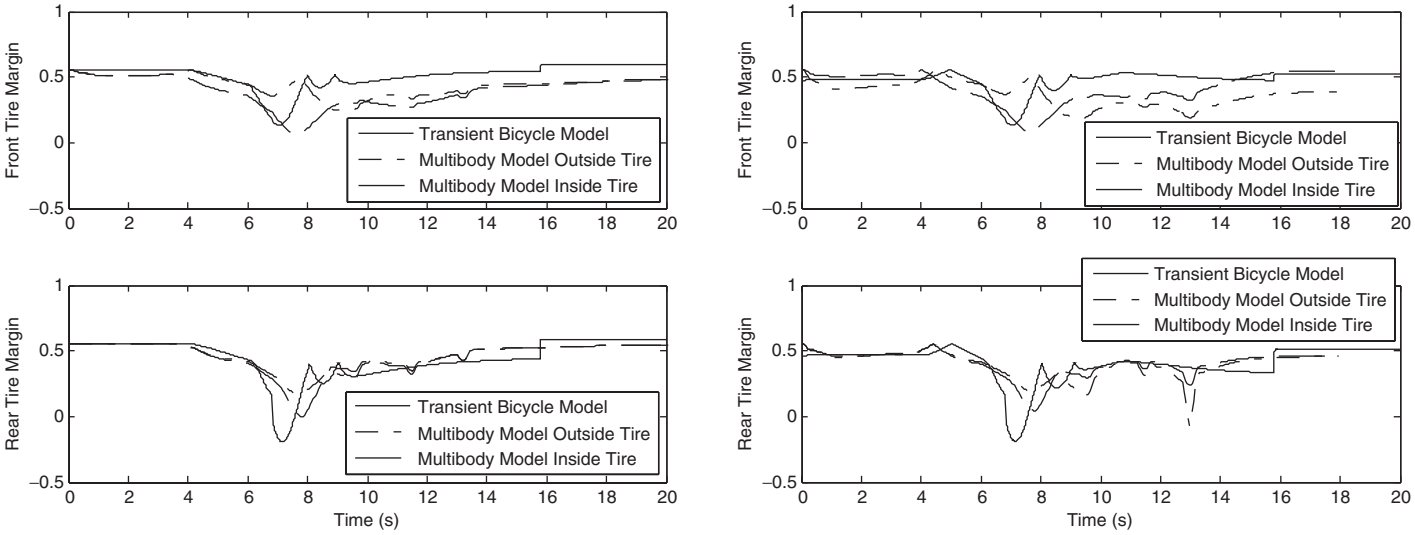

Figure 136. Lateral friction margin trajectories from transient bicycle and multibody models for full-size SUV [V = 55 mph, G = −9%, e = 0% (left plots) and 8% (right plots)] (a_x = −11.2 ft/s² and lane change).

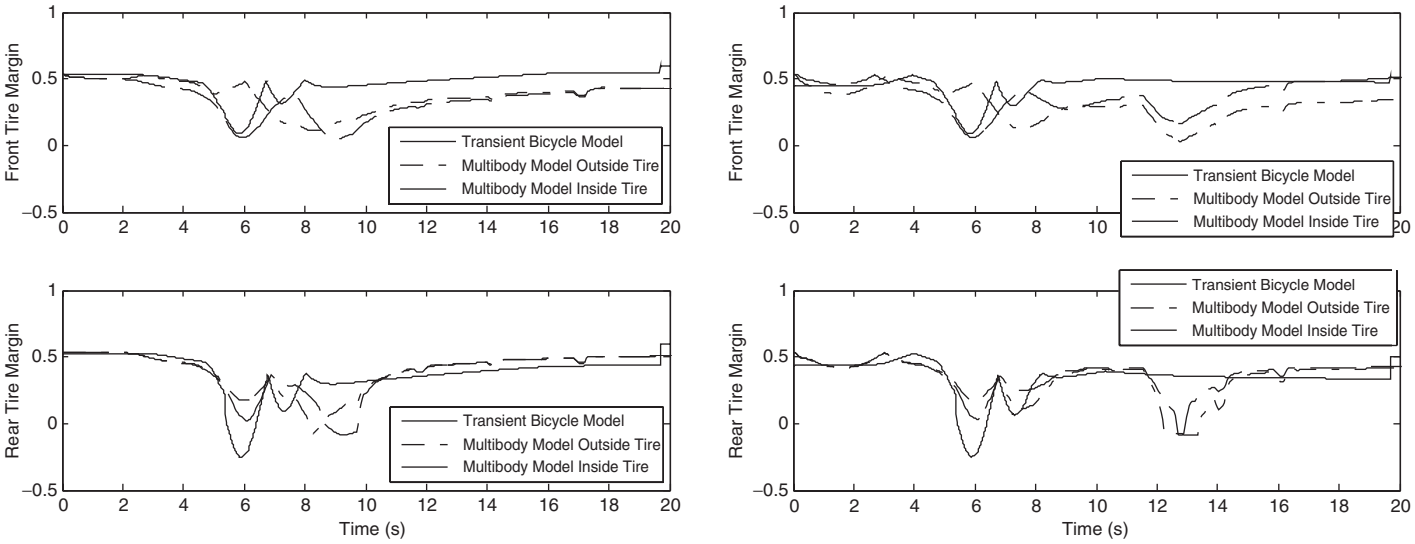

Figure 137. Lateral friction margin trajectories from transient bicycle and multibody models for full-size SUV [V = 85 mph, G = −9%, e = 0% (left plots) and 8% (right plots)] (a_x = −11.2 ft/s² and lane change).

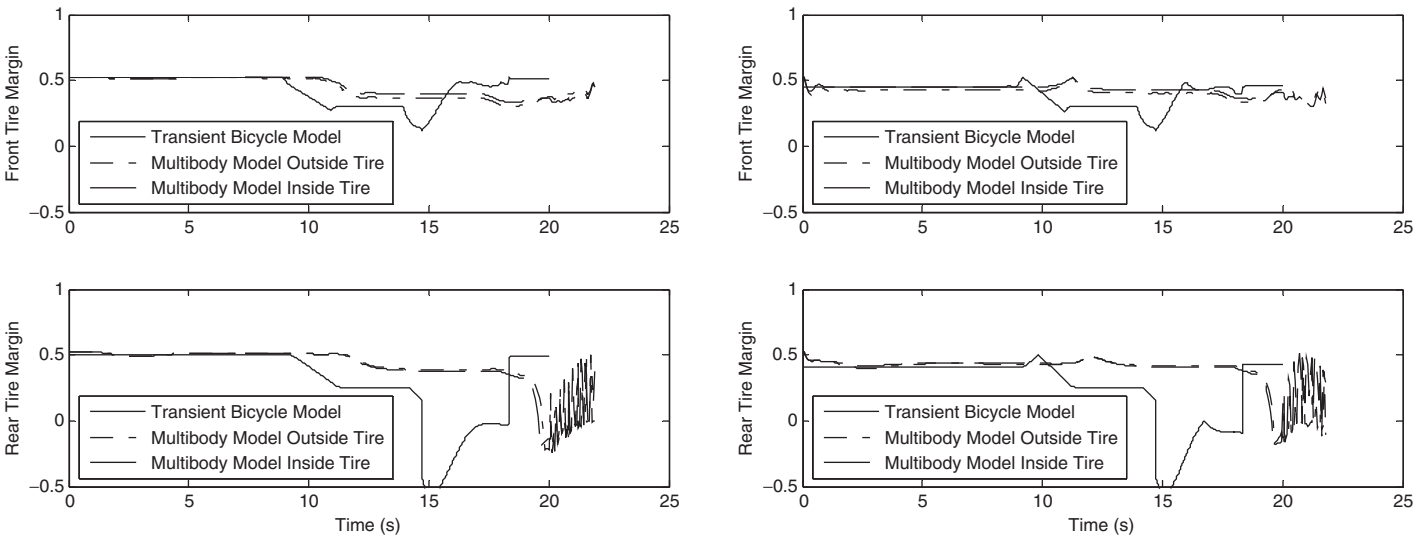

Figure 138. Lateral friction margin trajectories from transient bicycle and multibody models for single-unit truck [V = 25 mph, G = −9%, e = 0% (left plots) and 8% (right plots)] (a_x = −11.2 ft/s² and lane change).

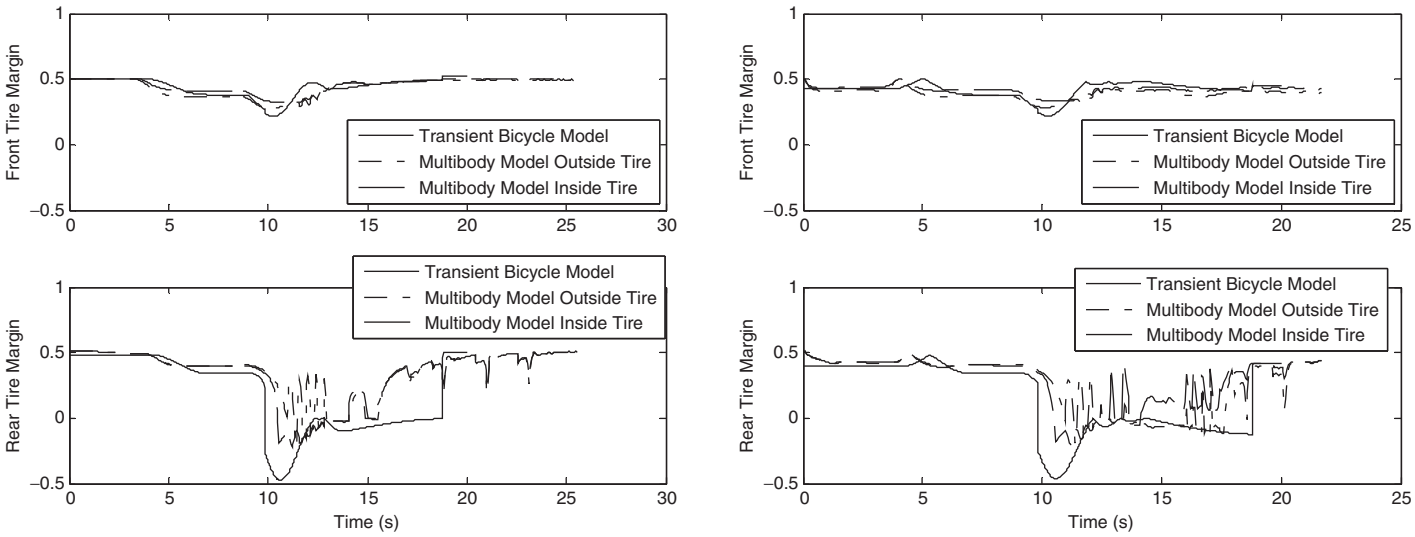

Figure 139. Lateral friction margin trajectories from transient bicycle and multibody models for single-unit truck [V = 55 mph, G = −9%, e = 0% (left plots) and 8% (right plots)] (a_x = −11.2 ft/s² and lane change).

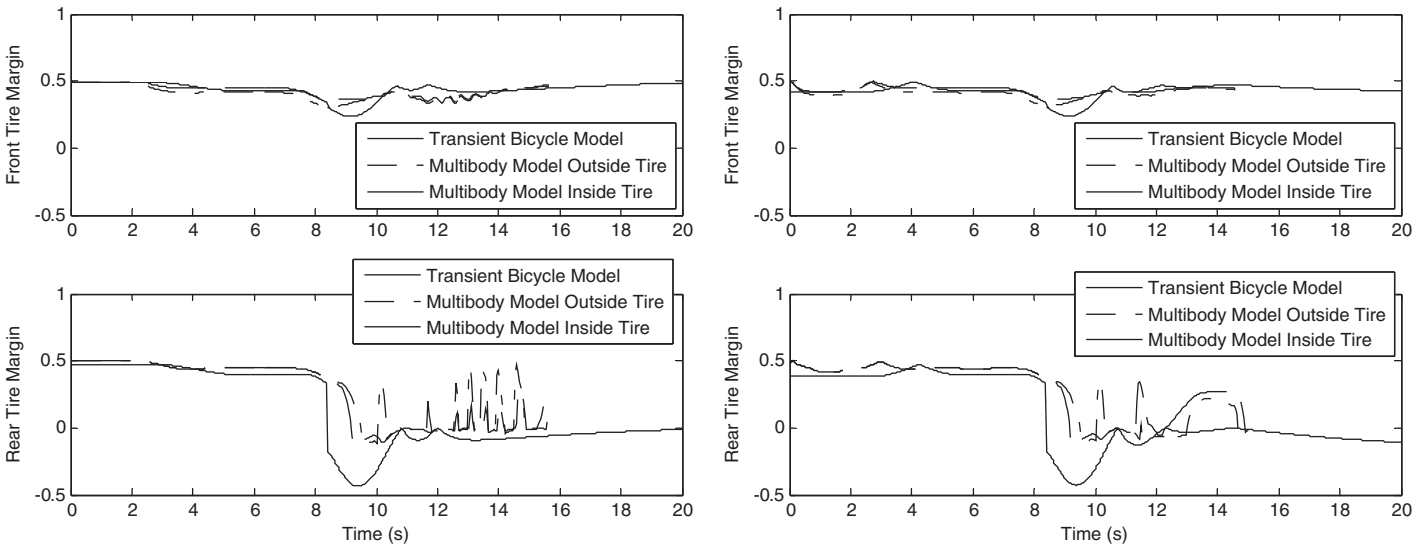

Figure 140. Lateral friction margin trajectories from transient bicycle and multibody models for single-unit truck [V = 85 mph, G = −9%, e = 0% (left plots) and 8% (right plots)] (a_x = −11.2 ft/s² and lane change).

to be nearly identical. The 0% superelevation cases of these figures represent the worst-case scenarios as identified in Section 4.9 for each vehicle. These situations had friction margins close to zero for most speeds with the transient model, and these low margins are confirmed in general by the multibody simulation results. One effect of larger superelevations appears to be that, where there are intervals of low margins in the maneuver, these intervals seem to last longer in the 8% superelevation case than in the 0% superelevation case. An example of this can be seen in Figure 133. In many of the cases, Figure 133 as an example, one can see the bias in lateral weight caused by the superelevated curve. This is caused by the multibody model's ability to account precisely for a vehicle's weight transfer and suspension dynamics during and after skidding occurs. The main message, however, remains that the effects of reasonable superelevation values on margins are small as long as appropriate guidelines for developing the superelevation in the tangent are followed.

Figures 132 to 143 also show that the multibody model matches the transient bicycle model fairly well for most of the traversal, with some caveats. First, the time traces between the transient model and the multibody model do not always align, but this is generally due to mismatched inputs between the two models, not necessarily due to model differences. Also, they exhibit the same sort of brake oscillations present in the preceding section on curve-keeping steering with stopping sight distance deceleration. This causes the simulations to sometimes over-predict or under-predict the lateral friction margins

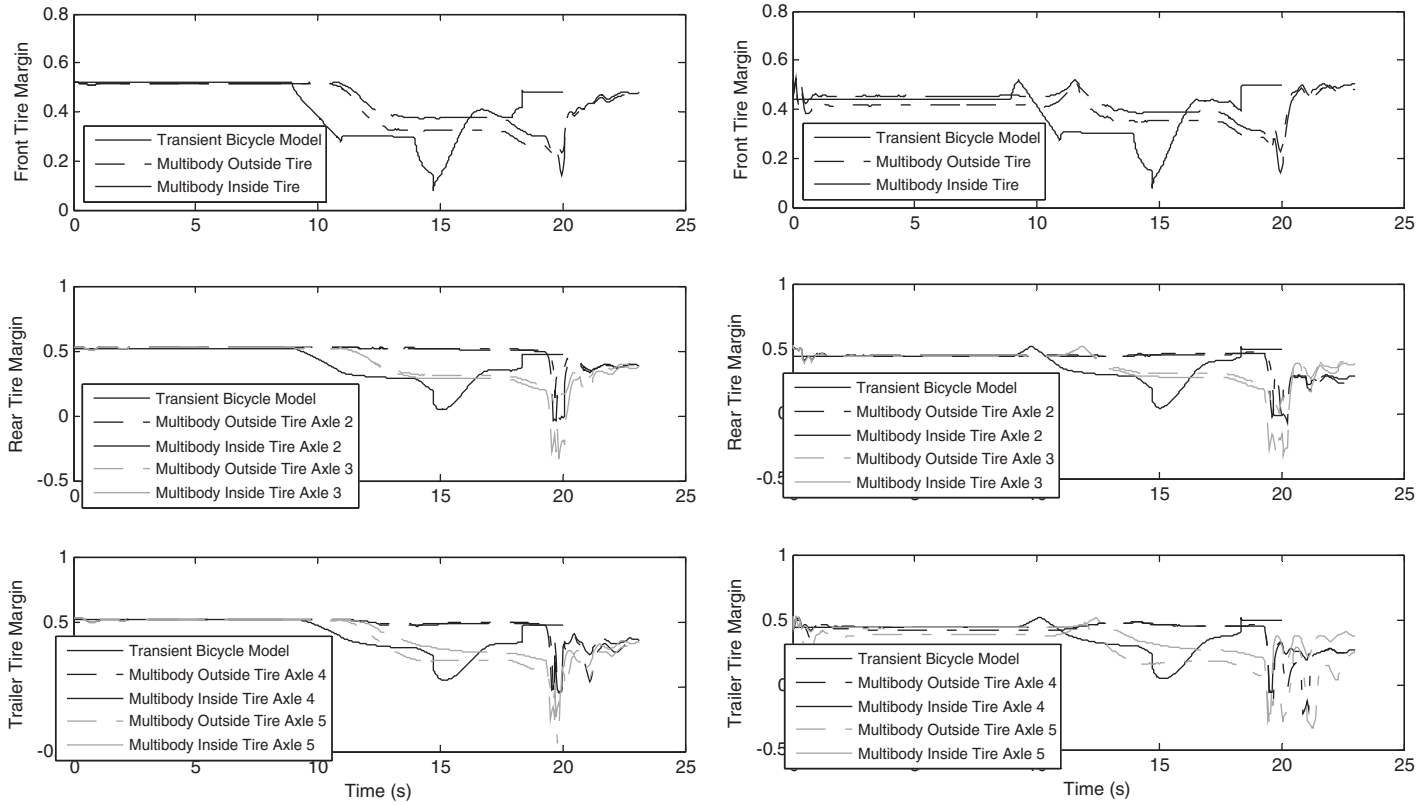

Figure 141. Lateral friction margin trajectories from transient bicycle and multibody models for tractor semi-trailer [V = 25 mph, G = −9%, e = 0% (left plots) and 8% (right plots)] (a_x = −11.2 ft/s² and lane change).

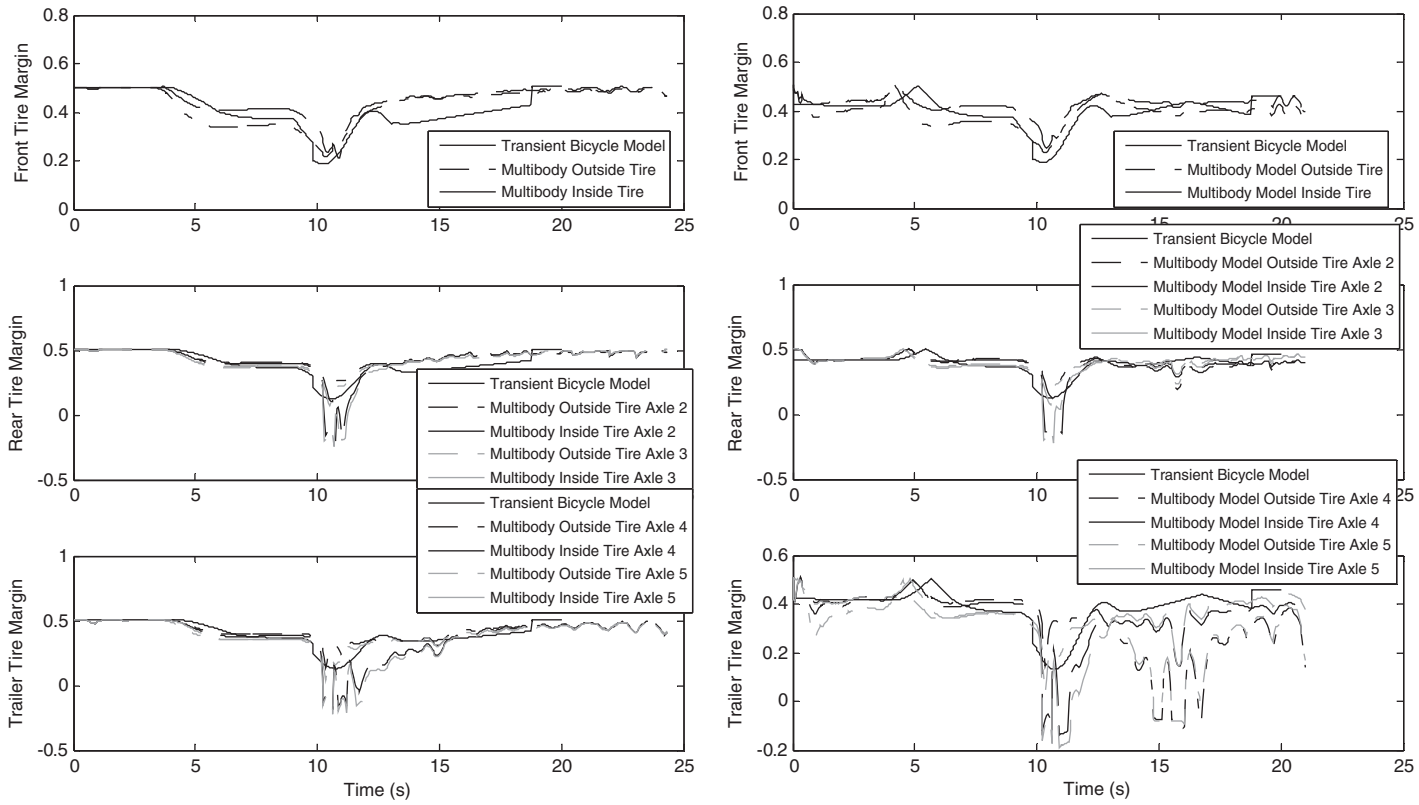

Figure 142. Lateral friction margin trajectories from transient bicycle and multibody models for tractor semi-trailer [V = 55 mph, G = −9%, e = 0% (left plots) and 8% (right plots)] (a_x = −11.2 ft/s² and lane change).

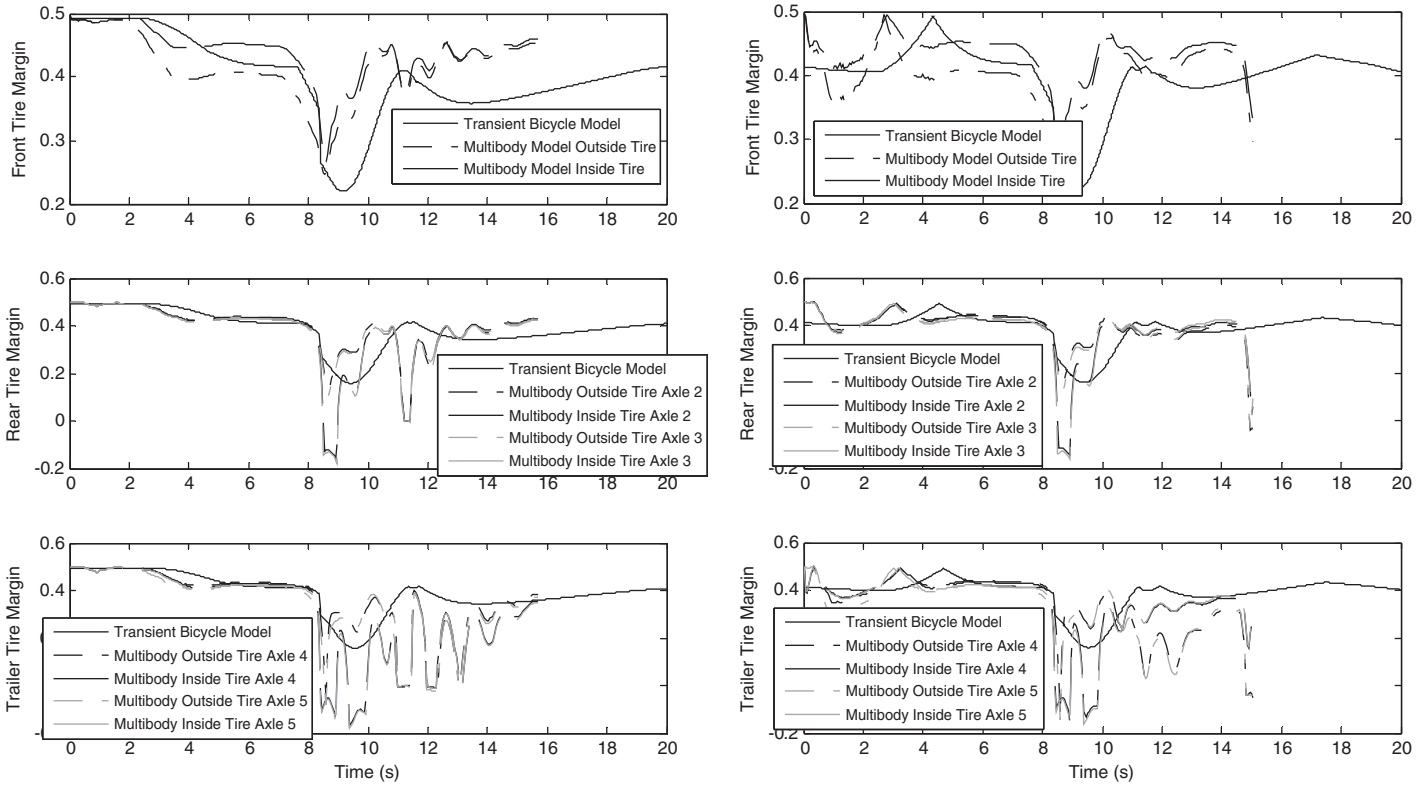

Figure 143. Lateral friction margin trajectories from transient bicycle and multibody models for tractor semi-trailer [V = 85 mph, G = −9%, e = 0% (left plots) and 8% (right plots)] (a_x = −11.2 ft/s² and lane change).

compared to the transient bicycle model, primarily because of the driver behavior used by the multibody simulation software.

Most significantly, the multibody model shows that the ABS may be activated for some of these maneuvers even when the simulations are conducted on high-friction roads. The effects of the input variations are illustrated in particular within Figures 138 to 143. The single-unit truck and the tractor semi-trailer models used by the multibody simulation software are both equipped with ABS, which activates during the traversals to help the vehicles avoid losing control. For these trucks, the ABS tends to activate in the multibody model in situations where the transient bicycle model predicted severely negative margins; so while ABS prevented the grossly negative margins, the multibody model does confirm that these situations would likely have had very negative margins if ABS were not available.

In summary even though the simulations using the transient bicycle model are capable of showing very negative lateral friction margins, and even though the road surface used in the multibody model was simulated with a high coefficient of friction to ensure that the demand predicted would be sufficient for all cases simulated, the ABS still activates during the stopping sight distance deceleration traversal with lane change for the two trucks considered. This prevented the lateral friction margins from going too far below zero and assisted the vehicle in staying under control. However, it also indicates quite clearly that lane changes combined with stopping sight distance decelerations will cause ABS activation even on high-friction roads.

4.10.2.6 Effect of Lane-Change Maneuver at Emergency Braking Deceleration

Given the variability of the multibody simulation results caused by the driver model, and given that nearly all scenarios predict negative margins, only a few scenarios are evaluated using emergency braking deceleration rates. In particular, Section 4.9 predicted that the E-class SUV, full-size SUV, and single-unit truck would skid considerable distances when a combined lane-change/emergency braking deceleration maneuver occurred. In previous sections, the lateral deviation distance was predicted assuming, among other things, that the driver made no corrective steering inputs and that ABS is not present—this situation is similar to a worst-case vehicle situation. However, in the multibody model, the vehicles are simulated with ABS, and there is a driver model present that steers the vehicle toward the desired path even in the presence of deviations. This is analogous to a best-case scenario. Thus, comparison of the multibody results with the results of Section 4.9 illustrates the range of tracking behavior that might occur in the presence of negative lateral friction margins.

Figure 144 shows the path tracking performance of four vehicles under emergency braking deceleration with a lane

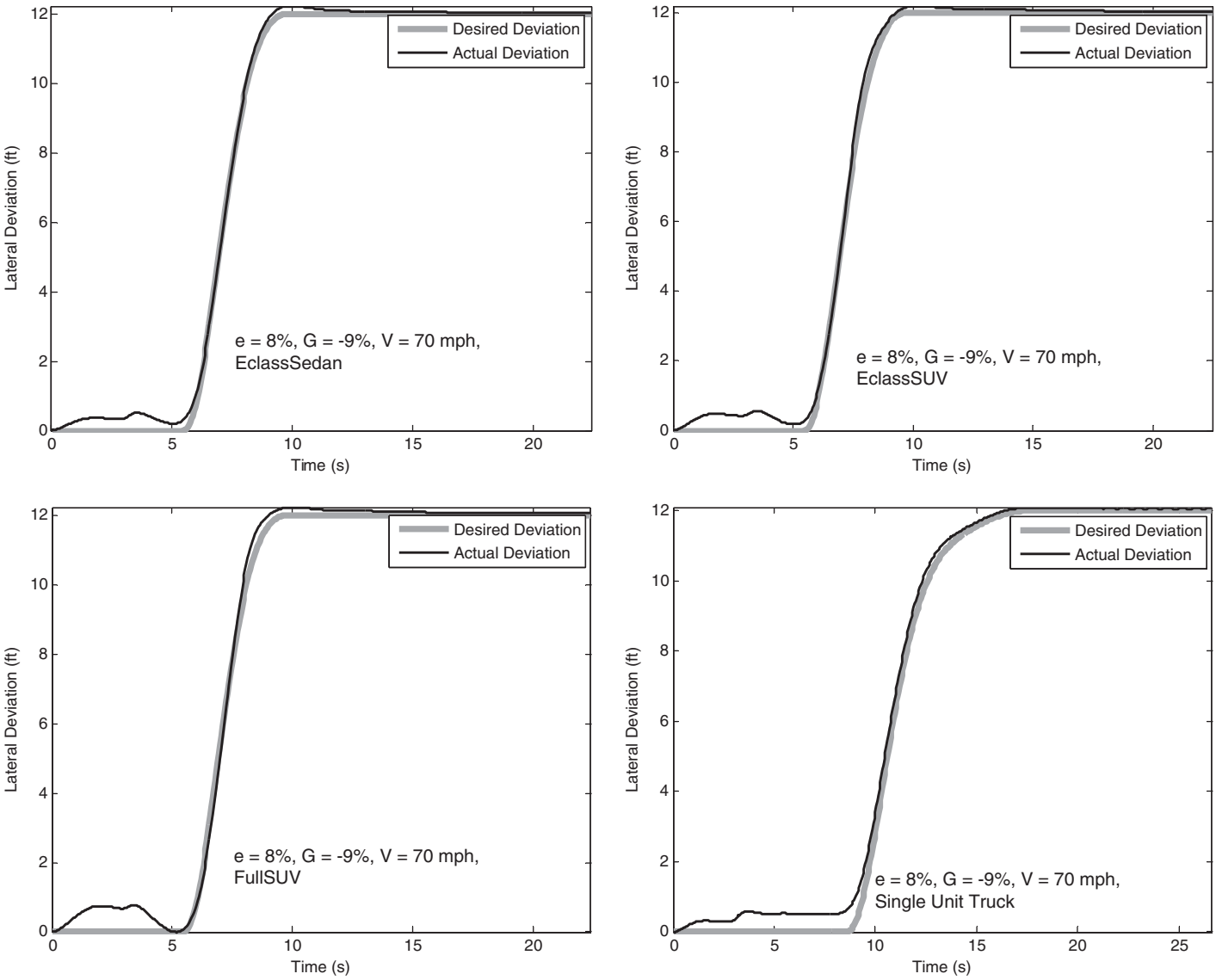

Figure 144. Lateral deviation distance from multibody models for E-class sedan, E-class SUV, full-size SUV, and single-unit truck (V = 70 mph, G = −9%, e = 8%) (a_x = −15 ft/s² and lane change).

change at 70 mph, predicted for the multibody simulation in situations where there are negative lateral friction margins. Note that the ABS was activating during the simulation, even for high-friction roads, which again indicates that the friction margins are extremely low. All four vehicles were able to maintain control through the curve through the use of ABS and the multibody software's driver model.

Figure 145 shows the time trajectories of the lateral friction margin for the same vehicles for the same traversal as shown in Figure 144. The margin trajectories between the transient bicycle model and the multibody model match in shape, although in the case of the full-size SUV and the single-unit truck—the two worst vehicles for lateral deviation distance during this type of traversal (see Section 4.9)—the effects of ABS are evident in the oscillations of tire force when the margins approach zero. The fast, pulsing action of the ABS on the simulated vehicles allows the multibody software's driver model to continue to navigate the prescribed maneuver without any significant skidding and subsequent lateral deviation. The fact that none of these vehicles departed significantly from the intended trajectory while traversing the curve suggests that the lane change on the curve is not so severe that an ABS-equipped vehicle will lose control.

Recall that the roads used in the multibody simulation possessed high coefficients of friction (corresponding to friction supply) so as not to distort the computation of friction demand as defined in Section 4.2. This was done to make the lateral friction margins comparable for as many driving scenarios as possible between Section 4.8 and this current analysis. But even high-friction roads did not stop the ABS from activating due to excessive wheel slip for large braking values

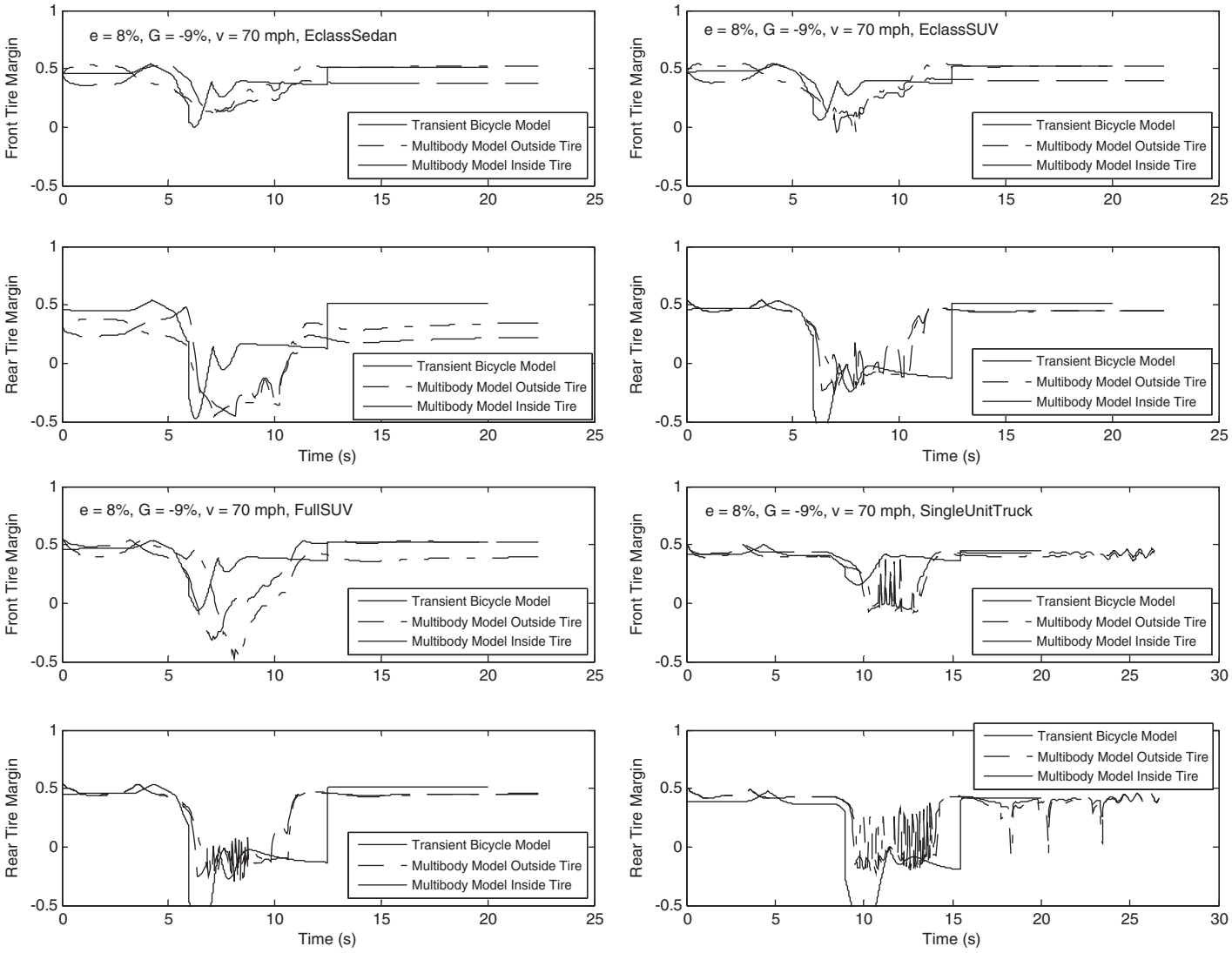

Figure 145. Lateral friction margin trajectories from transient bicycle and multibody models for E-class sedan, E-class SUV, full-size SUV, and single-unit truck (V = 70 mph, G = −9%, e = 8%) (a_x = −15 ft/s² and lane change).

or for the most aggressive maneuvers. Additionally, using a high-friction road to generate friction demand values could inadvertently allow the vehicles in the multibody simulation to maintain path tracking artificially well.

To analyze whether the high-friction simulations are artificially improving skid performance, another series of simulations was performed. This set of simulations used conditions identical to those run in Figures 144 and 145, but the road surface was given a low coefficient of friction of 0.50 for trucks and 0.55 for passenger vehicles, which represent the actual two-sigma low friction supply values in the lateral (cornering) direction for 70 mph as calculated in Section 4.2.

The results of the low-friction simulations, shown in Figure 146, are nearly identical to the high-friction road simulations shown in Figure 144. This suggests that even with low friction in the multibody model, the simulated driver is able to maintain control of the vehicle during the lane change. This result is clearly not a sweeping generalization about all human drivers and all low-friction environments. Drivers often panic when tires lose traction, even with ABS and/or stability control assisting them, and often do not make the correct control decisions necessary to keep a vehicle on a desired trajectory at the onset of a skid. However, the fact that the simulated driver is able to maintain lane following and a lane-change maneuver while the ABS system activates on a low-friction road suggests that the lane changes are physically possible on curves, even under emergency braking circumstances.

In the simulations presented so far, friction demand is subtracted from friction supply to obtain lateral friction margin; thus, in cases of negative margin, it is possible that the vehicle is not actually decelerating at the assumed rate. In the multibody simulation, this can cause the vehicle to achieve a

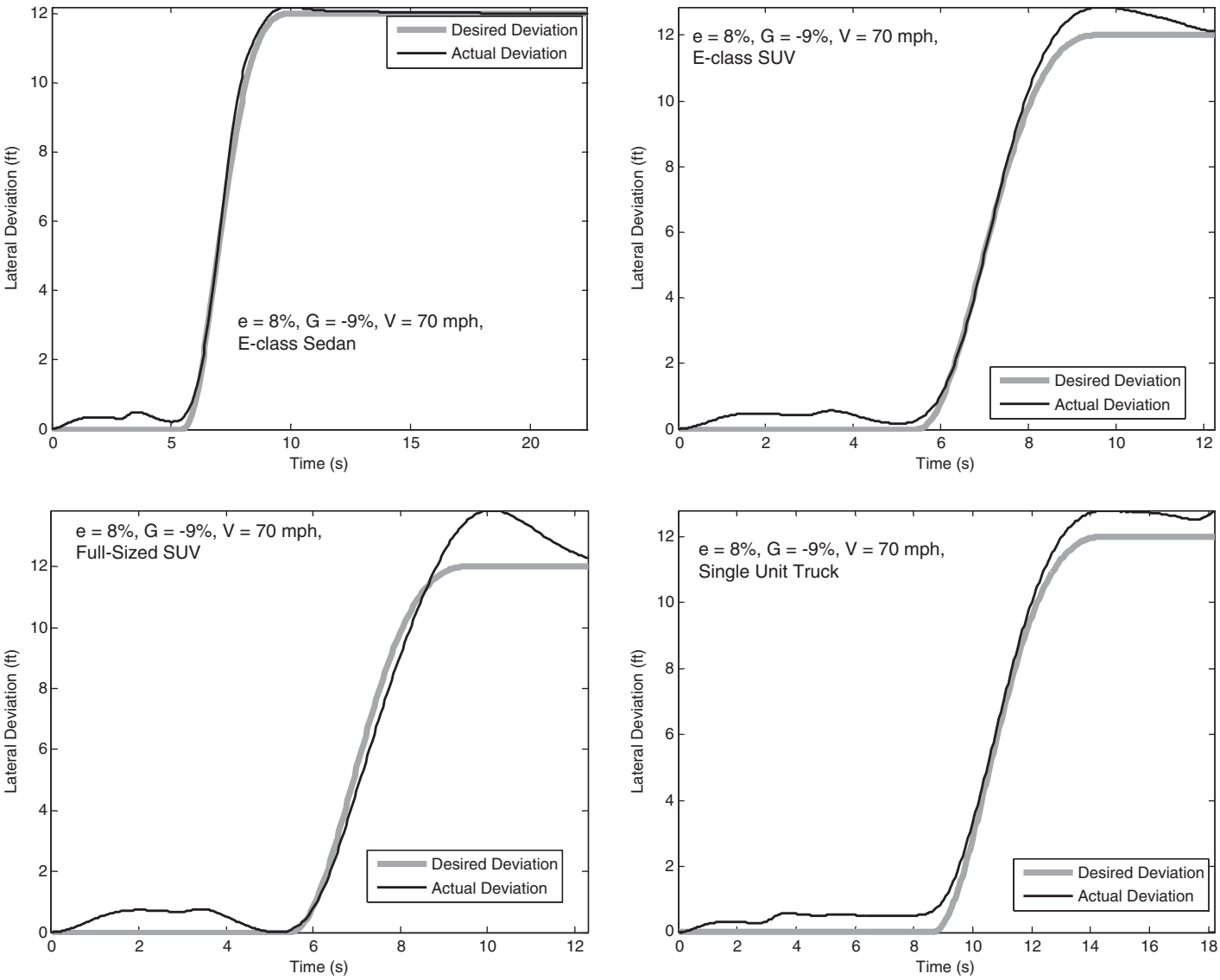

Figure 146. Lateral deviation distance for low-friction simulation from multibody models for E-class sedan, E-class SUV, full-size SUV, and single-unit truck (V = 70 mph, G = −9%, e = 8%) (a_x = −15 ft/s² and lane change).

lane change and/or lane follow, but not actually decelerate at the intended amount. Further investigations confirmed that the deceleration rates (as measured at the vehicle's sprung-mass center of gravity) for all vehicles were comparable to the desired deceleration rate of −15 ft/s².

4.10.3 Discussion

This section addresses a couple of key issues associated with the use of complex vehicle dynamics models for estimating lateral friction margins. The first issue deals with the accuracy of the vehicle simulations themselves. For two-axle vehicles, the transient bicycle model is a fairly good predictor of vehicle behavior with a worst-case driver, e.g., one who does not attempt to correct for any lane-keeping errors. In circumstances where the ABS inputs and driver corrections are both negligible, the results show that the transient bicycle model for two-axle vehicles produces margins that match quite well with the multibody models. For multiaxle vehicles, it was shown that if adjacent tractor or semi-trailer axles are averaged, then the multibody model largely agrees with the transient bicycle model. However, it was found that this averaging may hide some axle-specific variation in lateral friction margin that could result in low or even negative friction margins.

The second insight is that, as maneuvers become more aggressive, the agreement between different models becomes less exact, and more dependent on the driver model and on the presence or absence of ABS. Thus the outputs become harder to compare. It is expected that the multibody simulations' simulated driver behavior is more representative of

what a human driver will do during a traversal of a curve, but it is also acknowledged that these inputs may no longer be the worst case because a worst-case driver response cannot be defined. When the deceleration values exceed curve-entry deceleration values, oscillations in the braking input caused by the simulation trying to maintain the desired deceleration become significant and can lead to negative margin predictions. On the other hand, the ABS activates in the multibody software to prevent margins from becoming too negative and allows the vehicle simulated by the multibody software to maintain the desired path, when driven by the software's optimal preview steering controller (i.e., driver model).

4.10.4 Summary of Key Results from Step 9

In summary, the following findings were obtained from the analysis in Step 9:

1. The multibody model confirms the results of the transient bicycle models for two-axle vehicles for all but the most aggressive maneuvers, which makes them suitable for roadway design.
2. The transient bicycle models for tractor semi-trailers tend to predict vehicle behavior well for moderate maneuvers but should not be used to predict lateral friction margins for combined cornering, lane-change, and braking maneuvers. Disagreement between the transient bicycle model and the multibody model was found for these cases. The most disagreement was a function of either averaging of axle forces, the presence of ABS, or the specific responses of the simulated driver's braking inputs.
3. Lateral friction margins for the STAA Double are, for the cases that have been studied, slightly higher than those for the tractor semi-trailer.
4. The simulated driver's braking and steering control used by the multibody simulation software, which attempts to approximate human behavior, can cause any of the vehicles considered to temporarily skid. This was seen during a curve-keeping event with or without a lane change when decelerating at stopping sight distance levels on grades.
5. The single-unit truck and the full-size SUV both have positive lateral friction margins during combined curve-entry deceleration and lane changes. But both have negative lateral friction margins during stopping sight distance and emergency deceleration with or without lane-change events for all speeds.
6. Due to the driver model within CarSim and TruckSim, as well as the use of ABS in the multibody simulations, all vehicles were able to maintain the desired trajectory around the curve and through a lane change for all braking scenarios considered. This is in contrast to the results of Section 4.9, which did not consider ABS or driver corrections.
7. The path tracking performance of the simulated vehicle in the multibody model was not degraded when a low-friction road was simulated.

4.11 Step 10: Predict Wheel Lift of Individual Wheels during Transient Maneuvers

The objective of Step 10 was to use high-order multibody models to predict wheel lift of individual wheels. Using commercially available vehicle dynamic simulation software (i.e., CarSim and TruckSim), high-order multibody models were used to predict wheel lift of individual wheels as a vehicle traverses a sharp horizontal curve, taking into consideration a range of conditions such as the horizontal curvature, grade, and superelevation. Rather than simulating the full range of hypothetical geometries and vehicles considered throughout this research, this analysis focused on those situations identified in previous steps as areas of concern. Note, unlike the analyses in Sections 4.9 and earlier, in the multibody models the superelevation transition is simulated (i.e., designed) according to the *Green Book* policy.

4.11.1 Analysis Approach

To extend the results of Section 4.6, a more sophisticated method of identifying rollover margins was considered in this step using multibody models. The analysis considers the cases where the vehicle traverses a curve without a lane change, with a lane change, and with deceleration. The analysis focuses on vehicles identified in Section 4.6 as having low rollover thresholds as defined by Equation 27. This consists especially of the single-unit truck and the tractor semi-trailer truck. Note that tractor semi-trailer/full-trailer trucks are assumed to have the same rollover thresholds as tractor semi-trailer trucks. This assumption is made because in the static case, both vehicles are limited by the rollover threshold of their trailers. The CG height and track width of the trailers for both vehicles are assumed to be quite similar. Thus, the tractor semi-trailer results are assumed to represent the tractor semi-trailer/full-trailer as well. This assumption of similarity between the rollover margins for the tractor semi-trailer and the tractor semi-trailer/full-trailer is confirmed in the analysis that follows.

In Section 4.6 the rollover threshold, and hence the rollover margin, was defined according to the static configuration of the vehicle, and thus may not be appropriate to predict dynamic wheel-lift events. Thus, a new definition of proximity to wheel lift is needed. In this analysis, the load transfer ratio (LTR), a metric commonly used in the vehicle dynamics community to predict wheel lift and examine the

relative severity of a maneuver with respect to wheel lift, is utilized. The metric is defined for each axle as:

$$LTR = \frac{N_i - N_o}{N_i + N_o} \tag{89}$$

Where N_i and N_o are the normal (vertical) loads on an axle's inside and outside tires while cornering, respectively. Because the normal loads on a tire cannot be less than zero, this metric can only vary from −1 to +1. As defined, the LTR for an axle is −1 when the outside tire bears all of the axle's load (i.e., the inside wheel lifts) and +1 when the inside tire bears all of the axle's load. For a symmetrically loaded vehicle on a tangent roadway with 0% superelevation, the LTR for any axle would be 0.

As a vehicle traverses a horizontal curve, the LTR will tend toward −1 immediately prior to wheel lift. From a qualitative perspective, the LTR can be thought of as the portion of the total axle load carried by the outside tire. This constitutes a sort of "roll demand" that, when subtracted from unity, gives a per-axle dynamic rollover margin defined by the proximity of the LTR to a value that causes wheel lift, e.g.,

$$RM_{LTR} = 1 - \left| \frac{N_i - N_o}{N_i + N_o} \right| \tag{90}$$

This "dynamic" rollover margin, in contrast to the "static" rollover margin of Section 4.6 defined in Equation 27, represents the proximity of the axle to wheel lift.

4.11.2 Analysis Results

In Figure 147, the rollover margins are plotted for a single-unit truck and a tractor semi-trailer traversing a curve without making a lane change and keeping a constant speed, for a curve with a grade of −6% and 4% superelevation. These plots show the differences between the rollover margins of individual axles for speeds from 25 to 85 mph. Because the current AASHTO policy provides for higher levels of lateral acceleration at low design speeds, there is more weight shift at lower speeds than with higher speeds. This weight shift causes lower rollover margins for this steady traversal at lower speeds. The rollover margins increase with increasing design speed. For these test cases, the minimum rollover margins are approximately 0.4 to 0.48 for a speed of 25 mph.

To test the boundaries of the rollover margin envelope in the scope of the maneuvers considered in this research, the more aggressive maneuvers are of greatest interest. Figure 148 shows the rollover margins for a single-unit truck and a tractor semi-trailer considering curve-entry deceleration combined with a lane change for a −9% grade and superelevations of 0% and 8%. The plots indicate that both vehicles have a large amount of load remaining on the inside tire. In Figure 148, the −9% grade with 0% superelevation represents the worst case identified in Section 4.8 for lateral friction margins for both of these vehicles. It was assumed that this worst-case friction situation will likely generate the worst-case rollover margin, since in general lateral friction margins and rollover margins are both worst when lateral accelerations on a vehicle are highest.

In Figure 148 the worst-case margins occur at low speed for the tractor semi-trailer. The 8% superelevation case was simulated for the tractor semi-trailer/full-trailer at 25 mph to compare to the tractor semi-trailer. The results are shown in Figure 149, and the minimum rollover margins are nearly identical to the tractor-trailer (0.32 versus 0.36).

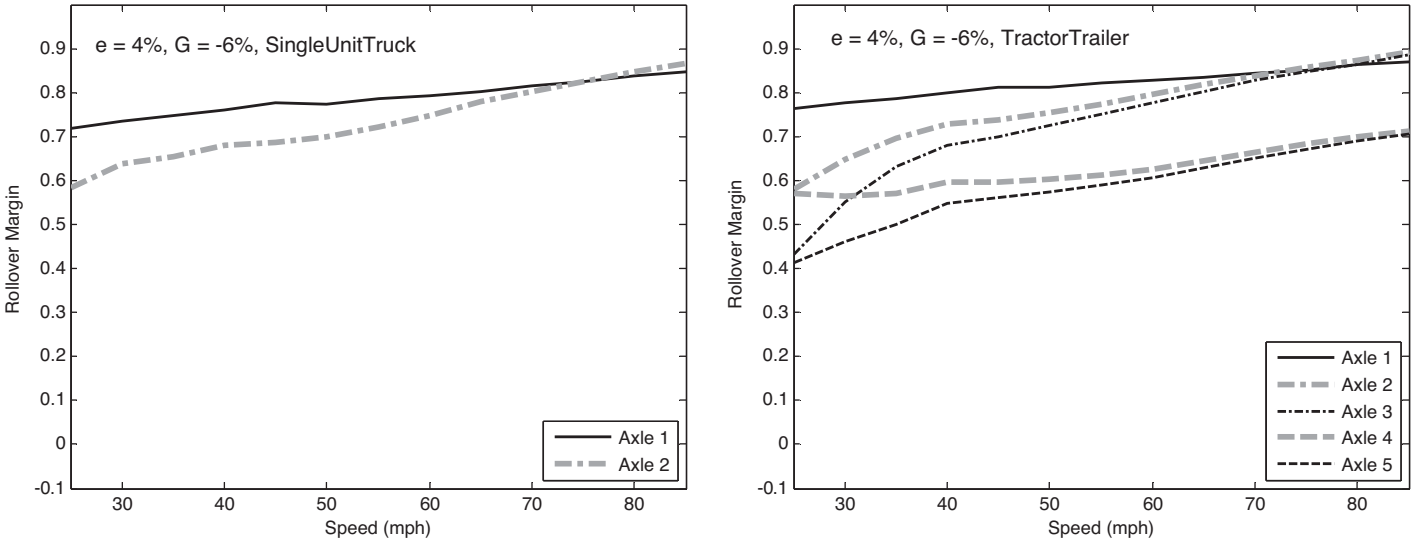

Figure 147. Rollover margins for individual axles of single-unit truck and tractor semi-trailer (G = −6%, e = 4%) (a_x = 0 ft/s²).

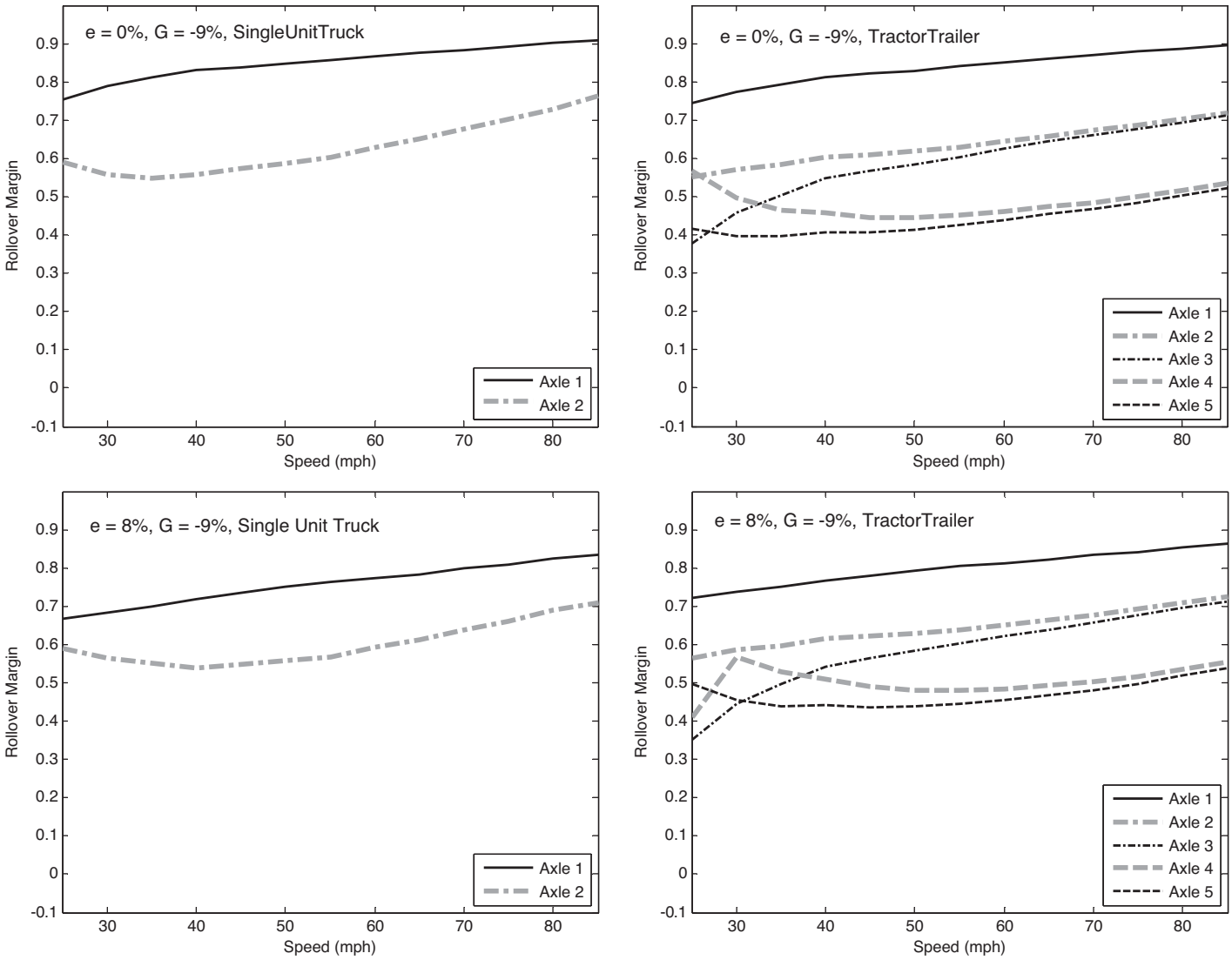

Figure 148. Rollover margins of individual axles for single-unit truck and tractor semi-trailer (G = −9%, e = 0% and 8%) (a_x = −3 ft/s² and lane change).

Considering an even more severe scenario, Figure 150 shows the rollover margins for a single-unit truck and a tractor semi-trailer considering stopping sight distance deceleration combined with a lane change for a −9% grade and superelevations of 0% and 8%. The results indicate that rollover margins for both vehicles are at least 0.4 or greater for this maneuver and roadway design. As it happens, the rollover margins in this case are actually higher than they are for the mild deceleration case, primarily due to the effect of the friction ellipse. At the higher deceleration level, more of the tire force is partitioned to braking and thus less is available for lateral acceleration. The previous sections showed that this situation begins to produce very low lateral friction margins, and thus the rollover margins are actually higher than expected.

When emergency braking deceleration is considered, the results of the rollover margin analysis for the single-unit truck are quite different than previous results. These rollover margins are shown in Figure 151. While the tractor semi-trailer still does not come close to lifting a wheel, the same is not true for the single-unit truck. The single-unit truck appears to lift a wheel from 50 to 65 mph under emergency braking deceleration with a lane change.

To understand the wheel-lift situations for the single-unit truck, the specific rollover margin trajectories are plotted for all wheel-lift speeds (i.e., 50 to 65 mph) in Figure 152. It is clear that the rollover margins are generally very positive through almost the entire trajectory, and only spike down to zero for an instant. This spike is most likely due to resonance in the suspension and/or braking systems associated with actions of the ABS controller on the simulated vehicle. The rollover margins near zero represent only a very momentary "wheel lift" on the inside tire, and do not present a condition where the

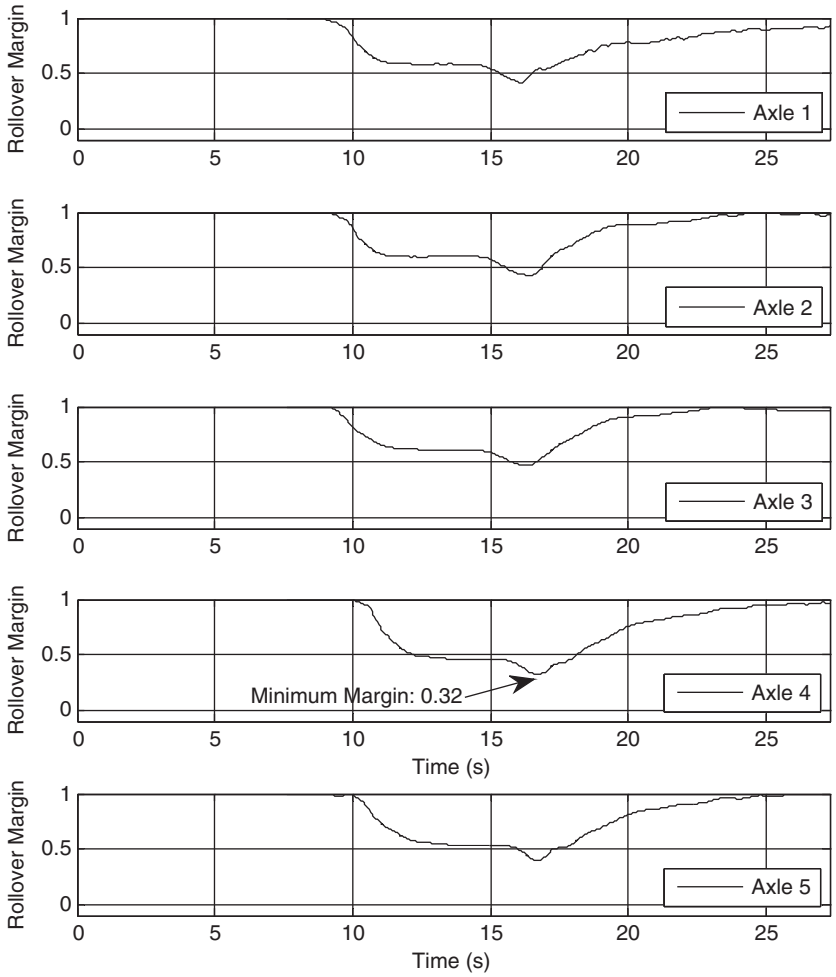

Figure 149. Rollover margins of individual axles for tractor semi-trailer/full-trailer truck (Double) (G = −9%, e = 8%) (a_x = −3 ft/s² and lane change).

vehicle will likely rollover. This is evidenced by the fact that the multibody simulation itself did not predict a rollover event, which the software is fully capable of simulating. Thus, even the vehicle with the highest center of gravity did not run the risk of rolling over during any of the worst-case maneuvers considered in this research. This confirms the assertion of Section 4.6 that skidding is a much more pressing issue for normal maneuvers on highways than is rollover.

Finally, the above situations were simulated for the E-class sedan, E-class SUV, and full-size SUV. The lowest margins observed were for the SUVs, and particularly the E-class SUV, but no margins were low enough to elicit any concern. The lowest rollover margin detected was 0.63. This occurred at 70 mph for an E-class SUV conducting an emergency braking maneuver with a lane change. Clearly, wheel lift is not a concern for passenger vehicles conducting the various maneuvers considered in this research.

4.11.3 Summary of Key Results from Step 10

In summary, the following findings were obtained from the analysis in Step 10:

1. For the vehicles considered in this research, rollover is not a direct concern for a vehicle traversing a sharp horizontal curve on a steep downgrade, not even when a vehicle performs a lane change, with or without braking while traversing the curve.
2. The single-unit truck exhibits momentary wheel lift at speeds of 50 to 65 mph for the case of emergency braking deceleration combined with a lane change on a steep grade of −9% and a superelevation of 0%. This momentary inside wheel lift is an artifact of the ABS's actuation and suspension behavior but does not represent a condition where the vehicle will likely roll-

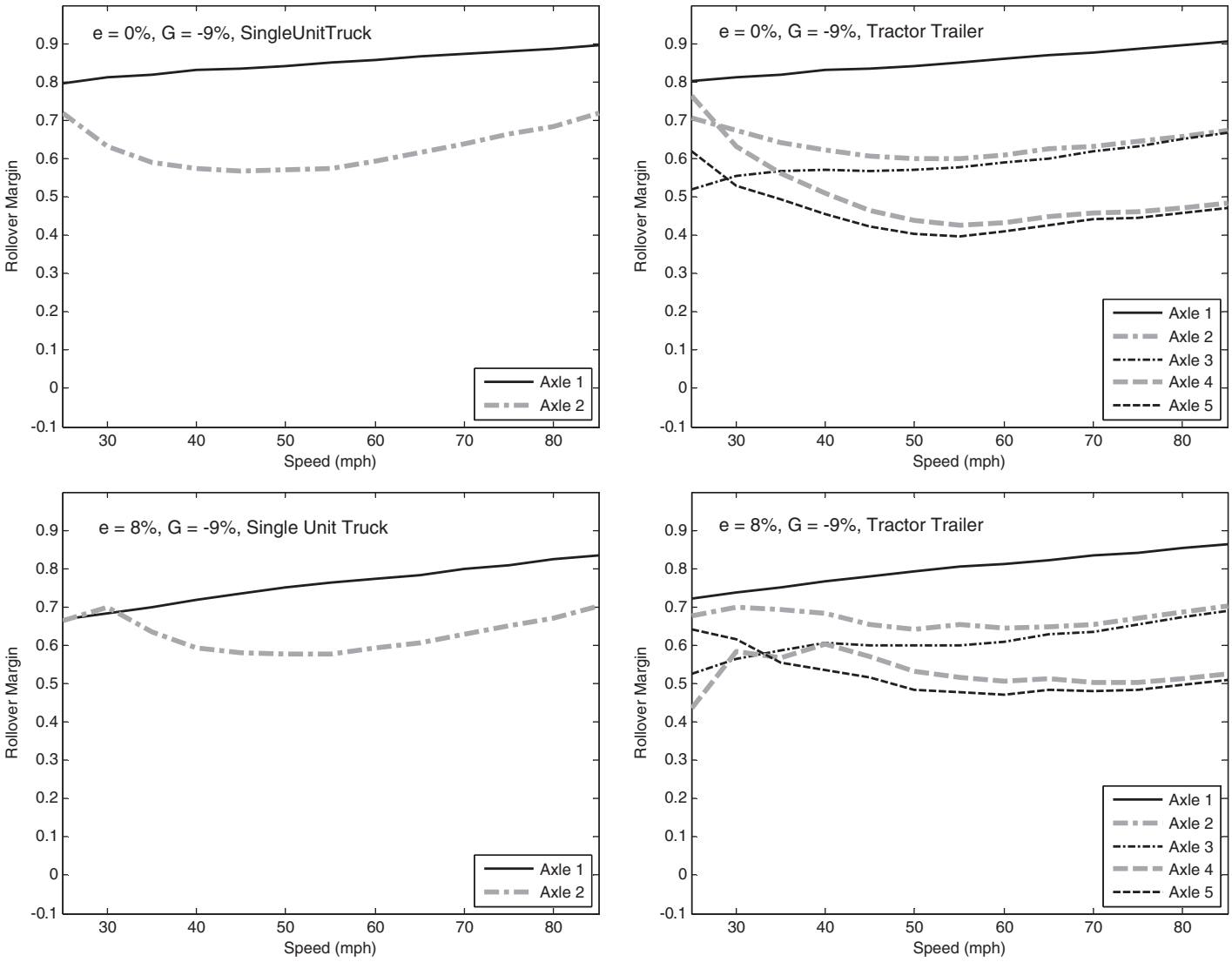

Figure 150. Rollover margins of individual axles for single-unit truck and tractor semi-trailer (G = −9%, e = 0% and 8%) (a_x = −11.2 ft/s² and lane change).

over for this worst-case roadway design and maneuver combination.

3. Assuming the CG height and track width of the trailers for both vehicles are the same, tractor semi-trailer/full-trailer trucks have very similar rollover margins compared to tractor semi-trailer trucks. This was evident based upon the static rollover margins estimated in Step 5 (see Section 4.6), and analyses using the "dynamic" rollover margin based upon the LTR confirmed the rollover similarities between both vehicles.
4. For tractor semi-trailer or tractor semi-trailer/full-trailer trucks with unusual loading, or those loaded to capacity, rollover may be more of a concern, especially for very aggressive avoidance maneuvers. But for the loading situations simulated here—considered quite typical for these vehicles—there appears to be adequate wheel-lift margins.

4.12 Step 11: Analysis of Upgrades

The objective of Step 11 was to analyze the effects of upgrades on lateral friction and rollover margins. Using the transient bicycle and multibody models, this analysis estimated lateral friction margins for passenger vehicles traversing horizontal curves on upgrades, assuming that passenger vehicles maintain their desired speed on the upgrade and curve. For tractor semi-trailers, the analysis accounted for reduced speeds on upgrades (i.e., crawl speeds) and for traversing upgrades at the design speed. Vehicle rollover issues were also considered.

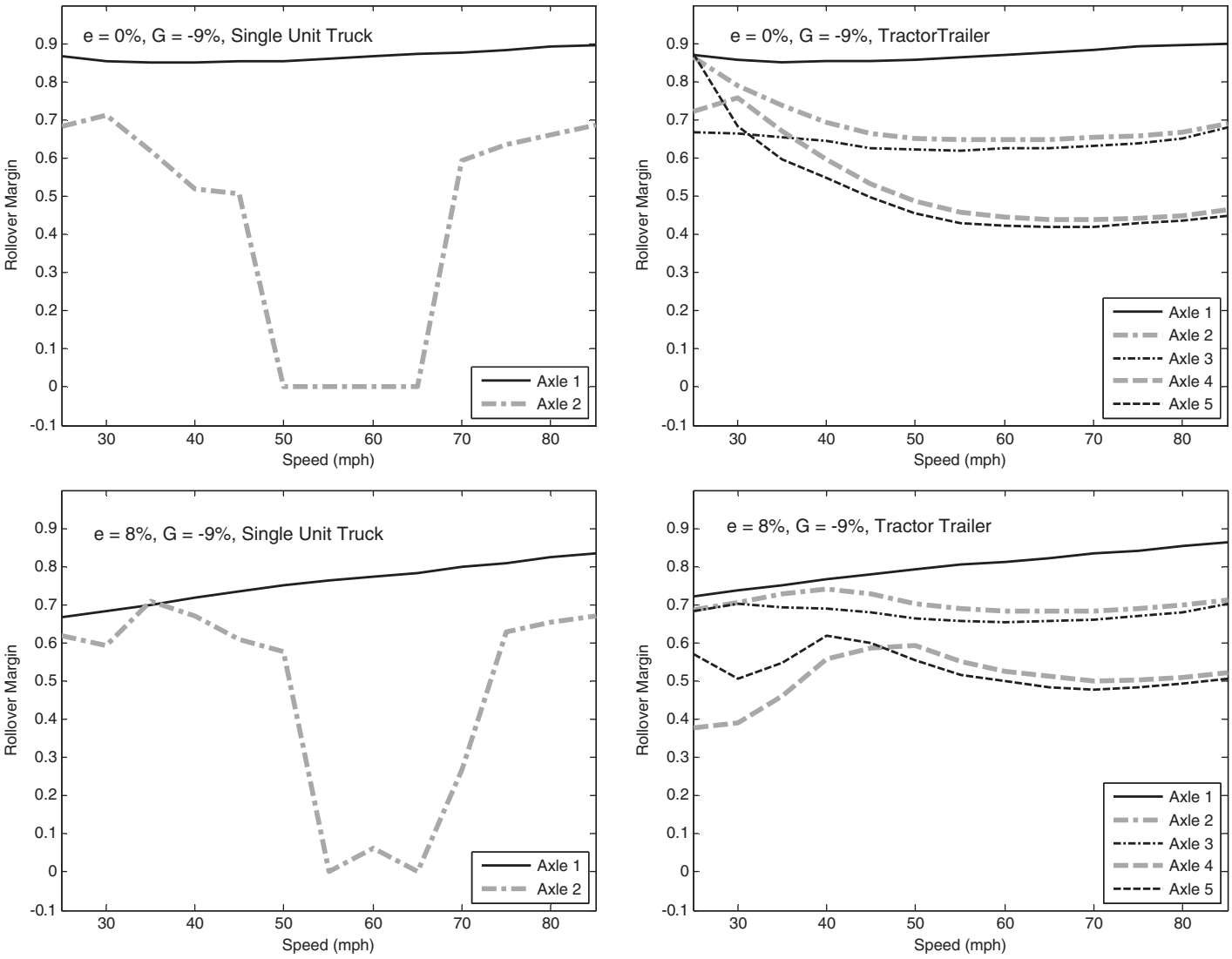

Figure 151. Rollover margins of individual axles for single-unit truck and tractor semi-trailer (G = −9%, e = 0% and 8%) (a_x = −15 ft/s² and lane change).

4.12.1 Analysis Approach

On upgrades, the direction of the grade requires traction forces instead of braking forces to be applied on vehicles. While this generally makes braking efforts easier, for situations without braking it means that more of the friction margin may be used. The primary difference between braking and traction is that, for braking, the brake forces are distributed among all tires, but for traction, the drive forces are distributed only to the drive axles. For trucks, it is unclear whether the traction forces required may cause the drive axles to skid during maneuvers on upgrades. If the vehicles require significant traction on the upgrade, skidding may occur for front-wheel-drive and rear-wheel-drive passenger vehicles as well.

This analysis extends the results of Section 4.9, using a modified version of the bicycle transient models. These modifications are specifically to add the effects of grade and to distribute traction forces only to the drive axles of the vehicle.

To calculate the theoretical crawl speeds of tractor semi-trailers on upgrades, Figure 153 is used to determine the force balance on the vehicle. In general, the traction force at the wheels, after losses due to transmission, rolling resistance, and other losses, requires a power output equal to the forces acting on the body, multiplied by the vehicle's speed:

$$P = F_x \cdot V \tag{91}$$

Here P represents the wheel-horsepower of the tractor semi-trailer, V represents the speed of the tractor semi-trailer, and F_x represents the forces acting in the longitudinal direction on the body of the vehicle. F_x is also equal to the final

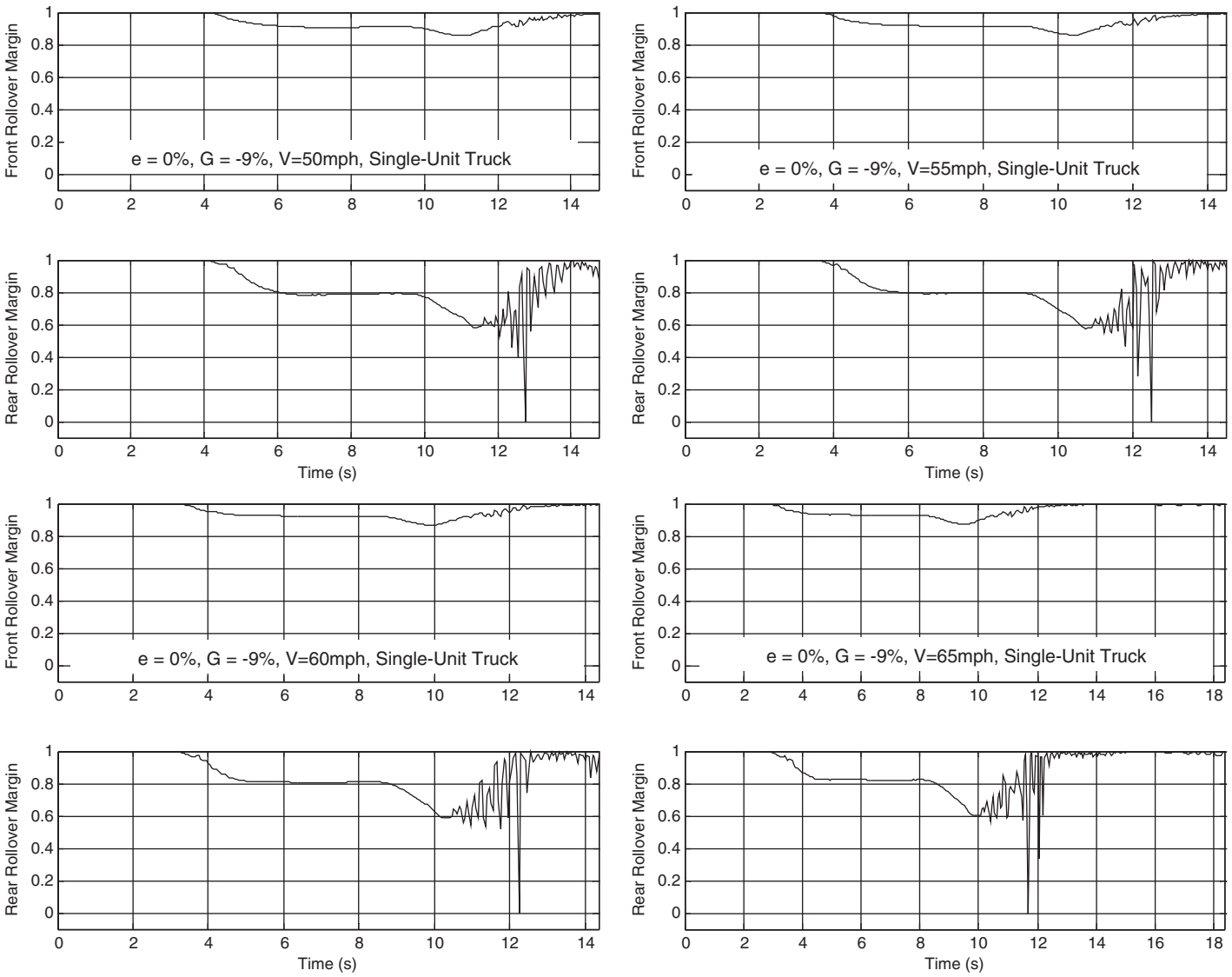

Figure 152. Rollover margin time trajectories for individual axles for single-unit truck (V = 50 to 65 mph, G = −9%, e = 0%) (a_x = −15 ft/s² and lane change).

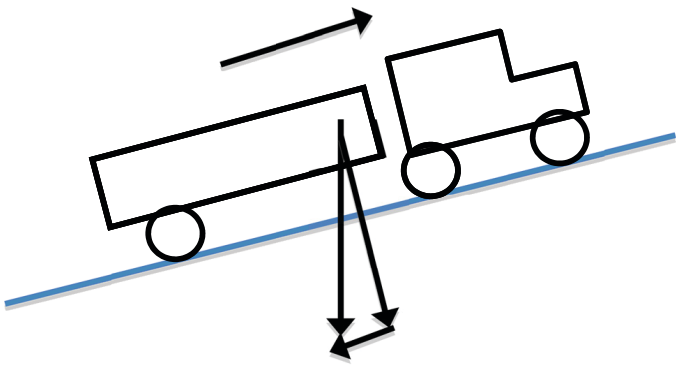

Figure 153. Force balance on a tractor semi-trailer to determine crawl speeds.

tractive force at the driving wheels when no braking is being applied. Summing forces on the whole tractor semi-trailer system yields:

$$\sum F = m \cdot \frac{dV}{dt} = \frac{P}{V} - mg\frac{G}{100} - C_d \frac{1}{2}\rho \cdot A \cdot V^2 \qquad (92)$$

Here, m is the total mass of the vehicle, g is the gravitational constant, C_d the drag coefficient, ρ is the density of air, and A the frontal area of the vehicle. When the tractor semi-trailer is no longer able to accelerate, it has reached its crawl speed and Equation 92 reduces to:

$$0 = \frac{P}{V} - mg\frac{G}{100} - C_d \frac{1}{2}\rho \cdot A \cdot V^2 \qquad (93)$$

which can be rearranged by multiplying by V to obtain:

$$0 = P - V_{crawl} \cdot mg\frac{G}{100} - C_d\frac{1}{2}\rho \cdot A \cdot V^3 \quad (94)$$

The wheel-horsepower, P, is related to the rated engine horsepower, P_{eng}; the static power load on the engine, P_{static}; and the rolling power coefficient, C_{roll}, by the following:

$$P = P_{eng} - P_{static} - C_{roll} \cdot V \quad (95)$$

So that one can write:

$$0 = \left(P_{eng} - P_{static}\right) - V_{crawl} \cdot \left(C_{roll} + mg\frac{G}{100}\right) - C_d\frac{1}{2}\rho \cdot A \cdot V^3 \quad (96)$$

Equation 96 can be solved many ways. For this equation, two of the roots form a complex conjugate pair, and the third real root represents the crawl speed, V_{crawl}, of the tractor semi-trailer.

Representative values (for a tractor semi-trailer) for terms in Equation 96 were assumed as follows (McCallen et al., 2006; TruckSim):

$C_d = 0.79$
$\rho = 0.0739$ lb/ft^3 (at 77°F)
$A = 84.0$ ft^3
$P_{eng} = 35$ Hp
$P_{static} = 413$ Hp
$C_{roll} = 1.15$ Hp/mph

Note, it was assumed that the driver shifts into a gear that allows maximum usage of the engine power at the crawl speed. These numerical values were used with Equation 96 to calculate crawl speeds across a range of grades. This solution was obtained for a tractor semi-trailer loaded with 22,000 lb. Comparisons of the theoretical crawl speeds with crawl speeds calculated within TruckSim for the same conditions/assumptions confirmed the accuracy of the theoretical calculations of crawl speeds for use in this analysis.

On upgrades, the direction of the grade requires traction forces instead of braking forces to be applied on vehicles. While this generally makes braking efforts easier, the traction force is concentrated on the drive axle. The traction force required for the upgrade is:

$$F_x = m_{truck} \cdot g \cdot \frac{G}{100} \quad (97)$$

While the normal force on the rear (drive) axle is:

$$F_z = m_{truck} \cdot g \cdot p_r \quad (98)$$

Here p_r is the proportion of the truck weight on the rear axle, and it is usually about 44% of the total mass of the truck. Thus, the normalized friction required is the ratio of these two values:

$$f_{x,traction} = G/(100 \cdot p_r) \quad (99)$$

The equation predicts that the worst-case longitudinal traction force will occur for the steepest upgrades. For example, for an upgrade of 9%, the demand traction friction is roughly 0.2. The supply friction for crawl speeds typical of trucks is approximately 0.62, and thus the traction forces require 32% of the available longitudinal force on the tire. The friction ellipse modifies the available *lateral* force by the longitudinal force used, or for this example by the numerical value of $\sqrt{1-0.3^2} = 0.95$. Thus, the maximum traction forces for 9% upgrades reduce the available lateral force by 95% of the non-traction values. Thus, the traction forces are not expected to significantly affect the lateral friction margins.

4.12.2 Analysis Results

4.12.2.1 Passenger Vehicles Traveling at Design Speed

For passenger vehicles, simulations were conducted at the design speed of the roadway as the power-to-weight ratios of these vehicles can be high enough to traverse steep grades at the design speed. Lateral friction margins were calculated for upgrades. For comparison, Figure 154 shows the lateral friction margins for upgrades from 0% to 9% and for downgrades from 0% to –9%. The lateral friction margins overall are slightly higher for upgrades due to the effect of grade. The exceptions are the constant-speed and the stopping sight distance deceleration cases. For the constant-speed case (a_x = 0 ft/s^2), upgrades have lower margins because the drive axle must utilize some additional friction to maintain the vehicle at speed. This pushes the margins for the constant-speed situations down to a level where they overlap with the curve-entry deceleration margins ($a_x = -3$ ft/s^2). For the stopping sight distance deceleration margins ($a_x = -11.2$ ft/s^2), these lateral friction margins are nearly identical between downgrades and upgrades.

4.12.2.2 Tractor Semi-Trailer Traveling at Crawl Speed on Upgrades

Figure 155 shows the minimum lateral friction margins across all axles for tractor semi-trailer simulations from the transient bicycle model for 0% to 9% grades, for curve-keeping situations with a very large superelevation (16%).

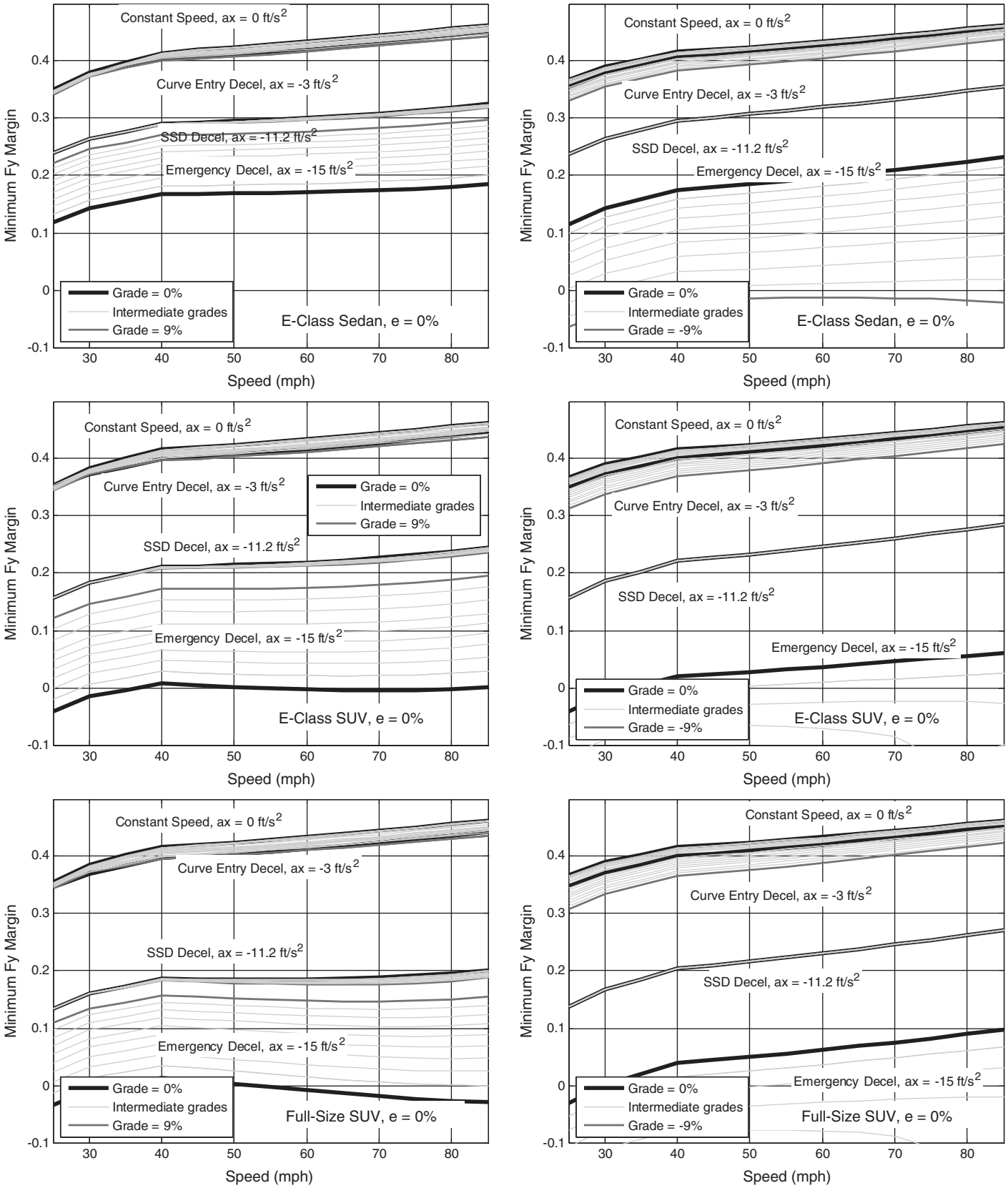

Figure 154. Lateral friction margins from transient bicycle model for passenger vehicles comparing upgrades (left plots) (G = 0% to 9%) to downgrades (right plots) (G = 0% to −9%), (e = 0%) (a_x = 0, −3, −11.2, and −15 ft/s²).

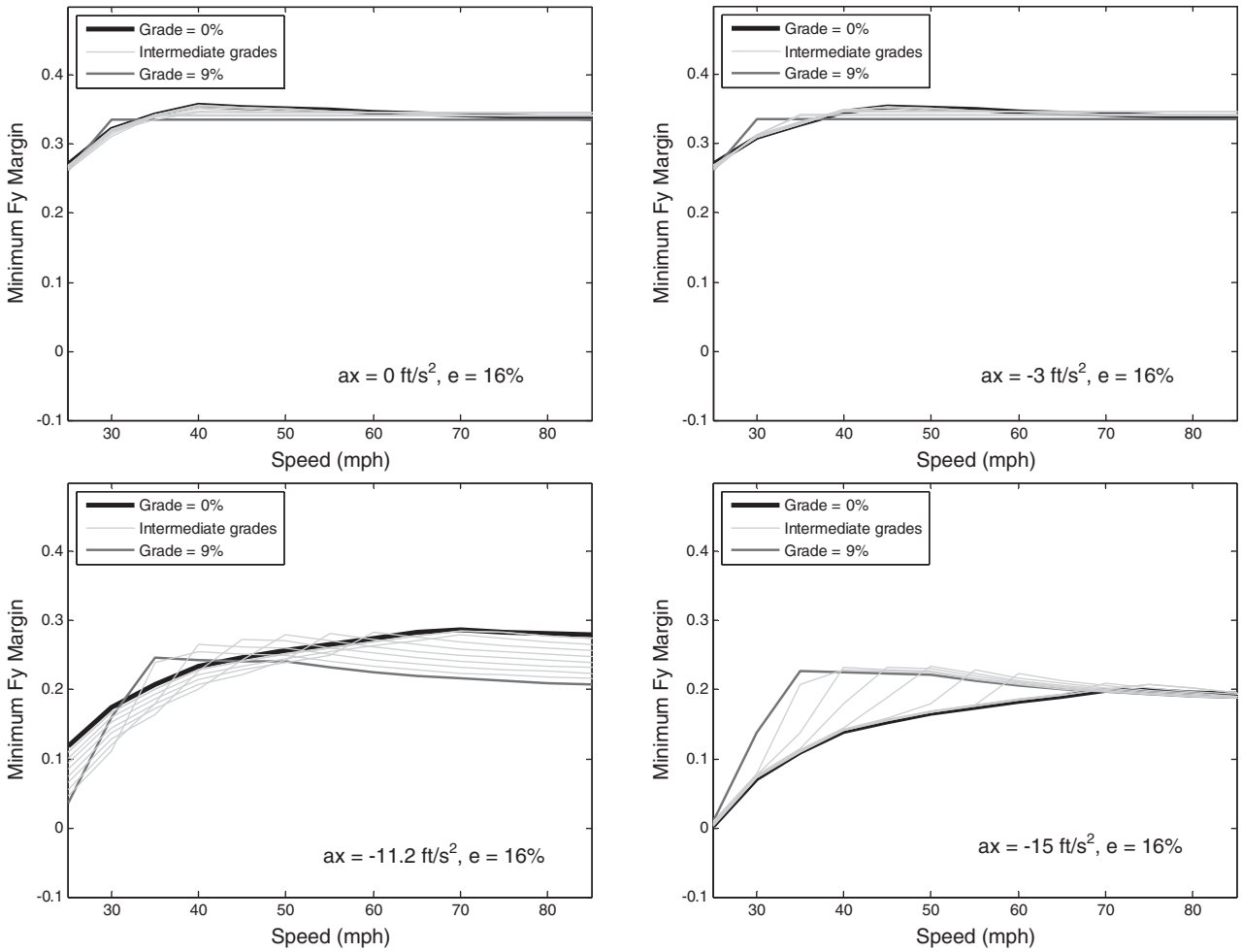

Figure 155. Lateral friction margins from transient bicycle model for tractor semi-trailer initially traveling at crawl speed (G = 0% to 9%, e = 16%) (a_x = 0, −3, −11.2, and −15 ft/s²).

Figure 156 shows the same situation with lane changes on the upgrade. The simulations were conducted assuming the vehicle was initially traveling at the crawl speed on the grade.

The presence of upgrades generally did not cause worse margins than the 0% grade case. In fact, for nearly all conditions, the upgrades caused the tractor semi-trailer to slow so significantly that the lateral accelerations were greatly diminished, resulting in much higher lateral friction margins because the vehicle traverses the curves at much slower speeds.

The single exception to this trend, that increasing grade improves the lateral friction margins, is the stopping sight distance deceleration case ($a_x = -11.2$ ft/s²) where margins become worse for increasing upgrades. This is because the decelerations become more aggressive for increasing grades, due to how the stopping sight distance decelerations are calculated. In all the cases where the grades are low enough that the vehicle can operate at the design speed, the addition of grade causes worse margins for the stopping sight distance deceleration case. This is particularly notable for low speeds (i.e., 35 mph or less), where the addition of grade can cause negative friction margins.

4.12.2.3 Tractor Semi-Trailer Traveling at Design Speed on Upgrades

There may be situations where a truck that has a slow crawl speed can traverse a steep upgrade at a high design speed. One example is when the upgrade is short and follows a long stretch of roadway with a downgrade or level grade. In these situations, the truck's momentum can maintain the vehicle's speed through much of the curve, resulting in much higher speeds in the curve. To study these situations, tractor semi-trailer simulations were conducted using the transient bicycle model at the design speed, rather than the crawl speed, for curve-keeping situations (i.e., no lane changes). The results, shown in Figure 157, are compared to the downgrades and show that the margins are generally higher for upgrades than for downgrades, particularly for

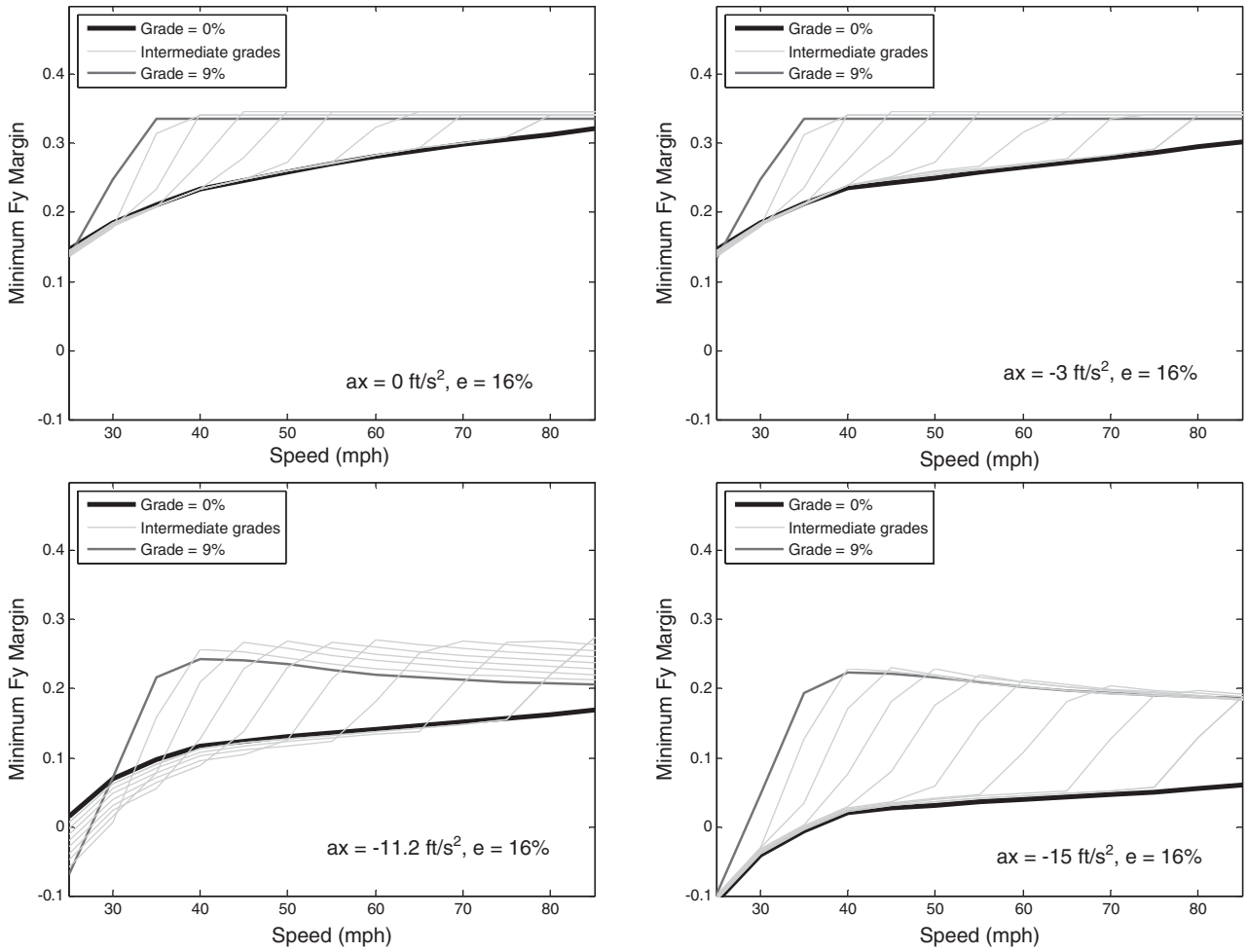

Figure 156. Lateral friction margins from transient bicycle model for tractor semi-trailer initially traveling at crawl speed (G = 0% to 9%, e = 16%) (a_x = 0, −3, −11.2, −15 ft/s² and lane change).

the emergency deceleration cases. Like the situation observed for passenger vehicles, there is a reduction of margin for the constant-speed cases due to the traction required to maintain speeds. For the stopping sight distance decelerations, there is a much larger sensitivity to grade: higher grades cause much larger reductions in margins, again due to the more aggressive deceleration demanded on upgrades versus downgrades. The worst margins are for low speeds, and the margins, while positive for all situations, are only marginally positive for the 25 mph case at both stopping sight distance and emergency braking decelerations.

4.12.2.4 Checking Transient Bicycle Model Results for Tractor Semi-Trailers Using the Multibody Model

Because the lateral friction margins for the tractor semi-trailer are low for the stopping sight distance situations at low design speeds, the stopping sight distance deceleration scenarios were examined more closely using the multibody model for the tractor semi-trailer traveling initially at the design speed of the roadway. The first set of simulations considered the apparent worst-case upgrade ($G = 9\%$) and superelevation ($e = 16\%$). Figure 158 shows the individual inside/outside tire margins for the tractor semi-trailer for the multibody model.

In Figure 158, the outside tire lateral friction margin disappears from the plot above 65 mph for axle 5, the very rearmost axle on the tractor semi-trailer. The margin is not shown here because it is actually infinitely negative as defined originally in Section 4.4, because the tire is lifted off the ground. This, along with the downward trend in friction margins with increasing speed, is in conflict with the predictions of the transient bicycle model.

To gain more insight into why the margins could disagree so drastically, and even become infinitely negative, consider Figure 159, which shows the rollover margins for the same roadway design and maneuver. The rollover margin for high

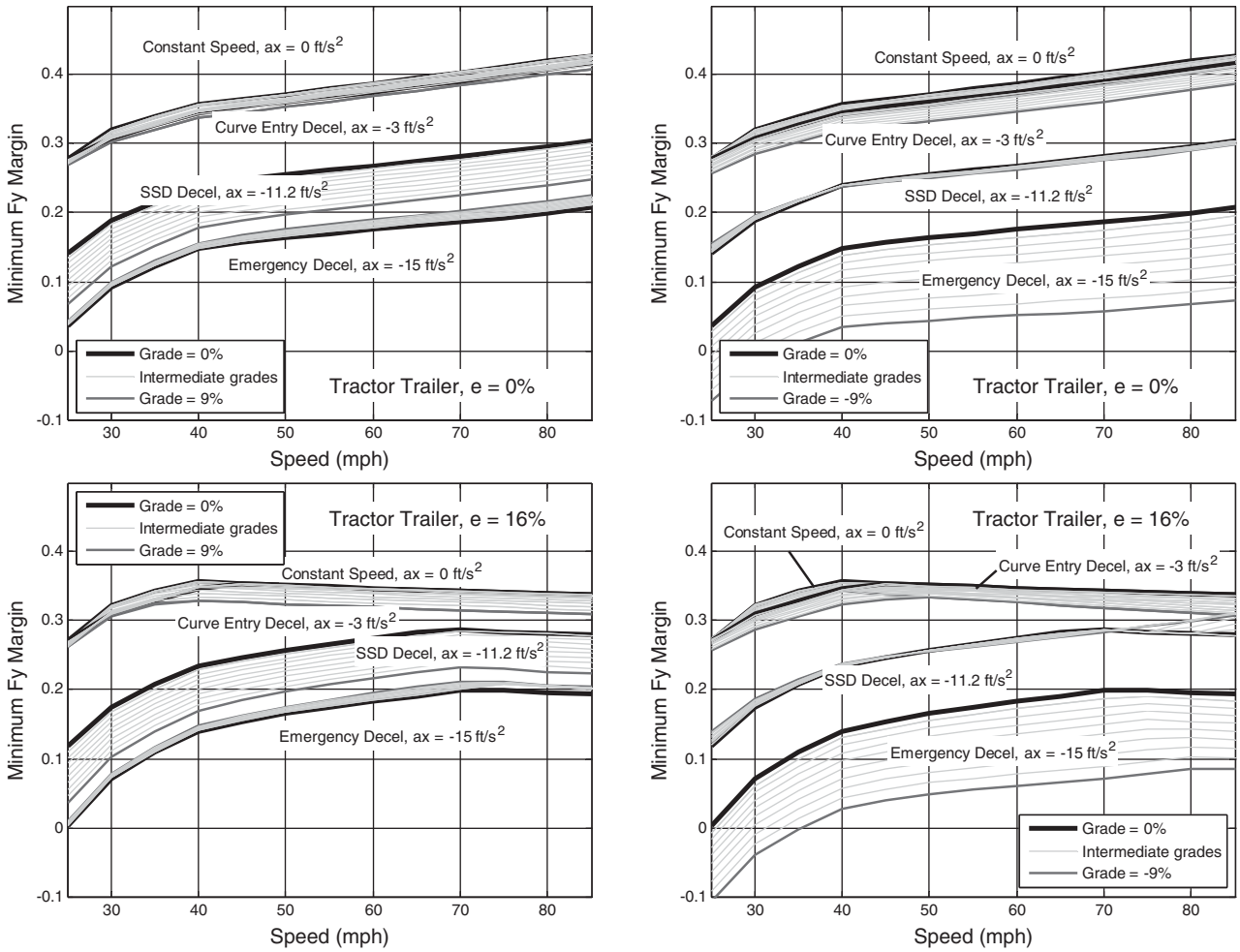

Figure 157. Lateral friction margin from transient bicycle model for tractor semi-trailers comparing upgrades (*left plots; G = *0% to 9%) to downgrades (*right plots; G = *0% to −9%) (*e = *0% and 16%) (*a_x = *0, −3, −11.2, and −15 ft/s²).

speeds is low and hits a minimum of zero for speeds from 70 to 80 mph. As defined in Section 4.11, a rollover margin of zero implies that a wheel has lifted on the axle, which implies a zero normal force on that tire. With a zero normal force, the friction demand approaches infinity, since friction demand is defined as the cornering force required on the axle divided by the normal (vertical) force on the axle. With an infinite friction demand, infinitely negative lateral friction margins are inevitable.

The low minimum rollover margins shown in Figure 159 are likely the reason for the decreasing trend in friction margins with speed as shown in Figure 158. With very little normal load in reserve, the "lighter" tires on an axle will often artificially decrease the minimum friction margin for a given maneuver, while the vehicle may still be controllable and maintain its intended path. Figure 160 shows both the normal force on each tire for the maneuver considered and the lateral deviation to offer more insight on the severity of the low rollover and friction margins seen for higher speeds. The plots show a pronounced oscillation in the vertical loads on the rear tractor and the trailer axle groups, yet a reasonable path tracking performance. The vertical load oscillation appears to coincide with the spike in lateral deviation shown, which is under 2 ft at its maximum. This indicates that the vehicle was able to maintain its path on the road, but that the trailer began to rock back and forth while the vehicle was decelerating, leading to a brief (under 1 s) wheel-lift event for axles 4 and 5 for the outside tire at approximately 17 s into the maneuver.

The most interesting point to note for this case is that it is the outside tire which lifts momentarily, leading to the predicted infinitely negative lateral friction margin and zero rollover margin for the 70 mph design speed maneuver. What this means, in the face of 16% superelevation, is that the high wheel is lifting off the ground, implying that the vehicle is leaning heavily toward the low edge of the road.

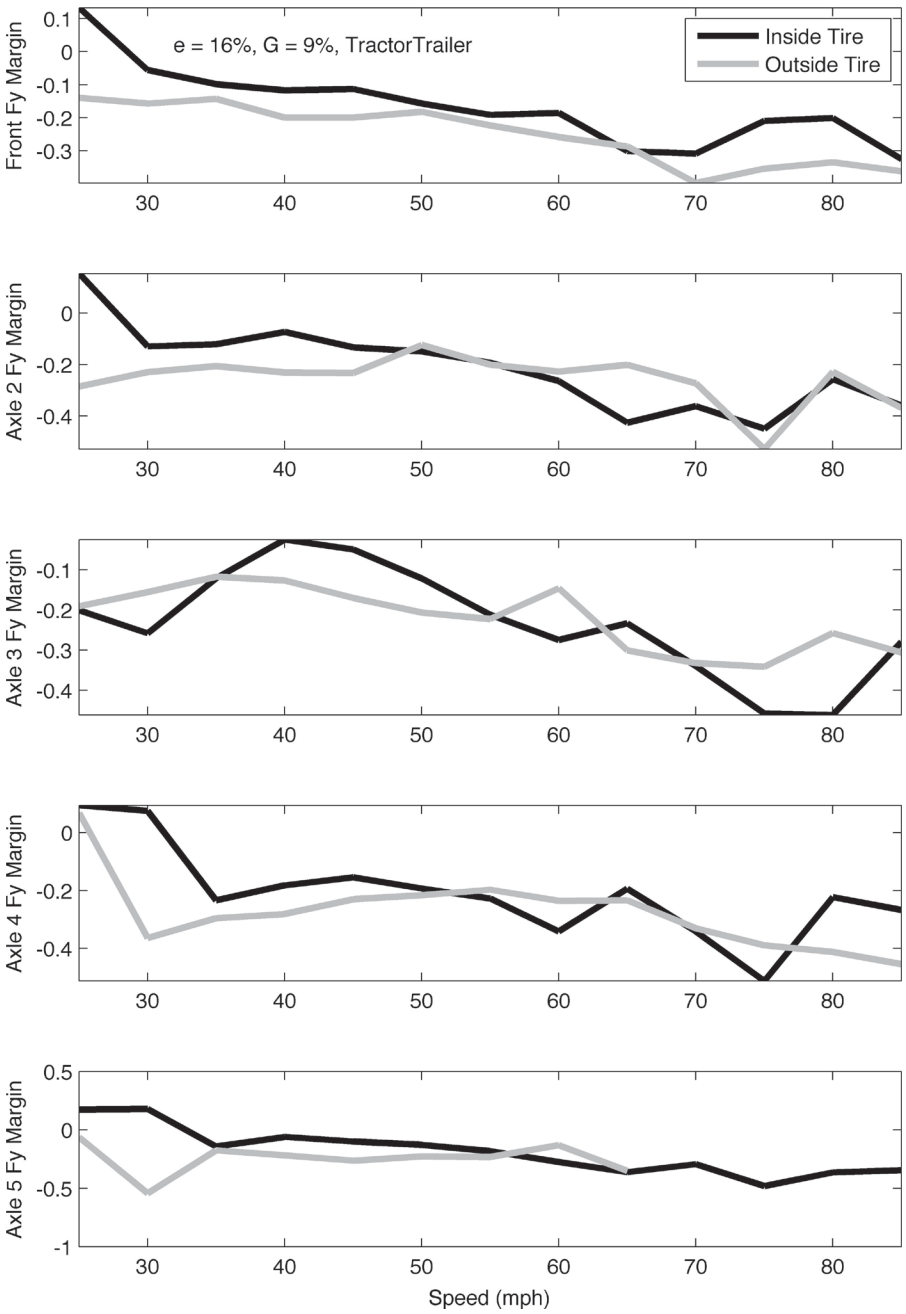

Figure 158. Lateral friction margins for inside and outside tires from multibody models for tractor semi-trailer (G = 9%, e = 16%) ($a_x = -11.2$ ft/s²).

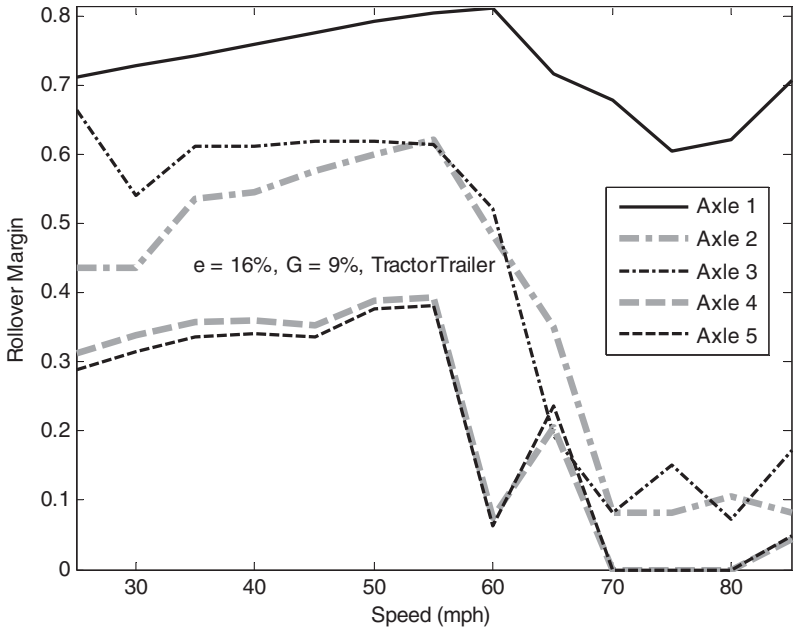

Figure 159. Rollover margins of individual axles for tractor semi-trailer (G = 9%, e = 16%) ($a_x = -11.2$ ft/s²).

Figure 161 depicts why this happens and gives some important context to the wheel-lift event. It shows the inputs as a function of time for the 70 mph curve-keeping maneuver.

Figure 161 brings several very important facts to light. First, for the multibody model, the vehicle speed decreases from 70 mph gradually as soon as the simulation starts. This is because, while the transient bicycle model simulates the vehicle at either the design speed or the crawl speed, the multibody model includes all engine effects and will naturally result in a decrease in speed toward the crawl speed from the moment the simulation begins. This also results in the time shift of the deceleration event between the transient model and the multibody model. The former initiates the deceleration at a particular time, and the latter initiates the deceleration at a particular distance on the curve. Second, notice the sine-wave-like steering input occurring in the multibody model just after 15 s. This is caused by the simulated driver attempting to maintain the desired trajectory within the lane. This corrective steering is caused for trucks because, at speeds below the design speed, the down-slope side of the vehicle is experiencing more braking force than the up-slope side of the vehicle, causing the vehicle to steer

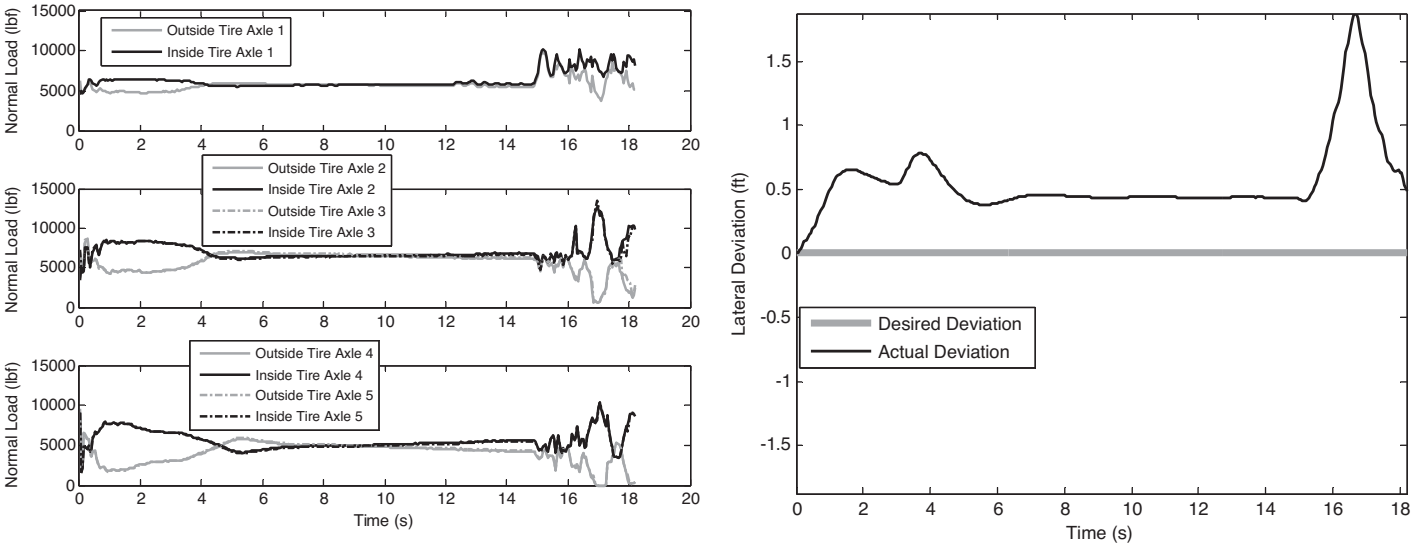

Figure 160. Vertical tire loads of individual axles (left plots) and deviation from intended path (right plots) for tractor semi-trailer (V = 70 mph, G = 9%, e = 16%) ($a_x = -11.2$ ft/s²).

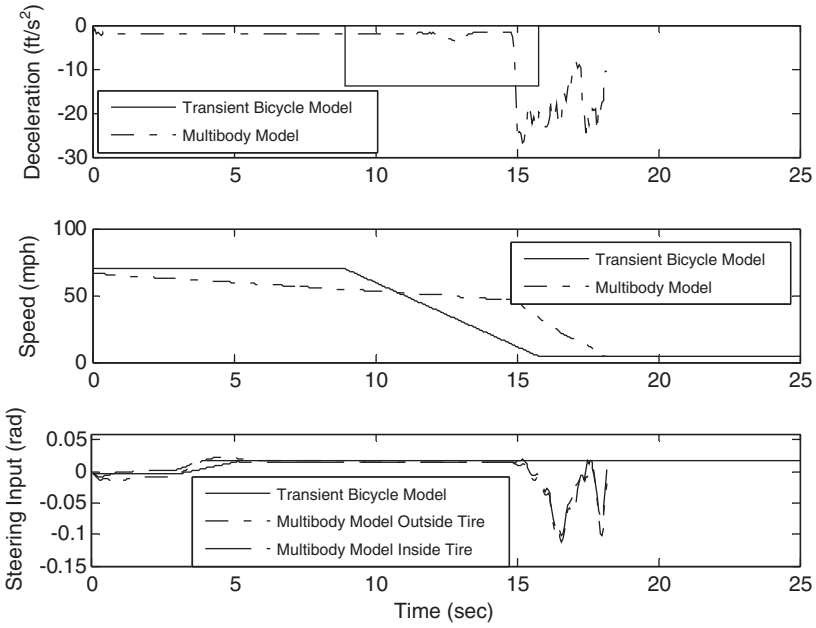

Figure 161. Trajectory of simulation inputs for transient bicycle and multibody models for tractor semi-trailer (V = 70 mph, G = 9%, e = 16%) ($a_x = -11.2$ ft/s²).

down-slope slightly. The simulated driver attempts to correct for this by steering up-slope slightly. This steering change creates a special situation unique to low-speed traversal of upgrades: this situation is potentially more demanding than the curve keeping with lane-change maneuver simulated in Section 4.9. For maneuvers near the design speed, this would not be a problem, but as the speed decreases during deceleration, the lateral acceleration required to maintain the turn also decreases. Thus, steering toward the uphill end of the cross-slope constitutes a maneuver that allows the superelevation to effectively decrease the vehicle's rollover threshold. This effect, chiefly due to the efforts of the simulated driver to stay on the road, combined with the inside/outside load differences on each axle, cannot be captured by the transient bicycle model.

These results suggest that special consideration may be needed in the choice of the design superelevation on upgrades to prevent tractor semi-trailers from lifting a wheel as their drivers attempt to decelerate and maintain their position on the road during a stopping sight distance deceleration event. To find a superelevation that avoids this issue for a 9% upgrade, Figure 162 shows the rollover margins for the tractor semi-trailer during the same curve-keeping maneuver, but for more moderate design superelevations of 8% and 12%.

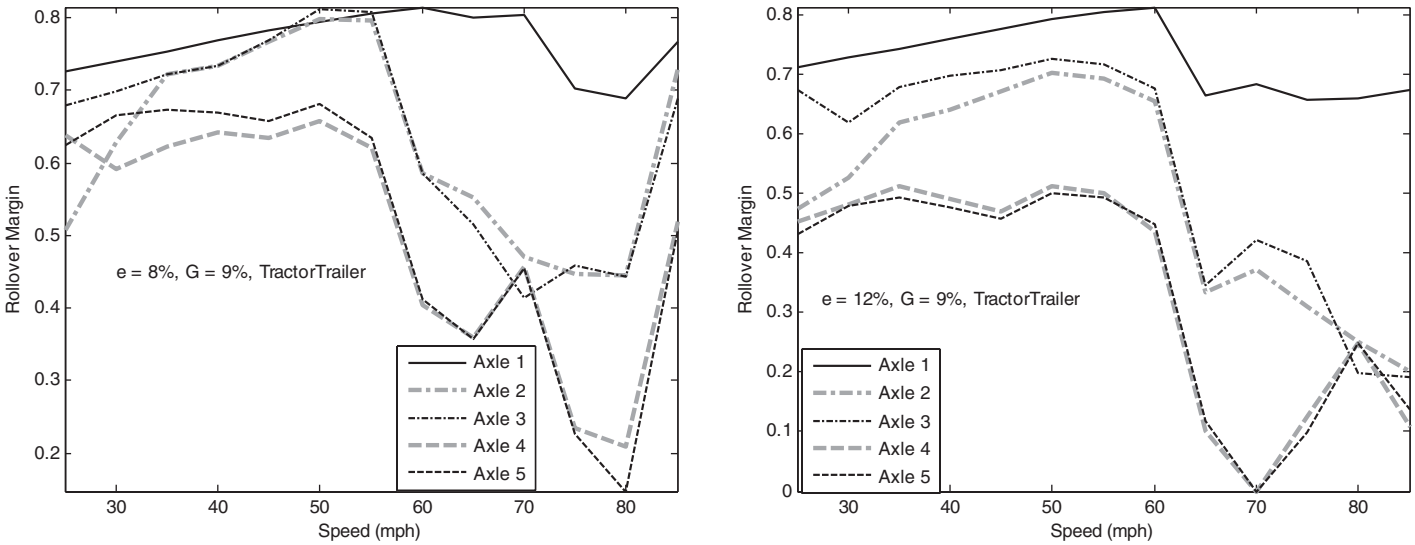

Figure 162. Rollover margins of individual axles for tractor semi-trailer (G = 9%, e = 8% and 12%) ($a_x = -11.2$ ft/s²).

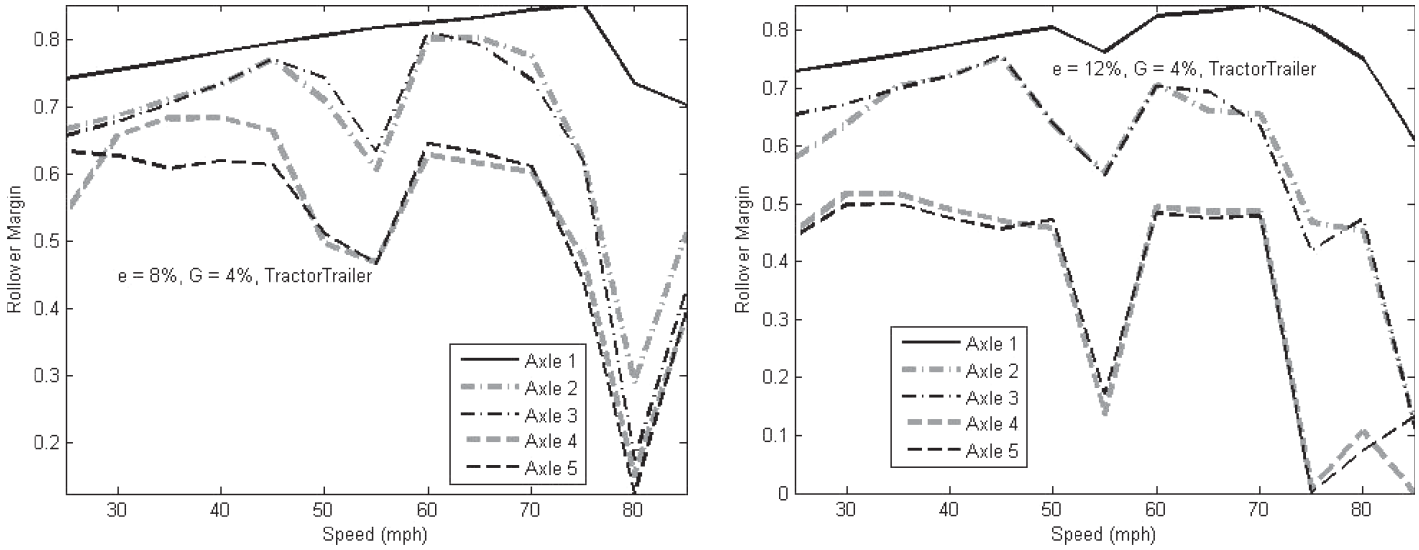

Figure 163. Rollover margins of individual axles for tractor semi-trailer (G = 4%, e = 8% and 12%) ($a_x = -11.2$ ft/s²).

The predicted rollover margins for a superelevation of 8% are positive for all speeds, although a minimum of 0.1 for the 80 mph traversal is still rather low. It appears that the 12% superelevation will still result in wheel lift at a 70 mph design speed.

To examine whether the same wheel-lift behavior observed at 9% upgrades and 12% superelevation is observed at different grades and/or intermediate superelevations, a battery of simulations was run for superelevations of 8%, 9%, 10%, 11%, and 12% for upgrades from 4% to 9%. The rollover margins for simulations of 8% and 12% superelevations are summarized in Figure 163 for a 4% upgrade, in Figure 164 for a 5% upgrade, and in Figure 165 for a 7% upgrade. The sensitivity analysis revealed that on upgrades of 4% and superelevations between 8% and 12%, the lowest speed at which wheel lift occurred for a tractor semi-trailer undergoing stopping sight distance deceleration was 75 mph at 12% superelevation. For upgrades of 5%, low rollover margins began to occur near speeds of 60 mph at 8% superelevation; and as superelevation increased, wheel lift occurred at speeds as low as 55 mph at 12% superelevation. For upgrades of 7%, low rollover margins occurred near speeds of 55 and 60 mph for all superelevations evaluated, but wheel lift did not occur until an initial speed of 70 mph at 12% superelevation. As

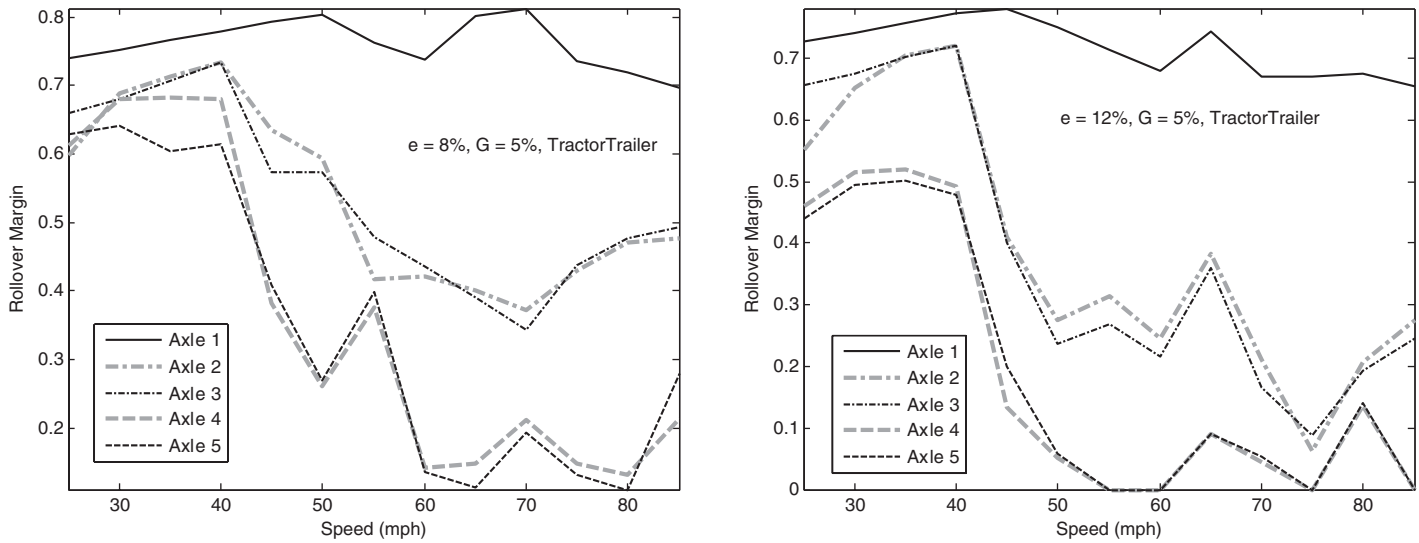

Figure 164. Rollover margins of individual axles for tractor semi-trailer (G = 5%, e = 8% and 12%) ($a_x = -11.2$ ft/s²).

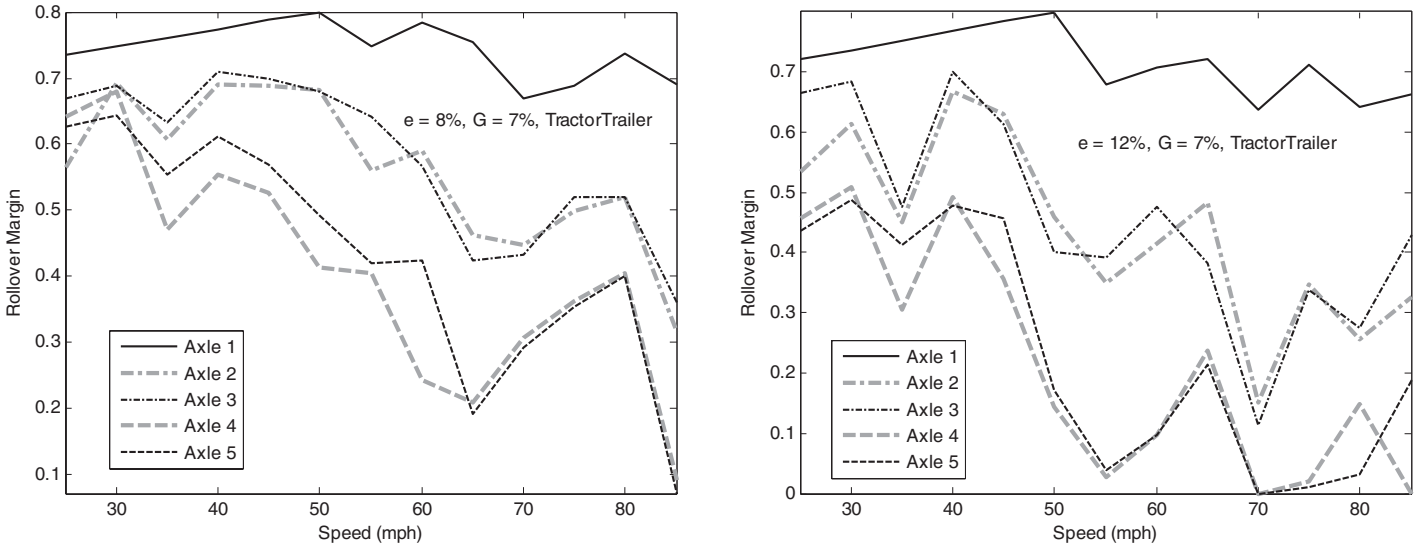

Figure 165. Rollover margins of individual axles for tractor semi-trailer (G = 7%, e = 8% and 12%) ($a_x = -11.2$ ft/s²).

a general rule, these results suggest that on upgrades of 4% and greater, the maximum superelevation should be limited to 9% for curves with design speeds of 55 mph and higher. Alternatively, if it can be verified that the available sight distance is such that deceleration at −11.2 ft/s² is unlikely to be required on upgrades of 4% and greater, minimum-radius curves could be designed using a maximum superelevation up to 12% on these steep upgrades.

4.12.3 Summary of Key Results from Step 11

In summary, the following findings were obtained from the analysis in Step 11:

1. For passenger vehicles on upgrades, the lateral friction margins predicted by the transient bicycle model were similar and/or generally higher than those observed on downgrades. The exceptions are the margins for the constant-speed and stopping sight distance deceleration cases. On upgrades, for the constant-speed case, the lateral friction margins are slightly reduced due to the traction necessary to maintain speed on upgrades. This reduction in margin is fairly minor and is similar in magnitude to the margin reductions caused by curve-entry deceleration. For stopping sight distance deceleration, lateral friction margins are nearly identical between upgrades and downgrades.
2. Upgrades in general require more traction forces, but for tractor semi-trailers the slower crawl speeds on upgrades significantly reduce the lateral forces. The result is that lateral friction margins are generally better for upgrades than downgrades for tractor semi-trailers.
3. As vehicles undergo stopping sight distance deceleration on upgrades, the net effect on lateral friction margins is to actually reduce friction margins in these braking situations.
4. Design superelevations on upgrades of 4% and greater should be limited to a maximum of 9% to avoid the possibility of wheel lift on tractor semi-trailers as predicted by the multibody model for speeds above 55 mph when undergoing stopping sight distance deceleration on the curve. Alternatively, if it can be verified that the available sight distance is such that deceleration at −11.2 ft/s² is unlikely to be required on upgrades of 4% and greater, maximum superelevation values up to 12% may be used for minimum-radius curves.

4.13 Summary of Analytical and Simulation Modeling

Results from Step 1 of the analysis provide comparisons between road friction measurements and the maximum side friction, f_{max}, used in the current AASHTO design policy for horizontal curves. The friction supply curves for both the lateral (cornering) and longitudinal (braking) directions for both passenger vehicles and trucks are higher than the maximum friction demand curves given by AASHTO policy. Thus, current horizontal curve design policy appears to provide reasonable lateral friction margins against skidding. These results suggest that if there is going to be an area of concern based upon AASHTO's current design policy, it will likely arise from the interaction of braking and cornering forces.

A series of analyses was undertaken incorporating more complex vehicle dynamics simulation models within the procedures to investigate margins of safety against skidding and

rollover for a variety of vehicles types when traversing sharp horizontal curves on steep grades. The point-mass model was the simplest model considered, while the transient bicycle and multibody models are more complex and simulate vehicles using multiple axles and multiple tires, respectively. Incorporating more complex vehicle dynamics simulation models to investigate margins of safety against skidding and rollover of vehicles traversing sharp horizontal curves on steep grades revealed several significant findings:

- When maintaining a vehicle operating speed at or near the design speed on a horizontal curve, grade and superelevation appear to have little effect on the margins of safety against skidding and rollover.
- When vehicles change lanes on a horizontal curve, the margins of safety against skidding decrease considerably for all vehicle types. When lane changing occurs in combination with severe braking (i.e., stopping sight distance or emergency braking deceleration levels), significant reductions in margins of safety against skidding can occur.
- The superelevation attained at the point of curve entry should be checked and compared to a lateral friction margin condition to ensure that the lateral friction margin on the curve entry is not less than the margin within the curve.
- The more complex models (i.e., the transient bicycle and multibody models) indicate that the point-mass model generally overestimates the margins of safety against skidding and rollover across all vehicle types.

SECTION 5

Crash Analysis

An analysis of the crashes that occurred at the field data collection sites was conducted to determine the statistical correlation between crash frequency/rate and margin of safety against skidding (i.e., lateral friction margin) and margin of safety against rollover (i.e., rollover margin) estimated from the vehicle dynamic simulation models. In theory, it was assumed that as margin of safety increases, crash frequency decreases. The questions that remain, however, are what is the rate of decrease and is there a threshold value for the margin of safety beyond which the decrease in crash frequency is negligible? These are the primary questions to be answered through the analysis of the crash data.

The crash analysis focused on determining the relationship between (1) margin of safety against skidding and single-vehicle run-off-road (SVROR) crashes and (2) margin of safety against rollover and single-vehicle rollover (SVROLL) crashes. The analysis did not include crashes involving multiple vehicles. Passenger vehicles and trucks were analyzed separately. The analysis was limited to crashes that occurred in the immediate vicinity of the horizontal curve at the field data collection sites. In most cases, the analysis was limited to crashes that occurred within the limits of the curve, but in some cases, crashes were also included if they occurred slightly upstream or downstream of the curve; it seemed reasonable to assume that these crashes could be curve related. Crashes that occurred further upstream from the curve on the tangent portion of the downgrade or upgrade were not included in the analysis. The analysis was also limited to crashes that occurred in the direction of travel corresponding to the speed and vehicle maneuver studies. The remainder of this section provides descriptive statistics of the data, describes the overall analysis approach, and presents the results.

5.1 Data Description

Site geometrics, margin of safety (MOS) data, 5-year crash data, and traffic volumes were available for 19 sites (16 downgrade and 3 upgrade) in five states. (Note: crash data were not available for site WA1, and therefore, this site was excluded from the analysis.) Basic site characteristics considered in the analysis (e.g., curve length, curve radius, superelevation, percent grade, and length of grade) are shown in Table 4 in Section 3.1.

Three separate margins of safety were considered in the analysis. Two margins of safety against skidding were estimated from the simulation models. One margin of safety estimate against skidding was based on the mean friction supply [MOS skid (mean supply)], and the second margin of safety estimate against skidding was based on the 2nd percentile friction supply (i.e., mean friction minus two standard deviations) [MOS skid (minimum supply)] measured at the site (see Section 3.4). A margin of safety against rollover (MOS rollover) was also estimated from the simulation models. For passenger vehicles, the estimated margins of safety are based upon simulations of an SUV, and for trucks the estimated margins of safety are based upon simulations of a tractor semi-trailer. The estimated margins of safety are also based upon the assumption that the passenger vehicle and truck were traveling at the mean speed for the respective vehicle type at the given site as measured in the field (Section 3.2).

The estimated margins of safety against skidding and rollover considered in the analysis for each site are shown separately for passenger vehicles and trucks in Table 26. The margins of safety against skidding (i.e., lateral friction margins) were calculated using the multibody model. The margins of safety against rollover were calculated using the methodology described in Section 4.6, with lateral acceleration obtained from the multibody model, or more specifically, the rollover margin was calculated using RM_{ay}.

Traffic volume—expressed as an average of the average annual daily traffic (AADT) and in million vehicle miles traveled (MVMT)—and curve length of each site and SVROR and SVROLL crash frequencies, all based on 5 years of data, are shown for each site in Table 27, separately for passenger

Table 26. Margins of safety by vehicle type and study site.

State	Site No.	MOS for passenger vehicles			MOS for trucks		
		Skid (mean supply)	Skid (minimum supply)	Rollover	Skid (mean supply)	Skid (minimum supply)	Rollover
CA	CA1	0.46	0.33	0.94	0.45	0.31	0.38
	CA2	0.39	0.26	0.71	0.47	0.34	0.25
	CA3	0.41	0.28	0.77	0.44	0.30	0.30
MD	MD1	0.47	0.37	0.93	0.42	0.33	0.33
	MD2[a]	0.38	0.35	0.91	0.49	0.45	0.42
	MD3	0.51	0.48	0.92	0.52	0.48	0.33
PA	PA1	0.48	0.34	0.86	0.26	0.11	0.18
	PA2	0.50	0.37	0.90	0.47	0.33	0.31
WA	WA2	0.44	0.31	0.84	0.46	0.32	0.30
	WA3	0.52	0.39	0.95	0.55	0.42	0.38
	WA4	0.42	0.30	0.87	0.44	0.31	0.32
	WA5[a]	0.47	0.34	0.94	0.59	0.45	0.45
	WA6	0.55	0.42	0.98	0.57	0.44	0.39
	WA7[a]	0.44	0.30	0.78	0.49	0.35	0.32
WV	WV1	0.35	0.26	0.81	0.22	0.13	0.29
	WV2	0.58	0.47	0.94	0.53	0.40	0.33
	WV3	0.35	0.26	0.84	0.22	0.12	0.27
	WV4	0.49	0.32	0.88	0.52	0.32	0.38
	WV5	0.46	0.33	0.91	0.39	0.25	0.32
Minimum MOS[b]		0.35	0.26	0.71	0.22	0.11	0.18
Maximum MOS[b]		0.58	0.48	0.98	0.57	0.48	0.39

[a] Upgrade sites.
[b] Range for 16 downgrade sites only.

Table 27. Traffic volumes and ROR and rollover crash frequencies by vehicle type and study site (5 years of data).

State	Site no.	Passenger vehicles				Trucks			
		5-yr Average directional AADT (veh/day)	MVMT	ROR crash frequency	Rollover crash frequency	5-year Average directional AADT (veh/day)	MVMT	ROR crash frequency	Rollover crash frequency
CA	CA1	35,520	31.764	36	7	1,480	1.323	5	6
	CA2	27,160	10.409	6	6	840	0.322	6	6
	CA3	27,645	6.559	0	0	855	0.203	0	0
MD	MD1	4,348	3.174	3	3	1,776	1.297	3	3
	MD2	7,288	6.650	0	0	2,695	2.460	0	0
	MD3	7,288	5.985	4	4	2,695	2.214	4	4
PA	PA1	6,222	2.157	5	5	468	0.162	5	5
	PA2	8,171	4.026	3	3	6,420	3.164	3	3
WA	WA2	5,700	2.497	3	4	1,800	0.788	4	4
	WA3	5,700	1.976	2	2	1,800	0.624	2	2
	WA4	5,700	3.433	4	4	1,800	1.084	4	4
	WA5	1,944	0.674	1	1	456	0.158	1	1
	WA6	4,810	2.897	1	1	1,690	1.018	1	1
	WA7	1,957	1.678	4	4	194	0.166	4	4
WV	WV1	11,357	9.327	16	5	2,493	2.047	5	5
	WV2	7,846	10.452	13	7	1,494	1.991	7	7
	WV3	11,942	2.179	1	1	498	0.091	1	1
	WV4	9,570	6.113	12	6	4,930	3.149	6	6
	WV5	31,029	28.314	15	11	4,231	3.861	11	11

vehicles and trucks. The years for which the traffic volume and crash data were obtained for each state are as follows:

- CA (2004–2008)
- MD (2007–2011)
- PA (2006–2010)
- WA (2004–2008)
- WV (2007–2011)

5.2 Analysis Approach

A crash prediction model was developed separately for each crash type and vehicle type based on the observed 5-year crash frequency, traffic volume (AADT), and site characteristics. Initially, both downgrade and upgrade sites were used in the crash prediction models, but after further investigation it was decided to only include downgrade sites in the analysis. A simple relationship of the following functional form was assumed:

$$N_{VT,CT} = \exp\begin{bmatrix} b_0 + b_1 \ln(AADT_{VT}) + b_2 MOS_{VT,CT} \\ + b_3 Var_3 + \cdots + b_n Var_n \end{bmatrix} \quad (100)$$

where:

$N_{VT,CT}$ = number of crashes/mi/year for given vehicle type (passenger vehicles or truck) and collision type (SVROR or SVROLL)
$MOS_{VT,CT}$ = MOS for given vehicle type and collision type
$AADT_{VT}$ = vehicles/day of given vehicle type
$Var_3, \ldots, Var_n$ = roadway characteristics (see list of parameters below)
ln = natural logarithm function
$b_0, \ldots, b_n$ = regression coefficients

In addition to AADT and MOS, the roadway characteristics ($Var_3, \ldots, Var_n$) considered in each model included:

- Superelevation
- Percent grade
- Length of grade
- Curve radius
- Shoulder width

The parameters in Equation 100 were estimated using a generalized linear model (GLM) approach with a negative binomial (NB) distribution and a log link using the combined crash data from all 5 years and average AADT across all 5 years. SVROR and SVROLL crashes were modeled separately for each vehicle type. A stepwise approach was used where first all parameters were included and then the least significant parameter(s) were eliminated, one at a time, until all remaining parameters were significant. This is known as backward stepwise selection. In general, a 10% significance level associated with the Type 3 χ_2-statistic was selected. However, in all cases, AADT and MOS were retained in the models. All analyses were performed using PROC GENMOD of SAS Version 9.3 (SAS, 2011).

In all, six models were investigated based on the following combinations:

- Passenger vehicles, SVROR crashes, and MOS skid (mean supply)
- Passenger vehicles, SVROR crashes, and MOS skid (minimum supply)
- Passenger vehicles, SVROLL crashes, and MOS rollover
- Trucks, SVROR crashes, and MOS skid (mean supply)
- Trucks, SVROR crashes, and MOS skid (minimum supply)
- Trucks, SVROLL crashes, and MOS rollover

5.3 Analysis Results

The NB regression analyses yielded mixed results. In some cases, the coefficients of model parameters, including AADT, were not statistically significant; the sign of the coefficient would be counterintuitive (e.g., the coefficient of MOS would be positive); and/or the model would experience convergence problems. A plausible explanation is that the number of sites is too small and the number of parameters too large and thus they could not provide sufficient evidence for a significant safety effect of one or more parameters. A case also can be made that the range of MOS values of a given type for the 16 downgrade sites is too narrow (see Table 26) to predict with confidence a relationship between margin of safety and crash frequency.

Of the six models considered, four were deemed usable, each based on only AADT and either MOS skid (minimum supply) or MOS rollover. The final analysis of variance results are shown in Table 28 for passenger vehicles and in Table 29 for trucks. The last column in these tables indicates whether the parameter is statistically significant at the 10% level. As shown, either AADT or MOS is statistically significant (if one includes the p-value of 0.1111), but never both.

Predicted crashes/mi/year and their 95% confidence limits were estimated over an MOS range of 0 to 1 using the four models shown in Tables 28 and 29. The median AADT (passenger vehicles or trucks) and median curve length from the 16 downgrade sites were used in the calculations. The four plots are shown in Figures 166 through 169. The vertical lines indicate the MOS range from the study sites on which the models are based; therefore, predictions outside that range are extrapolated and should be used with caution.

In general, the crash analysis indicates that as margins of safety against skidding and rollover increase, the predicted crash frequency decreases.

Table 28. Regression results for passenger vehicle SVROR and SVROLL crashes.

Parameter	Coefficient estimate	Standard error	Wald 95% confidence limits		Wald chi-square	Chi-square p-value	Significant at 10% level?
MOS Skid (minimum supply)							
Intercept	–4.2109	2.3960	–8.9069	0.4851	3.09	0.0788	—
ln($AADT_{PV}$)	0.6601	0.2100	0.2484	1.0717	9.88	0.0017	Yes
MOS Skid (minimum supply)	–1.5664	2.2580	–5.9919	2.8591	0.48	0.4879	No
Dispersion	0.1418	0.1145	0.0291	0.6905			
MOS Rollover							
Intercept	0.3988	2.5144	–4.5294	5.3270	0.03	0.8740	—
ln($AADT_{PV}$)	0.2724	0.1709	–0.0626	0.6074	2.54	0.1111	No (borderline)
MOS Rollover	–2.2449	1.7768	–5.7274	1.2376	1.60	0.2064	No
Dispersion	0.0000	0.0053	—	—			

Table 29. Regression results for truck SVROR and SVROLL crashes.

Parameter	Coefficient estimate	Standard error	Wald 95% confidence limits		Wald Chi-square	Chi-square p-value	Significant at 10% level?
MOS Skid (minimum supply)							
Intercept	1.0257	1.4512	–1.8187	3.8700	0.50	0.4797	—
ln($AADT_{Truck}$)	0.0734	0.1918	–0.3026	0.4493	0.15	0.7021	No
MOS Skid (minimum supply)	–2.1414	1.1872	–4.4683	0.1855	3.25	0.0713	Yes
Dispersion	0.0000	0.0115	—	—			
MOS Rollover							
Intercept	1.2242	1.3655	–1.4521	3.9005	0.80	0.3700	—
ln($AADT_{Truck}$)	0.2342	0.2100	–0.1773	0.6458	1.24	0.2647	No
MOS Rollover	–6.4837	2.8890	–12.1460	–0.8213	5.04	0.0248	Yes
Dispersion	0.0000	0.0000	0.0000	0.0000			

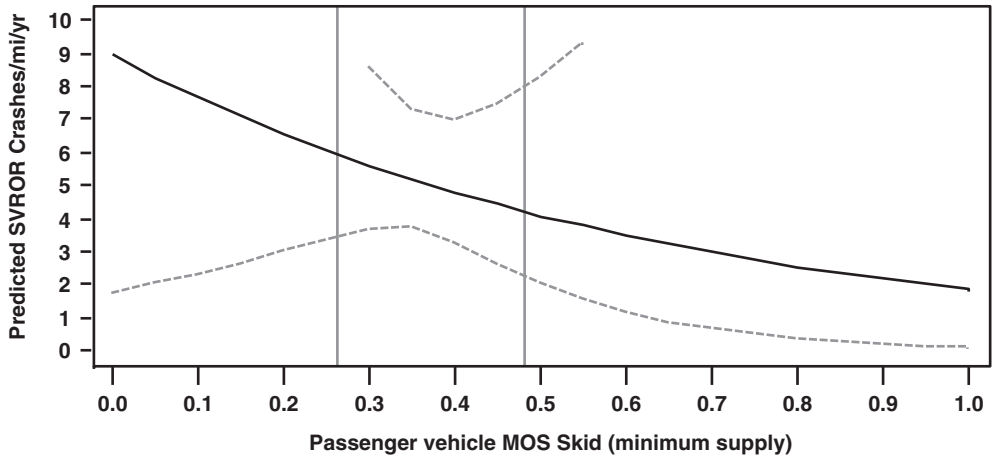

Passenger vehicle AADT = 7,300 veh/day (median); Curve Length = 0.34 mi (median)
Dashed lines represent 95% confidence limits
Vertical lines indicate interval of MOS values from 16 downgrade study sites

Figure 166. Passenger vehicles—predicted SVROR crashes versus MOS skid (minimum supply).

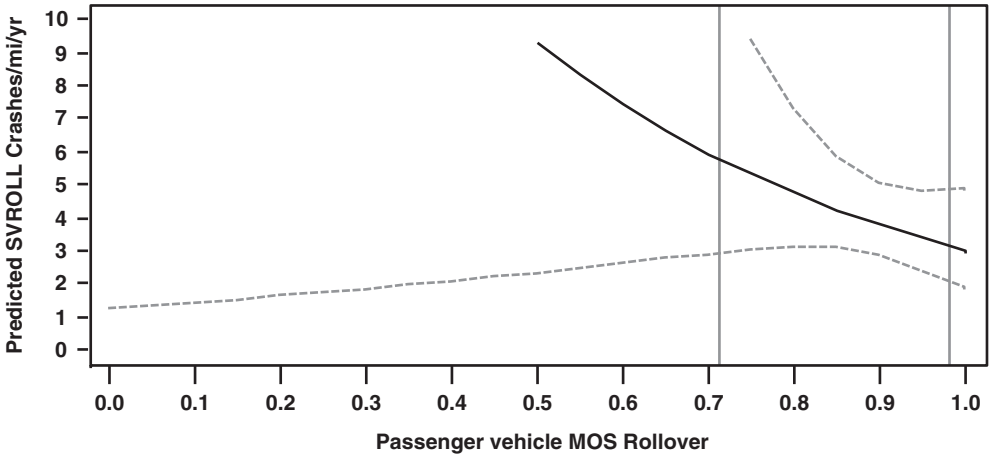

Passenger vehicle AADT = 7,300 veh/day (median); Curve Length = 0.34 mi (median)
Dashed lines represent 95% confidence limits
Vertical lines indicate interval of MOS values from 16 downgrade study sites

Figure 167. Passenger vehicles—predicted SVROLL crashes versus MOS rollover.

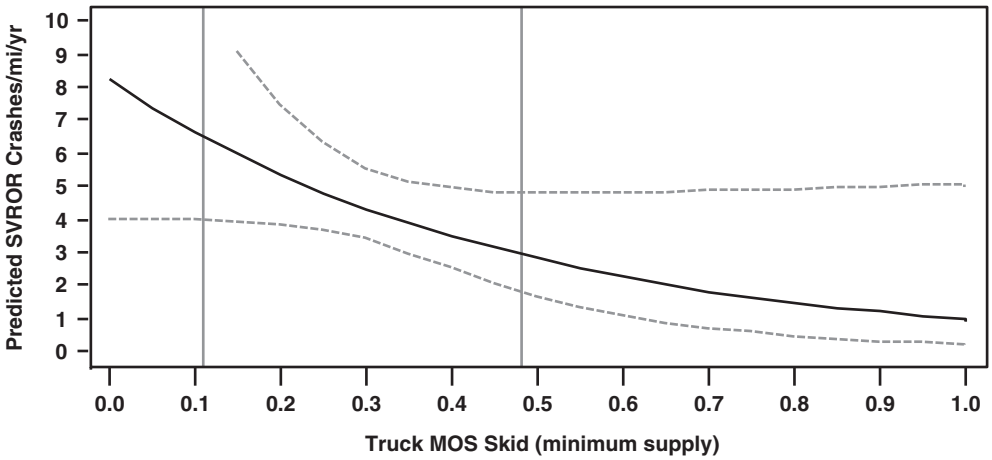

Truck AADT = 1,800 veh/day (median); Curve Length = 0.34 mi (median)
Dashed lines represent 95% confidence limits
Vertical lines indicate interval of MOS values from 16 downgrade study sites

Figure 168. Trucks—predicted SVROR crashes versus MOS skid (minimum supply).

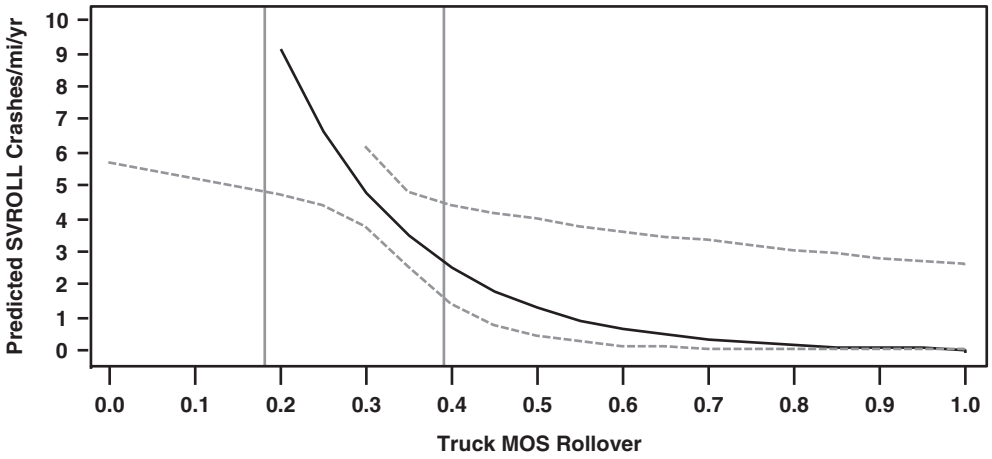

Truck AADT = 1,800 veh/day (median); Curve Length = 0.34 mi (median)
Dashed lines represent 95% confidence limits
Vertical lines indicate interval of MOS values from 16 downgrade study sites

Figure 169. Trucks—predicted SVROLL crashes versus MOS rollover.

SECTION 6

Conclusions, Geometric Design Guidance, and Future Research

The objective of this research was to develop superelevation criteria for sharp horizontal curves on steep grades. For this research, a sharp horizontal curve is defined as a minimum-radius curve as determined based upon the design speed, maximum rate of superelevation, and maximum side friction factor. Through a combination of field studies, crash analyses, and vehicle dynamics simulations, many horizontal curve–grade combinations were evaluated. This section of the report describes the general conclusions reached based on analyses performed in the study. Then, potential changes proposed for consideration in future editions of the *Green Book* and MUTCD are described, followed by recommendations for future research needs. Appendix C presents suggested modifications to text in the *Green Book* and MUTCD based upon the findings and conclusions of this research.

The vehicle types considered in this research are as follows:

- **Passenger vehicles**
  - E-class sedan
  - E-class SUV
  - Full-size SUV
- **Trucks**
  - Single-unit truck
  - Tractor semi-trailer truck
  - Tractor semi-trailer/full-trailer truck (double)

The vehicle-maneuver scenarios studied in this research are as follows:

- Vehicle maintains constant speed equal to the design speed of the curve (no deceleration, i.e., 0 ft/s^2).
- Vehicle brakes at a deceleration rate that drivers typically use when entering a curve (−3 ft/s^2).
- Vehicle brakes on the curve at a deceleration rate equivalent to that assumed for stopping sight distance design criteria (−11.2 ft/s^2).
- Vehicle brakes on the curve at a deceleration rate greater than that assumed for stopping sight distance design criteria, equivalent to the deceleration used in an emergency braking maneuver (−15 ft/s^2).

Each of these vehicle-maneuver scenarios was considered for a vehicle maintaining its lane position and also for a vehicle changing lanes while traversing the curve and decelerating, as described above.

The vehicle-maneuver scenarios were assessed, and it was concluded that the following scenarios occur so rarely that they do not represent a reasonable basis for design:

- Deceleration at rates greater than −11.2 ft/s^2 while traversing a curve (i.e., an emergency stop with deceleration greater than that assumed for stopping sight distance design criteria)
- Deceleration at rates of −11.2 ft/s^2 or greater (i.e., a controlled stop with deceleration greater than or equal to that assumed for stopping sight distance design criteria) while traversing a curve and simultaneously changing lanes on the curve

Thus, modifications to current AASHTO *Green Book* horizontal curve–superelevation design policy should be based on the assumption that a vehicle should be able to maintain its desired trajectory within the same lane while undergoing deceleration equivalent to that considered for stopping sight distance design criteria (−11.2 ft/s^2).

6.1 General Conclusions

- The AASHTO *Green Book* maximum side friction factors (f_{max}) used in horizontal curve design are below friction supply curves for lateral (cornering) and longitudinal (braking) directions, for both passenger vehicles and trucks, as measured in the field for design speeds greater than 20 mph. Thus, current horizontal curve design policy appears to provide reasonable lateral friction margins against skidding

in most situations. However, the more complex vehicle dynamics models (i.e., the transient bicycle and multibody models) indicate that the point-mass model generally overestimates the margins of safety against skidding and rollover across all vehicle types.

- There is no concern of a passenger vehicle rolling over while traveling at the design speed on a sharp horizontal curve with a steep downgrade, when designed according to current AASHTO *Green Book* policy.
- Based upon a review of the literature, the lowest rollover thresholds for tanker trucks (i.e., liquid-cargo tank trucks) are in the range of 0.28 to 0.30. Because carriers are discouraged from hauling half-filled tanks and because completely filled and empty tanks produce rigid-load behaviors that are generally more predictable and the rollover thresholds are closer to 0.56 than 0.30 and because crash data show that few crashes involve vehicles with rollover thresholds less than 0.35, horizontal curve design and superelevation criteria should not be based upon tanker trucks with rollover thresholds of 0.28 to 0.30. Rather horizontal curve design and superelevation criteria should be based upon more typical loading and truck configurations. For vehicles considered in the simulation modeling in this study, the minimum rollover threshold was 0.56.
- On downgrades, the lowest margins of safety against skidding and rollover generally occur at design speeds of 40 mph and lower for all vehicle types. This appears to be the result of higher side friction factors used in design for horizontal curves with lower design speeds.
- Steep vertical downgrade–sharp horizontal curve combinations that necessitate braking to maintain a constant speed (and maintain lane position) from the approach tangent through a horizontal curve for a passenger car sedan have large margins of safety against skidding (>0.33) for design speeds ranging from 25 to 85 mph (see Figure 87). Similarly, positive margins of safety against skidding (≥0.23) for passenger cars that decelerate at a rate of −3 ft/s^2 (similar to rates measured in the field for the present study and reported by Bonneson [2000b]) or at a rate of −11.2 ft/s^2 (stopping sight distance deceleration) exist for all design speed–downgrade combinations considered in the present study. Deceleration rates of −15 ft/s^2 (emergency braking) produce negative margins of safety for many design speeds for vertical downgrade–sharp horizontal curve combinations when the passenger car sedan enters the horizontal curve. However, the latter scenario does not seem likely to occur with sufficient frequency to constitute a reasonable basis for design.
- Steep vertical downgrade–sharp horizontal curve combinations that necessitate braking to maintain a constant speed (and maintain lane position) from the approach tangent through a horizontal curve for a E-class SUV have large margins of safety against skidding (>0.34) for design speeds ranging from 25 to 85 mph (see Figure 88). Similarly, margins of safety against skidding for a mid-size SUV that decelerates at a rate of −3 ft/s^2 exceed 0.3 for all design speeds for vertical downgrade–sharp horizontal curve combinations considered in the present study. When mid-size SUVs must decelerate at a rate of −11.2 ft/s^2 (stopping sight distance braking), positive margins of safety (>0.15) were produced for all design speeds for vertical downgrade–sharp horizontal curve combinations considered in the present study. Deceleration rates of −15 ft/s^2 (emergency braking) produce negative margins of safety for most designs considered in the present study. However, the latter scenario does not seem likely to occur with sufficient frequency to constitute a reasonable basis for design.
- The margins of safety against skidding for a full-size SUV were similar to those reported for the mid-size SUV (see Figures 88 and 89).
- Steep vertical downgrade–sharp horizontal curve combinations that necessitate braking for a single-unit truck to maintain a constant speed (and maintain lane position) from the approach tangent through a horizontal curve have large margins of safety against skidding (>0.25) for design speeds ranging from 25 to 85 mph (see Figure 90). Similarly, margins of safety against skidding for the single-unit truck that decelerates at a rate of −3 ft/s^2 exceed 0.10 for all design speeds for vertical downgrade–sharp horizontal curve combinations considered in the present study. Based upon the steady-state and transient bicycle models for a vehicle, when single-unit trucks must decelerate at a rate of −11.2 ft/s^2 (stopping sight distance braking) or a rate equivalent to emergency braking (−15 ft/s^2), significant negative margins of safety against skidding result across all design speed–downgrade combinations considered in the present study. However, based on multibody model analyses for deceleration rates of −11.2 ft/s^2 (and −15 ft/s^2) by a single-unit truck on a curve, the single-unit truck is able to maintain control on the curve when equipped with ABS.
- Steep vertical downgrade–sharp horizontal curve combinations that necessitate braking for a tractor semi-trailer to maintain a constant speed (and maintain lane position) from the approach tangent through a horizontal curve have large margins of safety against skidding (>0.28) for design speeds ranging from 25 to 85 mph (see Figure 91). Similarly, margins of safety against skidding for a tractor semi-trailer that decelerates at a rate of −3 ft/s^2 exceed 0.26 for all design speeds for vertical downgrade–sharp horizontal curve combinations considered in the present study, and when a tractor semi-trailer must decelerate at a rate of −11.2 ft/s^2, the margins of safety exceed 0.11. For emergency braking (−15 ft/s^2), a tractor semi-trailer will experience negative lateral friction margins at low design speeds (e.g., 35 mph or less). The margins of safety against skidding were slightly higher for the

tractor semi-trailer/full-trailer truck when compared to the tractor semi-trailer. However, the emergency braking scenario does not seem likely to occur frequently enough to constitute a reasonable basis for design.

- When maintaining a vehicle operating speed at or near the design speed on a horizontal curve, grade and maximum superelevation rate (e_{max}) appear to have little effect on the margins of safety against skidding and rollover for all vehicle types.
- Eck and French (2002) suggest that high superelevation rates (e.g., between 8% and 16%) make horizontal curves on steep downgrades more forgiving. The vehicle dynamics simulations in the present study suggest that maximum rates of superelevation (e_{max}) should not exceed 12% on downgrades because the superelevation transition occurring on the approach tangent can begin to reduce the margins of safety against skidding prior to curve entry. On curves designed with e_{max} greater than 12%, the margin of safety against skidding by a vehicle may be smaller in the superelevation transition area than on the curve proper. Thus, the results of this research do not support the recommendation by Eck and French that e_{max} values up to 16% should be considered in some cases. On upgrades of 4% and greater, e_{max} should be limited to 9% for minimum-radius curves with design speeds of 55 mph and higher, to avoid the possibility of wheel-lift events. Alternatively, e_{max} values up to 12% could be used for minimum-radius curves if it can be verified that the available sight distance is such that deceleration at –11.2 ft/s^2 is unlikely to be required.
- When vehicles change lanes in a horizontal curve, the margins of safety against skidding decrease considerably for all vehicle types considered in the present study. When lane changing occurs during a stopping sight distance or emergency braking maneuver, all vehicles exhibited negative margins of safety against skidding, as shown in Figures 132 through 143. For those situations (i.e., combinations of horizontal curvature, grade, and vehicle maneuvers) in which the transient bicycle model predicted skidding (i.e., negative lateral friction margins), the multibody model showed that if a vehicle has ABS, and the driver properly responds to minor lateral skidding, then the vehicle can maintain its intended path. In cases where the driver does not correct the steering input in response to a lateral shift, and the vehicle is not equipped with ABS, the transient bicycle model showed the lateral skidding of passenger sedan vehicles with negative margins of safety is small (i.e., less than 1.5 ft in lateral direction) across all combinations of vertical downgrade, design speed, deceleration rate, and lane-change maneuvers. A mid-size SUV, full-size SUV, and single-unit truck without ABS all exhibit large lateral shifts when the margin of safety against skidding is negative in certain conditions, most notably situations when more aggressive braking is needed such as deceleration rates similar to those used to develop stopping sight distance or emergency braking design criteria (–11.2 or –15 ft/s^2). The case of a tractor semi-trailer without ABS need not be considered because all tractor semi-trailers are mandated to have ABS. [Note: Federal Motor Vehicle Safety Standard No. 121 mandates ABS on all new air-braked vehicles with gross vehicle weight ratings of 10,000 lb or greater. ABS is required on tractors manufactured on or after March 1, 1997, and air-braked semi-trailers and single-unit trucks manufactured on or after March 1, 1998 (Allen, 2010).]
- Based on current AASHTO *Green Book* horizontal curve–superelevation design policy, a vehicle that performs an emergency braking maneuver (–15 ft/s^2 deceleration) on a steep downgrade–horizontal curve combination will likely skid off the roadway in many cases if the vehicle is not equipped with ABS.
- The method used in the current AASHTO *Green Book* policy to distribute superelevation and side friction on tangent–curve transitions is adequate and produces positive margins of safety against skidding and rollover for all vehicle types on horizontal curves designed using maximum superelevation and minimum curve radii. However, the superelevation attained at the point of curve entry should be checked and compared to a lateral friction margin condition to ensure that the lateral friction margin on the curve entry is not less than the margin within the curve.
- AASHTO policy uses superelevation to balance the effects of sharper curvature. This balance may be imperfect when axle-to-axle differences are considered. The balancing effect is slightly more conservative with higher superelevation rates, often resulting in lower lateral friction margins occurring for lower superelevations (e.g., 0% superelevation). However, differences in lateral friction margins between different superelevations are very small.
- The crash analysis performed in the present study showed that the predicted number of single-vehicle run-off-road and single-vehicle rollover crashes decreases as the margins of safety against skidding and rollover increase for both passenger vehicles and trucks.

6.2 Geometric Design Guidance

- Figures 30 and 32 of this report show passenger vehicle and truck tire measurements of skidding wet-tire friction in the lateral (cornering) and longitudinal (braking) directions. It is recommended that the lateral friction curves (two standard deviations below the mean) be integrated into AASHTO *Green Book* Figures 3-4 and 3-5, which show the maximum side friction factors (f_{max}) used in horizontal curve design for high-speed and low-speed streets and highways, respectively. Incorporating these curves into

Figures 3-4 and 3-5 of the *Green Book* would be informative to designers. The modified figures would, for the first time, illustrate friction measurements that take into consideration the effects of cornering. For a conservative design policy, horizontal curve–superelevation design policy recommendations should be based upon the 2nd percentile (i.e., mean friction minus two standard deviations) of the friction supply provided at the tire–pavement interface.

- For a simple horizontal curve, the maximum rate of superelevation (e_{max}) should not exceed 12% on a downgrade. If considering a maximum superelevation rate greater than 12%, a spiral curve transition is recommended to increase the margins of safety against skidding between the approach tangent and horizontal curve. On upgrades of 4% and greater, the maximum superelevation rate should be limited to 9% for minimum-radius curves with design speeds of 55 mph and higher, to avoid the possibility of wheel-lift events. Alternatively, if it can be verified that the available sight distance is such that deceleration at −11.2 ft/s^2 is unlikely to be required on upgrades of 4% or more (i.e., the available sight distance is greater than minimum stopping sight distance design values), e_{max} values up to 12% may be used for minimum-radius curves.
- For sharp horizontal curves (or near minimum-radius curves) on downgrades of 4% or more, the "Stay in Lane" sign (R4-9) should be installed in advance of the curve on multilane highways. Consideration may also be given to using solid white lane line markings to supplement the R4-9 sign.
- Sharp horizontal curves (or near minimum-radius curves) on downgrades of 4% or more should not be designed for low design speeds (i.e., 30 mph or less). In the event that such situations cannot be avoided, warning signs to reduce speeds well in advance of the start of the horizontal curve should be used.
- The following condition should be used to check that the superelevation achieved at the point of curvature (PC) of a simple horizontal curve (i.e., with no spiral transition curves) is less than the threshold value computed based on the given design speed–curve radius combination:

$$\frac{e}{100} < \frac{1}{1 + p_{tangent}} \times \frac{V^2}{gR}$$

where:

e = superelevation at PC of horizontal curve;
$p_{tangent}$ = proportion of the maximum superelevation that is attained at the PC of horizontal curve;
V = design speed (ft/s);
g = gravitational constant (32.2 ft/s^2);
R = radius of horizontal curve (ft).

If the condition presented above is met, the superelevation transition may be placed as indicated in *Green Book* Table 3-18. If the condition presented above is not met, designers should reduce the proportion of the maximum superelevation attained at the PC of the horizontal curve, or introduce a spiral transition curve between the approach tangent and simple horizontal curve. Based on an analysis completed for the present study, the condition above is satisfied for maximum superelevation–minimum-radius curves for all design speeds. However, the condition above may be violated when using greater than minimum horizontal curve radii. In such cases, it is important to check the superelevation condition above, and if the condition is not met, it is recommended that a lower proportion of the superelevation runoff (e.g., 70%) be introduced prior to horizontal curve entry.

6.3 Future Research

- Although not the primary focus of the present study, the vehicle dynamics simulations performed in the present study found that, for design speeds of 10 and 15 mph, the maximum side friction factors (f_{max}) used for horizontal curve design (0.38 and 0.32 for 10 mph and 15 mph, respectively) exceed truck rollover thresholds. Maximum side friction factors used for low-speed design also exceed or are very near rollover thresholds of 0.28 to 0.30 for partially filled tanker trucks. Additional research is recommended using a combination of simulation, field, and crash data to further investigate the relationship between truck rollover thresholds and maximum side friction factors used for horizontal curve design, particularly at low design speeds. Since low design speeds and a normal crown roadway cross section are often used in urban areas, the effects of adverse superelevation should also be investigated as part of this research.
- It would be of interest to include a tractor-trailer truck with a tanker trailer in the simulation analyses. However, existing models do not have the capability to simulate the dynamic effects of liquid sloshing in a tank trailer. When multibody models become sophisticated enough to simulate the dynamic effects of liquid sloshing in a tank trailer, the scope of this research should be revisited to incorporate tanker trucks in the analytical and simulation modeling analyses.
- Future research should be directed at collecting information concerning the relative propensity of emergency braking maneuvers under normal travel conditions to determine if these should be considered in horizontal curve–vertical grade geometric design policy. Naturalistic driving studies may provide the opportunity to collect these data from equipment installed on vehicles participating in such studies, provided that steering, braking,

and throttle conditions can be geo-located on the roadway network.

- The margins of safety against skidding and rollover are generally lowest for horizontal curves with low design speeds (40 mph or lower). This suggests that the difference between friction demanded by vehicles in relation to design side friction factors (f_{max}) is lower at low design speeds relative to higher design speeds. Because design side friction factors are based on driver comfort levels, future research should be directed at determining comfort thresholds acceptable to drivers on horizontal curves that are designed using low-speed criteria while taking into consideration vehicle dynamic capabilities.
- With a few exceptions, this research focused on simulating scenarios for maximum superelevation–minimum-radius curves for a range of design speeds. This research could be expanded to more thoroughly investigate conditions for above-minimum-radii curves. In particular, additional guidance could be sought for the design of above-minimum-radii curves for low design speeds and the need and use of "Stay in Lane" signs (R4-9) for above-minimum-radii curves on multilane highways and/or ramps.

References

Allen, K., 2010, *Effectiveness of ABS in Heavy Truck Tractors and Trailers*, Report No. DOT HS 811 339, National Highway Traffic Safety Administration.

American Association of State Highway and Transportation Officials, 2011, *A Policy on Geometric Design of Highways and Streets*, Washington, D.C.

Awadallah, F., 2005, Theoretical Analysis of Horizontal Curves Based on Actual Discomfort Speed, *Journal of Transportation Engineering*, Vol. 131, No. 11, American Society of Civil Engineers.

Barnett, J., E. R. Heule, and R. A. Moyer, 1937, Safe Side Friction Factors and Superelevation Design, *Highway Research Board Proceedings*, Vol. 16, Washington, D.C.

Biglarbegian, M., and J. W. Zu, 2006, Tractor-Semitrailer Model for Vehicles Carrying Liquids, *Vehicle System Dynamics*, Vol. 44, No. 11.

Bonneson, J. A., 1999, Side Friction and Speed as Controls for Horizontal Curve Design, *Journal of Transportation Engineering*, Vol. 125, No. 6, American Society of Civil Engineering.

Bonneson, J. A., 2000a, Kinematic Approach to Horizontal Curve Transition Design, *Transportation Research Record 1737*, Transportation Research Board, Washington, D.C.

Bonneson, J. A., 2000b, *NCHRP Report 439: Superelevation Distribution Methods and Transition Designs*, Transportation Research Board, Washington, D.C.

Bonneson, J. A., 2001, Controls for Horizontal Curve Design, *Transportation Research Record 1751*, Transportation Research Board, Washington, D.C.

Bundorf, R. T., 1968, *A Primer on Vehicle Directional Control*, Warren, Michigan: General Motors Technical Center.

Dugoff, H., 1968, On the Influence of Aerodynamic Forces and Moments on the Lateral Stability of Articulated Highway Vehicles, Presented at the First International Conference on Vehicle Mechanics, pp. 215–245.

Easa, S. M., and A. Abd El Halim, 2006, Radius Requirements for Trucks on Three-Dimensional Reverse Horizontal Curves with Intermediate Tangents, *Transportation Research Record 1961*, Transportation Research Board, Washington, D.C.

Eck, R. W., and L. J. French, 2002, *Effective Superelevation for Large Trucks on Sharp Curves and Steep Grades*, West Virginia Department of Transportation Research Project #153, West Virginia University, Morgantown, W.Va.

Ervin, R., M. Barnes, and A. Wolfe, 1985, *Liquid-Cargo Shifting and the Stability of Cargo Tank Trucks. Volume 2. Final Technical Report*, Report UMTRI-85-35/2, University of Michigan Transportation Research Institute, Ann Arbor, Michigan.

Fancher, P. S., R. D. Ervin, C. B. Winkler, and T. D. Gillespie, 1986, *A Fact Book of the Mechanical Properties of the Components for Single-Unit and Articulated Heavy Trucks*, Report No. DOT HS 807 125, National Highway Traffic Safety Administration, U.S. Department of Transportation.

Federal Highway Administration (FHWA), 1995, *Comprehensive Truck Size and Weight Study: Summary Report for Phase I-Synthesis of Truck Size and Weight (TS&W) Studies and Issues*, Washington, D.C.

Gillespie, T., 1992, *Fundamentals of Vehicle Dynamics*, SAE International Press.

Gillespie, T. D., and M. K. Verma, 1978, Analysis of the Rollover Dynamics of Double-Bottom Tankers. SAE Technical Paper 781065, Society of Automotive Engineers, Warrendale, Pa.

Glennon, J. C., and G. D. Weaver, 1972, Highway Curve Design for Safe Vehicle Operations, *Highway Research Record 390*, Highway Research Board, Washington, D.C.

Harwood, D. W. and J. M. Mason, 1994, Horizontal Curve Design for Passenger Cars and Trucks, *Transportation Research Record 1445*, Transportation Research Board, Washington, D.C.

Harwood, D. W., J. M. Mason, W. D. Glauz, B. T. Kulakowski, and K. Fitzpatrick, 1989, *Truck Characteristics for Use in Highway Design and Operation*, Vol. I. Research Report, FHWA Report FHWA-RD-89-226.

Harwood, D. W., D. J. Torbic, K. R. Richard, W. D. Glauz, and L. Elefteriadou, 2003, *NCHRP Report 505: Review of Truck Characteristics as Factors in Roadway Design*, Transportation Research Board, Washington, D.C.

Ito, K., 1990, Stability Analysis of Automatic Lateral Motion–Controlled Vehicle with Four-Wheel Steering System, *Proceedings of the 1990 American Control Conference* Vol. 1, San Diego, Calif.

Kontaratos, M., B. Psarianos, and A. Yotis, 1994, Minimum Horizontal Curve Radius as a Function of Grade Incurred by Vehicle Motion in the Driving Mode, *Transportation Research Record 1445*, Transportation Research Board, Washington, D.C.

Limpart, R., 1999, *Brake Design and Safety*, 2nd Edition, Society of Automotive Engineers, Warrendale, Pa.

MacAdam, C. C., 1981, Application of an Optimal Preview Control for Simulation of Closed-Loop Automobile Driving, *IEEE Transactions on Systems, Man and Cybernetics*, Vol. 11, No. 6.

MacAdam, C. C., P. S. Fancher, and L. Segel, 1985, *Side Friction for Superelevation on Horizontal Curves*, Final Technical Report Volume II, Report No. UMTRI-85-18-2, The University of Michigan Transportation Research Institute.

McCallen, et al., 2006, DOE's Effort to Reduce Truck Aerodynamic Drag through Joint Experiments and Computations, Lawrence Livermore National Laboratory, U.S. DOE. http://www1.eere.energy.gov/vehiclesandfuels/pdfs/hvso_2006/02_mccallen.pdf

Meyer, C. F., 1949, *Route Surveying*, First Edition. International Textbook Co. Scranton, Pa.

Milliken, W. F. and D. L. Milliken, 1995, *Race Car Vehicle Dynamics*, SAE International, August.

Modaressi-Tehrani, K., S. Rakheja, and I. Stiharu, 2007, Three-Dimensional Analysis of Transient Slosh within a Partly Filled Tank Equipped with Baffles, *Vehicle System Dynamics*, Vol. 45, No. 6, pp. 525–548.

Moyer, R. A., 1934, Skidding Characteristics of Automobile Tires on Roadway Surfaces and Their Relation to Highway Safety, Bulletin no. 120, Ames, Iowa: Iowa Engineering Experiment Station.

Moyer, R. A., and D. S. Berry, 1940, Marking Highway Curves with Safe Speed Indicators, *HRB Proceedings*, Vol. 20.

Olson, P. L., D. E. Cleveland, P. S. Fancher, L. P. Kostyniuk, and L. W. Scheider, 1984, *NCHRP Report 270: Parameters Affecting Stopping Sight Distance*, Transportation Research Board, Washington, D.C.

Pacejka, H. B., 2006, *Tire and Vehicle Dynamics*, Society of Automotive Engineers, Inc.

Psarianos, B., M. Kontaratos, and D. Katsios, 1998, Influence of Vehicle Parameters on Horizontal Curve Design of Rural Highways, *Transportation Research Circular E-C003*, Transportation Research Board, Washington, D.C.

SAS Institute Inc., 2011, *SAS 9.3 User's Guide,* Cary, N.C.

Stonex, K. A., and C. A. Noble, 1940, Curve Design and Tests on the Pennsylvania Turnpike, *Highway Research Board* Proceedings, Vol. 20, Highway Research Board, Washington, D.C.

Tan, C. H., 2005, *An Investigation of Comfortable Lateral Acceleration on Horizontal Curves*, PhD Dissertation, The Pennsylvania State University, University Park, Pa.

Varunjikar, T., 2011, *Design of Horizontal Curves with Downgrades Using Low-Order Vehicle Dynamics Models*, M.S. Mechanical Engineering Thesis, The Pennsylvania State University, University Park, Pa.

Vemulapalli, P. K., and S. N. Brennan, 2009, *Design and Testing of a Terrain Mapping System for Median Slope Measurement*, Presented at the 88th Annual Meeting of the Transportation Research Board.

Wong, J. Y., 2008, *Theory of Ground Vehicles*, John Wiley and Sons, Inc.

APPENDIX A

Nomenclature

This appendix presents the definition of terms/notation used throughout the report.

Notation	Definition	Location first used
a_r	Centripetal acceleration	Eq. 1
R	Radius of curve	Eq. 1
R_{min}	Minimum radius of curve, which is a function of the maximum rate of superelevation and the maximum demand side friction used in horizontal curve design	Eq. 9
$f_{tire\text{-}pavement}$	Side friction supply, which represents the available friction that can be developed between pavement and vehicle tires to prevent skidding along a horizontal curve, also referred to as the coefficient of friction	Page 11
F	Side friction factor, which represents the unbalanced portion of lateral acceleration or the portion of lateral acceleration that is not balanced by superelevation. The side friction factor represents demand side friction.	Eq. 5
f_{max}	Maximum side friction, which represents the maximum side friction demand set forth in the AASHTO *Green Book* for use in horizontal curve design. The values are based on driver comfort levels (i.e., tolerance for lateral acceleration). It is also referred to as the limiting side friction factor.	Eq. 9
e	Superelevation, typically defined by the rise (change in elevation) in feet per 100 ft across the road (i.e., in the transverse direction)	Eq. 5
e_{max}	Maximum rate of superelevation, which represents the maximum banking or cross slope of the roadway cross section within a horizontal curve. This value ranges from 4% to 12%, depending on climatic conditions, area type, terrain, and the frequency of very slow-moving vehicles in the traffic stream.	Eq. 9
α	Banking angle of road (in radians)	Eq. 4
V_{DS}	Design speed, which represents the selected speed used to determine the various geometric design features of the roadway	Eq. 9
V	Constant velocity	Eq. 1
N	Normal reaction from the road	Figure 2
F_c	The tire–pavement cornering force acting at the road toward the center of the rotation	Figure 2
W	Vehicle weight ($W = mg$)	Figure 2
m	Mass of the vehicle	Eq. 2
g	Gravitational acceleration	Eq. 4
F_y	Sum of forces acting in the *y*-axis direction	Eq. 2
N_y	Normal force acting in the *y*-axis direction	Eq. 2
W_y	Vehicle weight acting in the *y*-axis direction	Eq. 2
F_{cy}	Tire–pavement friction force acting in the *y*-axis direction	Eq. 2

Notation	Definition	Location first used
F_z	Sum of forces acting in the *z*-axis direction, point-mass model	Eq. 3
N_z	Normal force acting in the *z*-axis direction	Eq. 3
W_z	Vehicle weight acting in the *z*-axis direction	Eq. 3
F_{cz}	Tire-pavement friction force acting in the *z*-axis direction	Eq. 3
V_a	Curve approach speed	Figure 3
V_c	Speed at the mid-point of a horizontal curve	Figure 3
PC	Point of curvature	Eq. 76
SN_v	Skid number at a given speed	Eq. 11
P	Normalized skid gradient	Eq. 11
μ_s	Sliding friction	Table 2
μ_p	Maximum rolling (peak) friction	Table 2
F_x	Tire longitudinal force, or braking force	Eq. 12 (Figure 6)
F_y	Tire lateral force, or cornering force	Eq. 12 (Figure 6)
$F_{x,max}$	Maximum longitudinal force, e.g., the maximum braking force that a tire can generate	Eq. 12
$F_{y,max}$	Maximum lateral force, e.g., the maximum cornering force that a tire can generate	Eq. 12
N	Referred to as the utilized amount of tire–pavement friction or the measure of friction supplied (often referred to as friction reserve by vehicle dynamicists)	Eq. 12
f_x	Friction factor in the *x*-direction, defined as the tire's lateral force divided by the normal force on the tire. ($f_x = F_x/F_z$)	Eq. 13
f_y	Friction factor in the *y*-direction, defined as the tire's lateral force divided by the normal force on the tire. ($f_y = F_y/F_z$)	Eq. 13
$f_{x,\,max}$	The maximum extent of the tire's friction ellipse for longitudinal (braking) forces	Eq. 15
$f_{y,\,max}$	The maximum extent of the tire's friction ellipse for lateral (cornering) forces	Eq. 15
CG	Center of gravity	Eq. 27
t_{skid}	Time duration (in seconds) that a tire or axle is skidding	Eq. 88
$y_{Lat\ Dev}$	The lateral distance (in feet) that the vehicle will deviate from its normal lane position due to skidding	Eq. 88
z	The local deflection of a tire contact patch, in the LuGre tire model	Eq. 19
v_r	The relative velocity of a tire contact patch to the pavement surface below, as used in the LuGre tire model	Eq. 19
F_{xi}	The braking force of an element of the tire contact patch, in the LuGre tire model	Eq. 19
F_{zi}	The normal force on an element of the tire contact patch, in the LuGre tire model	Eq. 19
$\sigma_0, \sigma_1, \sigma_2$	Constants in the LuGre tire model	Eq. 19
a_x	Acceleration in the *x*-axis (braking)	Eq. 21
G	Grade, in percentage	Eq. 21
a'_x	The modified braking acceleration, used for calculating stopping sight distances in AASHTO guidelines	Eq. 26
T	Track width of the vehicle	Eq. 27
h	Height of the vehicle's CG above the road surface	Eq. 27
RM_{ay}	Rollover margin based on lateral acceleration, which represents the difference between current lateral acceleration and the maximum lateral acceleration that a vehicle can experience without overturning. A value of 0 indicates the onset of wheel lift.	Eq. 32
F_{zi}, F_{zo}	Normal load on the inside, outside tires of the vehicle	Figure 40
F_{yi}, F_{yo}	Lateral force (cornering force) from the inside, outside tires	Figure 40
ϕ	Roll angle of the vehicle relative to the road surface	Eq. 28
h_r	Height of the vehicle's roll axis above road surface	Eq. 28
a_y	Acceleration in the *y*-axis (cornering)	Eq. 29
R_ϕ	Roll gain, e.g., constant that gives the angle of body roll produced by suspension per unit of lateral acceleration, in rad/*g*	Eq. 31
F_{bf},F_{br}	Braking force from the front and rear axles	Eq. 35

Notation	Definition	Location first used
F_{cf}, F_{cr}	Cornering force from the front and rear axles	Eq. 36
N_f, N_r	Normal force from the front and rear axles on pavement	Eq. 37
a, b	Distance from CG to front and rear axles	Eq. 41/40
f_{yf}, f_{yr}	Lateral friction factors on front, rear axle (cornering)	Eq. 44
R_{tire}	Rolling radius of the tire	Eq. 46
G_f, G_r	Brake gain (front and rear axles), converts applied brake pressure to wheel torques	Eq. 46
P_f, P_r	Brake pressure applied to front and rear axles	Eq. 46
P_a	Brake pressure applied to proportioning valve	Eq. 47
P_a'	Brake pressure at which proportioning valve engages	Eq. 47
F_b'	Brake force at which proportioning valve engages	Eq. 48
$a_{x,p}$	Deceleration level at which brake proportioning valve engages	Eq. 49
f_{xf}, f_{xr}	Longitudinal friction factors on front, rear axle (braking)	Eq. 56
$f_{margin,f}$, $f_{margin,r}$	Front and rear axles margin of safety (cornering)	Eq. 59, 60
$f_{yf,supply}$, $f_{yr,supply}$	Lateral friction supply per axle on front and rear axles	Eq. 59, 60
r	The spin rate of the vehicle (rad/s) measured around the z-axis	Eq. 62
V_y	The lateral velocity of the vehicle, e.g., the sideways sliding velocity, measured at the CG	Eq. 63
I_{zz}	The moment of inertia of the vehicle about the z-axis. In the case of articulated vehicles, this is the inertia of the tractor only.	Eq. 64
α	The slip angle of the tire relative to the road	Figure 48
$C_{\alpha\phi}$, $C_{\alpha\rho}$	The front and rear cornering stiffness which predicts how much force a tire produces per radian of the tire's rotation to the road	Eq. 65
CC, CC_{offset}	The cornering coefficient and cornering coefficient offset for a tire that is used to calculate cornering stiffnesses from vertical load	Eq. 66
α_f, α_r	The front and rear tire slip angles	Eq. 67
δ	The steering angle of the front tire (radians), measured at the interface of the tire and the road surface. It is the angle between the longitudinal axis of the vehicle and the tire's centerline.	Eq. 67
R'	The rotation radius, as measured in the vehicle's body-fixed coordinate system	Eq. 73
$f_{yf,tangent}$, $f_{yr,tangent}$	The front and rear friction factors on the tangent, immediately prior to curve entry	Eq. 76
LTR	Load-transfer ratio of a vehicle, a measure of the percentage of load on a particular axle carried by the inside tire. A value of 1 means all load is on the inside tire; 0 is equally balanced inside/outside loading; and a value of −1 is when all load is on the outside tire. Values of −1 or 1 represent the onset of wheel lift.	Eq. 89
N_i, N_o	Normal force on inside, outside tires of an axle	Eq. 89
RM_{LTR}	Rollover margin defined by the proximity of the load-transfer ratio to an absolute value of unity, e.g., how close an axle is to experiencing wheel lift. A value of 0 indicates the onset of wheel lift	Eq. 90
Tractor Trailer Model		
m_1, m_2	Mass of tractor, trailer	Table 25
F_{cf}, F_{cr}, F_{ct}	Cornering force on tractor front axle, tractor rear axles, trailer axles	Table 25
F_{bf}, F_{br}, F_{bt}	Braking force on tractor front axle, tractor rear axles, trailer axles	Table 25
N_f, N_r, N_t, N_h	Normal force on tractor front axle, tractor rear axles, trailer axles, and on hitch	Table 25
f_t	Distance from hitch to trailer CG	Table 25
g_t	Distance from hitch to trailer axle	Table 25
d_h	Tractor CG to hitch distance	Table 25
h_1, h_2, h_h	Height of tractor CG, trailer CG, and hitch point	Table 25
L	The vehicle wheelbase, e.g., the distance from the front to the rear axle as measured from the center of the contact patch of each tire	Table 25

APPENDIX B

Vehicle Parameters Used in Simulation

Parameter Description	E-Class Sedan	E-Class SUV	Full-Size SUV	Single-Unit Truck	Tractor Semi-Trailer
Lead Unit Sprung Mass (lb)	3,640	3,500	5,010	9,810	13,900
Lead Unit Unsprung Mass (lb)	396	594	594	2,870	4,710
Lead Unit Total Mass (lb)	4,030	4,100	5,600	12,700	18,600
Trailer Sprung Mass (lb)					13,000
Trailer Unsprung Mass (lb)					3,450
Trailer Total Mass without Payload (lb)					16,500
Trailer Payload Mass (lb)					22,000
Lead Unit Yaw Moment of Inertia (lb-ft^2)	65,500	58,900	83,500	825,000	466,000
Trailer Yaw Moment of Inertia (lb-ft^2)					4,260,000
Trailer Payload Yaw Moment of Inertia (lb-ft^2)					1,180,000
Lead Unit Roll Moment of Inertia (lb-ft^2)	14,500	14,500	20,000	54,200	163,000
CG to Front Axle Distance (ft)	4.6	3.87	3.71	3.65	4.54
CG to Rear Axle Distance (ft)	5.4	5.81	5.96	12.8	13.9
Hitch to Lead Unit CG Distance (ft)					13.9
Hitch to Trailer CG Distance (ft)					19.7
Hitch to Payload CG Distance (ft)					24
Hitch to Trailer Axle Distance (ft)					45.2
Lead Unit Wheelbase (ft)	10	9.68	9.67	16.4	18.5
Nominal Cornering Stiffness Front (lbf/rad)	−51,000	−32,000	−43,000	−77,000	−100,000
Nominal Cornering Stiffness Rear (lbf/rad)	−44,000	−24,000	−29,000	−27,000	−240,000
Nominal Cornering Stiffness Trailer (lbf/rad)					−140,000
Cornering Coefficient (1/rad)	21.4	10.6	10.6	7.08	7.08
Cornering Stiffness Intercept (lbf/rad)	4,790	6,850	6,850	7,340	7,340
CG Height (ft)	1.94	2.36	2.56	3.85	3.34
Height of Hitch (ft)					3.61
Trailer CG Height Unloaded (ft)					5.45
Trailer CG Height Loaded (ft)					6.77
Track Width (ft)	5.25	5.17	6.23	6.39	9.44
Brake Gain Front (lbf-ft/psi)	4.07	4.07	5.09	4.07	
Brake Gain Rear (lbf-ft/psi)	3.05	3.05	3.56	3.05	
Tire Rolling Radius (ft)	1.19	1.26	1.32	1.67	
Brake Proportioning Valve Pressure (psi)	363	290	290		
Deceleration for Brake Transition (ft/s^2)	17.2	12.8	10.9		

APPENDIX C

Potential Changes Recommended for Consideration in the Next Editions of the *Green Book* and MUTCD

This appendix provides potential changes recommended for consideration in the next editions of the *Green Book* and *Manual on Uniform Traffic Control Devices* (MUTCD), based on findings and conclusions of this research. The recommendations are based upon a review of the 2011 edition of the *Green Book* and the 2009 edition of the MUTCD (with Revision Numbers 1 and 2 incorporated, dated May 2012). Recommended text is specified for selected sections of the documents as follows.

Text beginning on pg. 3-20 of 2011 Green Book

(1) Side Friction Factor

The side friction factor represents the vehicle's need for side friction, also called the side friction demand; it also represents the lateral acceleration a_f that acts on the vehicle. This acceleration can be computed as the product of the side friction demand factor f and the gravitational constant g (i.e., $a_f = fg$). Note that the lateral acceleration actually experienced by vehicle occupants tends to be slightly larger than predicted by the product fg due to vehicle body roll angle.

With the wide variation in vehicle speeds on curves, there usually is an unbalanced force whether the curve is superelevated or not. This force results in tire side thrust, which is counterbalanced by friction between the tires and the pavement surface. This frictional counterforce is developed by distortion of the contact area of the tire.

The coefficient of friction f is the friction force divided by the component of the weight perpendicular to the pavement surface and is expressed as a simplification of the basic curve formula shown as Equation (3-6). The value of the product ef in this formula is always small. As a result, the $1–0.01ef$ term is nearly equal to 1.0 and is normally omitted in highway design. Omission of this term yields the following basic side friction equation:

Metric	U.S. Customary	
$f = \frac{V^2}{127R} - 0.01e$	$f = \frac{V^2}{15R} - 0.01e$	(3-7)

This equation is referred to as the simplified curve formula and yields slightly larger (and, thus, more conservative) estimates of friction demand than would be obtained using the basic curve formula.

The coefficient f has been called lateral ratio, cornering ratio, unbalanced centrifugal ratio, friction factor, and side friction factor. Because of its widespread use, the term "side friction factor" is used in this discussion. The upper limit of the side friction factor is the point at which the tire would begin to skid; this is known as the point of impending skid. Because highway curves

are designed so vehicles can avoid skidding with a margin of safety, the *f* values used in design should be substantially less than the coefficient of friction at impending skid.

The side friction factor at impending skid depends on a number of other factors, among which the most important are the speed of the vehicle, the type and condition of the roadway surface, and the type and condition of the vehicle tires. Different observers have recorded different maximum side friction factors at the same speeds for pavements of similar composition, and logically so, because of the inherent variability in pavement texture, weather conditions, and tire condition. In general, research studies from the 1930s and 1940s show that the maximum side friction factors developed between new tires and wet concrete pavements range from about 0.5 at 30 km/h [20 mph] to approximately 0.35 at 100 km/h [60 mph]. For normal wet concrete pavements and smooth tires the maximum side friction factor at impending skid is about 0.35 at 70 km/h [45 mph]. More recent field measurements indicate that average peak side friction factors (representing the point of impending skid) range from about 0.50 at 140 km/h [85 mph] to 0.60 at 40 km/h [25 mph] for passenger cars on well-maintained roadways with high-type pavements and wet surfaces. For trucks, on well-maintained roadways with high-type pavements and wet surfaces, average peak side friction factors range from 0.50 at 140 km/h [85 mph] to 0.55 at 40 km/h [25 mph] *(69).* In all cases, the studies show a decrease in friction values as speeds increase *(46, 47, 60, 69*).

Horizontal curves should not be designed directly on the basis of the maximum available side friction factor. Rather, the maximum side friction factor used in design should be that portion of the maximum available side friction that can be used with comfort, and without likelihood of skidding, by the vast majority of drivers. Side friction levels that represent pavements that are glazed, bleeding, or otherwise lacking in reasonable skid-resistant properties should not control design because such conditions are avoidable and geometric design should be based on acceptable surface conditions attainable at reasonable cost.

A key consideration in selecting maximum side friction factors for use in design is the level of acceleration that is sufficient to cause drivers to experience a feeling of discomfort and to react instinctively to avoid higher speed. The speed on a curve at which discomfort due to the lateral acceleration is evident to drivers is used as a design control for the maximum side friction factor on high-speed streets and highways. At low speeds, drivers are more tolerant of discomfort, thus permitting employment of an increased amount of side friction for use in design of horizontal curves.

The ball-bank indicator has been widely used by research groups, local agencies, and highway departments as a uniform measure of lateral acceleration to set speeds on curves that avoid driver discomfort. It consists of a steel ball in a sealed glass tube; except for the damping effect of the liquid in the tube, the ball is free to roll. Its simplicity of construction and operation has led to widespread acceptance as a guide for determination of appropriate curve speeds. With such a device mounted in a vehicle in motion, the ball-bank reading at any time is indicative of the combined effect of body roll, lateral acceleration angle, and superelevation as shown in Figure 3-3.

The lateral acceleration developed as a vehicle travels at uniform speed on a curve causes the ball to roll out to a fixed angle position as shown in Figure 3-3. A correction should be made for that portion of the force taken up in the small body-roll angle. The indicated side force perceived by the vehicle occupants is thus on the order of $F \approx \tan(\alpha - \rho)$.

In a series of definitive tests *(47)*, it was concluded that speeds on curves that avoid driver discomfort are indicated by ball-bank readings of 14 degrees for speeds of 30 km/h [20 mph] or less, 12 degrees for speeds of 40 and 50 km/h [25 and 30 mph], and 10 degrees for speeds of 55 through 80 km/h [35 through 50 mph]. These ball-bank readings are indicative of side friction factors of 0.21, 0.18, and 0.15, respectively, for the test body roll angles and provide ample margin of safety against skidding or vehicle rollover.

From other tests *(11)*, a maximum side friction factor of 0.16 for speeds up to 100 km/h [60 mph] was recommended. For higher speeds, the incremental reduction of this factor was recommended. Speed studies on the Pennsylvania Turnpike *(60)* led to a conclusion that the

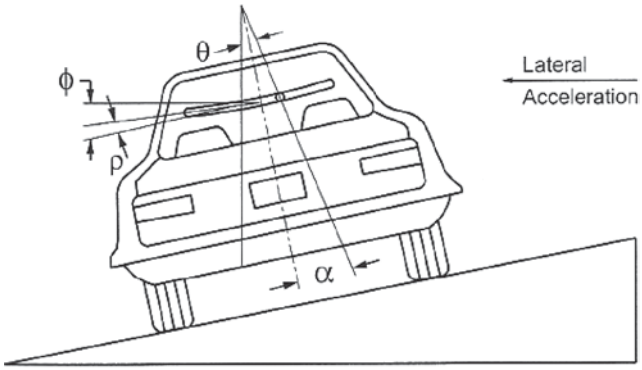

α = Ball-bank indicator angle
ϕ = Body roll angle
θ = Superelevation angle
ρ = Lateral acceleration angle

Figure 3-3. Geometry for ball-bank indicator.

side friction factor should not exceed 0.10 for design speeds of 110 km/h [70 mph] and higher. A recent study *(13)* re-examined previously published findings and analyzed new data collected at numerous horizontal curves. The side friction demand factors developed in that study are generally consistent with the side friction factors reported above.

An electronic accelerometer provides an alternative to the ball-bank indicator for use in determining advisory speeds for horizontal curves and ramps. An accelerometer is a gravity-sensitive electronic device that can measure the lateral forces and accelerations that drivers experience while traversing a highway curve *(20)*.

It should be recognized that other factors influence driver speed choice under conditions of high friction demand. Swerving becomes perceptible, drift angle increases, and increased steering effort is needed to avoid involuntary lane line violations. Under these conditions, the cone of vision narrows and is accompanied by an increasing sense of concentration and intensity considered undesirable by most drivers. These factors are more apparent to a driver under open-road conditions.

Where practical, the maximum side friction factors used in design should be conservative for dry pavements and should provide an ample margin of safety against skidding on pavements that are wet as well as ice or snow covered and against vehicle rollover. The need to provide skid-resistant pavement surfacing for these conditions cannot be overemphasized because superimposed on the frictional demands resulting from roadway geometry are those that result from driving maneuvers such as braking, sudden lane changes, and minor changes in direction within a lane. In these short-term maneuvers, high friction demand can exist but the discomfort threshold may not be perceived in time for the driver to take corrective action.

Figure 3-4 summarizes the findings of the cited tests relating to side friction factors recommended for curve design. Although some variation in the test results is noted, all are in agreement that the side friction factor should be lower for high-speed design than for low-speed design. ~~A recent study~~ Recent studies *(13, 69)* have reaffirmed the appropriateness of these side friction factors. To illustrate the difference between side friction factors for design and available side friction supply during cornering, Figure 3-4 also includes friction supply curves for passenger vehicle and truck tires for the skidding condition on wet pavement during cornering.

[**Comment:** Recommend adding supply friction curves from Figures 30 and 32 in the main body of the report, which are representative of more current research, to Green Book Figure 3-4. The data points for the curves to be added to Figure 3-4 are as follows, and the curves should be labeled accordingly.

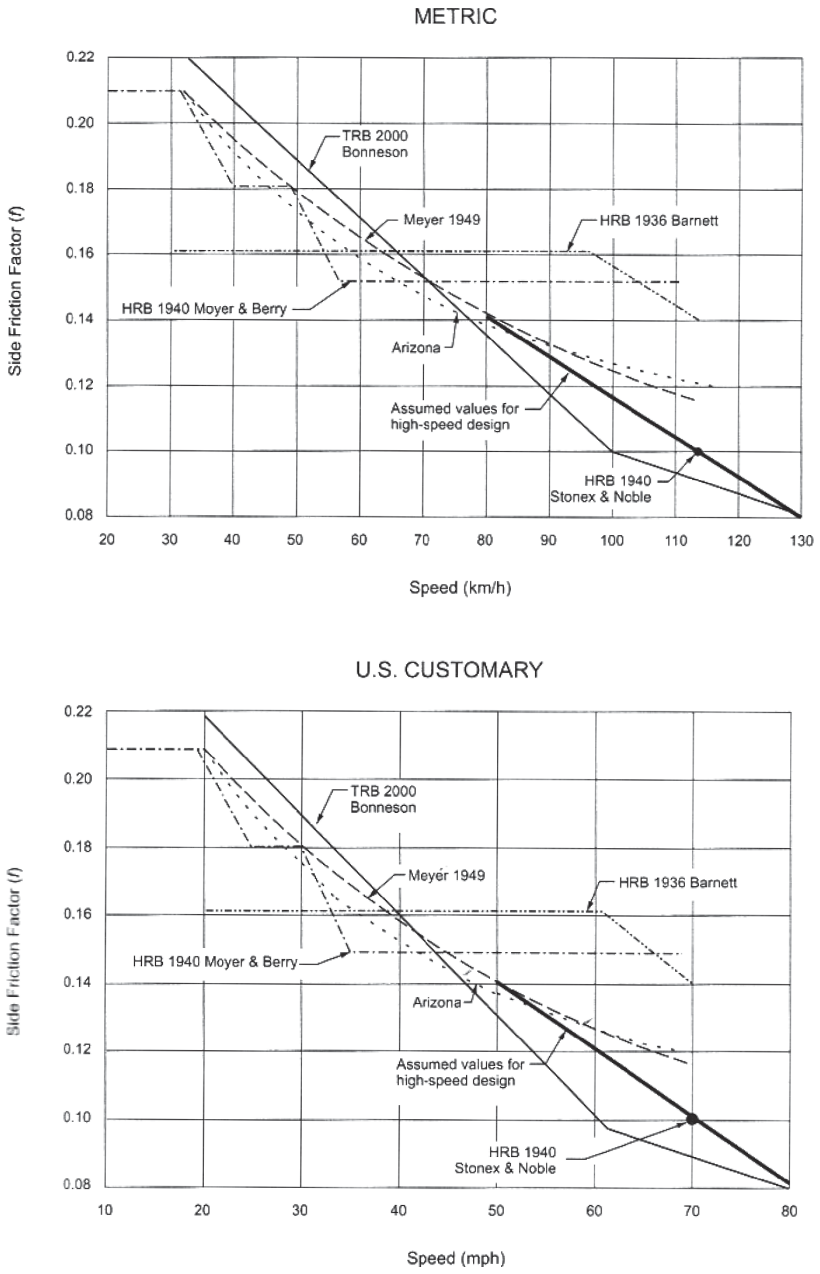

Figure 3-4. Side friction factors for high-speed streets and highways.

Speed (km/h)	40	48	56	64	72	80	89	97	105	113	121	129	137
Speed (mph)	25	30	35	40	45	50	55	60	65	70	75	80	85
Passenger vehicle tire measurements of skidding wet-tire friction in lateral (cornering) direction	0.59	0.58	0.57	0.56	0.55	0.54	0.53	0.52	0.51	0.50	0.49	0.49	0.48
Truck tire measurements of skidding wet-tire friction in lateral (cornering) direction	0.52	0.49	0.45	0.42	0.40	0.38	0.36	0.34	0.32	0.31	0.30	0.29	0.28

Note, the scale of Figure 3-4 will need to be adjusted to include the curves.]

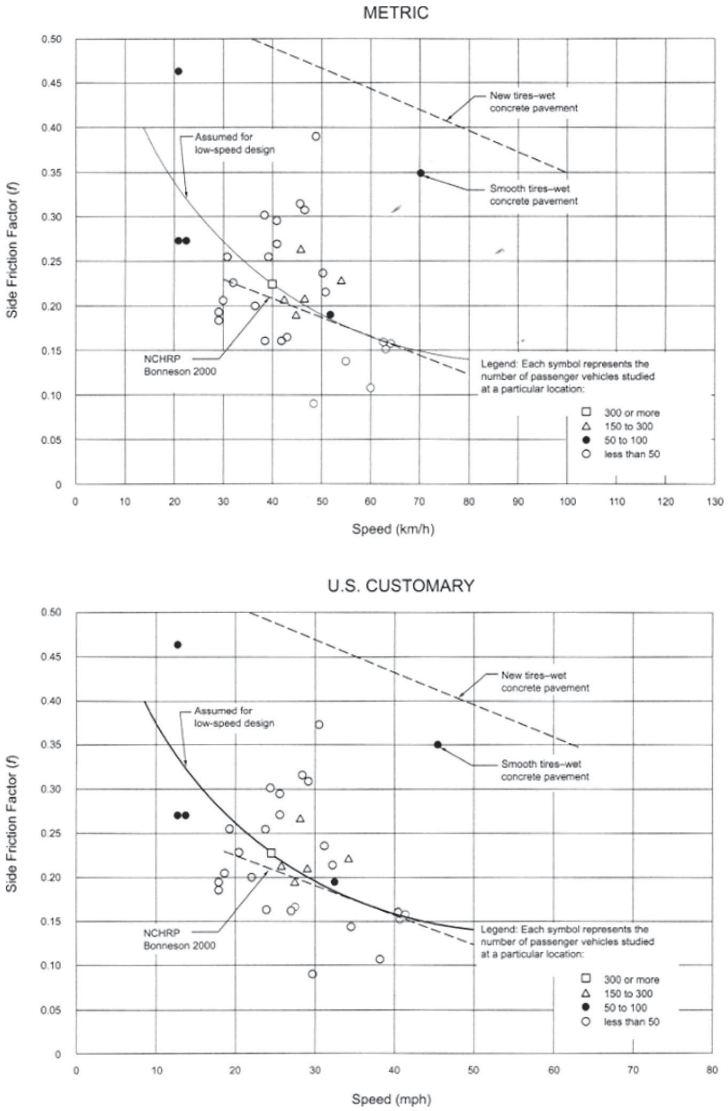

Figure 3-5. Side friction factors for low-speed streets and highways.

The maximum allowable side friction factors for low-speed streets and highways are shown in Figure 3-5. For travel on sharper curves, superelevation is needed. The curves are based on several studies *(14, 16, 23)* conducted to determine the side friction factor for low-speed intersection curves. A 95th percentile curve speed was used since it closely represents the 85th percentile tangent speed and provides a reasonable margin of safety against skidding *(13)*. These curves also approximated the assumed values for low-speed urban design based on driver comfort. Figure 3-5 also includes friction supply curves for passenger vehicle and truck tires for the skidding condition on wet pavement during cornering *(69)*. Comparisons of the side friction supply and the side friction factor ~~The~~ curves provide a~~n~~ sense of the ~~appropriate~~ margin of safety against skidding based upon the given side friction factors for design~~and a cost-effective limitation on superelevation~~.

[**Comment:** Recommend adding supply friction curves from Figures 30 and 32 in the main body of the report, which are representative of more current research, to *Green Book* Figure 3-5. The data points for the curves to be added to Figure 3-5 are as follows, and the curves should be labeled accordingly.

Speed (km/h)	40	48	56	64	72	80	89	97	105	113	121	129	137
Speed (mph)	25	30	35	40	45	50	55	60	65	70	75	80	85
Passenger vehicle tire measurements of skidding wet-tire friction in lateral (cornering) direction	0.59	0.58	0.57	0.56	0.55	0.54	0.53	0.52	0.51	0.50	0.49	0.49	0.48
Truck tire measurements of skidding wet-tire friction in lateral (cornering) direction	0.52	0.49	0.45	0.42	0.40	0.38	0.36	0.34	0.32	0.31	0.30	0.29	0.28

Note, the scale of Figure 3-5 will need to be adjusted to include the curves.]

The side friction factors vary with the design speed from 0.40 at 15 km/h [0.38 at 10 mph] to about 0.15 at 70 km/h [45 mph], with 70 km/h [45 mph] being the upper limit for low speed established in the design speed discussion in Section 2.3.6. Figure 3-6 should be referred to for the values of the side friction factor recommended for use in horizontal curve design.

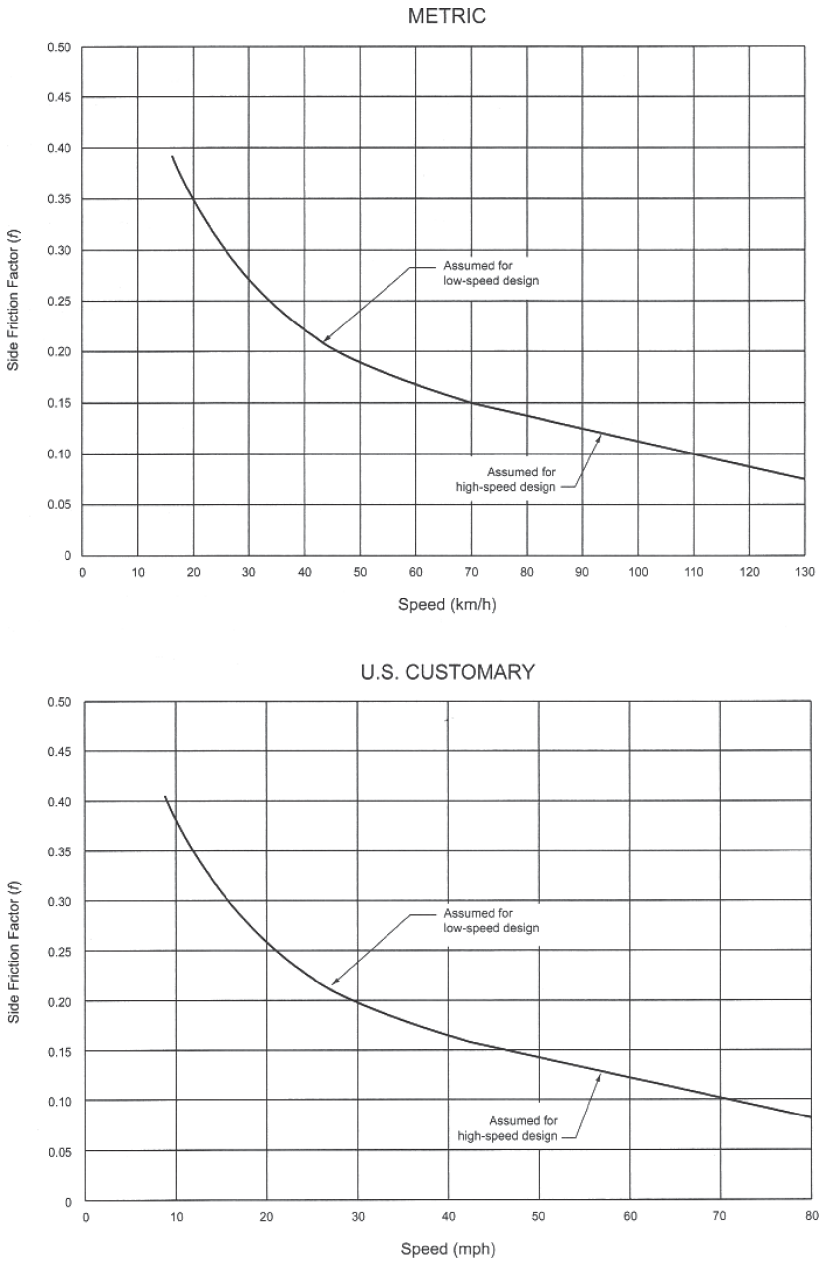

Figure 3-6. Side friction factors assumed for design.

Text beginning on pg. 3-33 of 2011 Green Book

(2) Effects of Grades

On long or fairly steep grades, drivers tend to travel faster in the downgrade than in the upgrade direction. Additionally, research *(13, 69)* has shown that the side friction demand is greater on both downgrades (due to braking forces) and steep upgrades (due to the tractive forces). Research *(69)* has also shown that, for simple horizontal curves, the maximum superelevation rate on steep downgrades of 4 percent or more should not exceed 12 percent. If considering a maximum superelevation rate on a horizontal curve in excess of 12 percent, a spiral curve transition is recommended to increase the margins of safety against skidding or rollover between the approach tangent and horizontal curve. Sharp horizontal curves (or near minimum-radius curves) on downgrades of 4 percent or more should not be designed using low design speeds (i.e., 50 km/h [30 mph] or less). In the event that such situations cannot be avoided, warning signs to reduce speeds well in advance of the start of the horizontal curve should be used.

On upgrades of 4 percent or more, the maximum superelevation rate should be limited to 9 percent for minimum-radius curves with design speeds of 90 km/h [55 mph] and higher, to minimize the potential for wheel-lift events on tractor semi-trailer trucks. Alternatively, if it can be verified that the available sight distance is such that deceleration at the rate assumed in stopping sight distance design criteria, 3.4 m/s^2 [11.2 ft/s^2], is unlikely to be required on upgrades of 4 percent or more, e_{max} values up to 12 percent may be used for minimum-radius curves.

Vehicle dynamics simulations have shown *(69)* that sharp horizontal curves with near or minimum radii for given design speeds on downgrades of 4 percent or more could lead to skidding or rollover for a range of vehicle types if a driver is simultaneously braking and changing lanes on the curve. For this reason, it may be desirable to provide a "STAY IN LANE" sign (R4-9) in advance of sharp horizontal curves on steep grades on multilane highways (*22*). Consideration may also be given to using single solid white lane line markings to supplement the "STAY IN LANE" sign and discourage motorists from changing lanes.

~~Some adjustment in superelevation rates should be considered for grades steeper than 5 percent. This adjustment is particularly important on facilities with high truck volumes and on low-speed facilities with intermediate curves using high levels of side friction demand.~~

~~In the case of a divided highway with each roadway independently superelevated, or on a one-way ramp, such an adjustment can be readily made. In the simplest practical form, values from Exhibits 3-21 to 3-25, presented in Section 3.3.5, can be used directly by assuming a slightly higher design speed for the downgrade. Since vehicles tend to slow on steep upgrades, the superelevation adjustment can be made without reducing the design speed for the upgrade. The appropriate variation in speed depends on the particular conditions, especially the rate and length of grade and the magnitude of the curve radius compared to other curves on the approach highway section.~~

~~On two-lane and multilane undivided roadways, the adjustment for grade can be made by assuming a slightly higher design speed for the downgrade and applying it to the whole traveled way (both upgrade and downgrade sides). The added superelevation for the upgrade can help counter the loss of available side friction due to tractive forces. On long upgrades, the additional superelevation may cause negative side friction for slow moving vehicles (such as large trucks). This effect is mitigated by the slow speed of the vehicle, allowing time to counter steer, and the increased experience and training for truck drivers.~~

Text beginning on pg. 3-66 of 2011 Green Book

Location with respect to end of curve. In the tangent-to-curve design, the location of the superelevation runoff length with respect to the Point of Curvature (PC) needs to be determined. Normal practice is to divide the runoff length between the tangent and curved sections and to avoid placing the entire runoff length on either the tangent or the curve. With full superelevation

attained at the PC, the runoff lies entirely on the approach tangent, where theoretically no superelevation is needed. At the other extreme, placement of the runoff entirely on the circular curve results in the initial portion of the curve having less than the desired amount of superelevation. Both of these extremes tend to be associated with a large peak lateral acceleration.

Experience indicates that locating a portion of the runoff on the tangent, in advance of the PC, is preferable, since this tends to minimize the peak lateral acceleration and the resulting side friction demand. The magnitude of side friction demand incurred during travel through the runoff can vary with the actual vehicle travel path. Observations indicate that a spiral path results from a driver's natural steering behavior during curve entry or exit. This natural spiral usually begins on the tangent and ends beyond the beginning of the circular curve. Most evidence indicates that the length of this natural spiral ranges from 2- to 4-s travel time; however, its length may also be affected by lane width and the presence of other vehicles.

Based on the preceding discussion, locating a portion of the runoff on the tangent is consistent with the natural spiral path adopted by the driver during curve entry. In this manner, the gradual introduction of superelevation prior to the curve compensates for the gradual increase in lateral acceleration associated with the spiral path. As a result, the peak lateral acceleration incurred at the PC should theoretically be about equal to 50 percent of the lateral acceleration associated with the circular curve.

To achieve this balance in lateral acceleration, most agencies locate a portion of the runoff length on the tangent prior to the curve. The proportion of runoff length placed on the tangent varies from 0.6 to 0.8 (i.e., 60 to 80 percent) with a large majority of agencies using 0.67 (i.e., 67 percent). Most agencies consistently use a single value of this proportion for all street and highway curves.

Theoretical considerations confirm the desirability of placing a larger portion of the runoff length on the approach tangent rather than on the circular curve. Such considerations are based on analysis of the acceleration acting laterally on the vehicle while it travels through the transition section. This lateral acceleration can induce a lateral velocity and lane shift that could lead to operational problems. Specifically, a lateral velocity in an outward direction (relative to the curve) results in a driver making a corrective steering maneuver that produces a path radius sharper than that of the roadway curve. Such a critical radius produces an undesirable increase in peak side friction demand. Moreover, a lateral velocity of sufficient magnitude to shift the vehicle into an adjacent lane (without corrective steering) is also undesirable for safety reasons.

Analysis of the aforementioned theoretical considerations has led to the conclusion that an appropriate allocation of runoff length between the tangent and the curve can minimize the aforementioned operational problems *(12)*. The values obtained from the analysis are listed in Table 3-18. If used in design, the values listed in Table 3-18 should minimize lateral acceleration and the vehicle's lateral motion. Values smaller than those listed tend to be associated with larger outward lateral velocities. Values larger than those listed tend to be associated with larger lateral shifts.

Theoretical considerations indicate that values for the proportion of runoff length on the tangent in the range of 0.7 to 0.9 (i.e., 70 to 90 percent) offer the best operating conditions

Table 3-18. Runoff locations that minimize the vehicle's lateral motion.

Metric					US Customary				
Design speed (km/h)	Portion of runoff located prior to the curve, No. of lanes rotated				Design speed (mph)	Portion of runoff located prior to the curve, No. of lanes rotated			
	1.0	1.5	2.0–2.5	3.0–3.5		1.0	1.5	2.0–2.5	3.0–3.5
20–70	0.80	0.85	0.90	0.90	15–45	0.80	0.85	0.90	0.90
80–130	0.70	0.75	0.80	0.85	50–80	0.70	0.75	0.80	0.85

on roadways with downgrades of less than 4 percent; the specific value in this range should be dependent on design speed and rotated width. Experience obtained from existing practice indicates that deviation from the values in Table 3-18 by 10 percent should not lead to measurable operational problems. In this regard, use of a single value for the proportion of runoff length on the tangent in the range of 0.6 to 0.9 (60 to 90 percent) for all speeds and rotated widths is considered acceptable. However, refinement of this value, based on the trends shown in Table 3-18 is desirable when conditions allow.

Research that considered minimum-radius horizontal curves on downgrades of 4 percent or more indicates that application of the proportion of runoff length values shown in Table 3-18 are acceptable to the design of curves using the maximum rate of superelevation and minimum curve radius for design speeds of 40 km/h [25 mph] or more *(69)*. However, when designing above-minimum-radius curves for specific design speeds, and applying the runoff location proportions shown in Table 3-18, the curve-radius/design-superelevation-rate combinations shown in Tables 3-8 through 3-12 may produce margins of safety against skidding or rollover that are lower on the approach tangent than within the limits of the simple horizontal curve. This is undesirable and should be checked using the following condition:

Metric	U.S. Customary
$\frac{e}{100} < \frac{0.077}{1 + p_{tangent}} \times \frac{V^2}{gR}$	$\frac{e}{100} < \frac{2.15}{1 + p_{tangent}} \times \frac{V^2}{gR}$
where: e = superelevation at PC of horizontal curve $p_{tangent}$ = proportion of the maximum superelevation attained at the PC of horizontal curve V = design speed, km/h g = gravitational constant, 9.81 m/s^2 R = radius of horizontal curve, m	where: e = superelevation at PC of horizontal cur $p_{tangent}$ = proportion of the maximum superelevation attained at the PC of horizontal curve V = design speed, mph g = gravitational constant, 32.2 ft/s^2 R = radius of horizzontal curve, ft

If the condition presented above is met, engineers can proceed with the superelevation transition as designed using the guidance included in this section. If the condition presented above is not met, designers should reduce the proportion of the maximum superelevation attained at the PC of the horizontal curve, or introduce a spiral transition curve between the approach tangent and simple horizontal curve. Based on theoretical considerations, the condition above is satisfied for maximum-superelevation/minimum-radius curves for all design speeds when applying the proportion of superelevation runoff values in Table 3-18. However, the condition above may be violated when using design superelevation rates that are approximately 50 percent or less than the maximum superelevation rate for a given design speed-minimum radius combination. In these cases, locating 70 percent of the superelevation runoff prior to the horizontal curve will increase the margins of safety on the approach tangent relative to the simple horizontal curve.

Limiting superelevation rates. Theoretical considerations indicate that, when a vehicle is traveling through a tangent-to-curve transition, large superelevation rates are associated with large shifts in the vehicle's lateral position. In general, such shifts in lateral position can be minimized by the proper location of the superelevation runoff section, as described above. However, large lateral shifts must be compensated by the driver through steering action.

In recognition of the potential adverse effect that large shifts in lateral position may have on vehicle control, the threshold superelevation rates associated with a lateral shift of 1.0 m [3.0 ft] are identified in Table 3-19. These limiting superelevation rates do not apply for speeds of 80 km/h [50 mph] or more when combined with superelevation rates of 12 percent or less.

Designs that incorporate superelevation in excess of the limiting rates may be associated with excessive lateral shift. Therefore, it is recommended that such superelevation rates be avoided. However, if they are used, consideration should be given to increasing the width of the traveled way along the curve to reduce the potential for vehicle encroachment into the adjacent lane.

Table 3-19. Limiting superelevation rates.

Metric		U.S. Customary	
Design speed (km/h)	Limiting superelevation rate (%)	Design speed (mph)	Limiting superelevation rate (%)
20	8	15	8
30	8	20	8
40	10	25	10
50	11	30	11
60	11	35	11
70	12	40	11
		45	12

On upgrades of 4 percent or more, the maximum superelevation rate should be limited to 9 percent for minimum-radius curves with design speeds of 90 km/h [55 mph] and higher, to minimize the potential for wheel-lift events on tractor semi-trailer trucks. Alternatively, if it can be verified that the available sight distance is such that deceleration at the rate assumed in stopping sight distance design criteria, 3.4 m/s^2 [11.2 ft/s^2], is unlikely to be required on upgrades of 4 percent or more, e_{max} values up to 12 percent may be used for minimum-radius curves.

New Reference for Green Book *pg. 3-184*

69. Torbic, D. T., M. O'Laughlin, D. W. Harwood, K. Bauer, C. Bokenkroger, L. Lucas, J. Ronchetto, S. N. Brennan, E. T. Donnell, A. Brown, and T. Varunjikar. *Superelevation Criteria for Sharp Horizontal Curves on Steep Grades.* Final Report for NCHRP Project 15-39, MRIGlobal, 2013.

Text on pg. 74 of 2009 MUTCD

Section 2B.33 STAY IN LANE Sign (R4-9)

Option:

A STAY IN LANE (R4-9) sign (see Figure 2B-10) may be used on multi-lane highways to direct road users to stay in their lane until conditions permit shifting to another lane.

Guidance:

If a STAY IN LANE sign is used, it should be accompanied by a double solid white lane line(s) to prohibit lane changing. Where the STAY IN LANE sign is intended to discourage lane changing on sharp horizontal curves on steep downgrades on multi-lane highways, consideration may be given to using a single solid white lane line marking to supplement the R4-9 sign.

Text on pg. 362 of 2009 MUTCD

Where crossing the lane line markings is discouraged, the lane line markings shall consist of a normal or wide solid white line.

Option:

Where it is intended to discourage lane changing on the approach to an exit ramp, a wide solid white lane line may extend upstream from the theoretical gore or, for multi-lane exits, as shown in Drawing B of Figure 3B-10, for a distance that is determined by engineering judgment.

Where lane changes might cause conflicts, a wide or normal solid white lane line may extend upstream from an intersection.

In the case of a lane drop at an exit ramp or intersection, such a solid white line may replace a portion, but not all of the length of the wide dotted white lane line.

Where a solid white lane line marking is intended to discourage lane changing by motorists on sharp horizontal curves on steep downgrades on multi-lane highways, a single solid white lane line may extend upstream, on, and downstream of the horizontal curve for a distance that is determined by engineering judgment.

Abbreviations and acronyms used without definitions in TRB publications:

A4A	Airlines for America
AAAE	American Association of Airport Executives
AASHO	American Association of State Highway Officials
AASHTO	American Association of State Highway and Transportation Officials
ACI–NA	Airports Council International–North America
ACRP	Airport Cooperative Research Program
ADA	Americans with Disabilities Act
APTA	American Public Transportation Association
ASCE	American Society of Civil Engineers
ASME	American Society of Mechanical Engineers
ASTM	American Society for Testing and Materials
ATA	American Trucking Associations
CTAA	Community Transportation Association of America
CTBSSP	Commercial Truck and Bus Safety Synthesis Program
DHS	Department of Homeland Security
DOE	Department of Energy
EPA	Environmental Protection Agency
FAA	Federal Aviation Administration
FHWA	Federal Highway Administration
FMCSA	Federal Motor Carrier Safety Administration
FRA	Federal Railroad Administration
FTA	Federal Transit Administration
HMCRP	Hazardous Materials Cooperative Research Program
IEEE	Institute of Electrical and Electronics Engineers
ISTEA	Intermodal Surface Transportation Efficiency Act of 1991
ITE	Institute of Transportation Engineers
MAP-21	Moving Ahead for Progress in the 21st Century Act (2012)
NASA	National Aeronautics and Space Administration
NASAO	National Association of State Aviation Officials
NCFRP	National Cooperative Freight Research Program
NCHRP	National Cooperative Highway Research Program
NHTSA	National Highway Traffic Safety Administration
NTSB	National Transportation Safety Board
PHMSA	Pipeline and Hazardous Materials Safety Administration
RITA	Research and Innovative Technology Administration
SAE	Society of Automotive Engineers
SAFETEA-LU	Safe, Accountable, Flexible, Efficient Transportation Equity Act: A Legacy for Users (2005)
TCRP	Transit Cooperative Research Program
TEA-21	Transportation Equity Act for the 21st Century (1998)
TRB	Transportation Research Board
TSA	Transportation Security Administration
U.S.DOT	United States Department of Transportation